# Groundwater Flow Conceptualization and Storage Determination of the Table Mountain Group (TMG) Aquifers

Report to the
**Water Research Commission**

*by*

***Y Xu, L Lin and H Jia***

Department of Earth Sciences
University of the Western Cape
Bellville 7535, South Africa

**WRC Report No. 1419/1/09**
**ISBN 978-1-77005-840-8**

**July 2009**

**DISCLAIMER**

This report has been reviewed by the Water Research Commission (WRC) and approved for publication. Approval does not signify that the contents necessarily reflect the views and policies of the WRC, nor doe mention trade names or commercial products constitute endorsement or recommendation for use.

# Executive Summary

The Table Mountain Group (TMG), located at the southernmost parts of the African continent, constitutes a major regional aquifer system in South Africa. The TMG aquifer comprises a thick sequence of hard sedimentary rocks dominated by fractured sandstones. Large-scale distribution of the TMG over various geological structures leads to a vast diversity in its hydrogeological properties which influence the dynamics of recharge, discharge and storage. An realistic estimation of these hydrogeological properties, with a focus on the aquifer porosity, permeability and storativity, is important for the sound evaluation and sustainable utilization of the groundwater resources in the TMG.

## Hypothesis

Although many initiatives have contributed to the investigation of the characteristics of the TMG aquifers and their implications for groundwater utilization in the region, the conceptual study of the TMG with the focus on aquifer properties, flow and storage dynamics has so far been limited because of the geometric and physical complexity of the fractured rock aquifer at various scales. This study is largely beased on the geological and geomorphological surveys, the examination of borehole core drilling samples, the observation of wellfield performance, the identification of groundwater flow dynamics, and the characterization of aquifer media at various scales. The aim is to improve the understanding of the TMG aquifers at both regional and local scales through the classification of hydrogeological units, the analysis of their aquifer properties and the quantification of groundwater recharge, discharge and storage. The findings obtained from this research would provide an insight into the fractured rock aquifers in the TMG area, and will have implications for sustainable groundwater management, hence forming a solid basis for the follow-up study of the TMG aquifers.

## Methodology

Data from previous studies and current research have been collated and analyzed to help establish the conceptual models and to quantify hydrogeological properties such as the hydraulic conductivity. Based on the study of hydrogeological settings and aquifer types, combined with the interpretation of aquifer hydraulic tests, it is evident that the hydraulic properties of the TMG aquifers are largely controlled by geological formations and structures at various scales. By analysing fracture networks and their associated patterns, it became clear that the most important single factor that controls groundwater flow in the TMG aquifers is the connectivity of the fractures. The study of aquifer media, especially the nature of the fractures and fracture networks is therefore conducted in detail. Subsequently, the established conceptual models of the fractured-media based on field observations and stochastic analyses are helpful tools for the better understanding of aquifer characteristics including flow and storage behaviors in the TMG aquifers.

## Aquifer hydraulic properties

With the information derived from field measurements and interpreted from the remote sensing, the anisotropic hydraulic properties of the fractured aquifers are estimated using a hydraulic conductivity tensor technique. Considering the fact that the fracture connectivity and the nature of fractured media at a given site may vary with depths, a tensor model is accordingly developed to estimate the hydraulic

properties on the surface and at depth by incorporating aquifer physical conditions. As a result, the estimated hydraulic conductivities at most sites fall in the range of $10^{-2}$~$10^{-3}$ m/d which is consistent with most of the pumping test results. However they decrease with depth according to a negative power law, which implies that the majority of fractures display a tendency of closure at greater depths. Site hydraulic tests also showed a similar vertical variation of the hydraulic conductivities.

The study revealed that fracture networks on a site scale occur as various fracture blocks nested in the system rather than as equally connected as originally postulated. A further simulation of fracture connectivity using the 3-D model of discrete fracture face analysis demonstrates that only limited fracture networks out of the bulk being considered allow groundwater circulation at both local and regional scales in the TMG aquifers.

Multiple approaches are employed to estimate the aquifer porosity and associated aquifer storativity. Results show that the porosity of the TMG sandstones is strongly scale-dependent, of which the value of core sample laboratory tests yields a upper limit of 1.0%~3.6%. The porosity of in-situ fracture measurements fall in the middle range of 0.05%~0.6%, whilst the application of lineament interpretation from remotely sensed data produces its lower limit of $1.2\times10^{-8}$%.

## Resource evaluation

For resource evaluation purpose, clarity is made regarding the nature of the TMG aquifer types. It is incorrect to classify an aquifer as the confined aquifer only because water level rises above where it gets struck. The rise of water level is a necessary condition for a confined aquifer but not sufficient condition for an aquifer being termed the confined. As the confining units in the TMG suffer from fault displacement, both confined and unconfined aquifers could be demarcated according to their geological settings even at a regional scale.

The spatial distribution of the TMG aquifers (including the Peninsula Aquifer and the Nardouw Aquifer), in both aerial and vertical extent, is quantified using a GIS technique for the first time. This provides the foundation for both the visualization of the aquifer geometry and the estimation of groundwater storage capacity. Different definitions of groundwater storage capacity, including total storage capacity, usable storage capacity, available storage capacity and sea level-related storage capacity, are demarcated and estimated for the TMG aquifers. For the purpose of evaluation of the TMG aquifer in its entirety, evaluation of the bulk groundwater resource is made based on assumptions that the TMG aquifers are homogeneous at a regional scale, and an average storativity value is necessary cross the entire aquifers. An available yield of $<1\times10^9$ $m^3$/year is proposed for the groundwater exploitation from the TMG aquifers based on the regional aquifer storage. The result suggests that the previously postulated bulk groundwater storage of TMG may be overestimated as use was made of an aquifer storativity derived at the local scale.

The estimation of groundwater recharge is largely derived from the previous work at UWC but some of the results are verified and assessed through a case study during this investigation. The main groundwater discharges from TMG aquifers – spring flow, groundwater abstraction and stream baseflow – are quantitatively estimated. The quantification of the former two components is accomplished by hydrocensus analyses. The surface water and groundwater interaction is also investigated, from which baseflow separations are performed to determine the order of magnitude of groundwater discharge into streams.

The response of TMG aquifer to pumping stresses in the areas of the

Kammanassie Mountains and Rawsonville is simulated by groundwater flow modeling. 3-D hydrogeological conceptual models are constructed, which helps to verify the understanding of the conceptual hydrogeological settings. The detailed groundwater-related data analyses are performed on the basis of previous and current data sets. The numerical model is then established to simulate the aquifer response to stresses including various pumping scenarios.

Some data processing techniques for general purpose are also developed in this research that can potentially be applied to similar studies.

## Implications

The finding of the WRC sponsored research project entitled "Groundwater Flow Conceptualization and Storage Determination of the Table Mountain Group (TMG) Aquifers" has formed a concrete basis for understanding groundwater flow dynamics and potential utilization of the TMG aquifer system in terms of aquifer media and spatial variations. Based on information acquired from this research, it bcomes feasible that more focused specific groundwater issues could be investigated to aid the sustainable utilization of the distributed groundwater resources in the TMG.

## ACKNOWLEDGEMENTS

This research project was funded by the Water Research Commission (WRC) with the assistance from Department of Water Affairs and Forestry (DWAF) and Council for Geosciences (CGS).

The project team is very grateful to the chairpersons of the Steering Committee, Dr Kevin Pietersen and subsequently Dr Shafick Adams for their effort and patience in managing the project. Many thanks are also given to the steering committee members for their inputs to the programme from start to finish as well as their suggestions and comments, for which the following organisations and their representatives are acknowledged:

| | |
|---|---|
| DWAF | Mr M Smart and Mr P Seward |
| CSIR | Dr H Beekman, Ms C Colvin, and Mr J Weaver |
| City of Cape Town | Mr RC Bishop |
| GWA | Dr R Murray |

The contribution of 29 geological cross-sections by the Council of Geosciences, Bellville Office (Appendix A) for TMG storage estimates is highly appreciated. The review of major TMG wellfields provided by SRK consulting (Appendix B) is acknowledged. Valuable reviews of the project were made by Prof GJ van Tonder of the IGS at the University of the Free State and Prof Balthazar Th.Verhagen at the University of Witwatersrand.

We would also like to acknowledge the field work team of DWAF for their plentiful assistance in the course of drilling and testing, as well as the staff and postgraduate students of the Department of Earth Sciences at UWC for their contributive roles in execution of the project. The VLIR – UWC Water Project has largely complemented this WRC project, though the VLIR project with a focus on ecohydrology will be reported separately. The final draft report was reviewed by Mr Paul Seward who provided valuable and constructive comment on the report.

# TABLE OF CONTENTS

# LIST OF FIGURES

# LIST OF TABLES

# 1. Introduction

## 1.1 Research Background

The Table Mountain Group (TMG) forms a huge aquifer system that extends from the northwest of the Western Cape to the northeast of the Eastern Cape, consisting of a suite of consolidated sedimentary rocks produced in the Ordovician-Devonian period. The significance of the TMG groundwater for water supply in the semi-arid areas of the nation has long been stressed due to the good water quality and high potential for abstraction from the high-yielding fractured sandstones. For the purposes of water supply and resource protection, the aquifer system has been selectively investigated since the 1980s on locations ranging from the Uitenhage artesian basin in the east to the Sandveld area in the west. An extensive monitoring network of boreholes and springs has been established, from which water level and water chemistry data are periodically collected. However, current understanding of the TMG aquifer system is limited as regarding the hydrogeological settings, hydraulic properties of aquifers, and accordingly the groundwater storage and circulation.

A theoretical study on the conceptual models of the TMG fractured rock aquifers, based on aquifer media characterization and analysis of aquifer properties, is therefore necessary for providing insight into groundwater flow and storage mechanisms of the TMG system. Based on previous studies, in situ hydraulic test data are available for the analyses of aquifer properties (Rosewarne, 2002). These data are valuable for the estimation of the intrinsic aquifer properties such as hydraulic conductivity ($K$), transmissibility ($T$), storativity ($S$) and porosity ($n$). These estimated aquifer parameters are critical in water resource evaluation, conceptualization, management, and groundwater development in the TMG area. An overestimate of $T$ and $S$, for instance, may lead to water withdrawals from an aquifer that exceeds its capacity. Current methods of determining hydraulic properties for the TMG aquifer through field tests nearly always assume that the aquifers form a hydrogeological continuum. This simplification can cause problems since the fractured rocks are anisotropic and complex in geometric and physical features, as a result of previous tectonic movement and current stress fields, and so aquifers may be less continuous and more heterogeneous than assumed in current aquifer test analyses.

Relevant studies associated with the TMG groundwater development have covered each field of hydrogeology ranging from aquifer delineation, through resource potential evaluation, groundwater recharge and quality, to exploration techniques (Pietersen and Parsons, 2002).

Exploration and monitoring of exploitation in the TMG aquifers has produced plenty of valuable information and form the basis for in-depth research. However, many issues remain unresolved regarding subsurface features of the TMG fractured rocks in which the key feature is the determination of flow paths and boundary conditions when using existing models to interpret the aquifer responses to external stresses. Previous studies have shown that the groundwater occurrence in the TMG region is prevalently dominated by secondary porosity, i.e. fractures or fracture networks. The significance of fractures controlling groundwater flow and storage in the aquifers has been long noted and studied by many investigators (Chevallier, 1999; Woodford and Chevallier, 2002; Hartnady and Hay, 2002a), for example. Very few studies have, however, extended as far as investigating the characteristics and patterns of the fractures which exert such a great impact on the aquifer properties.

A fractured rock aquifer is composed of a network of fractures that cut through a rock matrix. Understanding of the characterization of the fracture network requires information on the nature of both the fractures and the rock matrixes. Fractures may be characterized in terms of the dimensions, locations, and the nature of fracture walls. The rock matrix is characterized by its pore sizes and distributions, often expressed by effective porosity. Generally, the hydraulic conductivity of fractures is several orders of magnitude greater than that of the matrix. In the TMG sandstones, the fracture systems mainly control the permeability of rock masses and are major potential pathways for fluid flow. Because the distributions and attributes of fractures are not uniform either macroscopically or microscopically, the anisotropy of a fractured rock aquifer makes the determination of potential flow paths difficult. Ideally, fracture data should be gathered on fracture length, orientation, aperture, and density for developing a statistical or determinative model. Particularly the interconnection of fractures may play a key role on the determination of groundwater flow path. It is difficult to obtain all these data for the characterization of fractures at a regional or a local scale. However some useful knowledge can be inferred based on the structural analyses of an area or a site. The tectonic and depositional history of a given area is generally available in geological literature (McCarthy and Rubidge, 2005; Newton et al., 2006), providing a concrete background for understanding the formation of fractures in the TMG sandstones.

Hydraulic conductivity, aquifer transmissivity and storativity, are commonly used as the key aquifer parameters to determine the aquifer's capacity of yielding sufficient water supply, as well as quantification of flow and storage. However, uncertainty and diversity of these parameters often arise from various data sources at the same site or from multiple interpretation methods using the same data set. Therefore, it is necessary to employ multidisciplinary approaches, such as geophysical and geochemical methods, in-situ hydraulic and laboratory tests, and digital process and numerical model (Karasaki et al,. 2000; Kulatilake et al., 2003; Serzu et al., 2004), to estimate the parameters associated with groundwater flow and storage. Moreover, it is important to collate these data based on the understanding of the fracture network characteristics. Characterization of fractured rock as the basis of aquifer conceptualization is crucial, as it can present both geometric and hydraulic features of the fractures involved. The development of conceptual models on the basis of fractured medium analyses has rarely been done in the investigation area.

As quantification of groundwater flow and storages requires a proper understanding of the behavior and characteristics of aquifer system, especially fracture systems that function as both flow paths and storage media of groundwater, the impact of a variety of factors on the evolution of underlying geology and the mechanism that affects groundwater resources needs to be addressed (Mulhall and Demicco, 2004). The mechanism of groundwater storage, depending on the geometric and physical properties, and the recharge and discharge processes of the aquifers, is different in various aquifers, particularly in fractured rock aquifers of which the anisotropic properties are extremely difficult to determine. Therefore, the groundwater storage or storage capacity and sustainable yield on a regional scale is more practical to estimate using existing volumetric models and an average storativity or specific yield values. The estimation should also be based on the consideration of the three dimensions of the aquifer geometry, and the effects of groundwater withdrawal, recharge and discharge on the groundwater system as the whole.

The significance of groundwater and surface water interaction has been given more attention in recent decades from many hydrogeologists (Nathan, 1990; Winter et al., 1998 Chapman, 1999; Xu et al., 2002; Hughes et al., 2003). Intensive groundwater abstraction can affect the relationship between surface water and groundwater regimes. The majority of groundwater/surface water interactions have been frequently observed to occur as groundwater discharges into stream water, particularly in mountain areas. In regional groundwater resource estimation, the development of baseflow concepts and associated methods has provided important understanding and useful tools to study such relationships. Although the baseflow separated from each stream flow using long-term monitoring data cannot completely account for the groundwater discharges into the stream flow, it does approximate the amount gained from aquifer storage, especially if the interflow is not considerable and can be overlooked.

The subsurface flow system is usually more complex. It may be desirable to predict the behavior of an aquifer in response to pumping, the effects of recharge and discharge, boundary effect, and the effects of flow and transport in an anisotropic medium. Groundwater models are integrated tools in such predictions. A model is a simplified version of a real groundwater system that approximately simulates the complexity of reality in a manner that captures or represents the essential features and processes associated with groundwater issues. The simplification is introduced in the form of a set of assumptions that express the understanding of the nature of the system and its behavior (Bear and Verruijt, 1987). For solving groundwater problems the most commonly used methods are the numerical finite difference and finite element models (Wang and Anderson, 1982). The groundwater model can be used to improve the understanding of complex hydrogeological condition, and the results of model computation can be used to refine and optimize exploration and monitoring, as well as suggest scenarios for the management of groundwater abstraction on a sustainable basis.

## *1.2 Research aims and objectives*

In South Africa the TMG, the Karoo dolerite system, and the Dolomites comprise the major regional aquifers. The TMG aquifers have the potential to meet substantial bulk water supply requirements for irrigation and local municipalities in the Western and Eastern Cape Provinces. Geographically the TMG is the southernmost major hard-rock aquifer system in the African continent, and generally yields groundwater of high quality characterized by low salinity (Smart and Tredoux, 2001). With the increased water demand from irrigation and urban areas, South Africa has launched a number of research and investigation projects to facilitate integrated water resource management as required by the Water Act of 1998. The WRC project: "*flow conceptualization and storage determination in the Table Mountain Group (TMG) aquifer systems"*, aims to reveal the properties and characteristics of the TMG aquifer systems, and to be a pilot study for groundwater resources management in the area. The specific aims of the project are to determine the groundwater storage and the flow characteristics of TMG aquifer systems, by means of the aquifers' identification and conceptualization through previous data analyses and by field investigations. The project was carried out from 2003 to 2006 and comprised the following research tasks:

(1) Identification and verification of TMG hydrostratigraphic units

(2) Field investigations

(3) Define properties of aquifer media
(4) Assessment of seasonal and climate impact on hydrologic circle
(5) Define hydrogeological conceptual models
(6) Quantification of ground water flow and aquifer storage
(7) Visual presentation of the TMG aquifer systems
(8) Coordination of various research efforts
(9) Report writing

Prior to the late 1980s, groundwater development in the TMG aquifers was restricted to the areas with water shortages. It is only in the last decade that groundwater in the TMG sandstones has received wider attention in the area of agricultural activities, and for municipal and domestic development. The aim of groundwater investigations in the TMG is not just to establish well fields to provide significant water supplies to help alleviate future water shortages, but also to assess the potential ecological impact of large-scale groundwater use. Consequently a knowledge of how much groundwater is stored and how this water is distributed in the TMG area becomes essential. A comprehensive and quantitative estimation of this water resource has not been done yet on a regional scale, although previous studies have given some rough estimates. To provide a comprehensive understanding of the TMG fractured rock aquifers and a fundamental data set for the water resource management in the area, the major challenge of this study is to provide a proper perspective of the aquifer properties, based on conceptual understanding of the TMG aquifer media. This can be broken down into the following study objectives:

(1) A comprehensive conceptual understanding of the aquifer system and hydrogeological settings, based on the analysis of existing geological and hydrogeological information
(2) Characterisation of fractures and fracture network through surface measurements, remote sensing imagery interpretation, and borehole loggings
(3) Establishment of conceptual models on the basis of the TMG aquifer type and groundwater data
(4) Estimation of hydraulic properties using hydraulic tests (packer tests and pumping tests) conducted at different sites, and numerical modelling based on hydraulic conductivity tensors to be applied to various types of fracture network for both 2-D and 3-D problems
(5) Porosity and storativity quantification using the analyses of core samples, pumping and remote sensing data, and borehole geophysical logs

(6) Regional evaluation of the TMG groundwater resources involving the quantification of recharge, storage and discharge and an indication of sustainable yields based on a groundwater budget for the regional aquifer system
(7) Site-specific studies to gain a better understanding of the TMG aquifers and associated groundwater flow behaviour
(8) Quantitative analyses of the stream-aquifer interactions, and the identification of the most important component of groundwater discharge in the area
(9) Groundwater flow modelling, aiming to simulate the TMG aquifer response to pumping
(10) Development of applicable data processing approaches that may be used in future

## *1.3 Methodology*

The above-mentioned objectives cannot be achieved without a combination of available site-specific data, related experience, and scientific knowledge of the TMG hydrogeology, geology, and geomorphology. Effective characterization of aquifer properties based on the analysis of previous and current data requires not only an experienced interpretation of available data and a full understanding of the factors that control groundwater processes, but also the application of GIS techniques. Regarding groundwater as a resource, the relationships between recharge, storage and discharge are also addressed in this study in order to obtain a full understanding of the dynamic characteristics of the resource and how to manage it.

Combined with the estimation of hydraulic conductivity and transmissivity, existing data from previous studies and current research will be collated and analysed to help establish conceptual models of the TMG aquifers. Based on the understanding of these models, different interpretation methods are to be applied to the estimation of flow magnitude and groundwater storage. The applicability of these interpretation methods is also discussed, considering the media complexity for flow taking place in the fractured rocks.

# 2. Hydrogeological Setting

## *2.1 Introduction*

The outcrop of TMG extends from Vanrhynsdorp in the northwest to the Cape Peninsula in the south and then bends eastward to Port Elizabeth, covering an area of some 37000 $km^2$ (Fig. 2-1). Stratigraphically, the TMG consists of a thick sequence of consolidated sedimentary rocks deposited in a south-eastward trending trough of the Agulhas Sea 500~425 Ma ago, and has a deposit thickness ranging from 900 to 4000 m.

Based on the historical information on groundwater utilization from the TMG aquifers via borehole/spring abstractions, together with deductions from lithological characteristics, stratigraphic assemblage and structural fabrics of the TMG, it has been inferred that the TMG is a regional aquifer that extends to great depths (Issar, 1995; Weaver et al., 2002). In addition, it is acknowledged that the aquifer systems are mainly dominated by fractured sandstones, siltstones, and interbedded shales and mudstones. The TMG is underlain by Precambrian

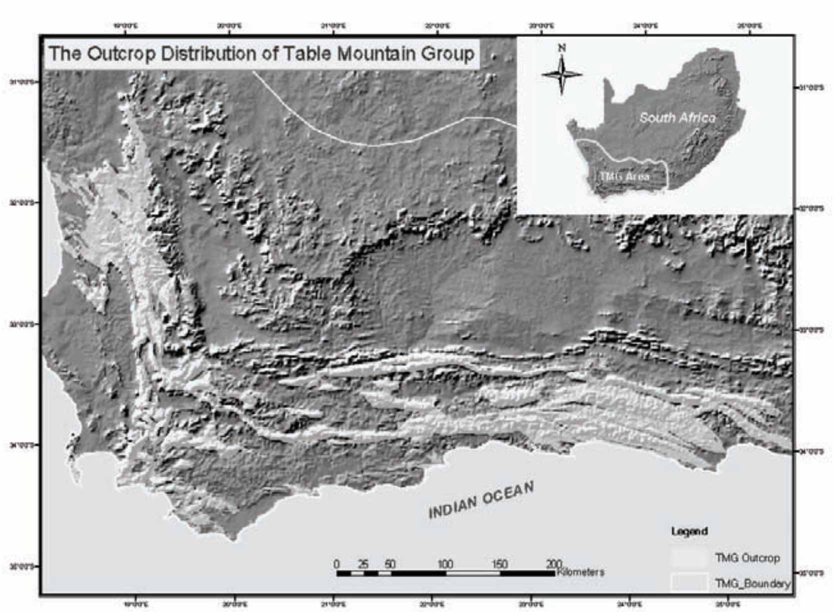


**Fig. 2-1** Extent of the TMG

rocks and overlain by mid- to neopaleozoic basin deposits, and is in some cases bounded by regional faults such as the Kango-Baviaanskloof and Worcester faults

## 2.2 Geological background

### *2.2.1 Geomorphology*

Regionally, the TMG geomorphology comprises mountains, wave-cut plains and intermountain drainage basins. The modern landform patterns of the TMG area largely resulted from post-Karoo morphogenetic processes including the denudation of mountains and the formation of half-grabens due to crustal uplift in inland areas, peneplain and transgression along the coastal areas.

The mountain peaks reach 1900~2250 m in Hex River Mountain, 1500~2000 m along Langeberg and 1700~2000 m on Swartberg Mountains. Compared with the overlying argillaceous rock formations and underlying basement rocks, the geomorphologic patterns of TMG are characterized by the highly prominent mountains and steep slopes with sparse or even no soil cover. From west to east, the Bokkeveldberg – Cedarberg – Skurweberg and Hex river mountains dominate, and further east are the Langeberg – Outeniekwaberg mountains. To the north there are Witteberg – Swartberg and Baviaanskloof mountains. In between these mountains there are basins and flood plains, most of which are covered by weathered material from argillaceous rocks and fluvial deposits.

Primary catchments that fall within the TMG area are – from west to east – the Berg, Olifants-Doring, Breede, Salt, Gourits, Gamtoos and Sundays rivers. The rivers cutting through various formations of the TMG and structural controls have contributed to the dramatic relief variations found in the area.

### *2.2.2 Stratigraphy*

South Africa has a long geological record spanning almost the entire geological history of the earth. Palaeoarchaean greenstone belts can be dated to ca. 3.5 Ga. The TMG was formed from the early Ordovician to the early Devonian during 500~425 Ma ago (Fig. 2-2).

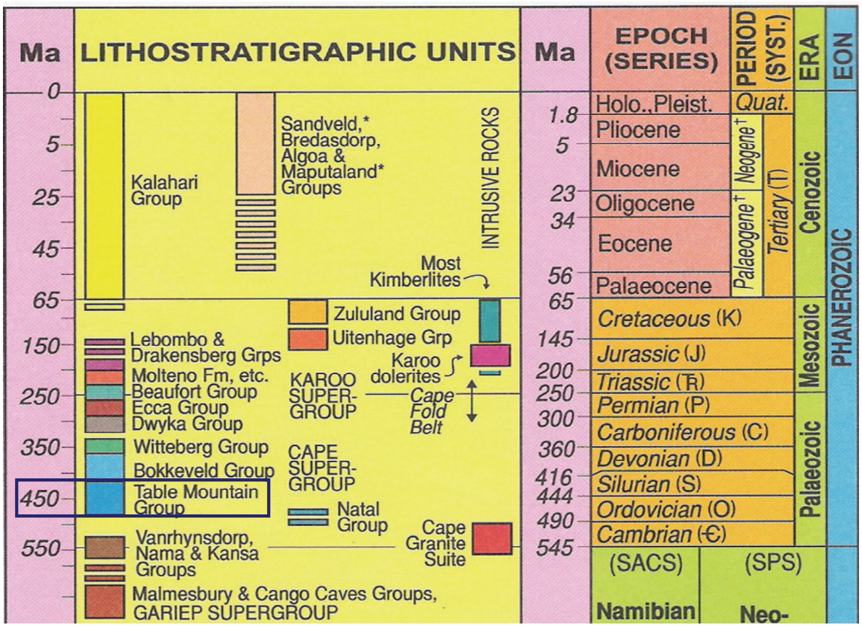


**Fig. 2-2** Stratigraphic position of the TMG (after Council of Geoscience, 2006)

**Table 2-1** Stratigraphic succession of the Table Mountain Group

| Group | Subgroup | Formation | Geological symbol | Thickness (m) subtotal | Thickness (m) | Lithology |
|---|---|---|---|---|---|---|
| **Bokkeveld** | | | D | 4000 | | Siltstones, shales, sandstones |
| **Table Mountain** | **Nardouw** | Rietvlei/Baviaa-nskloof | Dr/ S–Db | 1200 | 300 | Feldspathic quartz arenite |
| | | Skurweberg | Ss | | 500 | Quartz arenites |
| | | Goudini | Sg | | 400 | Arenite, minor siltstone, shale |
| | | Cedarberg | O–Sc | 70 | 50~150 | Silty shales and shaly siltstone |
| | **Peninsula** | Pakhuis | Opa | 2500~3100 | 100~150 | Tillite, diamictite, quartz arenites |
| | | Peninsula | Ope | | 1500~2000 | Largely thick-bedded, coarse-grained quartzitic arenites |
| | | Graafwater | Og | | 65~150 | Thin-bedded sandstone, siltstone, shale and mudstone |
| | | Piekenierskloof | Op | | 800 | Quartzitic sandstone with coarse-grained to gritty zones and rudites |
| **Basement** | | Underlying the TMG are the Malmesbury shales, the Gamtoos and the Kaaimans argillites, comprising a suite of moderately to lightly metamorphosed sedimentary rocks; and the Cape Granite Suite. | | | | |

The stratigraphy and lithology of the TMG have been depicted in detail by Du Toit (1954**),** Rust (1967; 1973), and De Beer (2002). The main stratigraphic units involved from the bottom to the top in the TMG aquifer system are the Piekenierskloof, Graafwater, Peninsula, Pakhuis, Cedarburg Formations, and the Nardouw Subgroup (Table 2-1). The basal

Piekenierskloof Formation, lying unconformably on basement rocks, consists of litharenites and rudites and is overlain by the semi-confining Graafwater shale/siltstone Formation. These two units are only found in the western branch of the TMG. The most significant and thickest Formation is the Peninsula, composed entirely of quartzitic arenites, being the preferred target for good quality water with high yields. This Formation occurs across the whole extent of the TMG with a thickness ranging from 1000 ~ 2000 m. A thin shale/ shaly siltstone layer with an average thickness of 70 metres makes up the Cedarberg Formation, which is as extensive as the underlying Peninsula Formation, and seemly acts as a confining layer or aquitard and effectively separates the lower Peninsula and upper Nardouw aquifers. At the top of the TMG is the Nardouw subgroup, which is divided into three members of interlayered shale, sandstone, siltstone and quartzite because of its variable composition.

The TMG stratigraphic units had undergone low grade of metamorphism due to folding and thrusting during the Cape Orogeny, resulting in phyllites and quartzites rather than shales and sandstones (Hälbich and Cornell, 1983). Recrystallization and polygonisation of quartz grains are typical in quartz arenites; these occurrences are commonly intensified in the rocks near fault zones. Recrystallization of mineral grains implies the reduction or disappearance of primary porosity and so groundwater in the TMG rocks can be regarded as being dominated by secondary porosity of fractures and joints. In spite of this, the TMG rocks still remain many of the original sedimentary fabrics and are generally referred to be sedimentary rocks (Newton et al., 2006) rather than metamorphic rocks.

### *2.2.3 Structural geology*

The TMG rocks have been reconstructed by several phases of crustal movements from the Permian to the Cretaceous, which created various types of discontinuities in the form of joints, faults and unconformities. Some of the discontinuities have been reactivated since the post Karoo tectogenesis which complicated the pre-existing fracture systems or zones. These secondary structural voids in TMG sandstones and siltstones constitute most of the fracture spaces allowing groundwater storage and movement.

The TMG region was at the margin region of Gondwanaland. The subduction on the southwest margin of Gondwanaland in the Late Carboniferous – Early Permian led to the transformation of an old passive margin into a foreland basin (the Great Karoo Basin) with southerly sourced sediments. The tectonic convergence at plate margins in the Permo–Triassic led to four episodes of development of the Cape Fold Belt known as Cape Orogeny during 278 Ma ~ 230 Ma (Hälbich, 1983). The formation of the Cape Fold Belt, which extends from

Australia through Antarctica and South Africa to South America (Fouché et al., 1992; McCarthy and Rubidge, 2005), caused a profound impact on the development of the TMG structural configuration and stratigraphical extension, and hence the hydrogeological setting.

The Cape Fold Belt is characterized by a series of northwest- to north-trending folds in the western branch, stretching from Stellenbosch to Vanrhynsdorp, and by folds striking approximately east-west in the southern branch from Swellendam in the west to Great Fish River in the east. The two arms of folds meet in the structural syntaxis in the center with more complex folding and faulting (De Beer, 2002) (Fig. 2-2). The Cape Orogeny largely formed the structural framework of the TMG (Hälbich, 1983), which also produced a series of south-dipping imbricate thrusts affecting both basement and cover rocks. Thrusts in the area, represented by Kango-Baviaanskloof and Worcester faults, can be roughly divided into three categories: back thrust, forward thrust, and pop-up structures (Newton et al., 2006). Both of the regional faults mentioned here are usually regarded as regional boundaries of groundwater regimes, and the pop-up structures are critical in searching for groundwater in the TMG fractured rocks (Newton et al., 2006).

Breakup of Gondwanaland during the late Jurassic to the Cretaceous created dextral shearing of the South African margin bounded by the Agulhas-Falkland fracture zone, and caused regional fragmentation and distortion of previous structural frames due to the compressive stresses being replaced by tensile stresses. Intraplate movements more easily took place along the existing thrust planes of relative weakness, which led to the development of half-grabens as the Oudtshoorn and Worcester basins where the Mesozoic strata (e.g. Uitenhage formation) were developed. Moreover, this tectogenesis turned most of previous thrust faults into normal faults with a gross throw of over 6000 m at the Worcester fault, for instance, and an impressive throw at the Kango-Baviaanskloof fault. Both in the eastern and western branches of the Cape Fold Belt, normal faults are widespread, especially where the faults have been rotated clockwise due to the right-lateral movement along Agulhas-Falkland fracture zone. In the structural syntaxis (Fig. 2-3), the features of normal faults are much complicated as a set of north-east striking faults strongly transect or rebuild both west-east and north-west trending faults and folds. However, the existence of this set of faults implies that a predominantly dextral strike-slip movement in this area has taken place (1/250000 geological map, 3319 Worcester sheet).

The normal faults developed in the TMG have long been the targets for groundwater exploration and exploitation. This can be successful for active faults where the fault zone

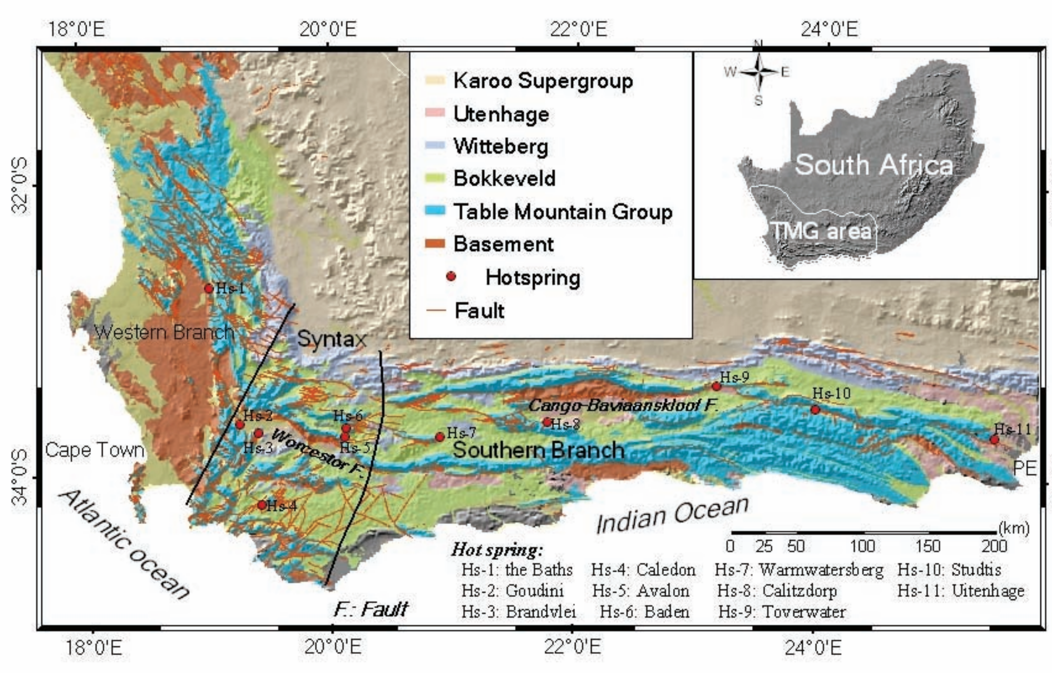


**Fig. 2-3** Map of Cape Fault Belt showing the stratigraphical and faulting distributions of the TMG, Pre-Cape rocks, and the younger Groups

materials are mostly uncemented, but unsuccessful when the fault zones are cemented and act as groundwater barriers. In fact, most of fault zones developed in the TMG sandstones and siltstones are regarded as being cemented and act as aquicludes (Newton et al., 2006), for example the Klein Bavaria fault north of Plettenberg Bay, the Brandvlei – Eikenhofdam fault, and the Kango fault etc.

## *2.2.4 Neotectonics*

The impact of neotectonic activity from the Miocene to the Quaternary on groundwater in the TMG fractured rocks is yet unknown and has rarely been studied. With the exception of earthquakes, neotectonic deformation and its impact on the occurrence and motion of groundwater is imperceptible in most cases. However, this long-term deformation has undoubtedly imposed a great influence on the TMG rocks, especially on discontinuities such as faults and joints. To have a better understanding of the TMG hydrogeology, it is necessary to take a look at post Karoo tectogenesis especially neotectonics. Currently, neotectonic information in South African onshore and offshore domains are derived from the interpretation of seismicity, fault rejuvenation, geomorphologic evidence, and estimation of stress field to meet the need of civil and industrial engineering work evaluations.

**1. Seismicity**

In general, an earthquake can exert an additional force on the rock masses within the seismic influence zone. This momentary external force may change the properties of fractures such as aperture and connectivity, both of which are critical in controlling groundwater flow paths in the fractured rocks. In particular rock masses nearby the epicenter are more fractured after an earthquake than before, and these rocks can be promising target for searching for groundwater (Andersen and Ainslie, 1994).

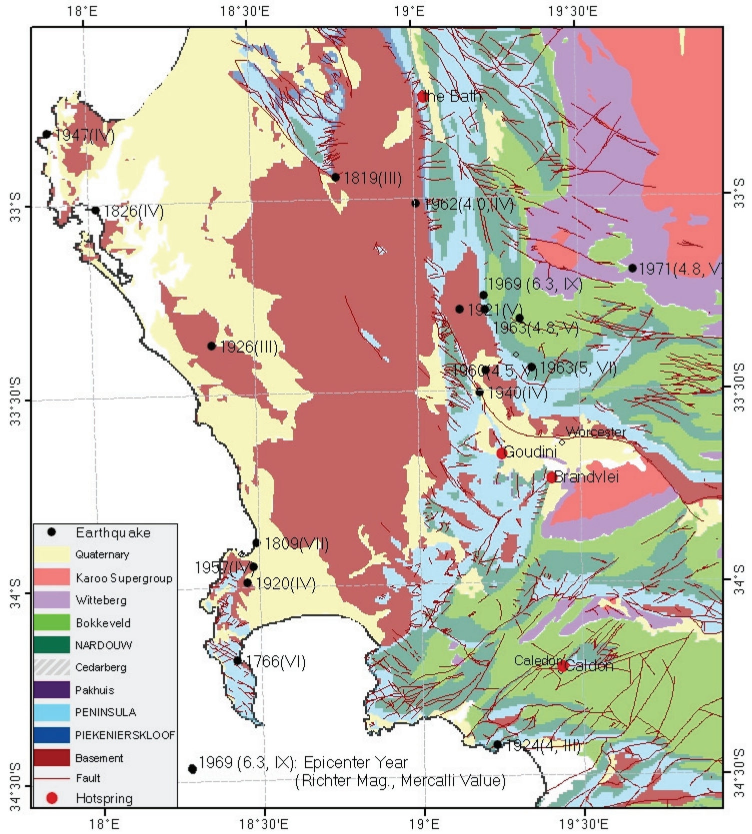


**Fig. 2-4** Occurence of earthquakes in the western branch of the Cape Fold Belt

South Africa is in an intraplate area such that earthquakes take place under poorly constrained forces (stresses) and affect the continental crust away from the seismic regions at the margin of tectonic plates (Andreoli et al., 1996). In the TMG area, seismic events characterized by low to moderate intensity are mostly concentrated in the western branch area of the Cape Fold Belt, from Ceres-Tulbagh to Cape Flat (Fig. 2-4). In the last two centuries, there have been about 40 seismic events taking place in this region. The worst hit area has been Ceres-Tulbagh where an earthquake on 29th September 1969 reached a magnitude of 6.3. The earthquake caused a hot spring at Goudini, some 50 km away from the epicenter, to dry up. Current hot "spring" water is obtained from a 350 m deep borehole drilled after the quake.

**2. Fault rejuvenation**

Although the mechanism of inland seismicity has not yet been satisfactorily explained (Ransome and de Wit, 1992; Andreoli et al., 1995), using both "ridge push" and crust uplift models, evidence for Late Tertiary to Quaternary neotectonic activity is rapidly growing, along with data derived from both onshore surveys, and offshore geophysical and borehole investigations. Of this, the rejuvenation of faults at various scales has most been documented. Fouché et al. (1992) concluded that the tectonic movement in this area, corresponding to plate drifting, did not terminate after the Gondwanaland segmentation. Andreoli et al. (1996) suggested that post Karoo structural activity in the southern African continental margin is mainly controlled by the structural configuration shown in Fig. 2-4 where one the major components is the Ceres-Prince Edward fabric that covers the TMG area ranging from the Groot River fracture zone (northern limit) to Gansbaai-Quoin Point (southern limit). According to Andreoli et al. (1996), faulting structures that predominate neotectonic activity in this area mainly comprise the offshore Agulhas-Falkland fracture zone, the Cape fracture zone which joins the Cape-Tzaneen Fracture zone in the north of the TMG, and the onshore Worcester fault which was partially reactivated in the Neogene. The stress field (Bird et al., 2006, Umvoto, 2003) in Fig. 2-5 implies that a NE 25° to NE 65° extension deformation dominates most of the TMG areas, but the direction and magnitude of principal stresses may change locally because the restriction of local structures, especially the discontinuities in rock formations, can divert stress distribution and concentration.

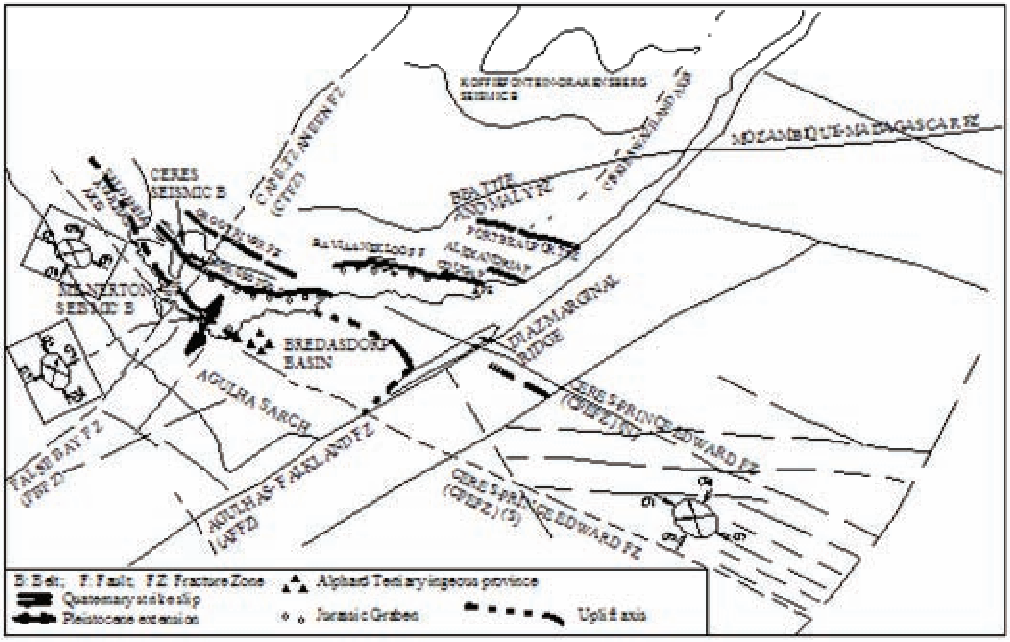


**Fig. 2-5** Post Karoo tectonic framework showing predominant structural features such as Agulhas-Falkland Fracture zone and Cape-Tzaneen Fracture zone running through Ceres-Prince Edward Fabric. These structural features control the post Karoo tectogenesis in the TMG area where some regional faults have shown evidence of reactivation. (modified from Andreoli, 1996; Friese, 2007).

Compared with the neotectonic activities taking place at plate margins, the reactivation of faults in the TMG region is of low magnitude in terms of deformation. In the eastern branch of the Cape Fold Belt, the Kango-Baviaanskloof fault, for instance, was shown to have a left-lateral strike slip with a comparatively recent offset measurable in metres through the investigation of slickensides and displaced river terraces at De Rust and Antoniesburge near Uniondale (Hill, 1988). In the western branch and structural syntaxis, the roughly W-E trending Worcester fault reveals a left-lateral slip movement (Andreoli et al., 1995). The rejuvenation of SE-trending Donkergat fracture zone between Quoin Pont and Gansbaai is well documented. The Miocene crust uplift along the SE-trending Saldanha-Cape Agulhas axis was reported by Partridge and Maud (1987). This neotectonic activity caused extensive jointing, faulting, and folding in the calcified dunes near Cape Agulhas.

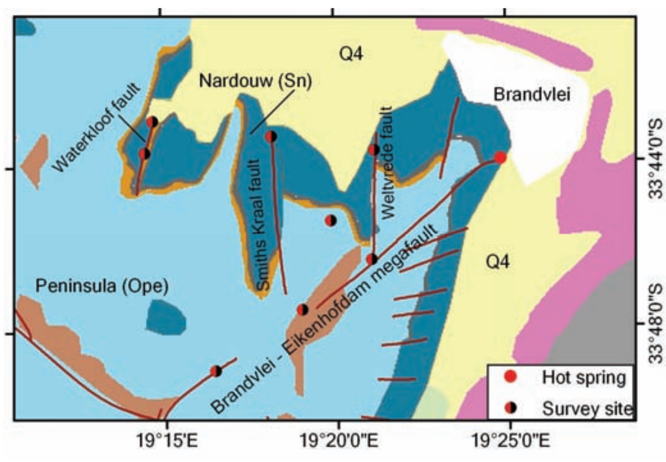


**Fig. 2-6** Brandvlei-Eikenhofdam megafault and its splay faults developed in the TMG and basement rocks

In the structural syntaxis, evidence for neotectonic activity is seismic events which are indications of crustal stress concentration at NW- and NE-trending faults. However, relatively recent fault movements can be tracked in some NS- and NE-trending faults, such as the Brandvlei – Eikenhofdam megafault and its splays (Fig. 2-6). At the fault zone of Brandvlei – Eikenhofdam fault near the Brandvlei hot spring, the SW-trending scratches, with uncemented iron oxides (Fig. 2-7) extensively developed in the fault core cleavages, have a plunge of 40°~50°. This probably indicates that this megafault has undergone a left-lateral strike-slip together with a SW-plunging movement in comparatively recent times. From field surveys of the fault zones of the splays, such as the NS-trending Waterkloof, Smiths Kraal, and Weltevrede faults in the south of Rawsonville (Fig. 2-7), the observed scratches, with coating/filling materials of quartz and iron oxide, imply that these faults have experienced a strongly disturbed period but then a low magnitude of displacement since post Karoo tectogenesis. In addition clean scratches, identified at depths of 110 m and 65 m in the borehole core samples from BH-1 and BH-2 nearby Waterkloof fault zone – where the fault core material consists of recemented cataclasites and slightly metamorphosed sandstones, also show the recent movement or stress concentration.

**Fig. 2-7** Picture showing Brandvlei – Eikenhofdam megafault zone (left) at Steynskloof. Scratches developed in the cataclastite cleavages having a WS-NE trend with a plunge of 43°, indicating a recent left-lateral strike-slip movement of the fault. Filling materials are partially cemented iron oxides (right). Note: the vehicle is facing approximately northeast**.**

## 2.3 Regional hydrogeological setting

### *2.3.1 Delineation of the TMG Aquifers*

In general the TMG is strongly compartmentalized by basement rocks, and by fault zones created in the Palaeozoic and reactivated during the Mesozoic tectonizations. Two major regional faults – the Worcester fault and Kango-Baviaanskloof fault – influence the TMG distribution to a very large extent. Reported throws of the two faults can reach 4000~6000 m, thus controlling the extension of the TMG at great depths. Isobaths of the base of the TMG (Fig. 2-8), derived from eight regional geological cross-sections and some 40 smaller geological cross-sections over the TMG area, shows that the TMG extends to a depth of 4000~6000 m in the central and northern areas. Unconformities are evident in the northwest and western areas where most of the TMG base is exposed along the contacts with basement rocks, especially at the eastern border of the Cape Flats. The thickness of the TMG Aquifer largely ranges from 500 m to 4000 m (Fig. 2-9). Both Fig. 2-8 and Fig. 2-9 indicate that the TMG, covered by Mesozoic sedimentary rocks, may extend a considerable distance beneath the Indian Ocean. The depth and thickness of the TMG suggest that most the Aquifer in the study area is currently inaccessible using current exploitation techniques. Eleven thermal springs occur in the Cape Fold Belt (Fig. 2-3) from deep TMG circulation water, temperatures ranging from 23-64°C (Meyer, 2002). Assuming that the natural thermal gradient is 2°C per 100 m and the average surface temperature 15°C, the circulation depth of these thermal springs is in the range of 500 m to 2500 m. In terms of a natural groundwater circulation system, this might suggest that the majority of the TMG rocks extending below the limits of those thermal water circulation depths cannot be regarded as aquifers.

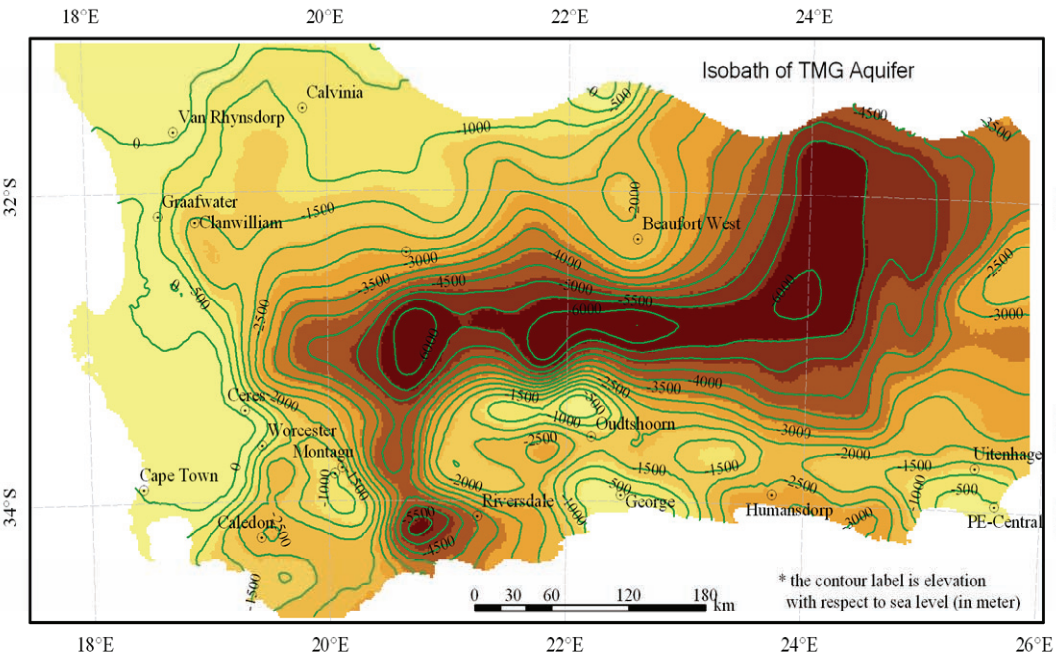


**Fig. 2-8** Map of isobaths showing the variation of the TMG base (buried depth) based on the study of cross sections through the whole TMG area

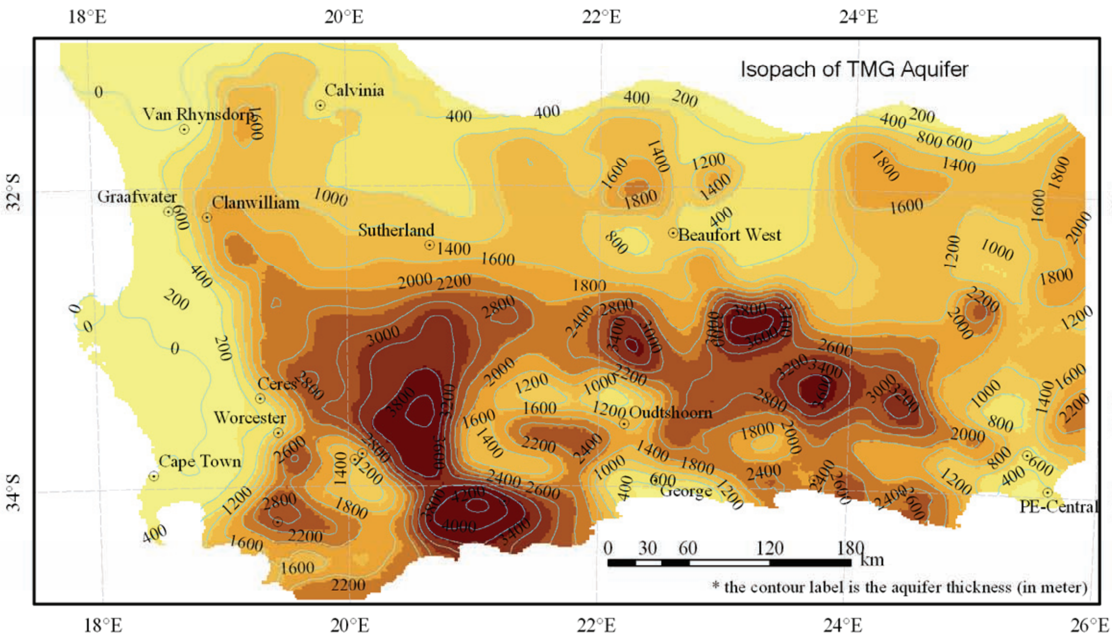


**Fig. 2-9** Map of isopachs showing the variation in thickness of the TMG aquifer based on the study of cross sections throughout the whole TMG area

### *2.3.2 Hydrogeological units*

The TMG aquifer system in the Cape Fold Belt is, in general, conceptualized into three aquifer units: the Peninsula Aquifer (Peninsula Formation), Nardouw Aquifer (Nardouw Group), and the Cedarberg Aquitard (Cedarberg Formation) separating the two main aquifers (Kotze, 2002). The Piekenierskloof Aquifer and the overlaying Graafwater Aquitard are restricted to the western branch of the Cape Fold Belt. This aquifer/aquitard demarcation is merely based on aquifer lithologies, although each of the units has unique hydrogeological characteristics in terms of aquifer porosities, fracture configurations, proximity to recharge areas, and so on. A lithological unit is not necessarily a hydrostratigraphic unit because the latter is normally defined as a formation, a part of formation or a group of formations in which there are similar hydrologic properties allowing for a grouping into aquifers and associated confined layers (Domenico and Schwartz, 1990). In fractured rocks, a hydrostratigraphic unit may consist of one or more lithological units with specific structural orientations and fracture networks that constitute a distinct groundwater circulation system for recharge, throughflow and discharge.

Regionally, the TMG aquifer system has been previously divided into five sections, namely the Western Section (the CAGE area: Hartnady and Hay, 2000), Central Section (Agter Witzenberg – Ceres – Hex – Koo Valley and Villiersdorp: Weaver et al., 1999), Klein Karoo Section: Kotze, 2002, eastern TMG Section (Plettenberg Bay to Port Elizabeth: Murray, 1996), and Coastal Belt (from Kleinmond to Mossel Bay: Fortuin, 2004).

By considering the type of openings (primary or secondary), lithostratigraphy, physiography, and climate, Vegter (2001) divided South Africa into 64 groundwater regions, of which 23 are within the TMG deposit area and 16 in its outcrop area. In Vegter's groundwater region demarcation and associated delineation, the TMG is not significantly different hydrogeologically from the adjacent Bokkeveld and Witteberg Groups.

The hydrogeological conditions of the TMG are more complex than the above delineations. The aquifer system within the Cape Fold Belt has complicated stratigraphic assemblages from Pre-Cambrian to Jurassic times, which experienced the tectonic events and low-grade metamorphism from the Permian to the Cretaceous, resulting in various water-bearing fold/fault systems. For this reason, it is necessary to demarcate the aquifer system into distinguishable hydrogeological units. This demarcation requires not only a detailed study on the aquifer media consist of basic stratigraphic units and structural fabrics, but also a careful identification of the boundaries of each proposed hydrogeological unit.

The hydrogeological boundary of the hydrogeological unit is firmly controlled by the features of lithology, geomorphology and faulting, which could form a regional groundwater barrier, or a recharge or discharge boundary. In the TMG area, the boundaries are summarized as follows:

1) Contacts between the TMG and the Pre-Cape basement rocks such as the Malmesbury, Kango, Gamtoos, and Kaaimans Groups; these contacts generally form the hydrogeological boundaries at the bottom of the TMG
2) Contacts between the TMG/Bokkeveld, and TMG/Witteberg forming the boundaries at the top of the TMG, whereby the TMG is mostly confined by the argillaceous rock formations
3) Regional faults such as the Worcester fault and Kango-Baviaanskloof fault
4) Basements coinciding with faults
5) Main rivers such as the Breede, and Olifants-Doring
6) Primary catchments
7) Discharge boundaries along the coastlines
8) Extent boundary in the north where the TMG dies out

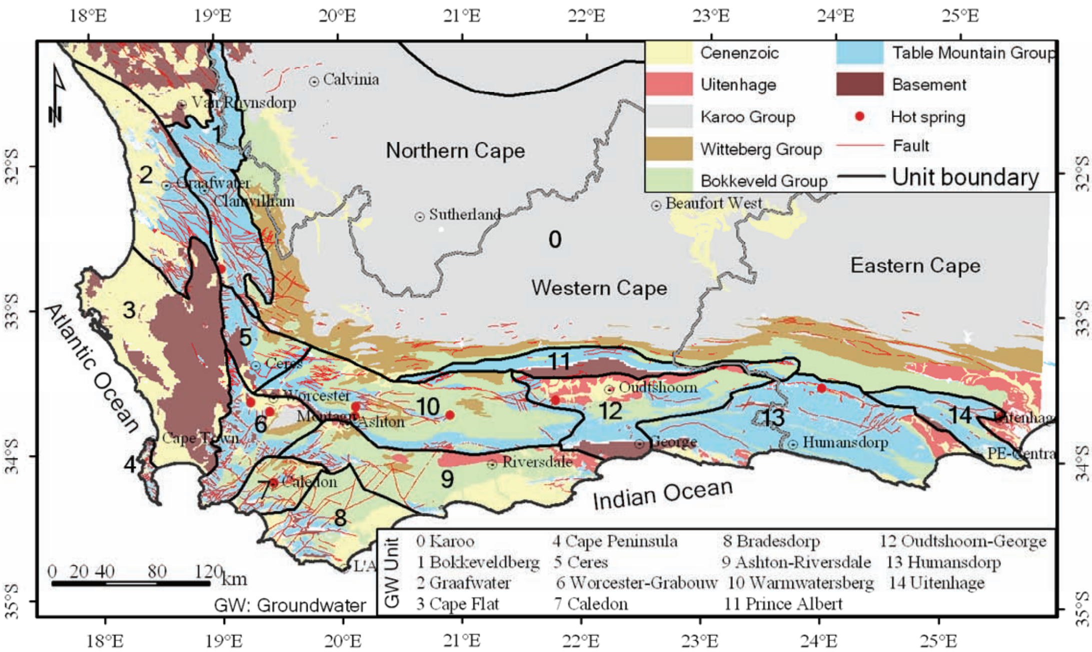

**Fig. 2-10** The TMG area divided into fifteen hydrogeological units

According to the elements of a hydrodynamic system and the boundary conditions of groundwater storage and flow as mentioned above, the TMG aquifer system can be divided into 15 hydrogeological units (Fig. 2-10). Although the Cedarberg shales act as an aquitard at an aquifer scale, they should not be regarded as regional hydrogeological boundaries, as these shales are susceptive to mechanical displacement into regional discontinuities. The Graafwater Formation is restricted the western branch of the TMG and is regarded only as a local aquitard and not important in the regional demarcation of hydrogeological units, which lithologically considers the TMG formations as a whole. Hydrogeological units classified at a scale of primary groundwater regions may not coincide with regional groundwater flow. These hydrogeological units are generally expected to provide a first-order focus for more detailed study at a regional scale. In this regard, there is no major difference in the demarcation used in this study from that of Xu et al. (2007) who divide the TMG into 19 units.

When the geological features and potential recharge areas and flow regimes are taken into more detailed account, the subdivision of each hydrogeological unit becomes necessary. The hydrogeological unit 6 (Worcester–Grabouw), for instance, can be subdivided into four subunits. Fig. 2-11 shows that Worcester fault and basement rocks in the north, Kleinmond-Robertson fault zone in the east, the TMG/basement contact in the west, and the coastline in the south constitute the boundaries of unit 6, whilst three other faults, including the Brandvlei-Eikenhofdam fault in the middle, form the secondary boundaries of the four subunits. In the process of subdivision, the Goudini and the Brandvlei thermal springs are separated into different subunits, for each thermal spring represents an independent deep-water circulation system. In terms of groundwater recharge, the hydrogeological subunit 6-4 (Fig. 2-11) receives the highest annual precipitation and subunit 6-2 the lowest among the four subunits.

For more detailed demarcation of hydrogeological subunits, there is still a lot of work that needs to be done, especially regarding the TMG geological structures and the identification of the flow characteristics of faults which can either be groundwater flow barriers or conduits. It is clear, from the subdivision of hydrogeological unit 6, that both faults and lithological contacts play a key role in controlling secondary boundaries. The result of such subdivision shown in Fig. 2-10 is still some way from a detailed study of a specific aquifer, but the basic approach of subdivision can be applied to the other hydrogeological units, providing a qualitative insight into scaled-down regional groundwater regimes through the studies of hydrogeological conditions.

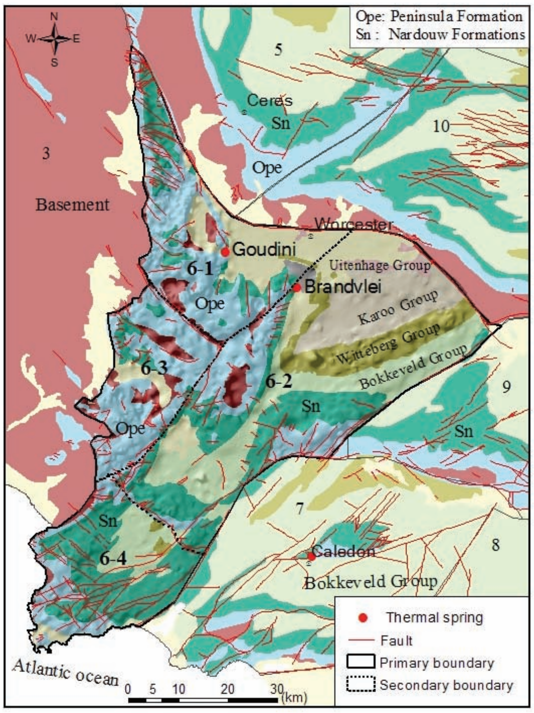


**Fig. 2-11** Subdivision of hydrogeological unit 6 into four sub-units based on structure, deep flow system, and recharge area.

## *2.4 Types of aquifers*

The TMG aquifers can be regarded as the fortuitous combination of lithologic, tectonic and climatic features. Currently, the majority of the TMG aquifer characterization is on the basis of aquifer formation analysis. Based on the analysis of the basic elements of aquifer system, Xu et al. (2007) summarize the TMG aquifers into four categories:

1) Horizontal strata aquifer system
2) Fold strata aquifer system
3) Fracture zone aquifer system
4) Composite aquifer system (Fig. 2-12)

The horizontal strata aquifers are limited to the Cape Peninsula and the far northwest of the TMG area where the gentle-dipping TMG terrain controls both the extension of the aquifer and the topographical features that influence the aquifer’s recharge (Fig. 2-13). Fold strata aquifer systems include aquifers consisting of synclines, anticlines and monoclines. This type of aquifer is assumed to be homogeneous and the folding is used to account for the occurrence of some thermal springs in the TMG where the aquifer strata are bounded by relatively low permeability layers (Fig. 2-14a). However, groundwater occurrence is not solely controlled by stratigraphy and its spatial distribution. There is almost no primary porosity in the TMG, sandstone as will be discussed in next chapter, and groundwater occurrence is dominated by various-scale fractures including faults, joints, and bedding planes. Because the characteristics of such structures are very heterogeneous, it is necessary to look beyond stratigraphy and folding, and carry out a detailed study of the fracture systems. As yet there are no conceptual models to describe the fracture block sandstone aquifers as illustrated in Fig. 2-14b.

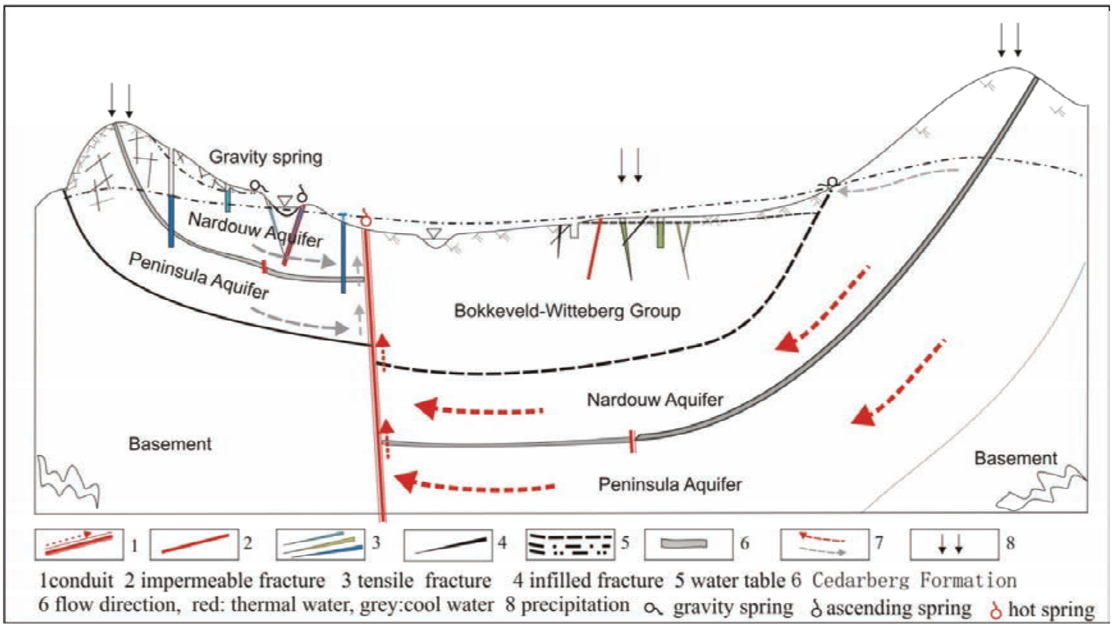


**Fig. 2-12** A model of the TMG composite fractured rock aquifer system (after Wu, 2005**)**

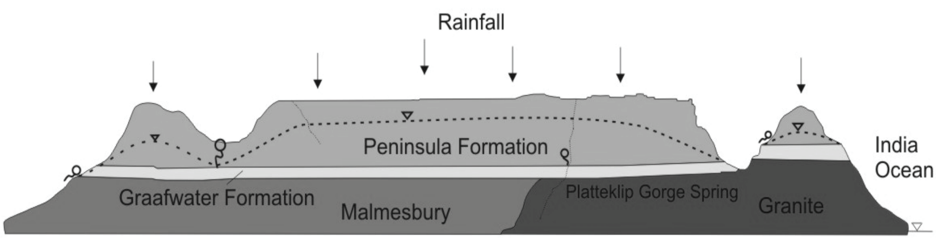


**Fig. 2-13** An example of a horizontal strata aquifer in Table Mountain, Cape Town (after Xu et al., 2007).

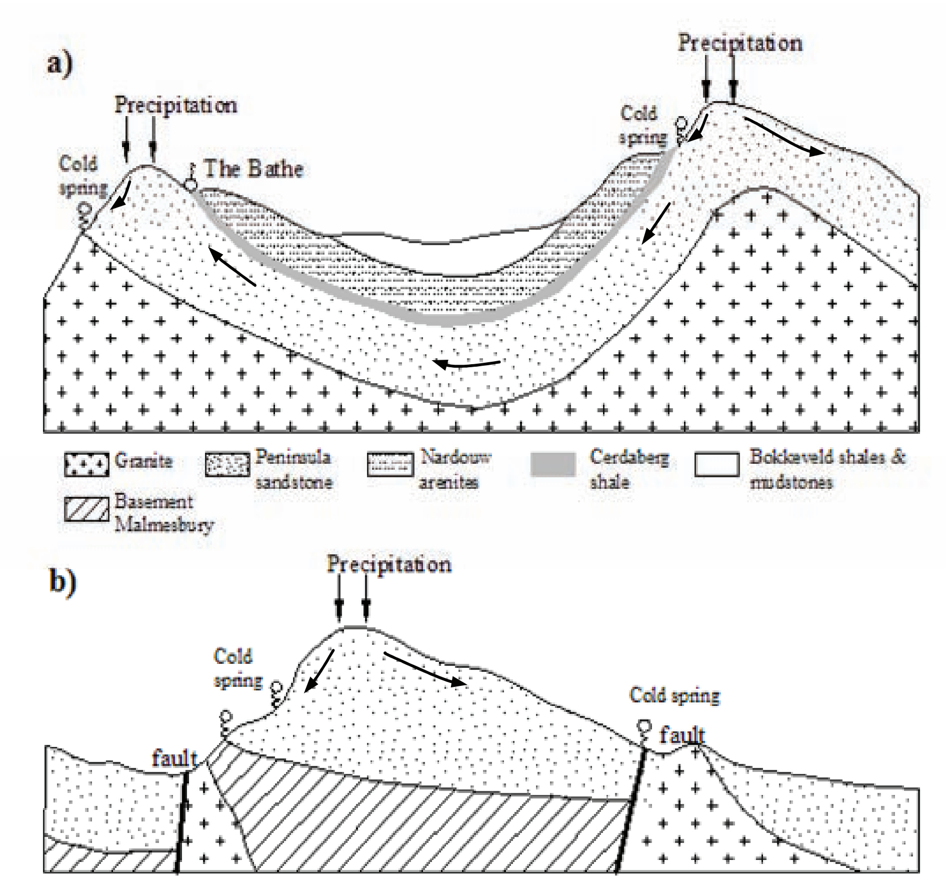


**Fig. 2-14** Lithology and structural controlled aquifers, a) Syncline, the Baths hot spring model, b) Fault and basement bounded outcrop model.

## 2.5 Current groundwater use

The TMG has become the focus of much investigation as a significant potential source of water supply for the southern regions of South Africa because of the large amounts of high quality water stored, accessible via high-yielding boreholes. The TMG area straddles large parts of the Water Management Areas (WMAs) of the Department of Water Affairs and Forestry (DWAF), namely the Olifants-Doring River in the west, Berg and Breede in the south, and the Gouritz and the Fish/Gamtoos River in the east (DWAF, 2002). The current annual abstraction from the aquifers of approximately $5.56\times10^7$ $m^3$ (Table 2-2), is only about 5.1% of the overall potential yield(about $9.0\times10^8$ $m^3$) and 4.3% of the total groundwater discharge ($1.29\times10^9$ $m^3$) estimated from the TMG aquifers (Jia, 2007). As surface water development has reached its peak in most areas, the development of TMG groundwater is critical for meeting future needs and ensuring economic development. The figure of groundwater use presented here is probably under-estimated due to data on much private abstraction not being readily available. However, considering current exploitation techniques and the cost of extracting groundwater from a maximum aquifer depth of 350 m below surface, the usable groundwater storage in the TMG rocks is estimated as $2.1\times10^9$ $m^3$ (Jia, 2007), which implies that there is still a big opportunity for groundwater development in the TMG Aquifer.

There are more than 30 major users of groundwater in the study area, among them numerous towns that are completely dependent on the TMG aquifer as their sole source of water supply, such as Steytlerville, Jeffreys Bay, St Francis Bay and Humansdorp in the east, and Bredasdorp, Napier, Struisbaai and Botrivier in the south. Many other towns are partially dependent on the TMG groundwater during the dry season. From Table 2-2 it can be determined that 67.9% of groundwater abstracted from the fractured rock aquifers in the TMG is used for farmland irrigation, 20.0% is thermal water for holiday resorts, and only 12.1% is used for municipalities. Other minor users are the smaller scale farmers, homesteads and stock farms. Groundwater extraction covers a wide area but is localized and focused on points of consumption.

**Table 2-2** Groundwater abstraction from the TMG aquifers
(After Meyer, 1998, 1999, 2001, 2002)

| **Area/Town** | **Water abstraction ($\times10^6$ $m^3$)** | | **Use** | **Year** |
|---|---|---|---|---|
| | **Amount** | **Percentage** | | |
| Albertinia | 0.1 | 0.18% | Town | 1999 |
| Brandvlei-Sandrift | 11.0 | 19.66% | Irrigation | 2001 |
| Bredasdorp | 0.5 | 0.89% | Town | 2001 |
| Calitzdorp | 0.1 | 0.18% | Town | 2001 |
| Ceres basin | 8.0 | 14.30% | Irrigation | 2001 |
| Dysselsdorp | 2.3 | 4.11% | Town | 1999 |
| Humansdorp | 1.1 | 1.97% | Town | 1998 |
| Jeffreys Bay | 1.8 | 3.22% | Town | 1998 |
| St Francis Bay | 0.55 | 0.98% | Town | 1998 |
| Struisbaai | 0.3 | 0.54% | Town | 2001 |
| 11 hot springs | 11.2 | 20.02% | Recreation | 1999 |
| Uitenhage | 5.7 | 10.19% | Irrigation | 1998 |
| Vanwyksdorp | 2.3 | 4.11% | Irrigation | 1999 |
| Witzenberg valley | 11.0 | 19.66% | Irrigation | 2001 |
| **Subtotal** | **55.59** | 100% | | |

## 2.6 Wellfields and study areas in the TMG

Prior to the late 1980s, large-scale abstraction in the TMG aquifers was restricted to the Hex, Ceres, Breede, and Agter Witzenberg Valleys, with some small-scale municipal use by the towns along the coastal and inland outcrop areas. Studies leading to development of important TMG wellfields were initiated for the Klein Karoo Rural Water Supply Scheme in 1987, Boschkloof near Citrusdal in 1997/98, Hermanus in 2001/02, and Koo Valley in 2002/03. The TMG Pilot Project for Feasibility Study for the City of Cape Town started in 2002, which is still on-going.

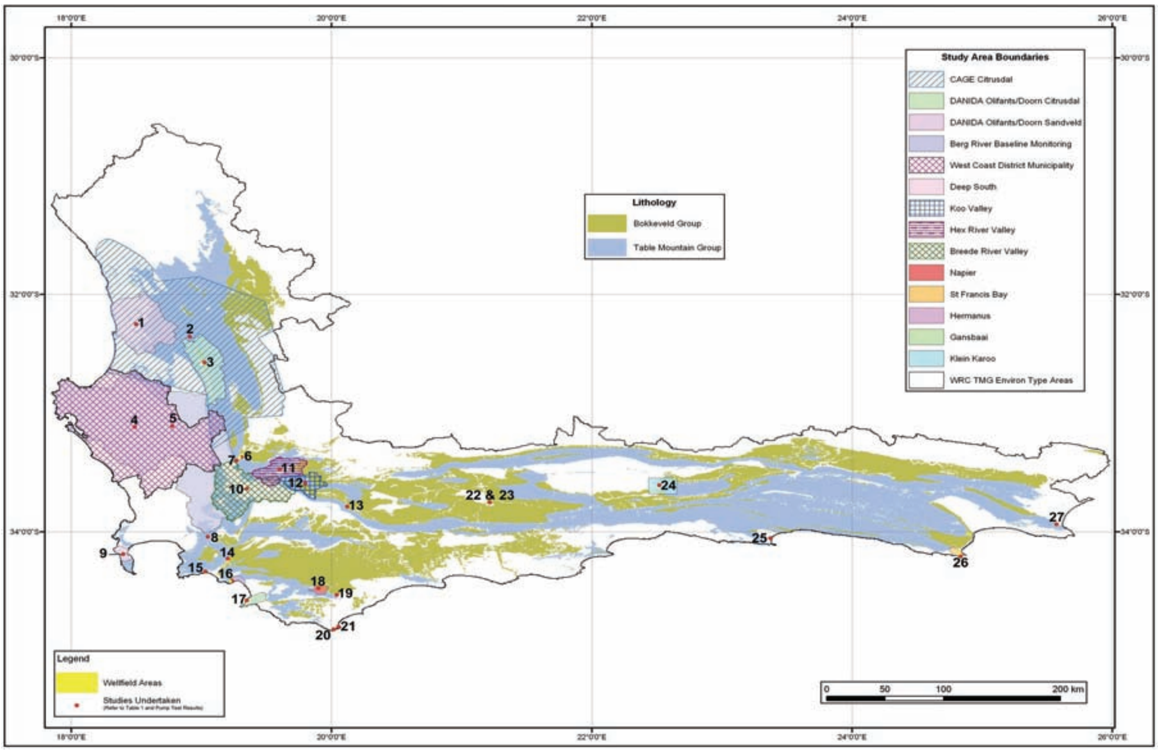


**Fig. 2-15 Wellfields developed in the TMG**

Previous studies on the groundwater resource in the TMG concentrated on the development of wellfields for water supply in the areas of Western and Eastern Cape provinces (Fig. 2-15). The Klein Karoo Rural Water Supply Scheme, commissioned in 1987, with a planned yield of 4.7 million $m^3$/a from two wellfield areas, an Eastern Wellfield near Dysselsdorp and a Western Wellfield near Calitzdorp. Borehole monitoring has shown that the actual capacity of the wellfields is closer to 1.3 million $m^3$/a. The earlier overestimation seems to be a result of poor understanding of the hydrogeological setting and incorrect analysis of pumping test data from which the hydraulic properties of the aquifers were overestimated (Kotze, 2002a & 2002b; Jolly, 2002). The scheme has also had problems of iron bacteria formation in the boreholes developed in the Nardouw formations, which has lead to clogging of screens and the need for continual rehabilitation of boreholes. As a result, the yield of Calitzdorp Wellfield has seriously declined.

Investigations with the aim of devloping a wellfield at Boschkloof near Citrusdal initiated in 1997~1998, culminated in five production boreholes, one of which had a very high blow yield of more than 100 l/s. These boreholes were developed in the Peninsula Formation near the intersection of two faults, and were expected to provide a large quantity of water to meet the needs of the municipality of Citrusdal. However, results from the evaluation of the pumping test data suggest that the long term sustainable yield of the wellfield may only be 25 l/s, and that there exists a mutual interference among the boreholes, and that abstraction might influence a nearby river some 80 m from the production boreholes. These boreholes have only been used intermittently by the municipality – usually when droughts cause a reduction in surface water supplies.

A more recent TMG wellfield development is a water supply scheme in the Koo Valley, to the north of Robertson and west of Montague. This water scheme was initiated in response to a period of drought in the area and a subsequent shortage of irrigation water for the farmlands in the Koo Valley. In order to have a sound estimate of sustainable yield in the wellfield, twenty-three exploration boreholes were drilled in 2002/2003. A sustainable yield of 60 l/s was estimated from a small number of pumping tests. However, subsequent groundwater abstraction and monitoring results show that this amount of water supply has also been overestimated, probably due to the overestimation of both hydraulic properties and recharge rates. These boreholes mostly only tap the Nardouw formations.

The biggest potential wellfield development project from the TMG Aquifer is taking place in the mountains to the east of Cape Town. This project is intended to develop a pilot wellfield with a yearly water supply of around 3.5 million $m^3$ for Cape Town Municipality. Yields of 100 l/s (3.2 $Mm^3/a$) have been targetted for some production boreholes. The aim of the investigation is to ascertain if the TMG aquifers can provide a significant bulk supply to help alleviate future shortages for the Cape Town Municipality. In addition the project aims to assess the potential ecological impact of large-scale groundwater abstraction from high yielding TMG wellfields. It was originally proposed that only confined areas of the TMG Aquifer be exploited, i.e. where the Peninsula Formation is confined by the overlying Pakhuis and Cedarburg formations. However, this has apparently proved to be more difficult than originally thought and may not be feasible.

## 2.7 Springs

Numerous springs, with a wide range of discharge rates occur in TMG area. These springs are classified by Meyer (2002) into three commonly occurring types:

Type 1: Shallow circulating springs

Shallow circulating springs are intermittent springs issuing from a network of joints, small fractures, contact zones of weathered mantle and bedrocks. They are seasonally controlled and cease to exist with the onset of dry weather conditions.

Type 2: Lithology controlled springs

There are three sub-types in this type: springs issuing from contacts with interbeds (Cedarberg Formation), springs on the TMG/Bokkeveld Group contact and springs issuing at unconformities. The yields of lithology-controlled springs are highly variable. The water quality from these springs is excellent.

Type 3: Fault controlled springs

There are eleven well-known hot springs occur in TMG area, which indicates that deep groundwater flow systems exist in the TMG terrestrial area. Among them the hottest spring is Brandvlei with an inferred circulation depth of 1800~2000 m. These springs are distributed along the Cape Fold Belt (Fig. 2-3) and have large constant flow rates. Five of the eleven hot springs are located in the syntaxis zone, which may indicate that deep fracturing is more common in this zone.

# 3. Aquifer Media and Characteristics

## 3.1 Introduction

On a regional scale, the TMG Aquifer acts as a homogeneous and isotropic entity, but in most cases can be regarded as heterogeneous and anisotropic at a local scale. Thin section studies from both the Peninsula and Nardouw rocks have shown that even in pure quartzitic sandstones from unfolded beds of the TMG, intergranular pore spaces are completely filled by secondary quartz overgrowths, making these rocks virtually impermeable in an un-altered state (Hälbich and Cornell, 1983; De Beer, 2002). It is only where the rocks are fractured by folding, and/or faulting that the rocks develop a secondary porosity and become fractured aquifer media.

The analysis of the TMG aquifer types in Chapter 2 provided a regional view of the aquifer fabrics and possible groundwater flow paths in which the aquifer media are generally homogeneous and isotropic. However, unlike porous media such as the Quaternary deposits on the coast and river valleys, the TMG rocks are extremely anisotropic.

Current methods used for analyzing groundwater flow and storage in fractured rocks are based on the assumption that groundwater flows through a geological continuum (Wang et al., 2002). These methods are generally applicable to porous media, but have limited applicability when groundwater is governed by highly anisotropic fractures or fracture network. Field observations show that there is almost no continuous groundwater level from one site to another. This suggests that water levels and associated maps are not capable of characterizing meso- to large-scale flows. Even in a single wellfield at the scale of hundred meters, the groundwater in boreholes does not completely communicate with each other, such as the Malkoppan site at Lambert's bay and the Gevonden site at Rawsonville where some of the nearby monitoring boreholes do not respond to the water level drop at the pumping holes. In fact, groundwater occurring in fractured rocks like the TMG sandstones is mainly flowing through the fractures, controlled by the fracture geometry and associated hydraulic properties. In the absence of fracture information, it is extremely difficult to fully understand the aquifer response to hydraulic tests and to determine the related aquifer properties. It is hence of crucial hydrogeological significance to study the properties of the fractured media.

Currently, among the hydrogeological problems faced in the TMG fractured rock aquifers, none is as challenging as the establishment of a conceptual model through the characterization of aquifer media. The study of such a problem is difficult in the TMG because of its regional and local complexity, though many efforts have been contributed to the understanding of the characteristics and patterns of the fractures that exert such a great impact on aquifer properties (Chevallier, 1999; Woodford and Chevallier, 2002; Hartnady and Hay, 2002a).

Based on previous studies and current research, this chapter describes the characterization of the TMG fractured media on regional and local scales done using remote sensing interpretation, core sample study, and analysis of fracture field measurement data. The aim is to develop an initial conceptual model that can be helpful in gaining a better understanding of the TMG fractured rocks, and can be applied to, and in turn be refined by, the quantification of aquifer properties. In addition, the study of aquifer media makes use of the delineation of aquifer types carried out in Section 2.4 of Chapter 2.

## 3.2 Faults

It is well known that faults play a key role in the occurrence of groundwater in the TMG sandstones. So far, almost all the major wellfields for water supply schemes in the TMG area have been developed in the vicinity of fault zones, such as Vermaaks River (Kotze, 2002), Boschkloof (Hartnady & Hay, 2002b), St Francis Bay (Rosewarne, 1993a), Ceres (Rosewarne, 1993b) and so on. Where the faults intersect the regionally oriented structure they may become a preferred locality for the production boreholes. This suggests that the secondary splays of regional faults could be preferred zones for locating groundwater.

However, through field investigation in the Vermaaks River fault, Hälbich and Greef (1995) found that there were hard breccias and cataclasites widely developed in both the 9 km long fault and its secondary splays. In Eastern Cape the Coega Fault cutting southeastward through the Uitenhage artesian basin separates the basin into two different groundwater systems (Maclear, 2001). In fact, most of the fault zones developed in the TMG sandstones and siltstones are found to be lithified and act as aquicludes (Newton et al., 2006).

Of particular interest in borehole siting for groundwater development is the architecture of the faults which could have a big effect on the mode of groundwater occurrence. The elements of a fault include the fault core and the fracture zones at both walls (Ciane et al., 1996). The current state of a fault is the result of geological processes; especially neotectonic activities that might have an additional impact on the fault fabric. However detailed information on neotectonics is yet not available except for some evidences to show that the area has undergone a relatively low magnitude of fault reactivation, as indicated by earthquake events in the western and southern branches of the Cape Fold Belt. Fig. 3-1 presents a conceptual model with four types of fault architecture that can occur in the TMG area regardless of the mode of faulting. The majority of the TMG faults fall in category **d)** where the fault cores are largely recemented and often serve as groundwater barriers (Fig. 3-1), whilst the fracture zones act as the conduit. While this helps explain why faults can be good local targets for groundwater, more detailed work needs to be done to gain a better understanding groundwater occurrence at the megafaults such as the Worcester and Cango Faults. The megafaults apparently influence the occurrence of thermal springs in the Cape Fold Belt.

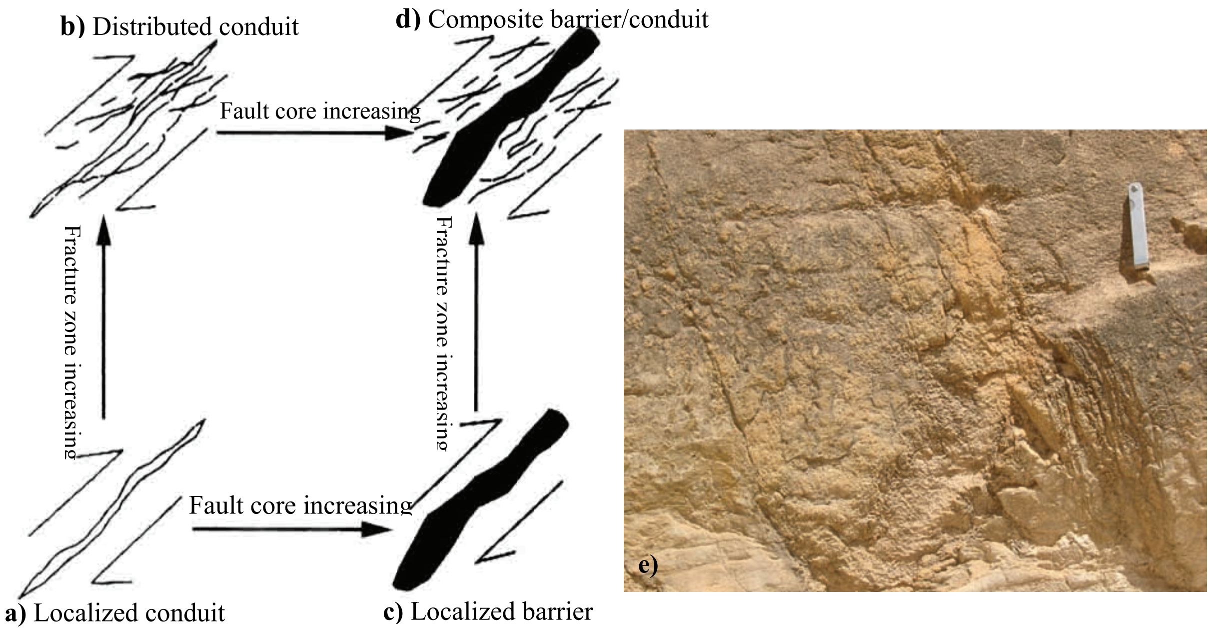


**Fig. 3-1** Models of fault showing the evolution of fault architecture (After Ciane et al., 1996).
[e) Breccias constituting fault core material is very common in the TMG area]

## *3.3 Fractures*

Fractures include joints and faults, as well as various discontinuities over different scales and lithologies due to crustal tectonic driving forces (Pollard and Aydin, 1988). They usually provide an ideal conduit for groundwater flow throughout the upper crust (Sibson and Scott, 1998). The following classification of fractures is based on the mode of rock deformation or displacement according to a broad mechanical classification (Pollard and Aydin, 1988; National Research Council, 1996):

i) Dilatant fractures

ii) Compaction fractures

iii) Shear fractures/faults

To designate the TMG fractures into the above classes, one must not only have data on a single fracture as mentioned above, but also analyses of fracture networks such as termination, hierarchy, and connectivity. In this study, it was extremely difficult to collect these data to identify the modes of such structures on the surface or in a borehole, although aerial and satellite imageries have been used to interpret the fractures and fracture networks. The geological structures of the TMG in the Cape Fold Belt have been developed and modified by multi-stages of tectonics. The development of these fractures is summarized in Fig. 3.2, which may help to explain the complexity of the fracture system in the study area. The structures have been developed by multistage tectonic events and modified by later morphogenetic

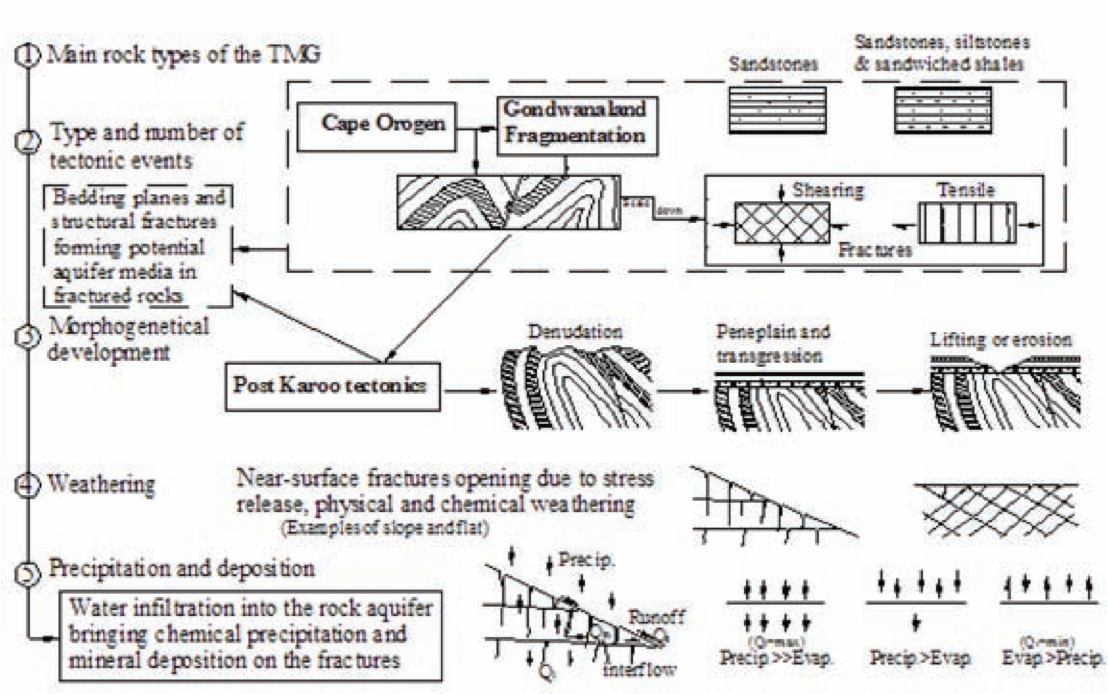


**Fig. 3-2** Factors impacting on the development of fracture systems in the TMG sandstone formations (modified from Ewer, 1985**)**

processes resulting in various types of folds and faults, and specific fracture systems in the TMG areas. The infiltration of meteoric water and precipitation of secondary minerals on the fracture walls tends to complicate the properties of the fractures. The most relevant fracture property for groundwater studies is the percentage of open fractures where groundwater could be stored and the interconnectivity of the open fractures where flow could take place.

The classification of fractures as open or closed may have more hydrogeological meaning to the study of a fractured rock aquifer if it is realized that open fractures are a precondition for groundwater flow in the aquifers.

## *3.4 Core sample case study − Riefontein deep borehole*

There are many approaches that can be used to study open fractures and their interconnectivity: borehole image scanning, borehole radar, injection and tracer tests, and so forth. Core logging is often unable to directly sort out the features of open fractures due to the deformation of many core samples by stress release and disturbance during drilling. But the surface characteristics and the mineral fillings and coatings of the core fractures may help to distinguish some susceptible zones of open fractures. Fracture scanning from core samples can yield useful information for the characterization of fracture networks that have a direct effect on groundwater flow. For this reason, a case study was done using data from the Rietfontein in the Sandveld area, where a core borehole was drilled to a depth of 800 m. In this study, the characteristics of the fracturing in the rock aquifer around a deep borehole in the TMG are examined and analyzed, using surface fracture measurements and core sample data. Information on fractures and fracture coatings was collected and analyzed by scanning borehole cores. The main objective is to provide a qualitative insight into the fracture characteristics and associated hydrogeological conditions by assessing fracture spatial correlation and the precipitation of secondary minerals on the fracture walls.

### 3.4.1 Introduction to site hydrogeology

The site is located at the farm Rietfontein, 10 km west of Graafwater, Western Cape (Fig. 3-3). Borehole G40145 was drilled between 1998 and 2001 to a depth of 800 m and screened to a depth of 168 m. It is the deepest of about 25,000 known boreholes in the TMG area. The borehole passes through the Piekenierskloof Formation – the basal formation of the TMG – from 0 to 754 m depth, and Precambrian metamorphic basement rocks for the remaining depth. During the drilling process, core samples were carefully collected for further analysis. Standard down-hole geophysical tests such as vertical electrical resistivity (VER), gamma (NN log), and rock density logs were completed to 380 m below the surface, in an attempt to identify the lithologies and fracture zones and to establish a conceptual framework for the hydrogeology in the vicinity of the borehole (Titus et al., 2002).

The Piekenierskloof Formation in the study area is 800 m thick and represents alluvial-fan and braided-river complexes deposited on an uneven bedrock topography created during the folding and lifting of Neoproterozoic Pan-African mountain belts along the west coast prior to $500\times10^6$ years ago. The lithology is characterized by mottled sublitharenites and quartzarenites, with a 100 m thick conglomerate at the base, followed by sandstones and siltstones. It is also characterized by minor sandwiched iron-rich shales which affect the groundwater quality in terms of color and smell. The basement rocks are slightly sulphur-bearing metamorphic rocks.

During the drilling of borehole G40145 (Fig. 3-3b and c), an initial artesian flow of 0.3 l/s was identified from three intervals (about 170 m, 210 m and 380 m below surface). Water samples have been collected monthly for both in-situ and laboratory analyses since April 1999. The average water temperature is 20.8ºC. Electrical conductivity (EC) has varied between 1350 and 2560 μS/cm, pH between 5.7 and 6.8, and the artesian flow yield has dropped drastically from 0.33 l/s to 0.01 l/s in only two years. The groundwater is sodium-chloride dominant with an average of 82% Na-Cl content (283.80 mg/l as Na, 534.34 mg/l as Cl) and with an absence of carbonate (Table 3-1). The major chemical constituents have changed over time with iron and sulphate showing the most significant changes. Similar to most of TMG groundwater (Smart and Tredoux, 2002), this borehole water is ferruginous with a dissolved iron content of 0.1~1.2 mg/l. The presence of iron gives an undesirable reddish color to the borehole surroundings due to the precipitation of $Fe(OH)_3$ from the borehole overflows (Fig. 3-3c).

**Table 3-1** Principal chemical constituents of groundwater from G40145

| Sampling date | Chemical content (mg/*l*) | | | | | | | |
|---|---|---|---|---|---|---|---|---|
| | $Na^+$ | $Ca^{2+}$ | $Mg^{2+}$ | $Si^{4+}$ | $K^+$ | $Cl^-$ | $SO_4^{2-}$ | $NO_3^-$ |
| 2000-8-25 | 298.98 | 29.59 | 34.75 | 5.03 | 10.84 | 556.82 | 37.59 | 0.04 |
| 2001-9-7 | 284.41 | 49.40 | 22.00 | 5.06 | 10.26 | 559.99 | 14.32 | 0.04 |
| 2003-11-17 | 268.00 | 25.30 | 29.43 | 3.84 | 7.93 | 486.21 | 6.00 | 0.11 |
| | $F^-$ | $PO_4^{3-}$ | $Fe^{2+}$ | $Mn^{2+}$ | $Zn^{2+}$ | $Cu^{2+}$ | $Cd^{2+}$ | $As^{3+}$ |
| 2000-8-25 | 0.28 | 0.03 | 1.18 | 2.00 | 0.004 | 0.002 | 0.002 | 0.05 |
| 2001-9-7 | 0.25 | | 0.88 | 1.96 | | | | |
| 2003-11-17 | 0.26 | 0.02 | 0.06 | 2.53 | 0.014 | 0.044 | 0.009 | 0.13 |

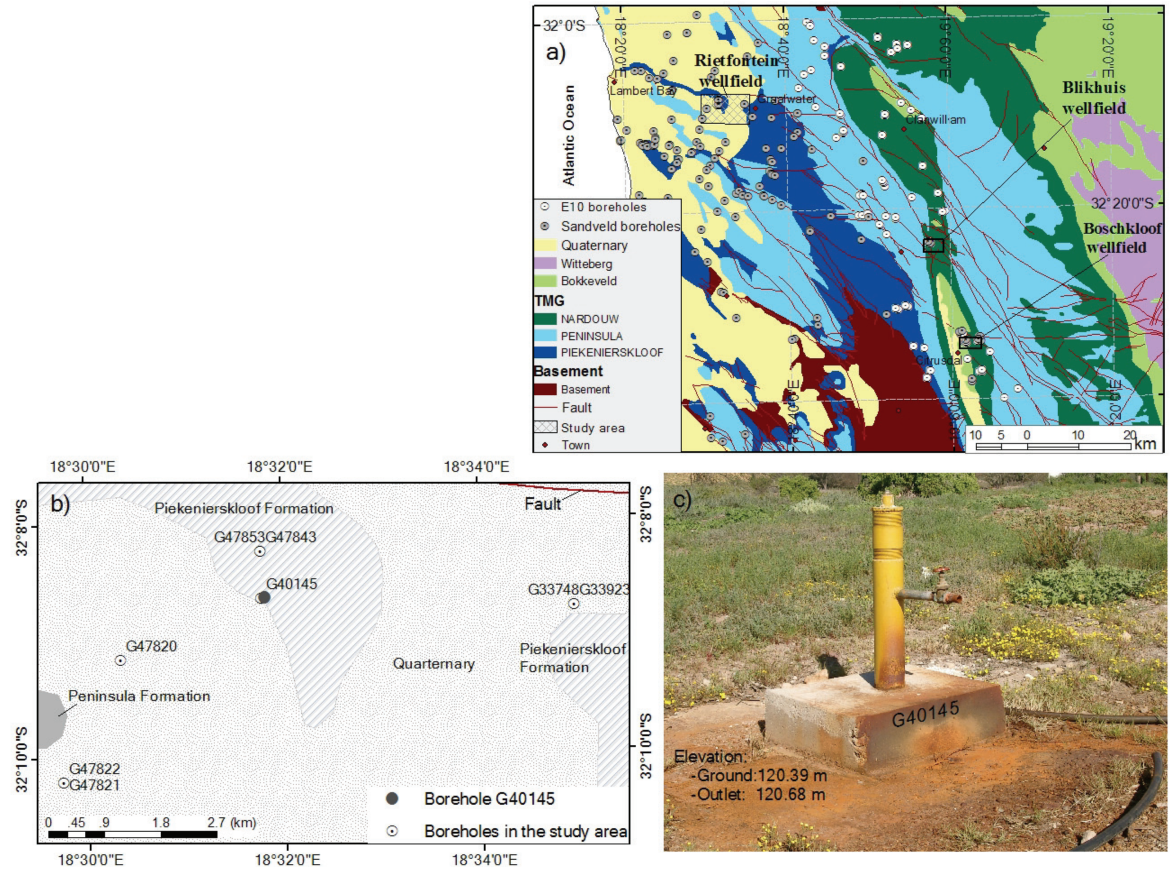


**Fig. 3-3** Maps of the study area, and Rietfontein deep hole. a) Geological settings of the western branch of TMG with faults and folds mainly extending NW-SE which terminate the W-E ones; b) Study area and the position of the Rietfontein deep hole G40145 at the core of an anticlinorium, in the west of Graafwater, Western Cape, and the surrounding holes drilled for groundwater exploration and production; and c) The diamond-drilled borehole G40145 with a diameter of 75 mm and a depth of 800 m sealed for monitoring purposes.

### 3.4.2 Fracture geometry

#### 3.4.2.1 Fractures from surface measurement

Borehole G40145 is situated at the core of an anticline extending to the northwest (see Fig. 3-3b). In order to study the effect of fractures on borehole hydrogeological conditions, it was necessary to determine the surface characteristics of the fractures in the vicinity of the deep hole. The measurement of fractures was carried out within an area of about 90×60 $m^2$ using a line scanning method which is roughly perpendicular to structural lines. The measured elements mainly comprised orientation, distance, aperture and roughness; and some of the fracture lengths were also traced. The fracture lengths traced range from 0.8 m to 20 m whilst the apertures have a wide range of 0.1 to 2 mm due to the effects of weathering. With respect to fracture orientations, Fig. 3-4 shows the spatial variation of the orientation and density of 289 measured fractures composed of bedding planes and steep structural fractures. According to the field measurements, the bedding planes trend to the NE from 50º to 90º with gently-dipping angles of 2º to 10º, while three sets of steep fractures were identified having average trends of N67E (67º east of north), S25W and S23E with the average dips of 78º, 71º and 77º, respectively.

### 3.4.2.2 Fractures from core logging

In general, down-hole geophysical data are useful for interpreting the variation of lithologies. But they can be inaccurate or even inapplicable for identifying fractures and associated properties at depth. Hence, it was necessary to re-scan and re-log the core samples to sort out the fractures developed in the lithologies of the Piekenierskloof Formation, especially when borehole image techniques were not applied during the drilling.

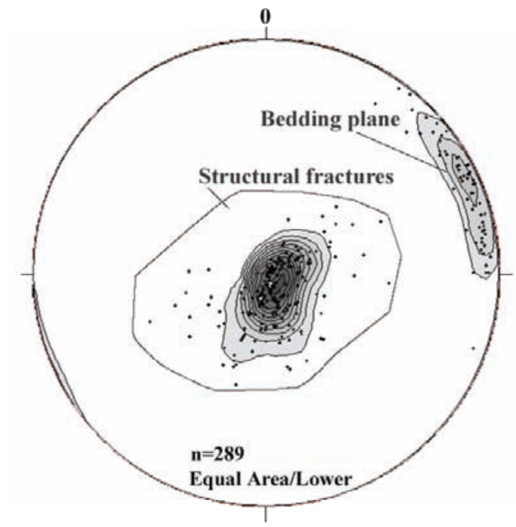


**Fig. 3-4** Spatial correlation and distribution of the fractures measured at Rietfontein, in which the solid polygons represent normals to the fractures, the density ranging from 0 to 27.85 with a contour interval of 2.7

Fig. 3-5 shows 4 typical core sections to illustrate the appearance of rocks of the Piekenierskloof Formation, the basic types of fractures, and the mineral fillings and coatings on the fracture surfaces. The fractures observed in the core are sub-horizontal bedding and steep structural fractures and are similar to the fractures present on the surface. Regardless of the dip direction, the dip angles of both bedding fractures (1°~12°) and steep structural fractures (60°~85°) from the top to the bottom of the hole are compatible with those observed on the surface.

Geometrically, the core fractures are not evenly straight but rough or undulating and have probably been deformed during drilling. For this reason, drill-induced fractures are excluded in the process of core logging. With respect to fracture shape and assemblage, 5 types of common patterns were delineated from the core sections (Fig. 3-6):

a) Bedding and steep fractures crossing each other, commonly developed in the brittle hard sandstones

b) Bedding (plane) fractures, dominant in most shale and other thin layers
c) Vertical and sub-vertical fractures intersecting bedding fractures
d) A complex of bedding and steep fractures intersecting with a few terminations
e) Intersection and termination of sub-vertical fractures

The assemblage patterns in Fig. 3-6a, c and d roughly represent the well-connected fractures developed in sandstones, while Fig. 3-6b and e indicate the poorly connected fractures in shales and some sandstones and siltstones. From the appearance of the topography and coating of the core fractures, it can be inferred that steep fractures are more likely to be open than other types. Bedding factures developed in shales and other thin layers are mostly closed except for those at sandstone/shale contact zones.

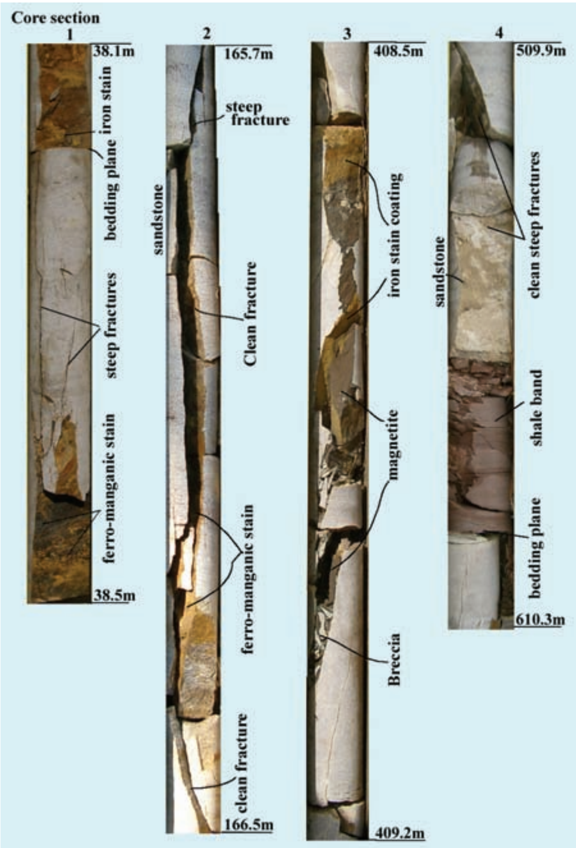


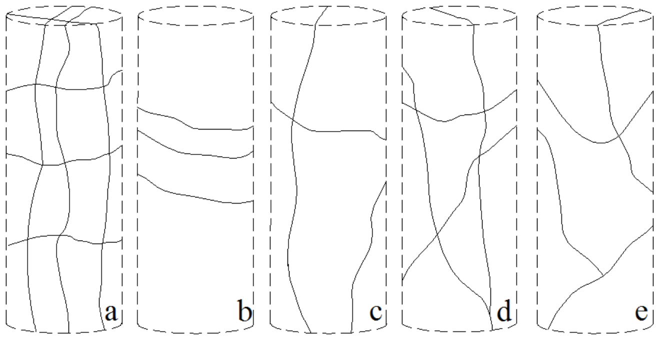


**Fig. 3-6** See figure on left. Types of fractures observed in the core from G40145 with respect to fracture shape and assemblage (please refer to the text for an explanation of a to e).

**Fig. 3-5** See figure on right side. Typical core sections from borehole G40145 at various depths ranging from the top to the bottom of the hole, showing not only lithology, but also fracture coatings. Most of the coatings on the fracture surfaces are iron and manganese stains (section 1, 2 3), while magnetite occurs as vein material. Note that the steep fracture in section 3 is partially coated and partially clean, and a clean fracture surface is shown in section 4.

#### 3.4.2.3 Fracture density at depth

Besides the above fracture patterns, fractures can also characterized by their density. The density of fracturing in fractures/cm was computed for all the fractures – bedding and structural fractures – observed between core depth tags without regard to the fracture orientation, fracture mode, or rock type. A frequency plot of 7242 fractures, observed with a logging interval of 2~6 m, following the intervals of core tags from the top cut-off at 14 m depth to the bottom at 785 m depth, is shown in Fig. 3-7. The core of TMG rocks ends at a depth of 754 m below surface. This plot, with an average density value of 0.114, shows that the density of fractures gently decreases with depth. There is a very weak spatial correlation – the correlation coefficients between fracture density and depth are 0.28, 0.33 and 0.16 with respect to linear, exponential and power distributions, respectively.

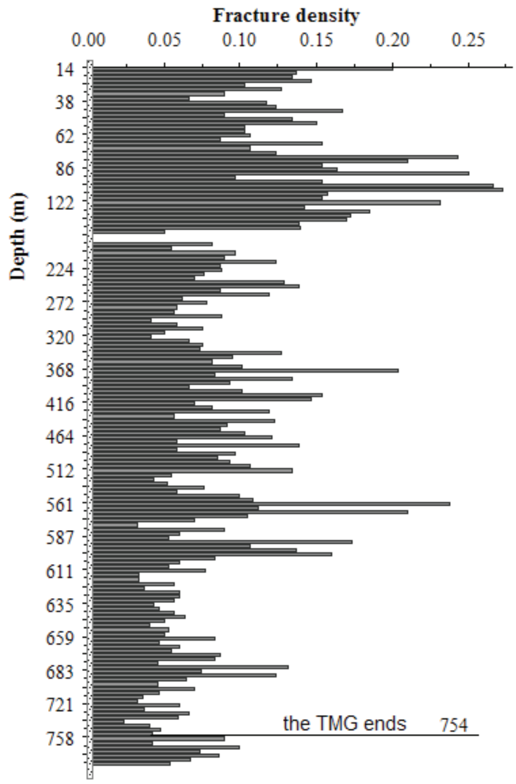


**Fig. 3-7** Fracture density (fractures/cm) plot versus depth of borehole G40145, computed at borehole depth intervals of 2~6 m except for the depths of 170~187 m due to core missing (Lin et al., 2007)

Snow (1968) points out that fracture spacing generally increases with depth, while apertures decrease in size. Although the density generally decreases with depth for the Rietfontein core, and 33% of fractures are concentrated in the top 160-m portion of this borehole, fractures are not substantially depleted with depth in the predominantly sandstone section. The general shape of the density plot is an undulating pattern where relatively highly fractured zones are located in the depth ranges of 70~125 m, 344~410 m, 560~598 m, and 668~697 m. However, these highly fractured zones and the logging intervals of higher densities are not consistent with the positions of hydraulically conductive zones which are open to groundwater flow into the borehole.

### 3.4.3 Hydraulically active fractures

As shown in Fig. 3-2, the processes of mineral filling and coating in a fracture network due to physical or chemical precipitation, and deposition due to groundwater circulation tend to change the nature of fracture walls. However these processes taking place underground are extremely complicated and difficult to detect directly. In general, coating materials may occur where the fractures are relatively open to flow, whereas fluid diffusion preferentially takes place where the water is comparatively stagnant, and chemical and physical precipitates clog the potential flow path, leaving few fractures to be hydraulically active. The relationship between fracture filling and coating, and hydraulically active fractures or flow paths is rarely studied in the TMG sandstones. Notable work in this field was done by Paces et al. (1996) who focused on the analysis of fracture coating data in a tunnel in the unsaturated zone of the Yucca Mountain, USA. A hydraulically active fracture for the purposes of this report refers to a fracture open to flow in both the past and present. Thus it represents the maximum number of fractures that could be open to groundwater flow.

The groundwater from borehole G40145 is weakly acidic, ferruginous, manganiferous and is also characterized by the absence of carbonates. The anions are mainly $Cl^-$, $SO_4^{2-}$ and $NO_3^-$ (Table 3-1). The cations such as $Fe^{2+}$, $Mn^{2+}$, $Ca^{2+}$, $Mg^{2+}$ and $Zn^{2+}$ are prone to precipitation as hydroxides through hydration during migration in this weakly acidic and oxidized environment and form the majority of the fracture fillings and coatings. This environment also provides desirable conditions for iron bacteria to establish themselves and create a reddish-brown ferric hydroxide ($Fe_2O_3 \cdot nH_2O$) precipitate.

Petrographic evidence suggests that most of the iron that now resides in oxidized authigenic phases was derived from solutes mobilized through dissolution of older iron-bearing authigenic minerals, particularly from the iron-rich shales. The presence of the secondary minerals in the form of fracture coatings thus provides an indicator of hydraulically active fractures.

Both total fracture length and the length with coatings were counted, while the length of a whole or a portion of a single fracture was counted as well to collect the fracture coating data. Most of the coatings are fixed on fracture surfaces. Unfortunately, the fracture coatings are too thin to sample, but they can be divided into 4 categories based on their physical features such as color, smell, and fabric:

a) Reddish-brown and loose iron stains, mainly limonite and less frequently hematite, with some minor manganese stains
b) Dark reddish and hard magnetite
c) Gray sporadic thin clay minerals marked by pyrophyllite deposits
d) Pyrite crystals.

Type-a coatings occur on the surfaces of fractures with little or no diffusion into the matrix rocks, implying that the groundwater in the rock aquifer was not stagnant. It is also obvious that the coating materials such as limonite and hematite have been transported and precipitated due to past or current groundwater flow; and that these coating materials are in turn indicative of hydraulically active fractures, and to a large extent groundwater flow has been mostly confined to the space where these fractures dominate. However, the other three types of coatings are probably not related to flow. In particular, the sporadically deposited pyrophyllite and magnetite were probably formed under great pressure and temperature (Velde, 1984) where the fractures can be regarded as closed to hydraulic activity. Pyrite crystals only occur at the very bottom of the hole, and may be attributed to the original fluid intruding from the sulphur-bearing basement rocks.

In order to characterize the spatial variation of the fracture coatings, a line-scan technique was used to compute the intensity of the coatings. Similar to the statistics of fracture density, the intensity of fracture coatings is expressed as the ratio of fracture length with coatings to the total fracture length. Plotting the intensity data against borehole depth reveals the downward distribution of hydraulically active fractures. On average 23.3% of the fractures are occupied by different types of coatings in the depth range of 14 to 800 m (Fig. 3-8). In the relatively shallow zone above a depth of 125 m, the number of hydraulically active fractures increases with depth with a maximum coating intensity of 0.9 at 122 m. Below 125 m, the number decreases and by 570 m hydraulically active fractures are absent. In particular, about 99% of hydraulically active fractures occupied by ferromanganese coatings are less than 400 m deep, while the most active ones are located between 85 and 135 m depth. At depths of less than 145 m, fracture coatings are mostly composed of ferromanganese substances both in gently-dipping bedding planes and steep structural fractures, but the coatings in steep fractures become predominant below that depth (Fig. 3-8a).

Using spatial variation and types of coatings to determine the degree to which fractures are hydraulically active, four zones are recognized as follows:

i) 0~150 m – High
ii) 150~400 m – Medium
iii) 400~570 m – Low
iv) 570~800 m (or deeper) – Inactive.

In this case, the relations of borehole depth with facture types and coating types provide a statistical basis for determining the degree of hydraulically active fractures and its hydrogeological implication. It is concluded that:

i) Groundwater flow is controlled by both gentle-dip bedding planes and steep fractures in the near-surface zone above 150 m, but is dominated by steep fractures in the deeper part of the aquifer below 150 m depth

ii) The majority of groundwater flow occurs above 400 m depth and tends towards zero below that depth

iii) No groundwater flow could take place below 570 m depth in the study area and adjacent areas of the TMG fractured rock aquifers with an analogous assemblage of structure and lithology

The depth model of groundwater circulation based on the above analyses is not necessarily applicable to all areas of the TMG rock aquifers. It may be extrapolated to areas with similar assemblages of structure and lithology. In terms of groundwater protection zoning and numerical flow modeling of the TMG area, the model may help to explain the properties of the fractured rock aquifers in general and to establish the conceptual model considering the lower limit of aquifer depth in particular.

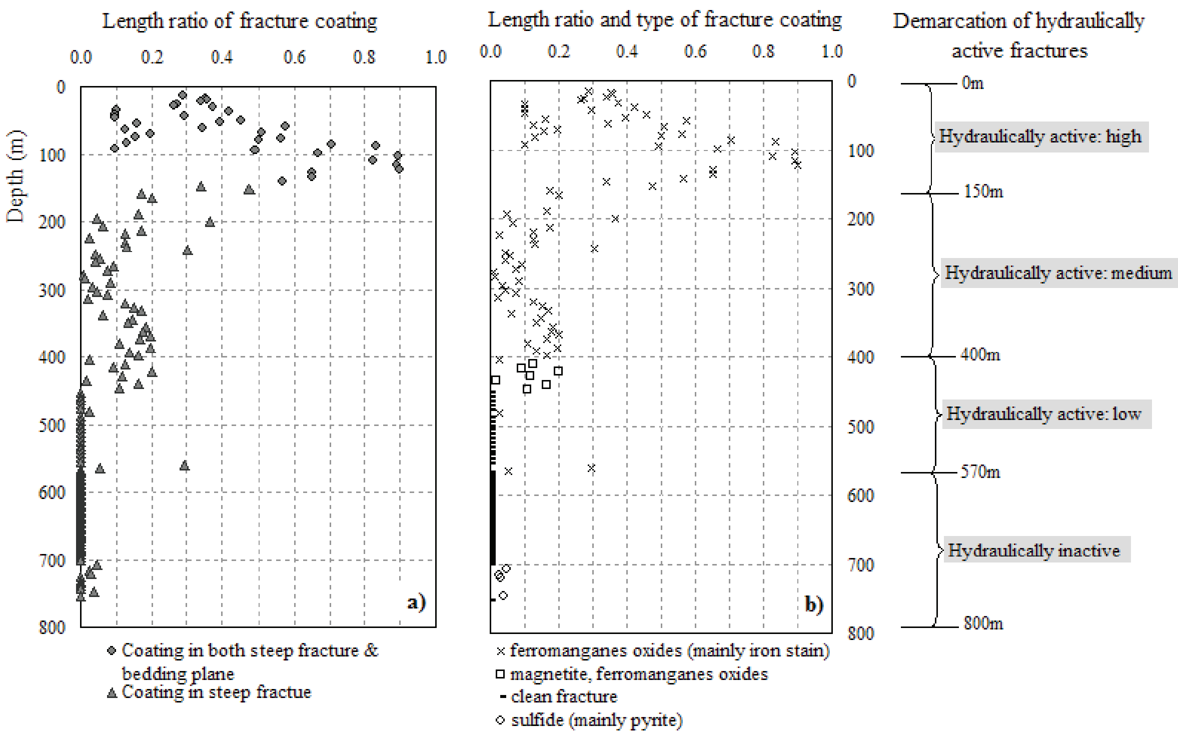


**Fig. 3-8** Types and variations of fracture coatings at borehole G40145 (Lin et al., 2007)

### 3.4.4 Implications of the hydraulically active fractures

The analyses of fracture coatings have clearly indicated the distribution of hydraulically active fractures, although such fractures cannot necessarily be regarded as flow paths. It can be assumed that the hydraulically active fractures represent the maximum number of currently open fractures and that most groundwater flow takes place in those interconnected open fractures.

From the demarcation of hydraulically active fractures, it appears that groundwater flow in the study area is controlled by the fractures without regard to their orientation in the near-surface zone above 150 m, but is dominated by steep fractures in the deeper parts (below 150 m). The main reason for this is that the sub-horizontal bedding fractures are more vulnerable to lithostatic pressures than the steep fractures and tend to close with increasing depth. It also appears that the majority of groundwater occurs above 400 m depth and is rarely found below 400 m depth. Furthermore, the top of the hydraulically inactive fracture zone clearly indicates that groundwater flow could not take place below a depth of about 570 m.

The main water strikes in the deep hole G40145 range from depths of 170 m to 380 m below surface, which is similar to other areas of the TMG fractured rock aquifers. At Boschkloof (Fig. 3-3a), for example, the strongest flow yields encountered in borehole BK1 and BK4 were 100~120 *l*/s and 95~109 *l*/s at depths of 154 m and 294 m, respectively (Hartnady and Hay, 2002b). In comparison the groundwater situation in a deep borehole (over 600 m in depth) at Blikhuis field is more typical, where the main water strikes are in the depth range of 345~370 m with an accumulative artesian flow of 3.35 *l*/s. Although another two conductive zones were found at 434~444 m and 475~485 m depths, the additional flow rate was merely 0.05 *l*/s and 0.3 *l*/s, respectively. There was no water encountered below 490 m in the Blikhuis deep hole (Hartnady and Hay, 2001c).

## *3.5 Application of remote sensing data*

With the increasing availability of high-resolution imagery, there have been more use of remote sensing techniques to study hydrogeological conditions on a large scale (Schowengerdt et al., 1979; Mabee et al., 1994; Kresic, 1995; Drury et al., 2001), for site investigation (Sander et al., 1996; 1997), groundwater monitoring (Rodell and Famiglietti, 2002), and groundwater protection and resource evaluation (Koch and Mather, 1997; Bressan and Anjos, 2003). As groundwater is not usually directly perceptible from remote sensing data, surface indicators have to be used to infer the subsurface conditions that control groundwater occurrence. Lineaments captured from imagery often provide a crucial clue on the interpretation and analysis of fractured rocks and associated groundwater flow regimes. The main assumption that underlies all lineament analyses is that the linear features (O'Leary et al., 1976; Waters et al., 1990), when properly identified, represent the surface manifestations of transmissive fracture frameworks of low permeability rocks (Degnan et al., 2002). Lineaments are usually characterized by azimuth and length distributions, length density ($L_d$, total length of lineaments per unit area), frequency ($L_f$, total numbers of lineaments per unit area), and intersection point density ($L_c$, total numbers of lineament intersection points per unit area). The preparation of lineament maps is hence important for groundwater study in fractured rocks, especially when they are incorporated with other pertinent maps using GIS.

### 3.5.1 Lineament mapping

The areas selected for lineament mapping are situated at the southern and western branches of the Cape Fold Belt, comprising a series of folds and faults extending approximately NW-SE, NE-SW, and E-W. Due to the lithologies and geomorphologies, many of the TMG outcrops are well exposed as bare rocks but are extremely difficult to access. This provides an opportunity to use remote sensing data to study the hydrogeological conditions on the basis of lineament analysis in the fractured rocks. As lineament analysis requires the location and distribution of lineaments that represent the fracture-correlated features, the choice of a study area should have very good rock exposures on the images. Areas with limited lineament distribution were excluded. This may reduce the representivity of the study areas, but increases the quality and consistency of lineament data. For this study, seven domain areas, with sizes ranging from 6.25~225 $km^2$ (Fig. 3-9) were selected.

Meaningful interpretation of lineaments that are associated with the structural framework is largely dependent on the quality of imagery, background knowledge, and the approach used for acquiring lineament data. In this study lineament mapping was done using Landsat $ETM^+$ imagery (UTM zones: S-34-30) that that cover the western half of the TMG area. The existing lithostratigraphic, geomorphologic, and structural information are used for reference during the mapping. The imagery comprises seven multi-spectral bands and one panchromatic band. In comparison with conventional aerial photography (1:50,000), this imagery has better spatial resolution, allows lineaments with a minimum length of 65 m to be traced. To enhance the confidence of lineament interpretation, multiple interpreters were employed during the lineament tracing. The data from various interpreters were carefully compared and then combined to one shape file. The major problem encountered during the lineament tracing was the sun azimuth effect (Woodford and Chevallier, 2002) which created a bias toward northeastern striking lineaments. After the mapping of a domain area was completed, each lineament length and orientation was computed for distribution and density analyses. The mapping and statistic results of the lineaments in the seven domain areas are presented in Fig. 3-9.

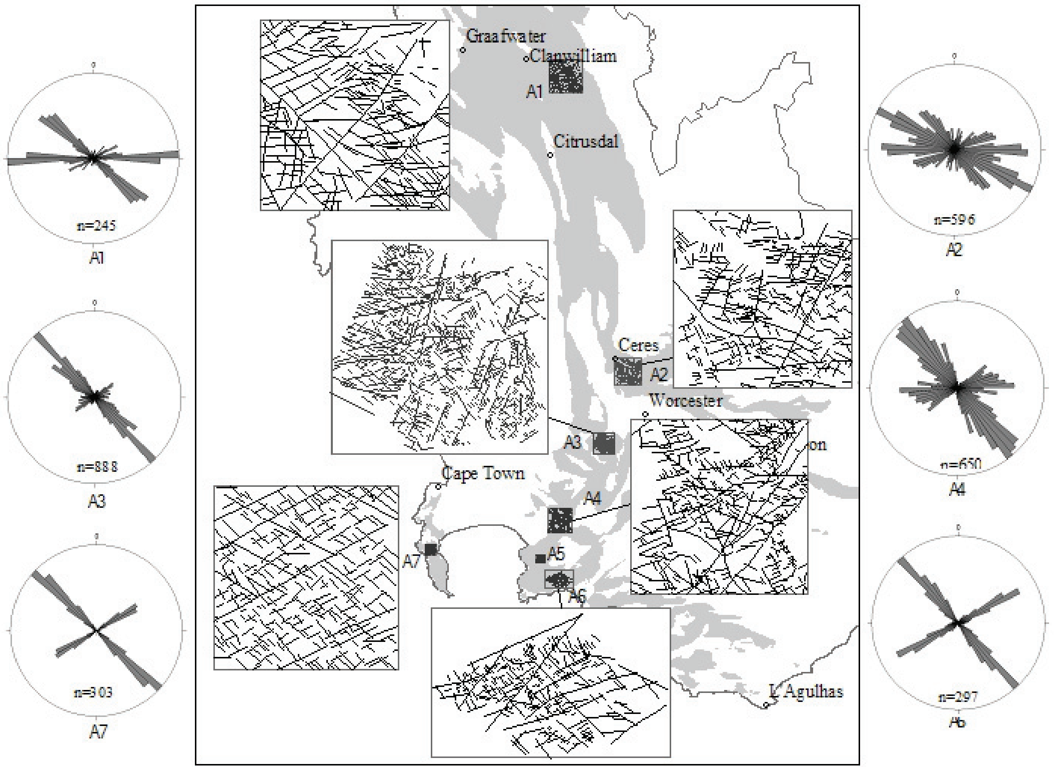


**Fig. 3-9** Map of selected domain areas for lineament analyses, showing captured lineaments and rose diagrams

Distribution patterns of lineament lengths and orientations are very useful for the study of fractured rock aquifers (Kulatilake and Panda, 2000), especially in the case where the measurement of fracture lengths and orientations on the surface is unable to yield sufficient data. A quantitative analysis was carried out to determine the distributions of lineament orientations and lengths in each domain area. Lineaments characterized by azimuth and length are computed using an in-house Visual Basic for Application (VBA) scripts developed in ArcMap. The results of directional analysis show that there are principally three trend directions: NE-SW, NW-SE, and approximately E-W in the seven domain areas (Fig. 3-9). According to the distribution of the lineament orientations, these areas can be grouped into four categories, suggesting different fracture patterns and tectonic stress conditions from the north to the south of the study area: 1) A1 in the northwest; 2) A2 in the core of structural syntax zone; 3) A3 and A4 in the middle south; and 4) A5, A6 and A7 in the south where the lineaments are merely striking to NE-SW and NW-SE. Moreover, the strikes of lineament closely have to a normal distribution with different orientation compartments as one of which is shown in Fig. 3-10.

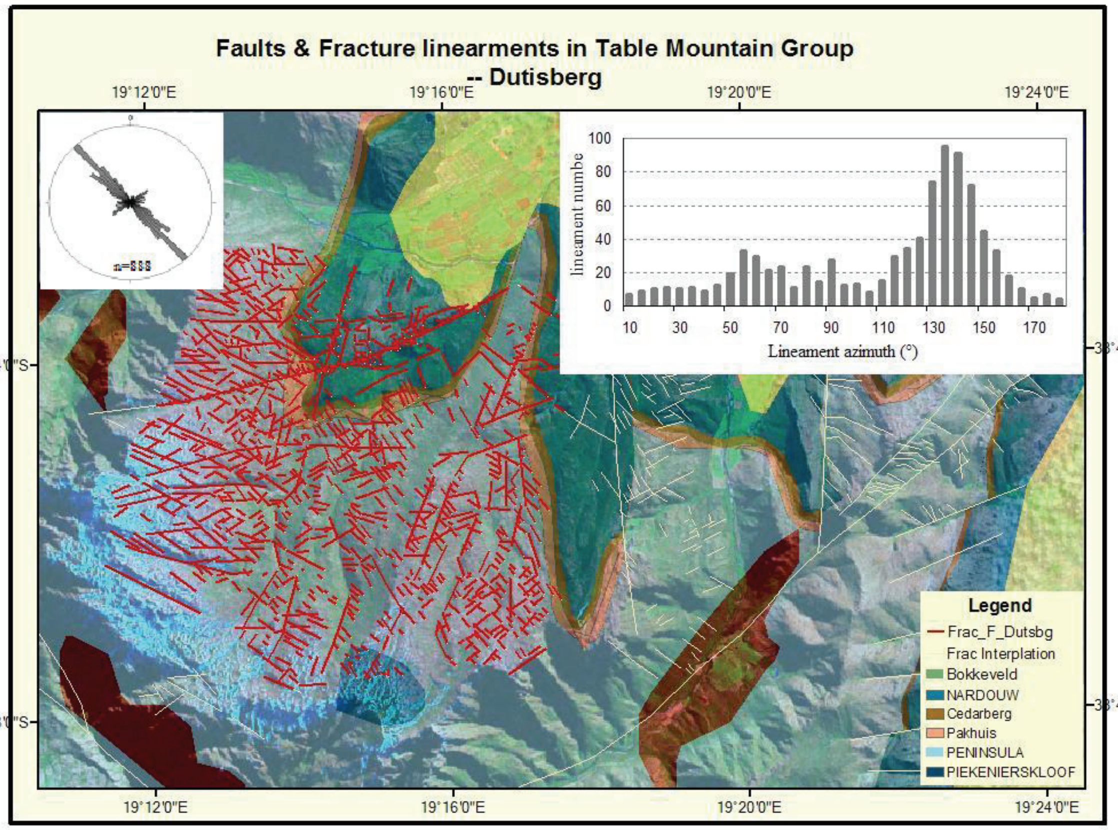


**Fig. 3-10** Map showing Lineaments (red color) captured from Landsat ETM+ image and their orientation pattern, incorporated with the geological information at domain area A3

### 3.5.2 Lineament analysis

Fracture length has a significant impact on connectivity in a fracture network. Studies of fracture connectivity pattern are largely derived from generated models via stochastic analysis of measured fractured data. Kulatilake et al. (2003) suggest that log normal, gamma, and exponential distributions are the best models to characterize fracture lengths based on probability analysis with data from field measurements in gneiss rock masses. An exponential distribution of fracture trace length is applied by Park et al. (2002) to study the hydraulic properties in granite. On a microscopic scale filamentary fracture tend to have a lognormal distribution according to X-ray scanning of core samples (Pyrak-Nolte et al., 1997). The different methods of fracture scanning and length computation used can lead to big differences in the derived length distribution patterns.

In this study, the length of lineaments is computed by points on each tracing line to avoid the possible bias for non-beelines. Recorded lineament length ranges from 60 m to 17450 m with mean values ranging from 351 m to 1984 m in the seven domain areas. No significant differences in the distribution of lineament length can be found from the number-length histograms (Fig. 3-11). They all appear to have a log normal distribution. This distribution pattern is thought to prevail in the TMG sandstone terrain, regardless of the size of a domain area. Since the fracture system distribution pattern is essentially the same regardless of the scale of the study areas, this distribution pattern can probably be applied to smaller-scale fracture systems.

On a microscopic scale, the aperture value of a fracture is usually proportional to fracture length (Zimmermann et al., 2003). This proposition is supported by the work of Gavrilenko and Gueguen (1998) who assume a linear relationship between fracture aperture and length. This work indicates that information of fracture aperture can therefore be inferred from fracture length. Based on lineament data analysis and field verification, Liu and Bodvarsson (2001) were able to establish a relationship between fracture aperture and fracture length which follows a power law with an exponent of 0.3~0.5:

$$B = c \cdot L^{d} \qquad ((3\text{-}1)$$

where $B$ = fracture aperture, $L$ = lineament trace-length, and $c$ and $d$ *are* constants. This relationship between fracture length and aperture tends to become meaningful in the study of large-scale hydraulic properties.

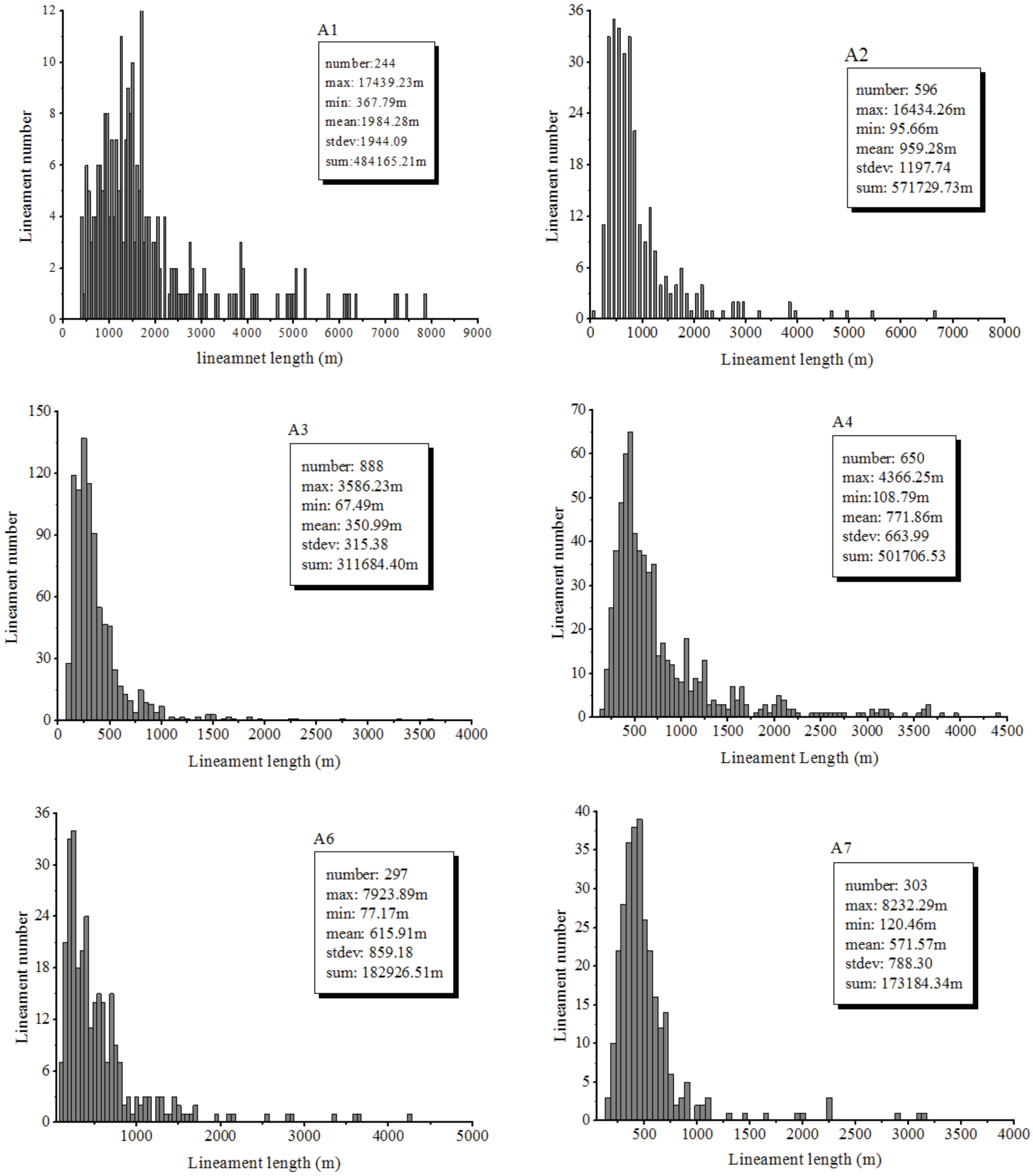


**Fig. 3-11** Histograms of lineament lengths

## *3.6 Fracture characterization with data from field measurements*

The fracture measurements carried out at medium to large scales by means of remote sensing imagery interpretation and statistics are intended to elucidate the framework of fracture networks with fracture lengths of more than 60 m. This is an effective approach to present the outline of fracture systems in a specific region where the rocks are well exposed. However some drawbacks inevitably arise from the misinterpretation of fractures when the lineaments are not actually controlled by fractures. The interpretation results therefore need to be confirmed in the field. Fracture data from site surveys and field measurements can be statistically analyzed for both the characterization of the TMG fractured rocks and the generation of hydraulic conductivity information.

### 3.6.1 Fracture field measurement and data statistics

Selected sites for detailed field surveys and investigations on much smaller scales were located in different structural domains of Cape Fold Belt. Ideally, fracture data should be gathered on fracture elements, i.e. length, orientation, aperture, and density for the purposes of developing a statistical or deterministic model. Most of the fracture element data could be properly collected in the TMG sites, except for fracture length because of the difficulty of tracing fractures buried by soils and vegetation for much of their length. In order to have sufficient measurements, the size of the sites is usually required to be more than 60 m in length and width (Fig. 3-12).


**Fig. 3-12** The TMG outcrops for fracture measurement. a) A close view of the TMG sandstone near a fault zone at the north of Grabouw; b) the Peninsula sandstone outcrop at Theewaterskloof; c) Peninsula sandstone at Simon's Town; and d) the Nardouw sandstone outcrop at Aseljagberg

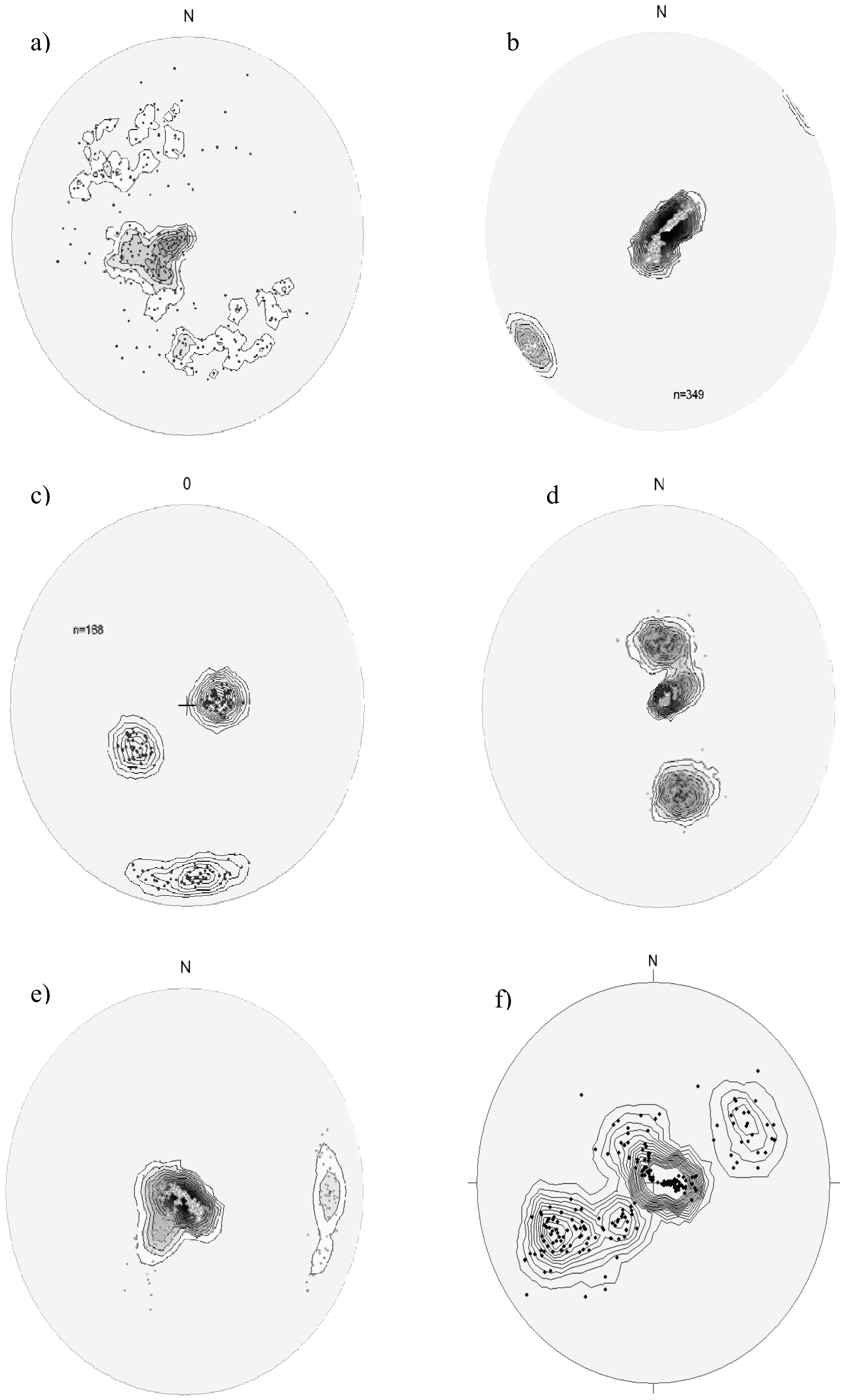


**Fig. 3-13** Spatial frequency distribution of fractures measured at sites in the Western Cape: a) Theewaterskloof east; a) Theewaterskloof west; c) Montague tunnel; d) Eselagberg; e) Gevonden; and f) Boschkloof, in which the solid polygons represent normals to the fractures.

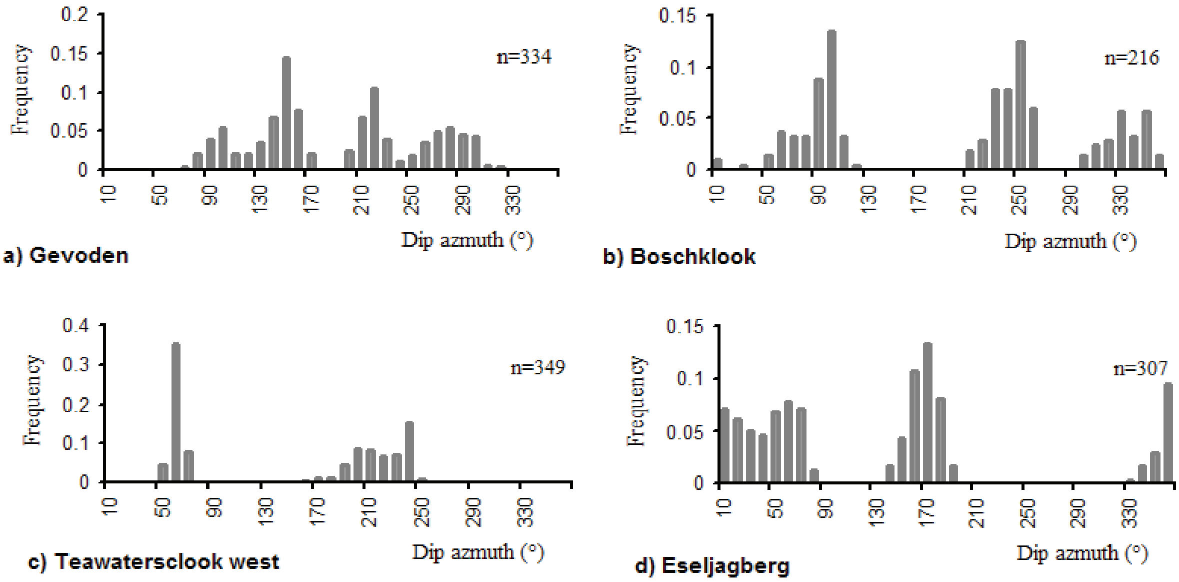


**Fig. 3-14** Frequency histograms of fractures vs fracture dip azimuth at 10° intervals, showing the dip directions at each selected site

Statistics on fracture geometries (dip azimuth and dip angle, spacing, aperture, and length) at selected sites are used to analyze the distribution of these parameters and form a solid basis for the study of aquifer properties such as hydraulic conductivity (Lin and Xu, 2006). With respect to the distribution of each fracture element, fracture length often obeys a log normal distribution, which has been proved by the data captured from satellite imagery. The fracture orientations and aperture approximate normal distributions. The fracture data measured at selected TMG sites show that there are mainly 3 to 4 sets of fractures (Fig. 3-13), including bedding fractures. The results suggest an approximately normal distribution of fracture orientation for an individual set of fractures (Fig. 3-14), which is quite similar to the results obtained from lineament analysis.

### 3.6.2 Stochastic analysis and connectivity of natural fractures

In the context of fracture hydrogeology, the interconnectivity of fractures has been recognized as one of the key features in controlling the flow system in fractured rocks (Margolin et al., 1998). Many efforts have contributed to the study of fracture connectivity through randomly reproducing fracture reality (Bradbury and Muldoon, 1994) largely based on the distribution of each fracture element (orientation, length, density). When these statistical data are incorporated with other parameters such as aperture and particularly connectivity of fractures, the hydraulic properties of fracture network can then be estimated (Mourzenko et al., 1999;

Dreuzy et al., 2000). In this regard, percolation theory can be an effective tool for delineating the connectivity of a fracture network. Random fracture analyses applied to quantitatively determine the percolation threshold mostly assume that fractures are well connected. In a study of fracture system at a uranium mine in France, Long and Billaux (1987, in Witherspoon, 2000) found that only 0.1% out of a total of 65740 generated fractures actually contributed to flow at the site scale. In situ borehole tests (Karasaki et al., 2000; Halihan et al., 2005) have also shown that fractures developed in a rock mass are not always fully connected. Fracture interconnection may depend on both geometric and physical properties such as orientation, aperture, length, termination, and fracture filling.

Based on the assumption that groundwater occurrence in the TMG sandstones is governed by fracture networks, fractures have been statistically generated in this study using the data derived from field measurements. The intention is to depict on a site scale the geometric interconnection of fractures with lengths ranging from metres to tens of metres, and subsequently to construct a conceptual model that may be applied to the estimation of hydraulic properties.

### 3.6.2.1 Statistically generated fractures

The statistical generation of fractures involves applying a random process to the distribution of fracture elements determined from site measurement data. Fundamental elements include fracture orientation (strike, dip azimuth and dip angle), fracture length, and the distance (spacing) of each set of fractures. The number of fractures measured has to be enough to meaningfully represent the population of fractures at the measuring site.

As discussed above, fracture orientation follows a normal distribution (Fig. 3-14). Log normal distribution is adopted for fracture length from the data of the remote sensing by considering the similarity of

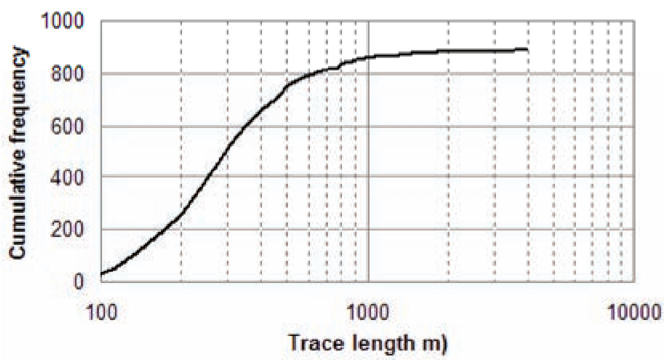


**Fig. 3-15** Plot of cumulative frequency against fracture trace-length with cut-off at 100 m, at site Gevonden (see Fig. 3-11-A3), approximately showing a lognormal distribution.

fractures at various scales (Fig. 3-15). It is extremely difficult to have enough trace-length data measured on a given TMG exposure, and so the fracture length population represents less than 40% of the measured fractures.

The random generation of fractures is based on the statistical data for each fracture set. With respect to the number of each fracture set, many key studies on discrete fracture network (DFN) use multiple fracture numbers that appear to meet a density value for the study of connectivity. Such an approach to fracture numbers at a study domain tends to amplify the uncertainty of the statistical results on fracture elements at the measurement scale. Rather than using an uncertain number, in this study the number of each set of fractures is determined by their spacing in a domain, and accordingly the position of fractures is assumed to be a uniform distribution.

Based on statistical feature of the fracture data, it is possible to use the "random number" function embedded in Excel to geometrically generate the fractures on surfaces and in profiles. The fracture data generated in Excel are loaded to ArcGIS. Geometric connectivity analysis is done in ArcGIS.

The realization of fractures on a 2-D plan (on surface) only needs to have the input of stochastically generated data of fracture strike, length and density (for the number of fracture sets). In order to remove the boundary effects in which position of each fracture offsets out side of the study domain, a central coordinate (x,y) is used to position each fracture during the generating process (Fig. 3-16).

Groundwater flow in the fracture system is however not a 2-D problem, but a 3-D one. This requires presenting the fracture media on 2-D profiles in which the generated fracture data of length, dip angle and density are necessary. However, unlike the generation of fractures on a 2D plan, the real dip angle of each fracture needs to be projected on the profiles with different strikes (direction) before the data can be generated. Fig. 3-17 illustrates the projection from a real dip angle ($\beta$) to apparent one ($\alpha$) which can be performed using the following relationship:

$$\tan\alpha = \sin\phi \cdot \tan\beta \qquad (3\text{-}2)$$

Where $\phi$ ($\phi$ = 0°~90°) is the included angle of profile strike and fracture strike. Fracture length is also changed by assuming the fracture takes a rectangle shape with an aspect ratio of 1.5:1; whereas the rotation of the profile does not have a big impact on the change in fracture length in profile.

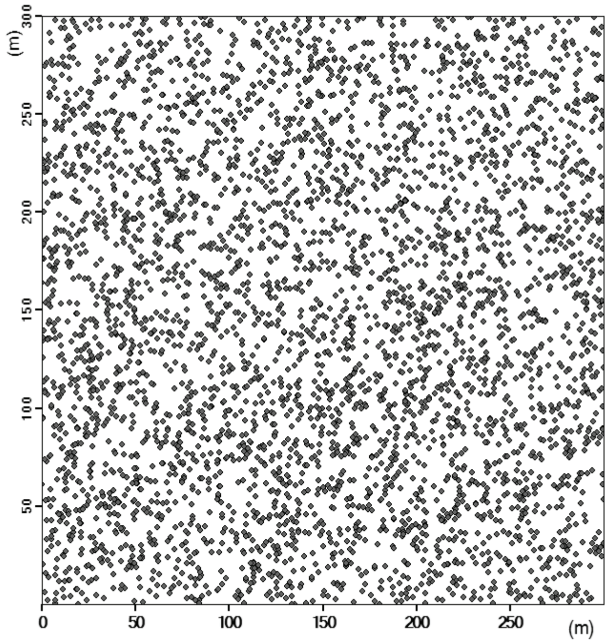

Fig. 3-16 Position of fracture central points generated by a uniform process in the study domain of 300 m×300 m for the Boschkloof site

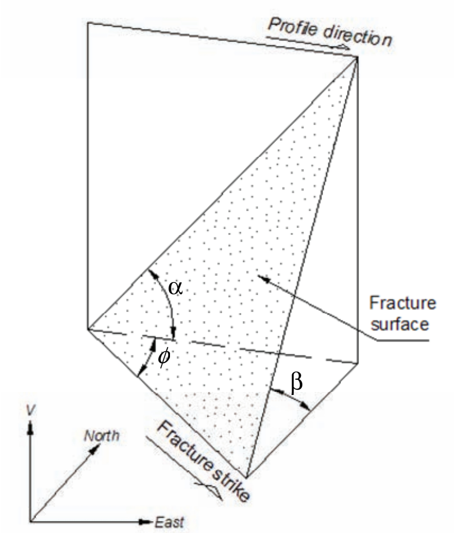


**Fig. 3-17** Relationship between fracture orientation and profile direction, in which $\phi$ is the included angle of fracture strike and profile direction, $\beta$ the fracture dip angle, and $\alpha$ is the apparent dip angle of fracture projected on the profile

#### 3.6.2.2 Application to field data

Fracture data for this part of study are derived from field measurement of the site Boschkloof in Citrusdal area (Fig. 3-3a), where there are five boreholes with the depths ranging from 174 m to 350 m drilled in the sandstone of the Peninsula formation in 1997~1998 (Fig. 3-18). The boreholes are located in the vicinity of a N-W trending fault that has been identified as a flow barrier, while the N-E trending fault is actually a lineament feature with unknown properties (Hartnady and Hay, 2002b). During the borehole drilling, the blow yield of the boreholes was reported to be very high compared with another wellfields developed in the TMG, especially in boreholes BK1 and BK4 where the blow yields value reached 95 *l/s* and 120 *l/s* respectively. The success of this wellfield motivated a full study of the TMG Groundwater. Characterization of this site and associated groundwater flow is based on the interpretation of stratigraphy, structure, and pumping test data and another field observation during the drilling (Hartnady and Hay, 2002b).

Table 3-2, Fig. 3-13f, and Fig. 3-14b collectively show the basic fracture data results from field measurement on the outcrops of Peninsula sandstone. A total of 216 fractures, about 5.2% of the fractures to be generated (Table 3-2), were examined. Five sets of fracture are identified. In table 3-2, sets 1 and 4 represent bedding fractures with relatively gentle dips. Steeply dipping fractures of set 2, 3 and 5 appear to dominate the density distribution in the sandstone because of their relatively low spacing. It should be pointed out that the fracture trace-length collected at the site ranges from 1.9 m to 35 m.

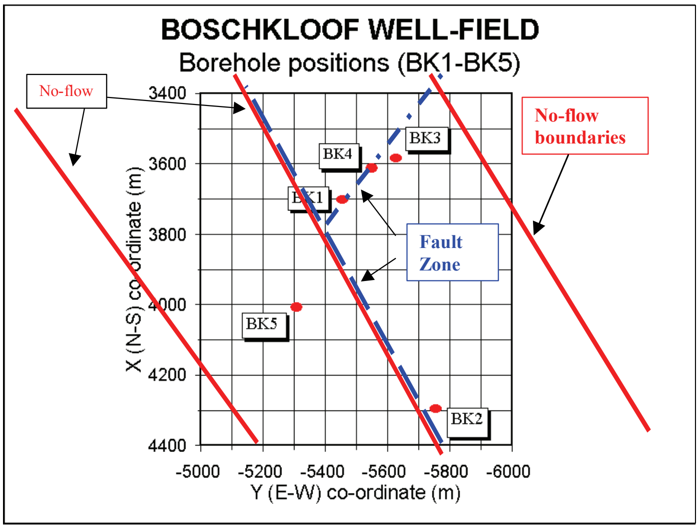


**Fig. 3-18** Map showing the position of boreholes at Boschkloof wellfield. Field measurement of fractures were taken on the Peninsula sandstone exposure between BK1 and BK3 (Courtesy of Gerrit van Tonder, also see Hartnady and Hay, 2002b). Note that the N-E striking fault is a lineament feature

Fracture generation is based on the statistical and parameter distribution of each fracture element as have been previously discussed. Fractures are generated in a study domain of 300×300 $m^2$, on 2-D plans and 2-D profiles with various profile directions. It was desirable to present the fracture networks on this site scale because both the borehole lengths are less than 350 m, and the lower limit of the main water strike is located at the depth of 294 m in borehole BK4.

The geometric nature of the fractures is different at depth, as discussed by Shapiro et al. (2007), due to the differences in lithology and stress state of fractures. For the generation of fractures on 2D profiles, partially based on the core sample study at the Rietfontein site, it is necessary to assume that the fracture orientation and density do not change much at depth in the locally homogeneous Peninsula sandstone.

**Table 3-2** Statistical results of 216 fractures measured at Boschkloof

| Set | Sample number | Dip angle/Dip direction (°) | | Length (m) | | | Spacing (m) | Number generated |
|---|---|---|---|---|---|---|---|---|
| | | Mean | Standard deviation | Mean | Standard deviation | Number measured | | |
| 1 | 57 | 40/244 | 10.28/40.09 | 16.31 | 1.66 | 16 | 0.41 | 730 |
| 2 | 50 | 77/330 | 10.44/17.48 | 7.29 | 1.40 | 22 | 0.27 | 1110 |
| 3 | 55 | 79/94 | 4.53/5.77 | 5.06 | 1.49 | 19 | 0.34 | 860 |
| 4 | 27 | 40/62 | 8.68/12.63 | 13.94 | 1.31 | 8 | 0.68 | 440 |
| 5 | 27 | 63/211 | 11.87/8.52 | 4.50 | 1.61 | 20 | 0.30 | 1000 |

#### 3.6.2.3 Connectivity pattern of fractures

Similar to many other stochastic studies, the fractures generated on both the 2D plan and vertical profiles better represent the assemblage of fractures than the real position of each fracture in the site because of their random coordinates. Therefore, each generated domain reflects the mode of fracture occurrence and the connectivity pattern that is embedded in the features of natural fractures.

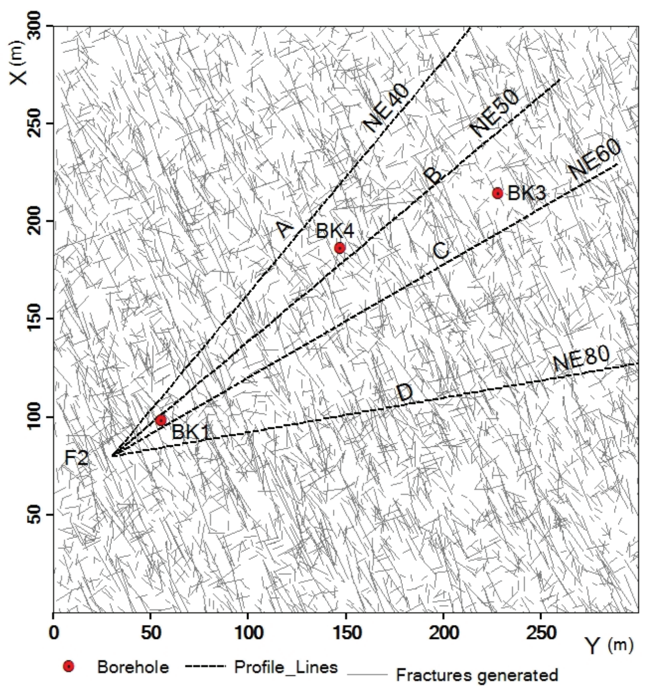


**Fig. 3-19** Fractures generated on a 2-D plan with data derived from the field measurements at Boschkloof wellfield. The study domain area is 300×300 m$^2$, in which the dashed lines are profiles A to D

To continue the field data application of the Boschkloof site, Fig. 3-19 shows these fractures in plan view. Four profiles with strikes from NE40° to NE80° are positioned for the fracture generation on vertical profiles. The intention of fractures generation on multiple profiles is to comparatively analyze the connectivity pattern with a view to elucidating some unique flow phenomena in the TMG fractured rocks. This will help to establish a site-scale conceptual model for studying aquifer properties and borehole hydrogeological condition in a statistical sense. This model can be used to average out a suite of relevant hydraulic properties to apply to groundwater modeling, or to effectively utilize a contour map of borehole water levels to present groundwater flow trends on a local or even a regional scale.

Fig. 3-20 shows the generated results including both the whole fractures (A1~D1) and the relatively large fracture clusters (A2~D2), together with three boreholes projected on four neighbor profiles with the intervals of strike azimuth from 10° to 20° in which profiles A, B, and C are close to the line determined by connecting borehole BK1 through BH4 to BK3, while profile D is relatively separate from the line (Fig. 3-19). It is clear that the interconnected fractures on each profile occur as distinct fracture blocks, commonly showing anisotropic features. It is also clear that the profile direction has an impact on the connectivity pattern in terms of the size and plunge of the connected blocks. On profiles A, B and C the largest connected block extends across most of the domains but none of them breaks through the boundary on both sides (bottom to top or left to right side) (Fig. 3-20A2, B2, and C2). This suggests that the connectivity patterns are collectively dependent on the factors of orientation, length, and density of fractures, and implies that in a study domain only part of the fractures are involved in flow systems. For example, on profile B the number of interconnected fractures from blocks 1 to 5 is 954, 127, 224, 99, and 167 respectively, accounting for 23%, 3.1%, 5.4%, 2.4%, and 4.1% of the total 4140 fractures.

Such connectivity patterns help explain the existence of multiple water strikes or conductive zones where groundwater is coming from different fracture (block) systems, but probably without hydraulic connection. However, the validity of the connectivity pattern needs to be tested against results from field observations. From borehole observations, the phenomena of multiple water strikes or several conductive intervals in a borehole, as well as the characteristic of no hydraulic communication between the holes in a wellfield are common in the TMG sandstone aquifers. At the Boschkloof site, for instance, at least two conductive intervals were identified in boreholes BK3 and BK4 (but only one in BK1), whereas borehole BK2 appears to be hydraulically isolated from the other three. Moreover, it was observed that the groundwater in boreholes BK1 (major water strike 98.7 m elevation) and BK4 (major strike 30.3 m elevation) were connected at the depth of the major water strikes (Hartnady and Hay, 2002b). The distance between BK1 and BK4 is 127.4 m, from which it is clear that the northeastern plunge of the conductive zone is 28°. This value falls in the fractures of set 4 with the dip angles ranging from 20° to 52° (Table. 3-2). Field observation (Hartnady and Hay, 2002b) also showed that groundwater in borehole BK3 was not necessarily connected to the other two although they were sited virtually on the same profile line. This evidence indicates that three boreholes were probably not sited on a single fault zone (Fig 3-18).

The drawdown observations during the constant discharge (CD) pumping tests conducted at borehole BK1 and BK4 show that the types of drawdown curve are different from each other (Fig. 3-21). Compared with borehole BK4, drawdown observed in BK1 during the CD test is very close to that of Theis flow, whereas drawdown in BK4 exhibits a stepwise mode. From both of the drawdown curves, it appears that the groundwater is coming from two different aquifers, although there is hydraulic connection between the both boreholes as discussed above.

The stepwise mode of drawdown is very common in the TMG sandstones and many other fractured rock aquifers in South Africa (Van Tonder et al., 2001) and is often explained as being caused by multiple boundary effects. This is true if only one flow system is intercepted by a borehole. When a borehole like BK4 intercepts at least two fracture flow systems, the question arises of whether the stepwise drawdown is attributed to the simultaneous dynamic response of these two flow systems to external pumping stresses. On one profile it is noted that the multiple generations of fractures by the same statistic data do not change the mode of connected fracture blocks, which means the stability of the connected blocks is quite high. On a single site, the connectivity patterns are directionally different, which always suggests the possibility of preferential flow path in the study domain and the necessity of studying groundwater problems in three dimensions. From site to site, the pattern of fracture connectivity varies mainly in terms of connected block size as shown by results from the Rietfontein and Gevonden sites in Fig. 3-22 and Fig. 3-23.

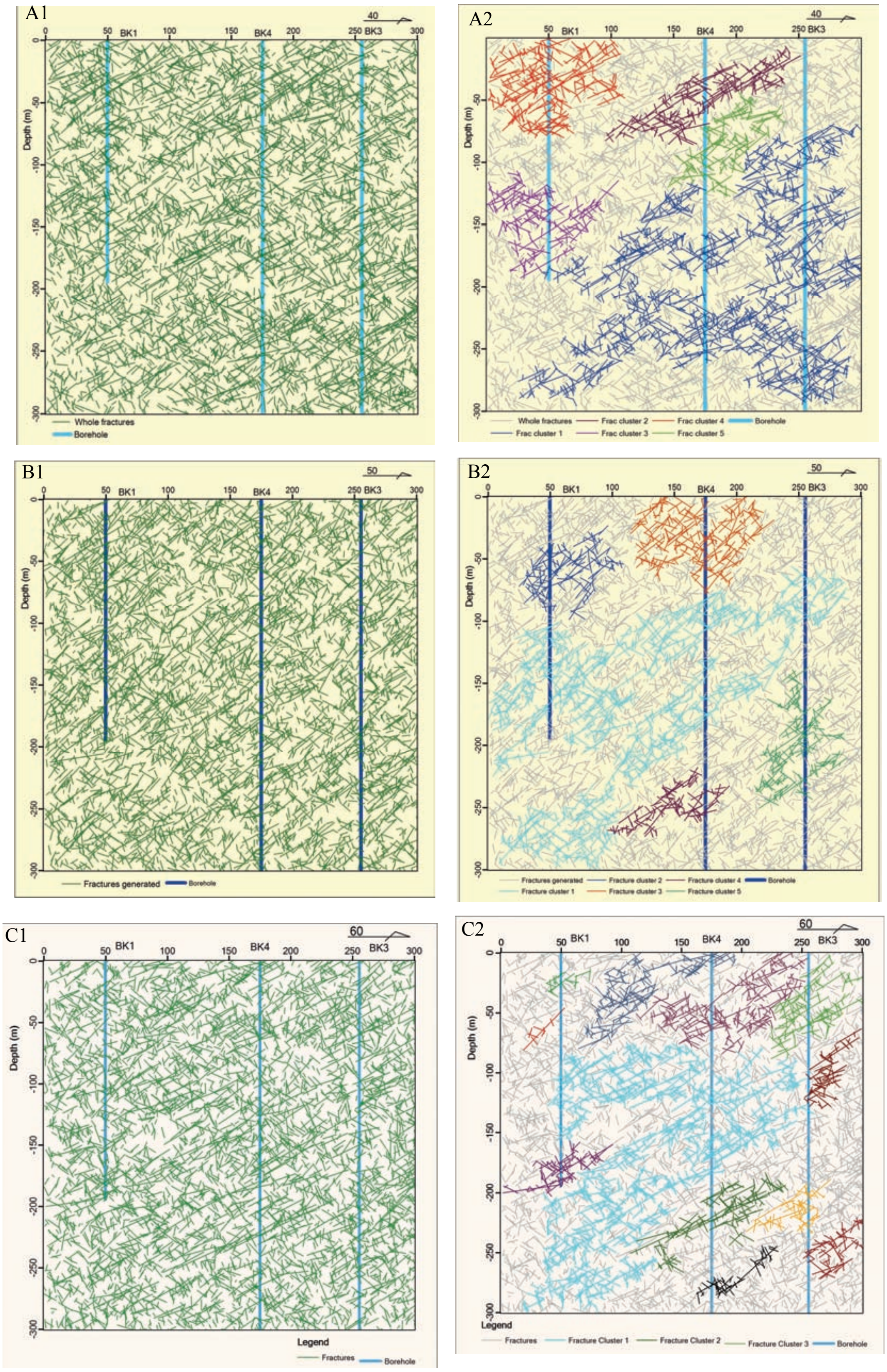


**Fig. 3-20** (continued on the next page)

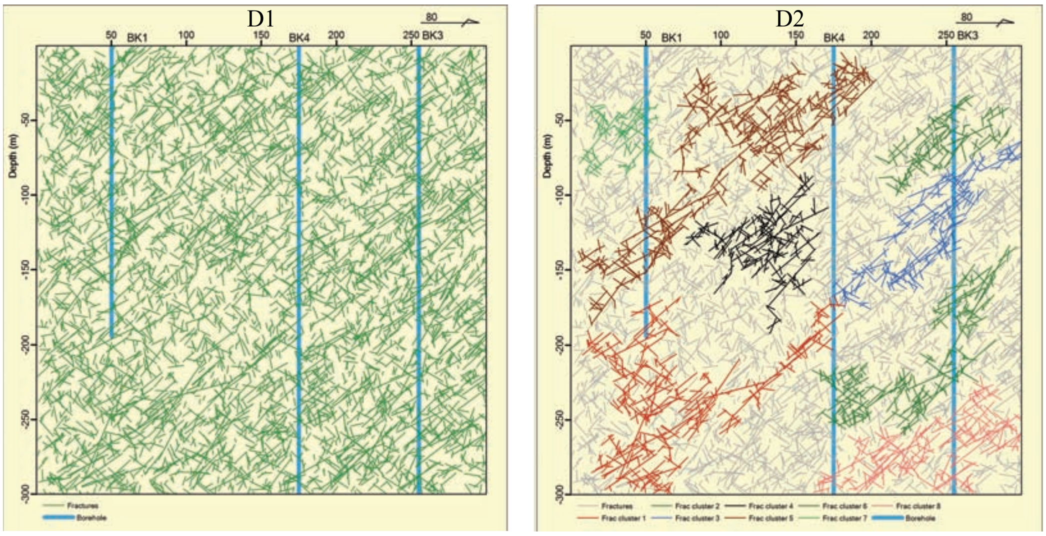


**Fig. 3-20** Fractures generated on four comparable profiles based on the data derived from surface measurements (Table 3-2) at a size of 300×300 m. 1) The left, the whole fractures on each profile. 2) The right, relatively large interconnected fracture blocks geometrically show the connectivity patterns at this site scale with the involvement of boreholes.

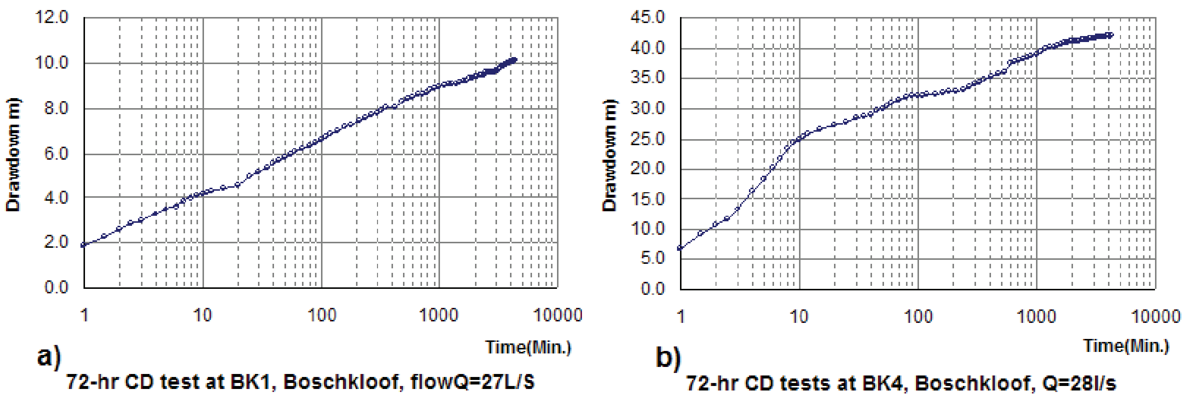


**Fig. 3-21** Drawdowns observed during 72-hour pumping tests at wells BK1 and BK4

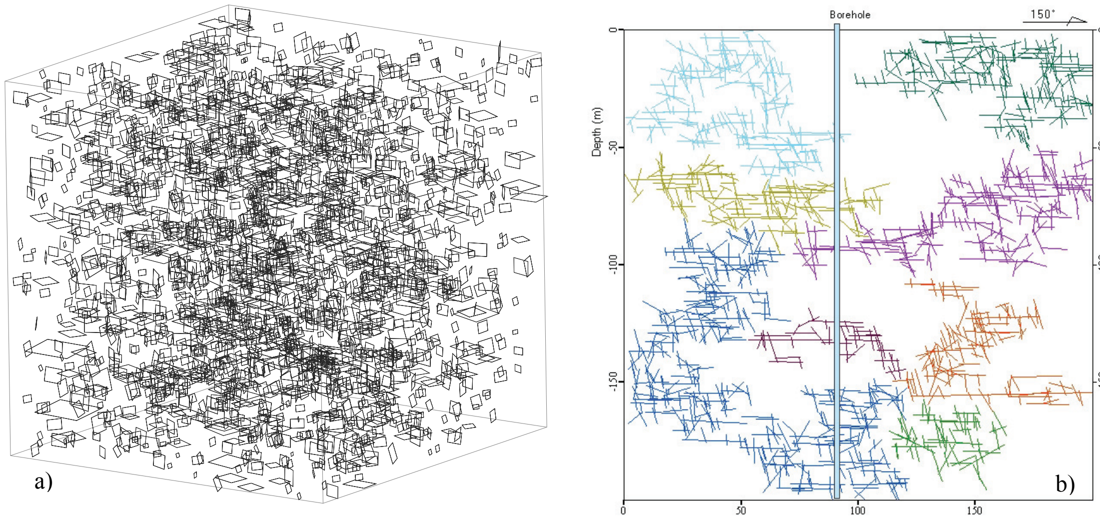


**Fig. 3-22** Fracture generated from data derived from surface measurements at Rietfontein at a size of 200×200×200 m. a) A northwestward view of 3-D visualization of rectangle fractures with a fracture length/width ratio of 1.5, in which the small black blocks indicate the well-connected fractures. b) The interconnected fracture blocks geometrically show a connectivity pattern at a borehole scale. Note that the fractures are projected and generated on profiles with a strike of 150º-330º.

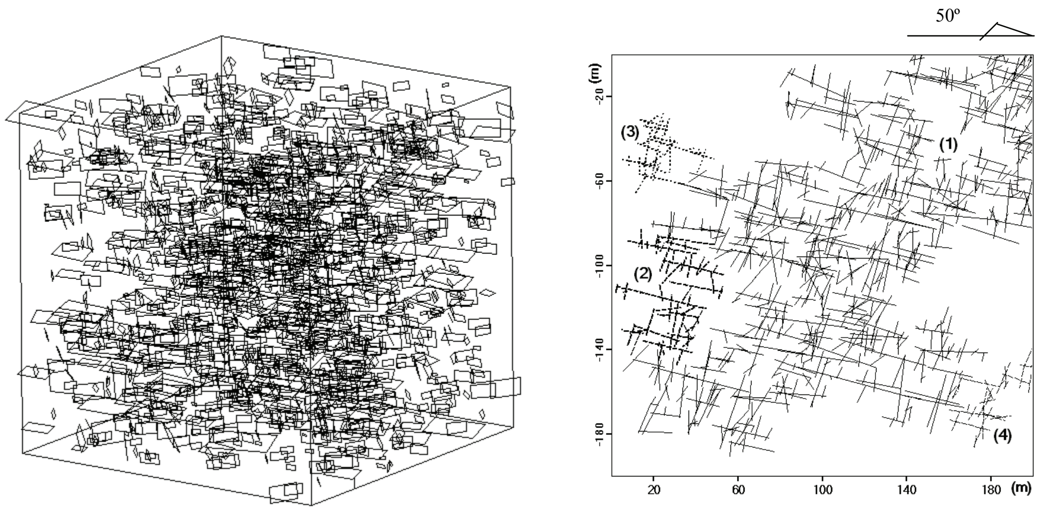


**Fig. 3-23** Fractures generated using the data derived from surface measurements at the Gevonden site at a size of 200×200×200 m.

## *3.7 Porosity and storativity*

### 3.7.1 Relationship between porosity and storativity

Porosity and storativity are both important hydraulic parameters for the estimation of groundwater storage. The former (*n*, percentage) is defined as the ratio of pore volume to the total volume of rock sample. The latter (*S*, dimensionless) is defined as elastic efflux or influx volume of water by per unit change in piezometric head in per unit area of a confined aquifer with a thickness of D. The relationship between the both can be expressed by the specific storage (*Ss*) which is developed by Jacob (1940):

$$Ss = \rho g(\alpha + n\beta), \quad (S = DSs) \tag{3-3}$$

where ρ is the fluid density, g the acceleration of gravity, $\beta$ the compressibility of the fluid (for water at 25C is $4.48\times10^{-10}$ $m^2/N$), and $\alpha$ is the compressibility of rock mass denoted by the reciprocal of its bulk modulus (*Kv,* $N/m^2$).

The *Ss* expression comes from one of the earliest studies to address the hydro-mechanical coupling problem. It was initially derived from compression process of porous media (soil) stressed by abstracting water from a confined aquifer. During the abstraction of confined water, decrease in water level leads to increase in the effective stress acts on the soil particles, resulting in the compression of the soil; in the meantime the decrease in piezometric head leads to the expansion of the confined water, resulting in elastic efflux. Extrapolating to an isotropic rock mass, the bulk modulus *Kv* is often estimated by Young's modulus through the relation:

$$E = 3Kv(1-2u) \text{ ($u$ is Poisson's ratio)} \tag{3-4}$$

However, for an anisotropic rock mass where fractures develop, the bulk modulus of the fractures must be introduced and the specific storage of the fractures takes a form similar to that of the matrix rocks:

$$Sf = \rho g(\alpha_f + n_f \beta) \tag{3-5}$$

in which $\alpha_f$ is the compressibility of fracture determined by the reciprocal of bulk modulus of the fractures (*Kf* $N/m^2$) which is generally less than *Kv* by a couple of orders of magnitude, and $n_f$ is the fracture porosity which can be estimated by total aperture of fractures. Thus, using *Ss* to represent the specific storage of a matrix, the specific storage of a fractured aquifer is sum of both *Ss* and *Sf* as illustrated in Fig. 3-24. In this regard, the fractured rock seems to resemble a dual porosity medium.

Assuming that the total aperture of fractures is generally in the order of millimetres to centimetres, and the aquifer thickness range from meters to tens of metres, it is clear that storativity of matrix rocks can be much higher than that of fractures at a borehole scale. It was reported by Woodford (2002b), based on a study by Van Tonder and Xu (1999), that storativity of highly permeable fractures are usually very low, in the order of $10^{-4}$ to $10^{-7}$, whilst that of the matrix is much higher (i.e. 0.005 to 0.05). This indicates that fractures in a rock aquifer can dominate the flow system, but groundwater storage is mainly controlled by the rock matrix. The ratio of both values suggests that storativity term contributed by fractures can perhaps be discarded in the estimation of aquifer storage. With respect to the TMG sandstones, the storativity of the rock matrix should perhaps be regarded as the contributions of fractures at various scales, because there is almost no primary porosity through the thin section studies, as mentioned in Chapter 2, although there may well be micro-fractures discernible at this level of examination. If this point regarding the absence of primary porosity is correct, the problem becomes one of resolving fracture porosity for fracture apertures at different scales.

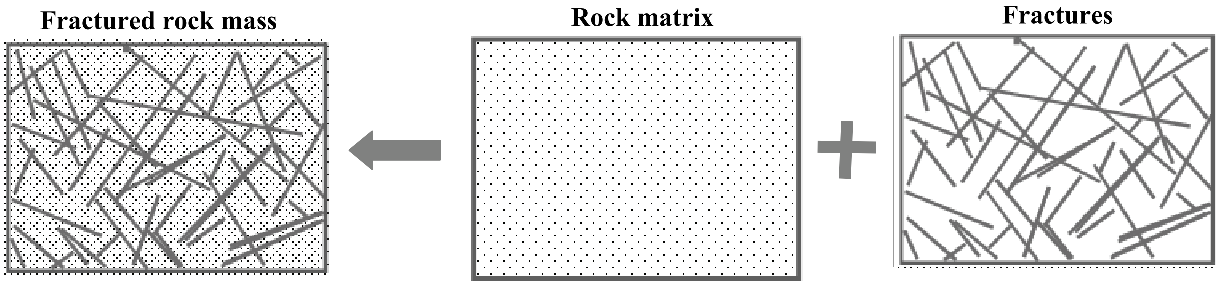


**Fig. 3-24** Schematic conceptual model of fractured and matrix rock media with different storativities

### 3.7.2 Porosity

As discussed above, the porosity of the TMG rocks may include two components, i.e. matrix porosity and fracture porosity; both of which may impact the storativity of the aquifers. Porosity can be expressed as follows (Cook, 2001):

$$n = n_f + n_m(1 - n_f) \qquad (3\text{-}6)$$

where $n$, $n_f$, and $n_m$ stands for total porosity, fracture porosity, and rock matrix porosity, respectively.

It is extremely difficult to determine both the matrix porosity and fracture porosity at the same time, because there is no clear boundary to distinguish one from the other at the scale of problem studied. Usually the porosity of a rock mass is obtained from laboratory test of rock samples, well pumping tests, and borehole geophysical logging (e.g. density, sonic, and neutron logs), or fracture aperture is used to represent the fracture porosity of a rock.

Fig. 3-25 shows some of geophysical logging results from the Rietfontein deep borehole (see also Fig. 3-3), including resistivity (Ohm/m), Gamma (cps), and density (g/cm$^3$) logging data, from which the lithologies of the Piekenierskloof formation in the borehole can be. In order to avoid the uncertainty of geophysical loggings, the logging results are compared to core photos and core logging information. According to Titus et al. (2002), the bulk density of sandstone is 2.65 g/cm$^3$ on average, siltstone is 2.45 g/cm$^3$, and shale (band) 2.35 g/cm$^3$. From the result of density logging, the porosity of the rock formation can be estimated using the following equation:

$$\rho = n\rho_f + (1-n)\rho_s \tag{3-7}$$

in which $n$ is the porosity, ρ is the bulk density, $\rho_f$ the pore fluid density, and $\rho_s$ matrix density. Assuming that the matrix density of sandstone is 2.75 g/cm$^3$, siltstone is 2.62 g/cm$^3$, and shale 2.57 g/cm$^3$, calculation of the porosity for different rocks then is performed.

**Table 3-3** Porosity estimated from the density logging result at Rietfontein deep hole

| **Lithology** | **Density (g/cm$^3$)** | | **Porosity (%)** | |
|---|---|---|---|---|
| | Range | Average | Range | Average |
| Clean sandstone | 2.53~2.72 | 2.65 | 1.7~12.6 | 5.7 |
| Fractured sandstone | 2.1~2.52 | 2.30 | 13.1~37.1 | 16.4 |
| Siltstone | 2.35~2.55 | 2.45 | 4.3~16.7 | 17.1 |
| Shale | 2.25~2.50 | 2.35 | 4.5~20.4 | 14.0 |

As can be seen in Fig. 3-25, there is no spatial correlation of the density logging data, so the porosity result derived from the density data is rather shown as a range rather than related to depth. Porosity of the rocks from the density logging shows a wide range in which many of the calculated values fall in the range of porous media. Although the results shown in Table 3-3 reveal an increasing trend in the porosity value from clean sandstone through siltstone and shale to highly fractured sandstone, these porosity data have limited applicability unless the lower limit of the porosity of each rock type represents a relatively intact rock. This is because the bore wall has been exposed for long periods during the lengthy drilling process, and consequently there is always a tunnel effect from stress concentration or release, resulting in the deformation of rocks near the bore wall and an increase in fracture porosity.

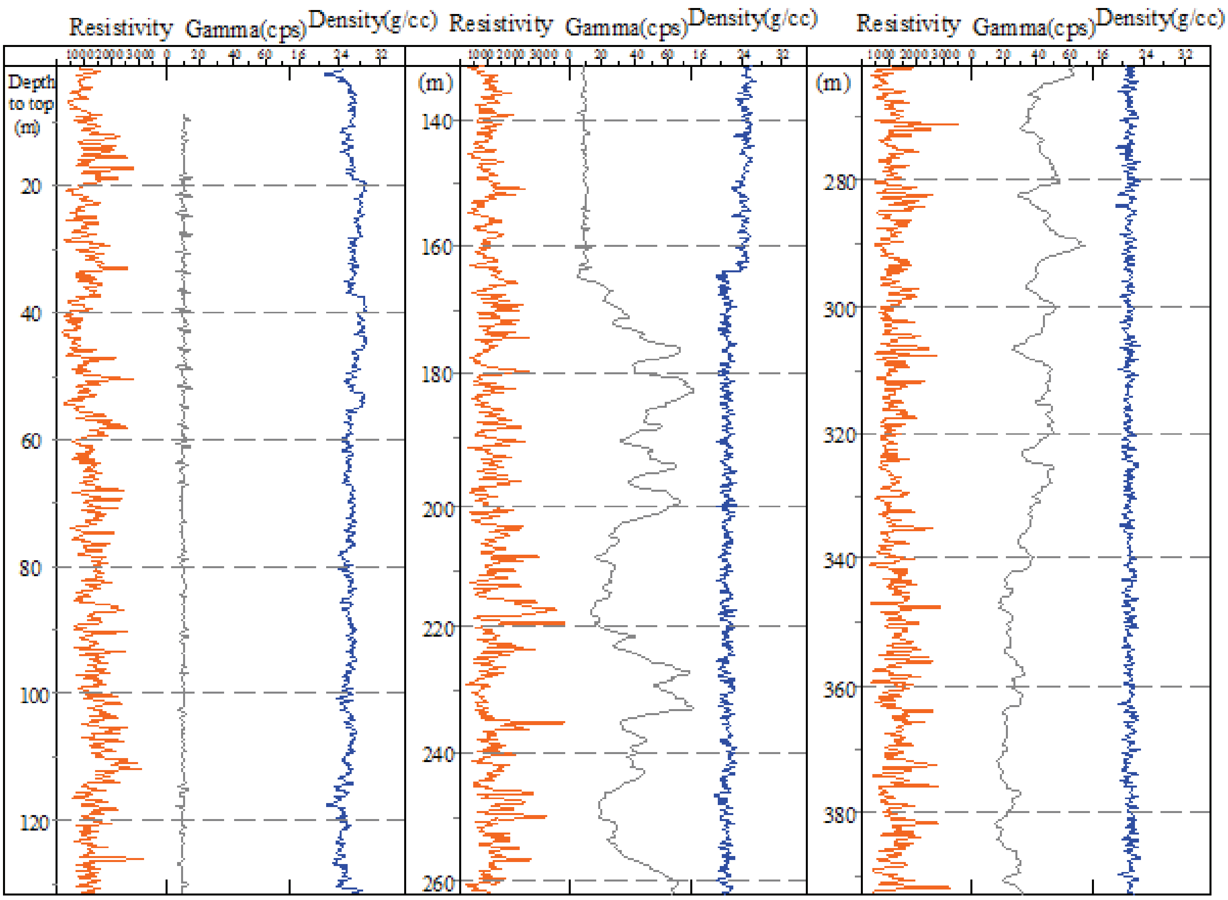


**Fig. 3-25** Geophysical resistivity, gamma and density logs for the Rietfontein deep hole

Table 3-4 shows a wide range of porosity results from various measurements, including laboratory test of core samples, in situ fracture aperture measurement, pumping tests, and the application of satellite imagery. Generally, the porosity of core samples and in situ aperture measurements represent a scale of metres. Porosity derived from pumping tests is actually derived from storativity of a rock mass on a scale of tens of metres, and is highly dependent on a sound estimate of the bulk modulus of the rock mass studied. Since remote sensing data can only be used for capturing fractures with lengths of more than 100 m, porosity from the interpretation of lineaments represents a study area in the scale of kilometers. The scale effect of porosity of the TMG rocks is schematically presented in Fig. 3-26.

Fig. 3-26 also reveals that porosity varies a lot even when measured at the same scale. For example, porosity analyses of a few of the TMG core samples have been carried out (Table 3-4), using the volumetric method. The results shows that the porosity of the TMG sandstones ranges from 1.0~3.6% with an average of 2.5%. These values greatly depend on both laboratory methods and the selections of core samples. Moreover, the effect of stress release on the core samples after they are taken away from the original site could have another impact on the estimation of porosity, from which difficulties regarding in-situ measurements and determining the variation of porosity at depth could arise. On the other hand, measuring only the visible fractures could lead to the porosity value underestimated because the ignored micro-fractures in the rock mass will have a significant contribution to porosity.

**Table 3-4** Porosity derived from core samples and pumping tests

| Type of measure | Sample Depth [m] | Porosity [%] | | Reference |
|---|---|---|---|---|
| | | Range | Average | |
| Core samples | 3322 -3420 [7 samples] | 1.9-2.3 | 1.5 | Core samples of Soekor boreholes. After, Roswell and De Swardt, 1967. non-TMG rocks |
| | 122-154 [11 samples] | 0.6-1.7 | 1.4 | |
| | 1-152 [49 samples] | 0.9-5.4 | 3.1 | |
| | 10-107 [7 samples] | 1.2-3.0 | 2.2 | |
| | 42.5-135.5 (5 samples) | 1.2-3.6 | 2.5 | Core samples of Gevonden BH1, TMG |
| | Unknown (1 sample) | 1 | 1 | Core samples of Gevonden BH2, TMG |
| Pumping tests | Koo Valley | 0.01-0.35 | 0.06 | Pumping tests, Jacob |
| | Kammanassie | 0.11-0.22 | 0.15 | Kotze (2002) |
| | Boschkloof | 0.1-0.01 | 0.05 | Umvoto (2000) |
| | Gevonden | 0.21-1.2 | 0.57 | Pumping tests, Jacob |
| Field measurement | Kirstenbosch, | 0.04 | 0.26 | Sandstone block measurement |
| | Rawsonville, | 0.52 | | Rock surface measurement |
| | Montague | 0.22 | | Rock surface measurement |
| Remote sensing | Rawsonville | | $1.24\times 10^{-6}$ | Area shown in Fig. 3-10 |

### 3.7.3 Storativity

Storativity can be obtained from the interpretation of well pumping tests, and from tests of rock mechanical properties and rock mass porosity. There is no available data for the latter. Currently the storativity and other hydraulic properties of the TMG aquifers are generally derived from the interpretation of well pumping tests. In almost all of the existing wellfields, from the west Citrusdal municipality through to the Klein Karoo semiarid area and beyond to the Uitenhage artesian basin, such hydraulic tests have been conducted by different researchers and a lot of information have been obtained, summarized in Table 3-5. These results show that storativity of the TMG fractured aquifers falls in a wide range from $10^{-2}$ to

$10^{-5}$, according to the interpretation of data through various methods based on the Theis theory for confined aquifer. Uncertainty in the results from the testing data is quite common in the fractured rock aquifers because of, inter alia, the diversity of observed drawdown curves, and difference in the interpretive methods. Because of this it would make more sense to express storativity as a range of values, rather than single value, for regional studies.

For the estimation of storage and the characterization of flow, an $S$ value of less than $10^{-3}$ has been applied to groundwater resource evaluation for the TMG aquifers at a national scale (Vegter, 1995). Based on the study of Jia (2007), the recommended storativity range for regional studies of the Peninsula Aquifer and Nardouw Aquifer respectively is listed in Table 3-6. In terms of practical application, the scale-dependency of storativity should be considered, and it is suggested that storativity follows the same pattern as porosity (Fig 3-26).

**Table 3-5** Storativity of the TMG aquifer refers to various formations and areas

| Wellfield | Formation | Reference | Storativity | Transmissivity ($m^2$/d) | Analysis method |
|---|---|---|---|---|---|
| Citrusdal | Peninsula | Umvoto-SRK (2000) | 1×10-3 to7×10-4 | <10 to 200 | FC* Recovery |
| Struisbaai | Peninsula/Nardouw | Weaver (1999) | 8.6×10-3 | 15 to 200 | Cooper-Jacob |
| Uitenhage | Peninsula/Nardouw | Maclear (2001) | 2×10-4 to5×10-2 | <10 to 400 | Unknown |
| Kleinmond-Bot River | Nardouw | Parsons (2001) | 1 to 5×10-4 | 70 to 320 | Jacob and FC |
| Klein Karoo | Peninsula/Nardouw | Kotze (2000) | 1×10-4 to1×10-2 | 10 to 200 | FC |
| St Francis-on-sea | Nardouw | Rosewarne (1990) | 1.8×10-3 to 3.3×10-3 | 55 | Gringarten & Witherspoon |
| Rawsonville | Peninsula | UWC Groundwater Group (2006 to 07) | 6.9×10-4 to 2.8×10-5 | 9 to 30 | Cooper-Jacob, fault bounded |
| * Flow characteristics method | | | | | |

**Table 3-6** Recommended storativity values for TMG aquifers (Jia, 2007)

| Aquifer Type | Range | Storativity | |
|---|---|---|---|
| | | Specific yield (Unconfined) | Storage coefficient (Confined) |
| **Nardouw** | Low | $7.0\times10^{-5}$ | $7\times10^{-6}$ |
| | Medium | $3.5\times10^{-4}$ | $7\times10^{-5}$ |
| | High | $3.5\times10^{-3}$ | $7\times10^{-4}$ |
| **Peninsula** | Low | $1\times10^{--4}$ | $1\times10^{-5}$ |
| | Medium | $5\times10^{--4}$ | $1\times10^{-4}$ |
| | High | $5\times10^{-3}$ | $1\times10^{-3}$ |

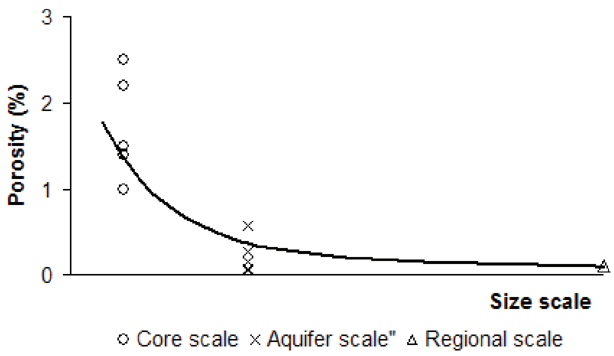


**Fig. 3-26** schematic depiction of scale effects on porosity in the TMG

## *3.8 Transmissivity of the TMG*

### 3.8.1 Theoretical Background of Analytical Methods

In a flow system the permeability (*k*) of the aquifer is one of the key hydraulic parameters that characterizes the aquifer's ability to transmit groundwater from a high hydraulic head point to a lower one. The hydraulic conductivity (*K*) is often used to represent aquifer's permeability. When the aquifer thickness (D) is taken into account, the transmissivity (*T*) term can be used. This parameter of permeability is meaningful for groundwater management for a specific aquifer. The relationship between K, *k*, D and *T* is as follows:

$$K = k \cdot \frac{\rho g}{v}, \quad T = KD, \qquad (3\text{-}8),$$

in which, $v$ is dynamic viscosity of fluid (N·s/m$^2$).

In general, well pumping tests provides an effective approach for estimating the average transmissivity of an aquifer; this approach is largely based on standard methods such as the Dupuit, Hantush and Theis solutions, for a broad variety of aquifers and different boundary conditions (Renard, 2005). The most common interpretation techniques based on the Theis solution include straight line analysis and type curve matching of observed drawdown. This simplified Theis is generally termed the Cooper-Jacob well function and normally causes less than a 5% error in drawdown when $u<0.1$. This drawdown can be alternatively presented as:

$$\begin{cases} s == a_p + b_T \log t \\ a_p = b_T \log \dfrac{2.25T}{r^2 S}, \quad b_T = 0.183 \dfrac{Q}{T} \end{cases} \tag{3-9}$$

During a constant discharge pumping test, the drawdown ($s_i$) and time ($t_i$) are recorded in the form of unequally spaced data. Assuming the relationship between drawdown $s$ and log time $t$ is linear as described in Eq. (3-9), using straight-line techniques the determination of parameters $a_p$ and $b_T$ in Eq. (3-9) may be carried out by means of least-square method from which $T$ and $S$ are estimated. In a single well test, given a well of $r_w$, parameters $a_p$ and $b_T$ are determined as follow:

$$b_T = \frac{n\sum_{i=1}^{n}(s_i \cdot \log t_i) - \sum_{i=1}^{n} s_i \sum_{i=1}^{n} \log t_i}{n\sum_{i=1}^{n}(\log t_i)^2 - (\sum_{i=1}^{n} \log t_i)^2}, \quad a_p = \frac{\sum_{i=1}^{n} s_i - b_T \sum_{i=1}^{n} \log t_i}{n} \quad (i = 1,2,...,n) \tag{3-10}$$

This kind of straight-line technique is frequently used to estimate both aquifers' transmissivity and storativity with data from pumping tests. However, problem arises when the observed data set do not follow a straight line.

### 3.8.2 Results from hydraulic test

In the TMG fractured aquifers, $T$ values estimated by methods using the Theis formula generally fall in a wide range from 9 to 400 $m^2/d$ – a range of two orders of magnitude (Table 3-5). From these results, it is extremely difficult to establish a regional understanding of the aquifer properties. The variation in the $T$ values is largely due to the complexity of the aquifers with diverse hydrogeological settings, reflecting the anisotropic nature of the hydraulic properties from both site to site, and even borehole to borehole at a single site

By considering the observed drawdowns during pumping tests in the TMG aquifers, it is possible to conceptualize four categories of drawdown curves (Fig. 3-27). These categories represent different modes of aquifer response to stresses by pumping tests:

a) Approximate straight-line type with the linear relation of drawdown with log time, for which the straight-line interpretation technique cab be applied
b) Stepwise drawdowns commonly observed during constant-discharge pumping tests in the TMG fractured aquifers, from which estimation of aquifer hydraulic properties

generally yields multiply results; and applicability of the *T* and *S* values seem to be very limited

c) An "S"-type of drawdown curve, from which the early-time and late-time *T* and *S* values are generally calculated to represent the intrinsic aquifer properties

d) This type of drawdown curve is seldom observed in the TMG aquifers, the determined *T* and *S* values can be very small

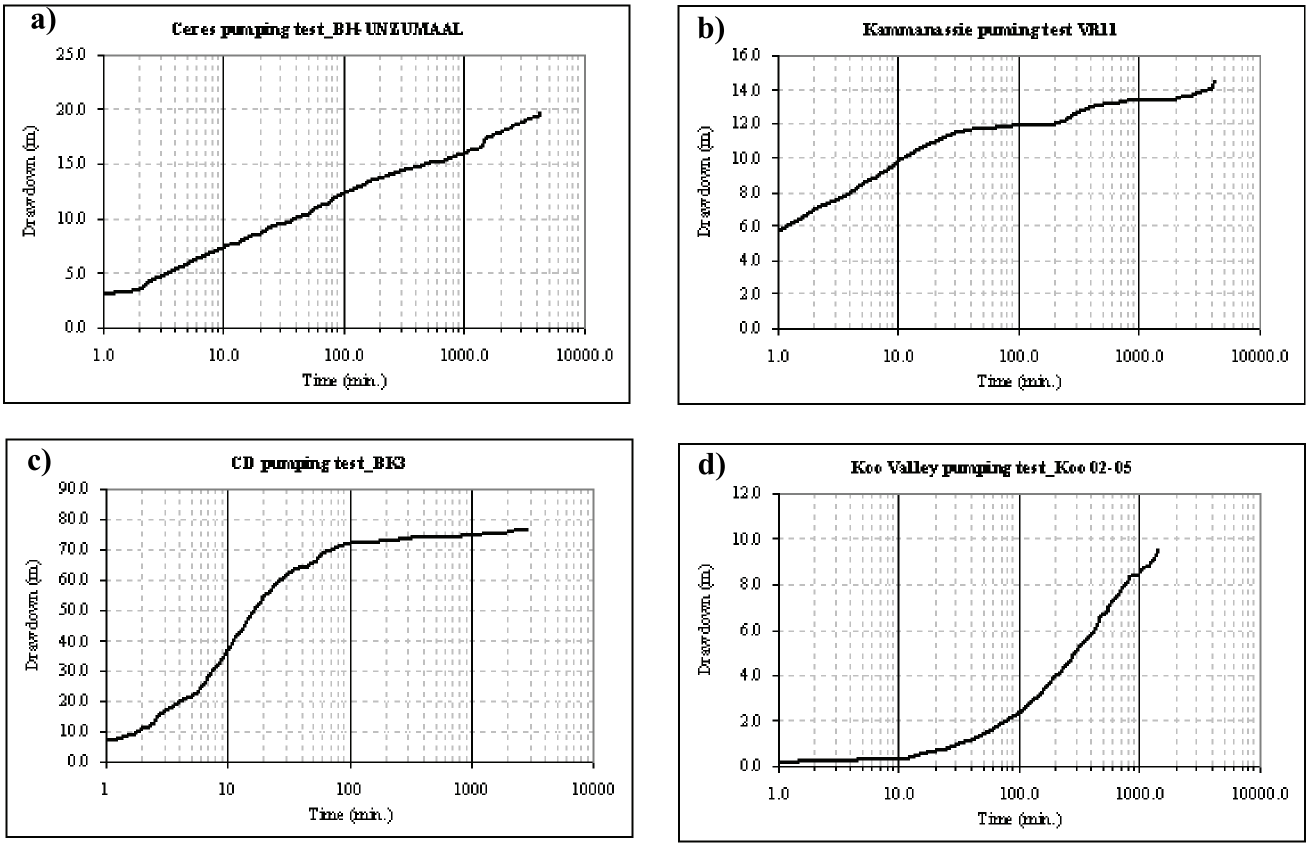


**Fig. 3-27** Four general types of observed drawdowns and log time plots for pumping tests in the TMG

### 3.8.3 Discussion of hydraulic tests

The mechanism of aquifer response to pumping test was not considered in previous studies of the TMG in which the estimation and explanation of aquifer's hydraulic properties are largely based on the analysis of drawdown curves. As discussed above (Fig. 3-27), a drawdown curve of type-a can be regarded as a drawdown behavior in a relatively homogeneous aquifer with a sharp response to the external stress, being similar to that of pumping test in porous media. Drawdown curves of type-b and type-c commonly show the aquifer response to well water abstraction that is lagging tens of minutes behind the commencement of the test. According to Van Tonder et al. (2002), the initial stage in both type-b and type-c is attributed to the well bore storage and skin effects. This means that the hydraulic properties must be estimated with the data collected at the late time. After these effects, drawdown of type-b and type-c might divert to a "stepwise flow" and a radial flow respectively; at the late stage the latter can be regarded to be similar to that of type-a. The type-d can be conceptualized as flow to the pumping well is from an aquifer with a closed boundary, or flow from the main fracture system only, and probably has the least hydrogeological significance in terms of water supply.

The stepwise type of drawdown is very common in the TMG sandstones, and many other fractured rock aquifers in South Africa, and is often explained as being set off by multiple boundary effects. It can be assumed that, along with the expansion of the cone of depression, multiple fracture flow systems with different hydraulic properties tend to provide water to a pumping well due to the change in pressure head, as schematically illustrated in Fig. 3-28. Based on this assumption, it is necessary to take a look at the contribution to the cone of depression made by different fracture flow systems at a given time. Simplified from Theis, we have:

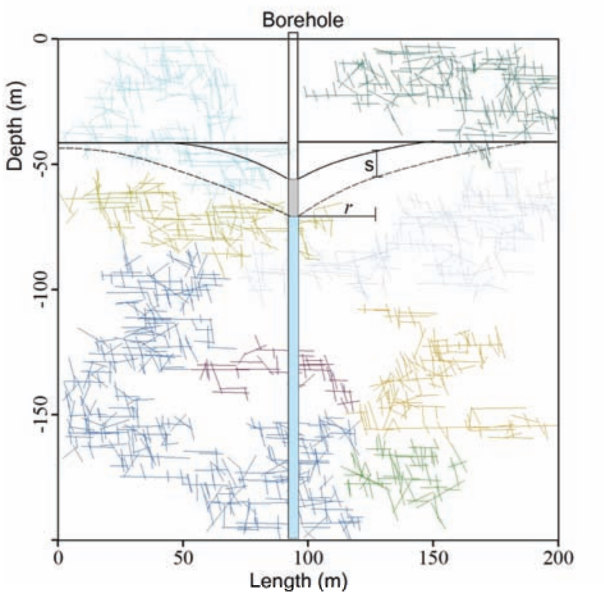

**Fig. 3-28** Schematic section showing the expansion of the depression cone in fracture flow systems

$$s = \frac{Q}{2\pi T} \ln \frac{1.5(T_f \cdot t / S_f)^{1/2}}{r} \tag{3-11}$$

in comparison with the drawdown of the Dupuit formula, the radius $R$ of the cone at the given time $t$ is:

$$R = 1.5(\frac{T_f t}{S_f})^{1/2} \tag{3-12}$$

in which $T_f$ and $S_f$ is, respectively, equivalent transmissivity and storativity. These parameters represent the averages of the hydraulic properties of fracture networks involved in the flows to the abstraction well.

The analysis of pumping data based on the above solutions should also integrate with the field geological observations. As has been discussed, almost all the wellfields developed in the TMG are fault-related, but very few site-specific studies in the TMG area have taken such structures into account when using the Theis or Cooper-Jacob methods to estimate both $T$ and $S$ values. In general, when a fault acts as a no-flow boundary, the image well method

(Ferris et al., 1962) can be applied by positive superposition of the drawdown of the image well at the pumping well. Using this method, the *T* and *S* values have been estimated for the Gevonden site using the data from pumping test. The result listed in Table 3-5 shows that, in comparison with an infinitely extended aquifer model at this site, the *T* values estimated from the fault-barricaded aquifer are much higher, but the *S* values almost go to the lower limit for TMG aquifers.

## 3.9 Hydraulic conductivity of the TMG aquifers

In terms of aquifer permeability, in-situ hydraulic tests yield the transmissivity or hydraulic conductivity as an average for the testing scale; for a pumping test this scale can be tens of metres, while the result of a packer test normally represents the scale of metres. As groundwater flow is largely controlled by fractures or fracture networks in a fractured rock aquifer, the directional hydraulic conductivity is crucial in the characterization of flow in an anisotropic aquifer.

### 3.9.1 Anisotropic fracture flow – theoretical challenges and proposed solution

Darcy's law is always used to estimate the groundwater flow in both porous and fractured media, and depends on realistic estimates of aquifer hydraulic conductivities and hydraulic gradients at the scale of problem. With respect to a fracture set with a mean aperture of *b* and a parallel face distance of *d*, the following classic expression is adopted for flow through the set of conduits (Talobre, 1957; Jaeger, 1972):

$$q = \frac{gb^3}{12\mu d} \cdot J \qquad \text{(3-13)}$$

where $\mu$ is the kinetic viscosity of fluid ($10^{-6}$ $m^2/s$ for water at 20ºC), *g* the acceleration of gravity and *J* hydraulic gradient.

Eq. (3-13) represents an idealized type of flow behavior that has been intensively studied, both experimentally and numerically, by many researchers. The term of $gb^3/12\mu d$ in Eq. (3-13) is usually referred to as the hydraulic conductivity *K* for the set of fractures involved. For the determination of *K* value, many theories and methods have been developed. These can be grouped into three main methodologies:

1) *K* tensor approach based on statistic or stochastic methods of *in-situ* fracture geometry and physical measurements
2) Fracture property field and laboratory tests for the parameter K evaluation.

3) Inverse analysis of continuous or discontinuous problems depending on numerical models and parametric calibrations

The estimation of $K$ values through either pumping or packer test is based on the assumption that the groundwater is flowing through a geological continuum. It is often an expensive exercise to use local scale hydraulic tests as the basis for estimating and predicting regional aquifer properties. In addition, the large variation in $K$, both at boreholes between boreholes, usually makes it difficult to determine the representativeness of the parameters for regional ground water assessments. Even where a representative elementary volume (*REV*) can be defined, it may not be appropriate to directly apply the local test results to a regional aquifer. In porous media the *REV* can be very small, whereas in fractured media the *REV* may be very large or may not even exist in some cases (Kulatilake and Panda, 2000; Wang et al., 2002).

Statistical methods for determining hydraulic conductivity tensors were developed in 1980s (Hsieh and Neuman, 1985; Oda, 1985; Tian, 1988). The results from these methods can successfully indicate 3-D principle $K$ values and directions by means of coordinate rotation of data derived from the surface measurements. The initial assumptions of the tensor approach include:

1) groundwater flow is exclusively governed by fractures
2) the fractures through a rock matrix are well-connected
3) Flows between fracture sets do not interfere, or no deflection flow occurs

For the ideal flow pattern with $M$ sets of fractures involved in a study area, the hydraulic conductivity of the fracture sets is expressed in the form of a matrix which reflects a form of flow superposition:

$$\begin{cases} \overline{\overline{K}} = \sum_{i=1}^{M} \frac{g b_i^3}{12 \mu d_i} \cdot K_{jl}^i, \quad j,l = x,y,z \\ K_{jl}^i = [I - \overline{n}^T \cdot \overline{n}] \end{cases} \tag{3-14}$$

where $\overline{\overline{K}}$ is the $K$ tensor matrix accounting for the anisotropic nature of studied media, $I$ is the unit matrix, and $\overline{n}$ is the direction cosine vector whose components are expressed in terms of the dip azimuth $\beta$ and dip angle $\alpha$ of the fracture sets in the coordinate system where the x, y axes are pointing to the north and east direction, respectively, while z axis is pointing upward. The elements of the matrix are depended on the geometric and physical parameters of fractures, which were studied by others (Tian, 1989). From Eq. (3-14) two key $K$ parameters, namely principal $K$ values and orientations, and their corresponding composite $K$ value can be estimated by employing the techniques of linear algebra.

However the complexity of $K$ in fractured rocks is far beyond what the existing models could handle since there are many geometrical and mechanical factors that impact on the flow through fracture gaps (Snow, 1969; Cook, 2001). Among them, fracture aperture is known to be most critical in controlling the quantity of flow, and so the study apertures became a focal point of this study. The factors affecting the aperture of fractures include geometrical and mechanical properties of the fracture walls such as rigidity, roughness, mineral fillings, and stress levels surrounding the fractures, in which the roughness has a crucial impact on the aperture around surface zone (Lomize, 1951; Louis, 1974; Patir and Cheng, 1978). Therefore, an expression of equivalent aperture due to roughness is suggested to calibrate the original $K$ tensor model. By taking into account crustal stress, lithostatic and hydraulic pressures that act on fractures, together with the equivalent aperture, an expression of hydraulic aperture can be developed for model calibration purposes.

### 3.9.2 Methodology

#### 3.9.2.1 Adaptation of hydraulic conductivity tensor approach

The direction of groundwater velocity ($V$) and hydraulic gradient ($J$) is usually not coincident with each other over time in fractured rock media. There is an included angle $\theta$ between $V$ and $J$, and the $J$ component on flow direction is

$$J_V = J \cdot \cos\theta \tag{3-15}$$

In an anisotropic medium, $K$ is not a scalar any more compared with an isotropic medium. The flow velocity is correspondingly expressed as follows:

$$\left.\begin{aligned} \vec{V}_x &= -(K_{xx}\frac{\partial H}{\partial x} + K_{yx}\frac{\partial H}{\partial x} + K_{zx}\frac{\partial H}{\partial x})\boldsymbol{i} \\ \vec{V}_y &= -(K_{xy}\frac{\partial H}{\partial y} + K_{yy}\frac{\partial H}{\partial y} + K_{zy}\frac{\partial H}{\partial y})\boldsymbol{j} \\ \vec{V}_z &= -(K_{xz}\frac{\partial H}{\partial z} + K_{yz}\frac{\partial H}{\partial z} + K_{zz}\frac{\partial H}{\partial z})\boldsymbol{k} \end{aligned}\right\}. \tag{3-16}$$

Where $\boldsymbol{i}$, $\boldsymbol{j}$ ,$\boldsymbol{k}$ are the unit vectors on coordinate x, y, z respectively. Its parameter term is generally presented in the form:

$$\overline{\overline{K}} = \begin{bmatrix} K_{xx} & K_{xy} & K_{xz} \\ K_{yx} & K_{yy} & K_{yz} \\ K_{zx} & K_{zy} & K_{zz} \end{bmatrix} \tag{3-17}$$

Eq. (3-17) is the hydraulic tensor matrix, in which $K_{xy}$=$K_{yx}$, $K_{yz}$=$K_{zy}$, and $K_{xz}$=$K_{zx}$. Note that in Eq. (3-14) the expression of the row matrix $\bar{n}$ is:

$$\bar{n} = [\cos\beta_i \sin\alpha_i \quad \sin\beta_i \sin\alpha_i \quad \cos\alpha_i], \quad i = 1,\cdots,M. \tag{3-18}$$

The above $\overline{\overline{K}}$ is a symmetric square matrix with three different eigenvalues and corresponding orthogonal eigenvectors satisfying the following relation:

$$(K_{ij} - \lambda_i \delta_{ij})U_i = 0, \quad U_i = [U_{ix} \quad U_{iy} \quad U_{iz}]^T, \quad i = 1,2,3. \tag{3-19}$$

where $\delta_{ij}$ is Kronecker's symbol, $\lambda_i$ the eigenvalues and $U_i$ is the corresponding eigenvectors associated to $\lambda_i$. Eq. (3-18) is the representative of a homogeneous equation group and the solutions of $\lambda_i$ and $U_i$ ($i$=1, 2, 3) may be obtained from (3-20) and (3-21) respectively.

$$|K - \lambda I| = 0 \tag{3-20}$$

$$\begin{cases} (k_{xx} - \lambda)U_x + k_{xy}U_y + k_{xz}U_z = 0 \\ k_{yx}U_x + (k_{yy} - \lambda)U_y + k_{yx}U_z = 0 \\ k_{zx}U_x + k_{zy}U_y + (k_{zz} - \lambda)U_z = 0 \\ U_x^2 + U_y^2 + U_z^2 = 1 \end{cases} \tag{3-21}$$

Using $U_i$ ($i$=1,2,3) as the basic vectors, the $K$ tensor reduces to the diagonal matrix:

$$\overline{\overline{K'}} = diag[\lambda_1, \quad \lambda_2, \quad \lambda_3] \tag{3-22}$$

Hydrogeologically λi ($i$=1, 2,3) represent three principal $K$, namely $K_{p1}=\lambda_1$, $K_{p2}=\lambda_2$ and $K_{p3}=\lambda_3$, and the direction of $K_{pi}$ is given by $Ui$. Whereby, the $K$ value of a given sample site can be represented by the geometric mean of the three principal $K$:

$$K_{comp} = \sqrt[3]{K_{p1} \cdot K_{p2} \cdot K_{p3}} \tag{3-23}$$

Furthermore, the relationship between $K$ components $K_x$, $K_y$ and $K_z$ along x, y, and z axes defined above and principal $K$ tensor can be established via $U_i$

$$\begin{cases} K_x = K_{p1}U_{1x}^2 + K_{p2}U_{2x}^2 + K_{p3}U_{3x}^2 \\ K_y = K_{p1}U_{1y}^2 + K_{p2}U_{2y}^2 + K_{p3}U_{3y}^2 \\ K_z = K_{p1}U_{1z}^2 + K_{p2}U_{2z}^2 + K_{p3}U_{3z}^2. \end{cases} \tag{3-24}$$

Assuming that the flow direction is known (Fig. 3-27), using Eqs (3-15) and (3-16) we have the following expression for $K$ along flow direction:

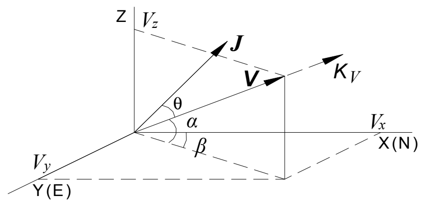


**Fig. 3-29** Relationship between flow direction and hydraulic conductivity.

$$K_V = \frac{\vec{V} \cdot \vec{V}}{\vec{V} \cdot \vec{J}} = \frac{(K_x \frac{\partial H}{\partial x}\boldsymbol{i})^2 + (K_y \frac{\partial H}{\partial y}\boldsymbol{j})^2 + (K_z \frac{\partial H}{\partial z}\boldsymbol{k})^2}{K_x(\frac{\partial H}{\partial x}\boldsymbol{i})^2 + K_y(\frac{\partial H}{\partial y}\boldsymbol{j})^2 + K_z(\frac{\partial H}{\partial z}\boldsymbol{k})^2} = \frac{1}{\frac{1}{V^2}(\frac{V_x^2}{K_x} + \frac{V_y^2}{K_y} + \frac{V_z^2}{K_z})} \tag{3-25}$$

Alternatively, using the projective relations of $V_x/V=cos\beta\cdot sin\alpha$, $V_y/V=sin\beta\cdot sin\alpha$ and $V_z/V=cos\alpha$ (see Fig. 3-29), one may also write that

$$\frac{1}{K_V}=\frac{\cos^2\beta\sin^2\alpha}{K_x}+\frac{\sin^2\beta\sin^2\alpha}{K_y}+\frac{\cos^2\alpha}{K_z}. \quad (3\text{-}26)$$

The above analyses indicate that the three types of $K$ values, namely geometric mean of $K_{pi}$ ($i$=1,2,3), axial $K_j$ ($j$=x,y,z) and flow direction $K_V$, are physically different. However, they are related through the $K$ tensors and vector projections. The former ($K_{comp}$) may be accounting for the $K$ value at a measuring site in the form of scalar that is averaged from three anisotropic principal $K_{pi}$. The $K_i$ ($i$=x,y,z) are the projections of three principal $K_{pi}$ along original system. Note that the quantity of $K_V$ is not simply the quadratic sum of $K_i$ ($i$=x,y,z) as it used to be because the flow direction $K$ is more physically determined by the components of flow velocity and head gradient than geometrically determined by axial $K$. There exists a non-linear relationship between $K_V$ and $K_i$ ($i$=x,y,z). Accordingly, if there exist not less than two sets of known values of $K_V$ and $K_i$ ($i$=x,y,z) obtained from hydraulic tests and surface measurements respectively, it is possible to deduce the flow direction using the following linear equation:

$$(K_x^{re}-K_y^{re})x_1+(K_y^{re}-K_z^{re})x_2=K_V^{re}-K_z^{re} \quad (3\text{-}27)$$

where $x_1=\cos^2\beta\sin^2\alpha$, $x_2=\sin^2\alpha$, $K_V^{re}=1/K_V$, $K_i^{re}=1/K_i, i=x,y,z$.

The above-mentioned equations have been programmed in an MS Excel Workbook. For the model testing, the basic data were measured at sites of *TMG* outcrops. The aperture (*b*) and distance (*d*) are geometric mean values and the angles arithmetic ones. The computed results, using the above-mentioned models, are listed in Tab.3-7. The geometric mean of $K$ in Tab.3-7 ranges from 1 to 21 m/d which is much higher than those of borehole tests mostly ranging from $5\times10^{-2}$ to $1.5\times10^{-3}$ m/d. This is because of the inevitable magnification of results when applying the measured data to the smooth plate model. Particularly the apertures, measured at road cuttings and open quarries where the fractures that have long been undergone disturbance and stress release, tend to be dilated compared to their original status.

The tensor method provides a tool to estimate $K$ values for well-connected and fractured rocks. It is usually applied to the rock formations without considering relevant hydraulic test data. For purely fractured rocks the method may lead to the overestimate of $K$ values when the fractures are not fully connected, while it can underestimate $K$ values for fractured porous media with significant permeability in matrix rocks. Although the $K$ from the tensor approach may account for the anisotropic nature of studied media, it should be noted that the basic data for the $K$ computations are mean values of fracture sets. No matter what types of mean values are taken in the calculation, they are derived from in-situ measurements; so the accuracy of the computed *K* is dependent on the quality of the measurements. In particular, the aperture usually measured by feeler gauge on a rock exposure is the most sensitive factor in determining *K*. To minimize the possible influences of weathering or disturbance, multiple readings of aperture value need to be taken at a single fracture. Moreover, JRC (joint roughness coefficient) can be sensitive to the *K* values; thus both the field-scale length profiles and the lab-scale core fractures need to be comparatively scanned to estimate JRC.

**Table 3-7** Calculated *K* values from surface fracture measurements

| *K* Values / Site No. | Principal *K* values (m/d) | | | | Axial *K* values (m/d) | | |
|---|---|---|---|---|---|---|---|
| | $K_{p1}$ | $K_{p2}$ | $K_{p3}$ | Geometric mean | $K_x$ | $K_y$ | $K_z$ |
| 1-Robertson | 2.313 | 1.880 | 0.437 | 1.239 | 1.940 | 2.029 | 0.662 |
| 2-Simon's Town | 13.816 | 11.858 | 2.176 | 7.091 | 13.039 | 12.261 | 2.550 |
| 3-Bot Rivier | 38.538 | 31.257 | 8.622 | 21.818 | 23.741 | 26.521 | 28.153 |
| 4-Grabouw | 13.258 | 11.804 | 1.869 | 6.639 | 11.121 | 10.263 | 5.549 |
| 5-Theewaterskloof | 6.355 | 6.007 | 0.543 | 2.748 | 1.554 | 5.507 | 5.844 |

### 3.9.2.2 Calibration of hydraulic conductivity tensor method

Equation (3-13) for groundwater flow in fractures is derived from the Navier-Stokes differential equation for pressure-induced laminar flow between two flat parallel plates where the hydraulic aperture is assumed to be uniform. The actual conditions in the TMG are quite different, as the rocks, including fractures, have undergone phases of deformations and distortions. What can be measured at rock outcrops is the mechanical aperture (Olsson and Barton, 2001) mostly ranging from 1 to $10^{-3}$ mm. The hydraulic aperture discussed here is regarded as the effective aperture for groundwater flow and can be obtained or inferred from both tracer tests (Charles, 1988) and laboratory experiments. Taking into account the main influencing factors, i.e. roughness and stress condition, Eq. (3-14) can be rewritten by adding the correction coefficients due to fracture roughness and stress condition respectively:

$$\overline{\overline{K}} = \sum_{i=1}^{M} \frac{gb_i^3}{12\mu d}_i C_{er} \cdot C_{es} \cdot K_{jl}^i , \quad j,l = x,y,z \cdot \tag{3-28}$$

Where $C_{er}$ is the correction coefficient of roughness and $C_{es}$ the correction coefficient of stress condition. From Eq. (4-28), it can be shown that the hydraulic aperture is the following:

$$b_h = (C_{er} \cdot C_{es})^{1/3} b. \tag{3-29}$$

Let $b_{er}=C_{er}^{1/3}b$, where $b_{er}$ may be regarded as the equivalent aperture due to fracture roughness. Correspondingly, let $b_{es}= C_{es}^{1/3}b_{er}$, where $b_{es}$ is the equivalent aperture due to stresses acting on the rough fracture surface, namely the hydraulic aperture. The following sections are focused on the discussion and determination of the $C_{er}$ and $C_{es}$, respectively, with the objective of calibrating the tensor model.

**1. Fracture roughness**

In the TMG rocks, fractures have rough walls and variable apertures. The influence of roughness on fracture apertures has long been discussed and analyzed by many others. Among them the important contributions are those of Lomize (1951), Louis (1974) and Barton et al. (1985). A compilation of their formulae for aperture correction coefficient due to roughness is listed in Table.3-8. A comparison of *K* values obtained from the different models is plotted in Fig. 3.30.

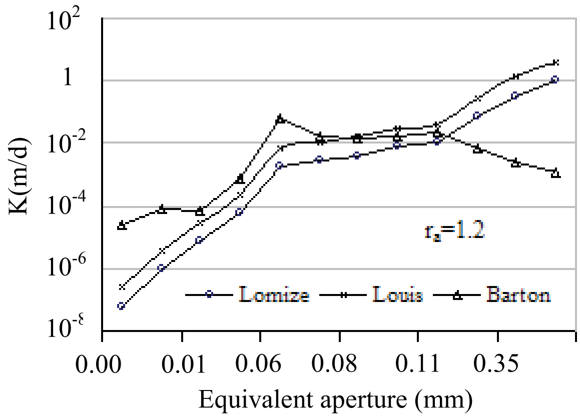


**Fig. 3-30** *K* Versus $b_{er}$ according to various roughness models using data measured from the TMG sites

**Table 3-8** Mechanical aperture correction coefficient $C_{er}$

| Formula | Source | Remark |
|---|---|---|
| $C_{er}=\frac{1}{1.0+6.0(r_a)^{1.5}}$ | Lomize (1951) | $r_a$—relative roughness<br>$r_a=\Delta/b$, Δ-asperity |
| $C_{er}=\frac{1}{1.0+8.8(r_a)^{1.5}}$ | Louis C (1974) | $r_a=\Delta/D_h$, $D_h$-hydraulic radius |
| $C_{er}=\frac{b^3}{(JRC)^{7.5}}$ | Barton et al. (1985) | b—mechanical aperture (mm)<br>*JRC*—joint roughness coefficient |

Given the parameter measurements, it seems more practicable to apply Barton's *JRC* model for macroscopic fracture sets. That is

$$b_{er}=\frac{b^2}{JRC^{2.5}} \tag{3-30}$$

in which $b$ is the mechanical aperture measured by a feeler gauge and *JRC* is the joint roughness coefficient, measured with a profile meter, and $b_{er}$ is the equivalent aperture calibrated by roughness.

It used to be assumed that groundwater flow is dominated more by bedding fractures within the zone of weathered bedrock than by structural joints because of the larger mechanical apertures within the bedding fractures. However in most of the *TMG* rocks around the measuring sites, the bedding fractures tend to have a relatively higher *JRC* value in the range of 2~6. Comparatively, the *JRC* of the structural or conjugate joints is mainly in the range of 1~3. By applying the equivalent aperture $b_{er}$ to the tensor model introduced, the difference of *K* values between bedding and structural fractures is quite small and the results are listed in Table 3. Note that the *K* value for the joint set at site 5 is about one order of magnitude higher as that of bedding fractures. It is attributed to the relatively rougher surfaces in bedding fractures producing more impedance to flow than that of structural joints even though bedding fractures are much longer than structural joints.

**Table 3-9** *K* values for bedding and structural fractures

| Index | Bedding Fracture | | Structural joint set | |
|---|---|---|---|---|
| Site No. | Mean JRC | Mean K (m/d) | Mean JRC | Mean K (m/d) |
| **2** | 3.5 | $4.35\times10^{-4}$ | 1.4 | $3.88\times10^{-4}$ |
| **4** | 3 | $8.21\times10^{-4}$ | 1.5 | $7.13\times10^{-4}$ |
| **5** | 3.5 | $9.29\times10^{-5}$ | 1.25 | $2.681\times10^{-4}$ |

The impacts of roughness due bedding and structural fractures on *K* values at the *TMG* sites are shown in Table 3-9. The *K* results in Table 3-10 are roughly consistent with those from pumping tests in the *TMG* aquifers.

**Table 3-10** Fracture *JRC* and corresponding *K* values

| Index / Site No. | Mean JRC | Mean Length (m) | Mean *K* (m/d) | Axial *K* (m/d) | | |
|---|---|---|---|---|---|---|
| | | | | $K_x$ | $K_y$ | $K_z$ |
| **1** | 1.7 | 29.2 | $1.45\times10^{-3}$ | $6.05\times10^{-3}$ | $5.24\times10^{-3}$ | $9.70\times10^{-4}$ |
| **2** | 2.4 | 34.74 | $2.33\times10^{-3}$ | $3.02\times10^{-3}$ | $2.33\times10^{-3}$ | $2,04\times10^{-3}$ |
| **3** | 2.2 | 9.25 | $1.623\times10^{-2}$ | $1.88\times10^{-2}$ | $2.18\times10^{-2}$ | $2.13\times10^{-3}$ |
| **4** | 2.3 | 20.50 | $1.47\times10^{-3}$ | $2.06\times10^{-3}$ | $1.03\times10^{-3}$ | $1.62\times10^{-3}$ |
| **5** | 2.4 | 14.52 | $1.77\times10^{-3}$ | $2.04\times10^{-3}$ | $1.16\times10^{-3}$ | $2.95\times10^{-3}$ |

## 2. Combined stress conditions

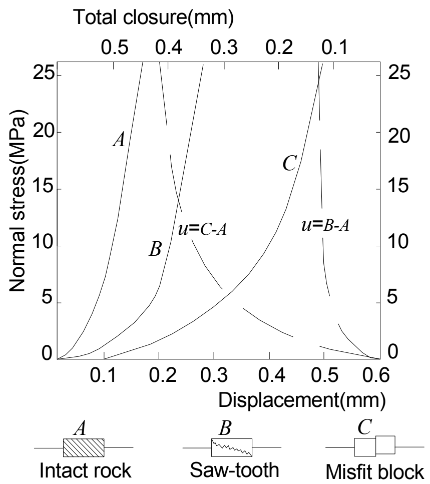


**Fig. 3-31** Rock mass displacement and fracture closure under normal stress (after Goodman, 1974)

The properties of a rock mass may change substantially under a certain stress or confined conditions, as opposed to those on the surface. In most cases, crustal stresses or lithostatic pressure acting on a rock mass tends to cause volumetric reduction. The functional dependency of rock properties with respect to the change in stresses or confined conditions has been studied by many researchers (Goodman, 1974; Bandis et al., 1983). In terms of hydromechanical coupling in fractured rocks, Rutqvist and Stephansson (2003) give a full review that can be traced back to Jacob's storativity expression in 1940s. Bandis et al. (1983) establish an expression for fracture displacement under normal stress conditions:

$$u_n = \frac{\sigma_N u_{\max}}{K_{ni} u_{\max} + \sigma_N} \tag{3-31}$$

In this expression, $u_n$ is the displacement under the normal stress $\sigma_N$ acting on the fracture surface, $K_{ni}$ the initial normal stiffness of fracture and $u_{max}$ is the maximum closure (Fig. 3-31). For shear tests of fractures, Barton et al. (1985) also develop an empirical formula to express the relationship between normal and shear displacements:

$$du_{ns} = du_s \tan d_m \tag{3-32}$$

where $d_m$ is the mobilized dilatation angle and it can be determined as follow (Olsson and Barton, 2001):

$$d_m = \frac{1}{M} JRC_m \log_{10}(JCS/\sigma_N) \tag{3-33}$$

where $M$ is the damage coefficient, $JRC_m$ the mobilized joint roughness coefficient, and $JCS$ the compressive strength of the joint wall.

It is assumed that an arbitrary fracture surface, with a dip azimuth of $\beta$ and dip angle of $\alpha$, is subject to a combined three dimension stresses $[\sigma_x, \sigma_y, \sigma_z, \tau_{xy}, \tau_{yz}, \tau_{zx}]^T$, the normal stress $\sigma_N$ and shear stress $\tau_s$ acting on the surface may be expressed as:

$$\begin{cases} \sigma_N = l^2\sigma_x + m^2\sigma_y + n^2\sigma_z + 2lm\tau_{xy} + 2mn\tau_{yz} + 2nl\tau_{zx} \\ \tau_s = [(l\sigma_x)^2 + (m\sigma_y)^2 + (l\sigma_z)^2 - \sigma_N]^{\frac{1}{2}} \\ l = \cos\beta\sin\alpha, \quad m = \sin\beta\sin\alpha, \quad n = \cos\alpha \end{cases} \tag{3-34}$$

In the present case, because rocks are normally subjected to compression by lithostatic pressure, it is convenient to denote the normal and shear stresses on the oblique fracture surface in the case of $\sigma_x = \sigma_y$.

$$\begin{cases} \sigma_N = \dfrac{\sigma_z + \sigma_x}{2} + \dfrac{\sigma_z - \sigma_x}{2}\cos 2\alpha + \tau_{zx}\sin 2\alpha \\ \tau_s = \dfrac{1}{2}(\sigma_z - \sigma_x)\sin 2\alpha + \tau_{zx}\cos 2\alpha \end{cases} \tag{3-35}$$

From which the maximum and minimum values of $\sigma_N$ and maximum value of $\tau_s$ may be obtained with respect to the derivatives of $\partial\sigma_N/\partial\alpha=0$ and $\partial\tau_S/\partial\alpha=0$:

$$\begin{cases} \dfrac{\sigma_{\max}}{\sigma_{\min}} = \dfrac{\sigma_z + \sigma_x}{2} \pm \sqrt{(\dfrac{\sigma_z - \sigma_x}{2})^2 + \tau_{zx}{}^2} \\ \tau_{\max} = \dfrac{\sigma_{\max} - \sigma_{\min}}{2} \end{cases} \tag{3-36}$$

Fractures mainly control the deformation of a rock mass, and they may respond to the change of normal or shear stresses even when no failures occur; these can be described by the relations between the stress and strain increments:

$$\begin{cases} d\sigma_N = K_n \cdot d\varepsilon \\ d\tau_s = G \cdot d\gamma \end{cases} \tag{3-37}$$

where $K_n$ ($kN/m$) is the stiffness of fracture walls, $k_n=E/(\pi L_f)$; $G$ is the fracture rigidity modulus, $G=E/2(1+v)$, $E$ the elastic modulus ($MPa$), $L_f$ the fracture length (m), and $v$ is the Poisson's ratio. Hence the increments of strain may be expressed in terms of the increments of displacement:

$$\begin{cases} d\varepsilon = du_n/(b_{er} - u_n) \\ d\gamma = du_s/b_{er} - u_s \end{cases} \tag{3-38}$$

in which $b_{er}$ is the equivalent aperture due to roughness, $u_n$ the normal displacement and $u_s$ shear displacement of the fracture. Combining Eqs (3-37) and (3-38) yields:

$$\begin{cases} d\sigma_N = \dfrac{K_n}{b_{er} - u_n} \cdot du_n \\ d\tau_s = \dfrac{G}{b_{er} - u_s} \cdot du_s \end{cases} \tag{3-39}$$

The first equation in Eq. (3-42) may be integrated with respect to $\sigma_N$ and $u_n$ respectively. This yields:

$$u_n = b_{er}[1 - \exp(-\frac{\sigma_N}{K_n})] \cdot \tag{3-40}$$

In the case of shearing displacement in Eq. (3-40), the integration may be performed using Eq. (3-35) ~ (3-36) and assuming that $d_m \approx tand_m$:

$$\int_0^{\tau_s} \frac{d\tau_s}{G} = \int_0^{u_{ns}} \frac{1}{b_{er} d_m - u_{ns}} du_{ns} \cdot \quad (3\text{-}41).$$

and thus:

$$u_{ns} = b_{er} \frac{1}{M} JRC_m \log_{10}(JCS / \sigma_N)[1 - \exp(-\frac{\tau_s}{G})] \quad (3\text{-}42)$$

Eqs (3-41) and (3-42) give expressions for the fracture displacement under normal stress and shear stress, respectively. Note that in these equations the normal stress term can be applicable to effective stress, i.e. $\sigma_e = \sigma_N - r_w h_w$. Considering the relationship between changed fracture aperture and the displacement under combined stress conditions, we have the hydraulic aperture $b_h$:

$$b_h = b_{er} - u_n + u_{ns} = b_{er} C_{es}^{1/3} \quad (3\text{-}43)$$

$$C_{es} = \{\exp(-\frac{\sigma_e}{K_n}) + \frac{1}{M} JRC_m \log(JCS / \sigma_e)[1 - \exp(-\frac{\tau_s}{G})]\}^3 \cdot \quad (3\text{-}44)$$

Using Eqs (3-29) and (3-30), the final hydraulic aperture expression obtained is:

$$b_h = b \cdot \frac{b}{JRC^{2.5}} \cdot \{\exp(-\frac{\sigma_e}{K_n}) + \frac{1}{M} JRC_m \log(JCS / \sigma_e)[1 - \exp(-\frac{\tau_s}{G})]\} \quad (3\text{-}45)$$

### 3.9.3 Application to the field data

It can be seen from the above hydraulic aperture expression that the hydraulic aperture is affected by both the physical and the mechanical properties of the fractures, particularly the roughness and the stress level on fracture walls. The importance of this hypothetical model is that most of fractured rocks in the TMG area (thicknesses up to 4500 m) are inaccessible with current investigation tools; and except for some wellfields that can be used for exploration purpose, the majority of TMG area is uninvestigated. To overcome this predictive models for hydraulic conductivity and flow behavior are necessary, and these might become key tools if validated.

#### 3.9.3.1 Hydraulic conductivity at borehole sites

The formulated model of hydraulic apertures was applied to the Rietfontein, Boschkloof and Gevonden borehole sites. Using the fracture data as listed in Table 3-11 and the basic properties of rock materials given in Fig. 3-32, the computed $K$ results are listed in Table 3-12. The hydraulic conductivity calculated for the Rietfontein site is $6.89 \times 10^{-4}$ m/d ($7.97 \times 10^{-9}$ m/s), the K for Boschkloof site is 4.00×$10^{-3}$ m/d (4.63×$10^{-8}$ m/s), and Gevonden site 5.45×$10^{-4}$ m/d (6.32×$10^{-9}$ m/s). The derived *K* for the Boschkloof site is much less than that obtained from pumping test; it is about one order of magnitude less than the *K* value estimated with pumping test data at the borehole BK3 from which the *K* was estimated as 1.9×$10^{-7}$ m/s using the FC method (Hartnady and Hay, 2002). However, in comparison with the packer test results from the borehole BH-1 and BH-2 at the Gevonden site, the average *K* value obtained through tensor method (6.32×$10^{-9}$ m/s) roughly matches the packer test results which mostly fall in the range of 6.14×$10^{-2}$ to 4.68×$10^{-5}$ m/d ($10^{-7}$ to $10^{-10}$ m/s) (Fig. 3-33). This suggests that the *K* value estimated by the tensor method possibly represents the hydraulic conductivity of fractured rocks at a relatively small scale, i.e. a scale of metres.

**Table 3-11** Data sets of fractures from surface measurements

| Site | Statistic mean / Item | | Dip $\beta$ (°) | Dip angle α (°) | Physical aperture (mm) | Spacing (mm) | Roughness (JRC) | Mean length (m) |
|---|---|---|---|---|---|---|---|---|
| Rietfontein | Basic data set | Set 1 | 66.80 | 6.42 | 0.22 | 463.30 | 2.20 | 12.55 |
| | | Set 2 | 67.43 | 78.28 | 0.15 | 290.00 | 1.20 | 8.86 |
| | | Set 3 | 205.30 | 71.07 | 0.17 | 271.10 | 1.40 | 6.99 |
| | | Set 4 | 157.25 | 77.11 | 0.03 | 437.20 | 1.00 | 5.16 |
| Boschkloof | Basic data set | Set 1 | 243.88 | 40.09 | 0.19 | 408.10 | 2.10 | 16.31 |
| | | Set 2 | 330.48 | 76.76 | 0.15 | 270.00 | 1.30 | 7.29 |
| | | Set 3 | 93.89 | 79.02 | 0.17 | 341.43 | 1.30 | 5.06 |
| | | Set 4 | 62.41 | 39.70 | 0.21 | 680.00 | 1.20 | 13.94 |
| | | Set 5 | 221.33 | 62.44 | 0.25 | 303.57 | 1.50 | 4.50 |
| Gevonden | Basic data set | Set 1 | 95.13 | 19.73 | 0.16 | 854.29 | 3.0 | 20.78 |
| | | Set 2 | 212.87 | 71.43 | 0.27 | 520.00 | 1.5 | 8.72 |
| | | Set 3 | 145.34 | 81.88 | 0.05 | 421.82 | 1.5 | 9.12 |
| | | Set 4 | 274.18 | 80.82 | 0.10 | 529.09 | 1.2 | 8.56 |
| Distribution | | | normal | normal | | uniform | | log-normal |

### 3.9.3.2 Hydraulic conductivity at depth

The decrease in hydraulic conductivity with depth perhaps implies that fractures tend to be closed with depth. Fig. 3-32 shows the relationship between the calculated hydraulic conductivity and depth at the three sites. It is clear that the reduction of hydraulic conductivity (K) with depth roughly follows a negative exponential law with different exponents. At the Rietfontein site, for example, the *K* value on the surface is 7×$10^{-4}$ (m/d), but then decreases to

$9.4\times10^{-6}$ (m/d), $1.29\times10^{-7}$ (m/d) and $8.2\times10^{-11}$ (m/d) at depths of 200 m, 400 m and 750 m, respectively. Unfortunately, there are no in-situ hydraulic test data available in this area to confirm the model predictions.

In 2006 some packer tests were conducted along with the core drilling in boreholes BH1 (from 19.2 m to 113 m) and BH2 (from 7 m to 200 m) at the Gevonden site where a network of five holes, which penetrate Peninsula formation and the bottom of the Nardouw subgroup of the TMG, has been established for the study of aquifer properties and groundwater monitoring. Fig. 3-33 presents the results of single-packer tests with a test interval of 6 m in the two boreholes. In comparison, the reduction of tensor-calculated *K* values with depth exceeds that that of packer tests. Although the *K* values are different, it is clear that the *K* generally decreases with depth. The relationship between hydraulic conductivity and depth for the two boreholes has the same pattern.

**Table 3-12** Computed *K* values based on the data set of Table 4-9

| | Item | | i=1 | i=2 | i=3 |
|---|---|---|---|---|---|
| **Rietfontein** | Principal K (m/d) | $K_{pi}$ (m/d) | $1.22\times10^{-3}$ | $1.01\times10^{-3}$ | $2.65\times10^{-4}$ |
| | | Dip (°) | 312.26 | 46.77 | 203.45 |
| | | Dip angle (°) | 9.43 | 25.31 | 62.75 |
| | Axial K | | $K_x=7.827\times10^{-4}$ | $K_y=5.923\times10^{-4}$ | $K_z=1.120\times10^{-3}$ |
| | Geometric mean of $K_{pi}$ | | $6.89\times10^{-4}$ | | |
| **Boschkloof** | ***Principal K (m/d)*** | $K_{pi}$ (m/d) | $5.92\times10^{-2}$ | $5.74\times10^{-2}$ | $3.18\times10^{-3}$ |
| | | Dip (°) | 205.410 | 135.463 | 249.662 |
| | | Dip angle (°) | 37.742 | 23.892 | 42.780 |
| | Axial K | | $K_x=4.53\times10^{-3}$ | $K_y=3.77\times10^{-3}$ | $K_z=4.17\times10^{-3}$ |
| | Geometric mean of $K_{pi}$ | | $4.00\times10^{-3}$ | | |
| **Gevonden** | ***Principal K (m/d)*** | $K_{pi}$ (m/d) | $2.528\times10^{-3}$ | $2.503\times10^{-3}$ | $2.567\times10^{-5}$ |
| | | Dip (°) | 32.179 | 123.115 | 213.221 |
| | | Dip angle (°) | 71.427 | 0.315 | 18.570 |
| | Axial K | | $K_x=9.470\times10^{-4}$ | $K_y=1.836\times10^{-3}$ | $K_z=2.274\times10^{-3}$ |
| | Geometric mean of $K_{pi}$ | | $5.457\times10^{-4}$ | | |

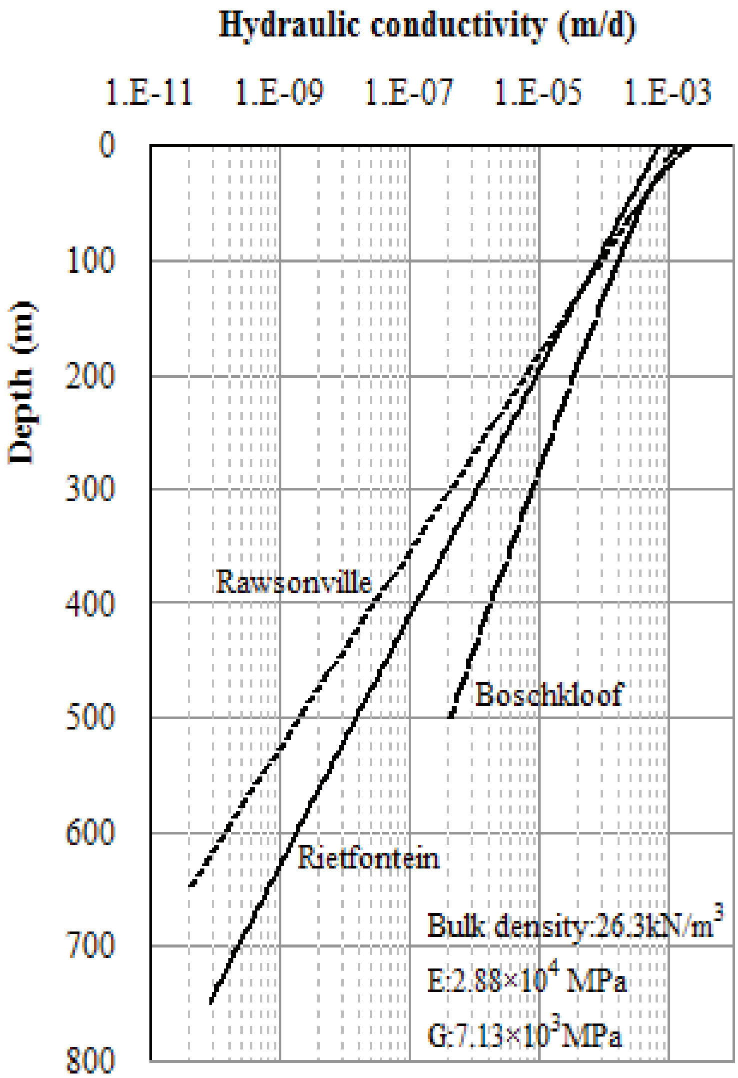


**Fig. 3-32** Hydraulic conductivity plot against depth of the Rietfontein, Boschkloof and Gevonden (Rawsonville) sites, using a tensor approach, based on the data measured on the surface and taking into account the impacts of fracture roughness and lithostatic pressure

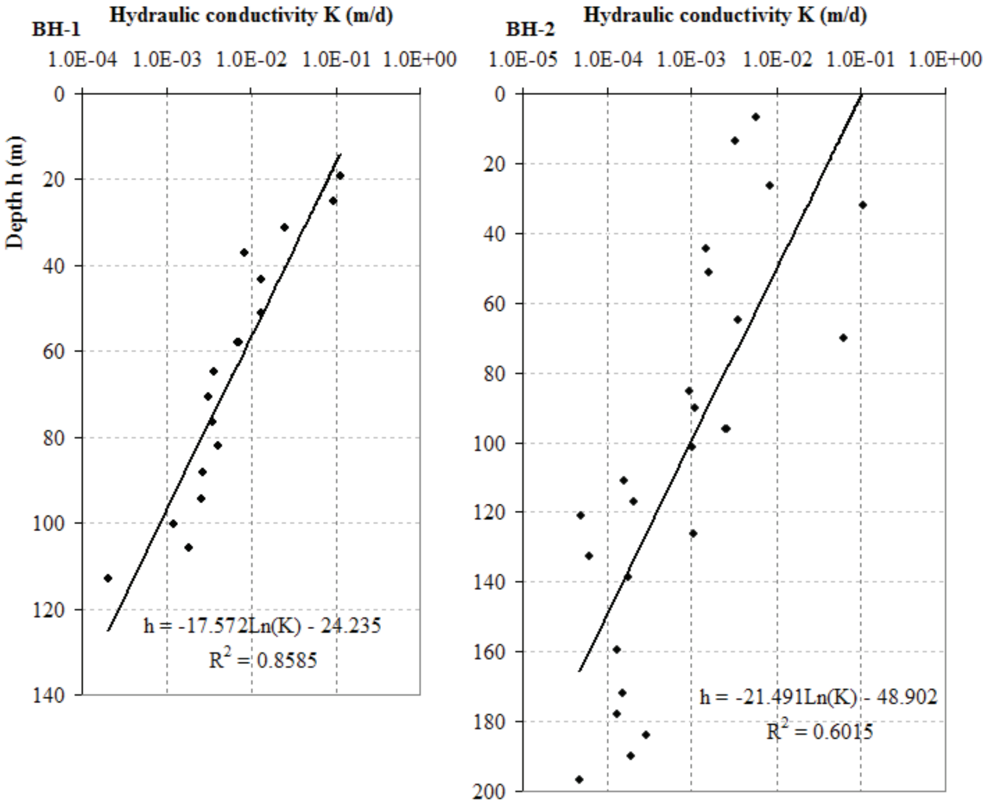


**Fig. 3-33** Hydraulic conductivity plot against depth of the TMG sandstone aquifer where single-packer tests were conducted with an interval of 6 m in boreholes BH1 and BH2 at the Gevonden site. In the trend line equations, h is the depth from the surface and $R^2$ the coefficient of confidence

# 4. Groundwater Flow Conceptualization and Quantification with Case Studies

## *4.1 Introduction*

Because of the complexity of the geometric and hydraulic properties of the TMG aquifers, the study of site-specific groundwater problems has been the main target for hydrogeologists involved in relevant research. So far the most thorough case study has concentrated on the Kammanassie wellfield, where carefully designed borehole networks have been developed, and investigations into aquifer properties (Kotze, 2002), groundwater recharge (Wu, 2005), numerical modeling for groundwater storage evaluation (Jia, 2007) have been carried out. Although discrepancies between the results of these studies have arisen as a result of the different project aims, the wealth of data produced is definitely helpful in understanding the fractured rock aquifers.

Between 2005 and 2006, a new groundwater research and monitoring site with a five-borehole network was established near Rawsonville. Research at this site is dedicated to the analyses of the field observations such as borehole core logging, groundwater monitoring, hydraulic tests, and the examination of fracture characteristics, with the objective of establishing a site-specific conceptual model for the estimation of the aquifer's hydraulic properties.

A number of ongoing research studies covering the broad type areas have been conducted, usually coinciding with existing wellfields where quantitative information can be correlated and analyzed. Based on these data, groundwater flow models may also be constructed. In this study the Kammanassie wellfield area is also selected as a case area to study the response of TMG aquifers to long-term pumping. Both the past pumping scheme and the future pumping scheme are modeled using different scenarios.

## *4.2 Gevonden (Rawsonville) site*

### 4.2.1 Site hydrogeology

There are 5 boreholes located on the farm Gevonden, 6 km west of Rawsonville, Western Cape. A perennial stream runs northwards with the water originating from a catchment of about 80 km$^2$ in which the mountain heights reaches 2000 m while the elevation of the study site is about 290 m. In this study area, the majority of the TMG outcrop consists of Peninsula Formation. The bottom of Nardouw Groups and the Cedarberg Formation occur in the very north of the study area. The TMG aquifer is bounded by basement rocks in the west and southwest and faults (Brandvlei-Eikenhofdam megafault and Smiths Kraal fault) in the east and southeast (Fig. 4-1). The Waterkloof fault cuts through the research site and extends some 15 km north-eastwards. Controlled by fault structures and the NE-trending TMG terrains, the geomorphologic features of the area are mainly characterized by steep, bare rock slopes of Peninsula outcrops, a stream course with three waterfalls with the altitudinal drops of 14 to 40 m, and a 6 m thick pluvial boulder soil. Several springs on the stream are identified, but are not linked to one another in a regional flow system because the water head gradient may reach more than 1/20 by a rough estimation on the 1/50000 topography map. This suggests that the observed flow systems on the surface are very local ones that seem to be controlled by fractured blocks.

Core drilling of boreholes BH-1 and BH-2 commenced in the mid of November 2005 by the drilling teams from the Department of Water Affairs and Forestry (DWAF) and ended in December 2006. Two percussion boreholes (BH-3 and BH-4) were drilled in September 2006 and BH-5 is an existing borehole (Fig. 4-1, Table 4-1). Some of the borehole details and field observations are now presented:

- BH-1 inclines to the west with a plunge of 60° and was drilled to a depth of 250 m (270 m in length). This borehole penetrates the bottom of Nardouw Group and Cedarberg Formation, and taps the top of Peninsula Formation. The artesian flow of 0.15-0.3 *l/s* was identified from three conductive zones at depths of 67.5 m, 95.3, and 213.0 m. In order to conduct long-term monitoring of the Peninsula aquifer, 179 m of steel casing was installed to the bottom the Cedarberg shale to seal the two conductive zones above the Peninsula Formation, resulting in a flow of about 0.2 l/s
- Borehole BH-2 was drilled to a depth 201 m and cased to 65 m. This borehole was sited on the fault core zone with the aim of elucidating both the fault core and fault fracturing zone. The water level in this borehole is 1.8 m from the top
- Based on the groundwater observations in boreholes BH-1 and BH-2, the percussion borehole BH-3 was sited between BH-2 and the existing borehole BH-5, in an attempt to link the three as a whole. BH-3 was drilled in September of 2006. During drilling, water level and flow rate in BH-2, BH-5, and BH-1 were monitored. It was found that when the air-lift water was pumped out of BH-3, water levels subsequently dropped in both BH-2 and the BH-3, but no flow changed in artesian borehole BH-1. In order to monitor the link between groundwater

found in the three boreholes and that from the regolith, an 8 m deep borehole (BH-4) was drilled some 45 m away from BH-3 (Fig. 4-1).

Water samples from these boreholes have been routinely collected for both in situ and lab analyses since the start of drilling. The average water temperature ranges from 18.5 to 20ºC.

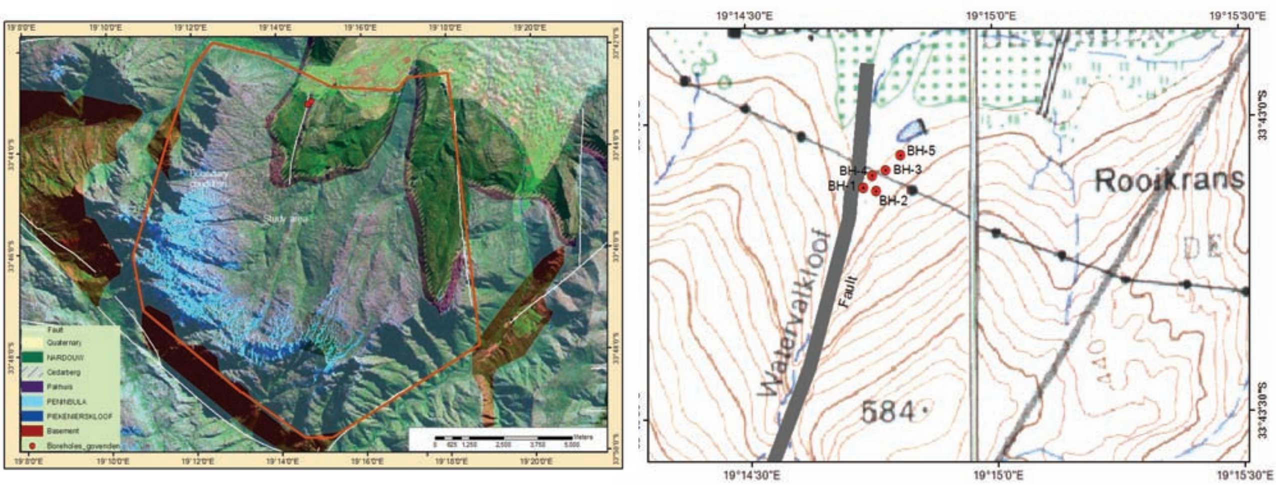


**Fig. 4- 1** Study area and boreholes – Rawsonville site

In the deep boreholes, water electrical conductivity (EC) varied between 40 and 60 µS/m, and pH between 5.2 and 6.8, while the EC in the shallow hole ranged from 130 to 160 µS/m. The physical features of groundwater are significantly different from those of stream water listed in Table 4-2. Groundwater from the fractured rocks is sodium-chloride dominant, but in late 2006 the water type changed because of inflows of stream. The major chemical constituents vary with time with iron showing the most significant changes. The borehole water is ferruginous with a dissolved iron content of 0.15~1.5 mg/*l*. The presence of iron gives a reddish color on the borehole surroundings at BH-1 due to the precipitation of $Fe(OH)_3$ from the artesian overflows.

**Table 4- 1 Basic information of the boreholes at the Gevonden site**

| Borehole No | Coordinate (º) | | Type | Depth (m) | | Inclination | Formations |
|---|---|---|---|---|---|---|---|
| | E | S | | Bore | Casing | | |
| BH-1 | 19.24615 | 33.71846 | Ø75 mm,core drilling | 250 | 156 | 60º/W | Nardouw to peninsula |
| BH-2 | 19.24659 | 33.71853 | Ø75 mm,core drilling | 201.1 | 65 | Vertical | Peninsula |
| BH-3 | 19.24696 | 33.71790 | Percussion | 200 | 16 | Vertical | Peninsula |
| BH-4 | 19.24654 | 33.71809 | Percussion | 8 | 6 | Vertical | Regolith |
| BH-5 | 19.24755 | 33.71749 | Percussion | 175 | | Vertical | Peninsula |

**Table 4- 2 Physical properties of borehole and surface water**

| item \ Water source | | BH1 | BH2 | BH3 | BH4 | BH5 | Stream |
|---|---|---|---|---|---|---|---|
| Ground elevation(m) | | 286.83 | 285.92 | 283.34 | 284.63 | 284.98 | |
| T (º) | | 20.15 | 19.25 | 18.5 | 18.9 | 20.05 | 14.50 |
| Water level | m to top | 0 | 1.8 | 3.05 | 2.59 | 5.57 | |
| | m | 286.83 | 284.12 | 280.29 | 282.04 | 279.41 | |
| pH | | 6.8 | 5.5 | 5.8 | 5.6 | 5.2 | 4.41 |
| EC (μS/m) | | 50~60 | 40~70 | 36~40 | 130~160 | 43~50 | <10 |
| Formation | | Nardouw | Peninsula | Peninsula | Regolith | Peninsula | Surface water |

### 4.2.2 Characterization of the fractured aquifer

The core logs and the site surveys show that the normal fault plays a key role in controlling the occurrence of groundwater. The 80 m wide fault core, identified to be cemented cataclasites, acts as a groundwater barrier that separates the fractured rock aquifer into eastern and western parts. In the eastern (hanging) wall of the fault, groundwater occurs as a static water level, but appears as an artesian flow in the west (foot) wall (Fig 4-2). The conductive zones intercepted by the boreholes are not at the fault core but at its fracture zones.

With respect to the aquifers at the Rawsonville site, there are three independent flow systems; of these two are fractured aquifers on both sides of the fault, and the other is the shallow groundwater flow through the boulder soil. These observations, together with the additional field surveys and borehole logging, help not only to improve the understanding of the role of faults in TMG aquifers, but also to establish a site-specific conceptual model, partially presented in Fig. 4-2.

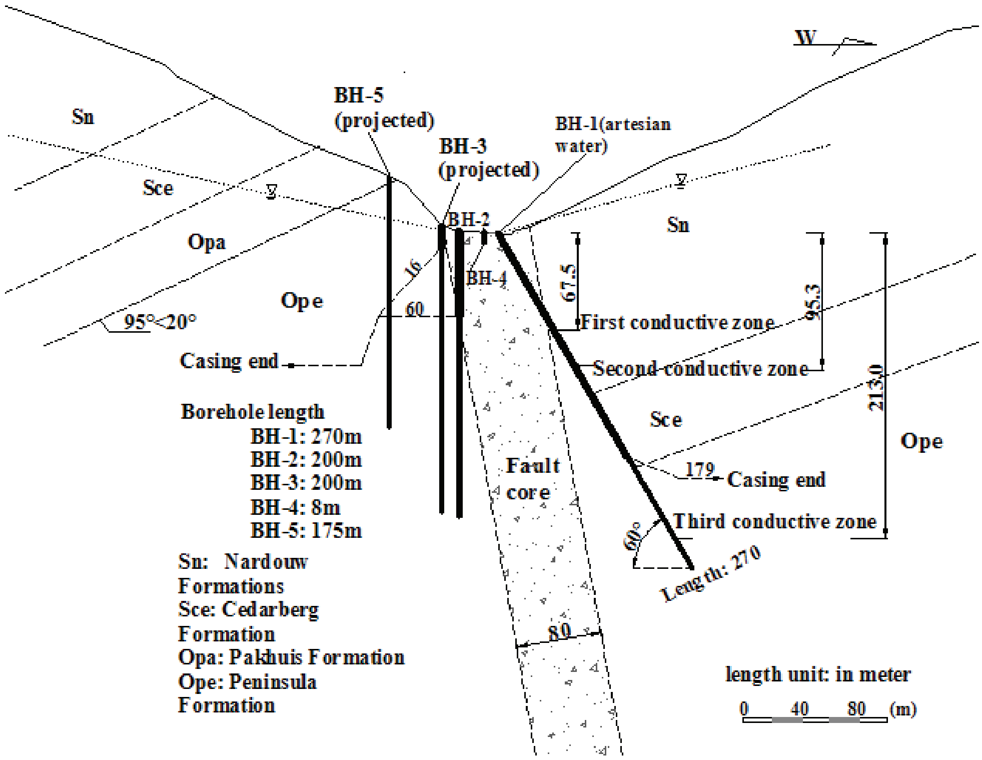


**Fig. 4- 2** Schematic hydrogeological cross section, together with the borehole construction, Gevonden site

### 4.2.3 Field logs

#### 4.2.3.1 Core log

The core drilling project was initiated to interpret the geological and hydrogeological characteristics in the vicinity of the site. Boreholes BH-1 and BH-2 were drilled using diamond core drilling rigs. The in situ core logging was done along with the drilling to avoid the weathering and disturbance of core samples. Lithologies, fractures and associated hydrogeological information from the core samples were carefully logged, using standard core logging techniques as well as by photographic capturing.

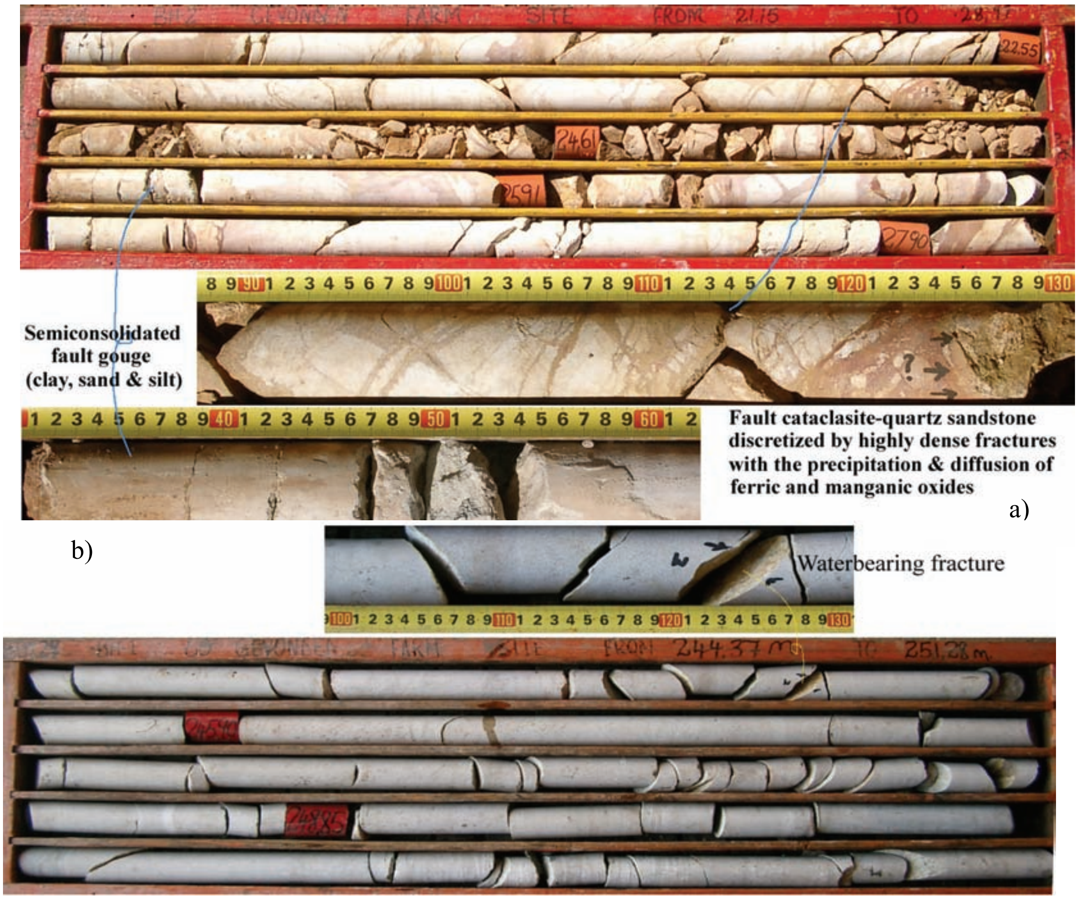


**Fig. 4- 3** Core trunks of BH-1 and BH-2. a) Fault core material at shallow zone of BH-2. b) the Peninsula sandstone and the sub-vertical conductive single facture at BH-1

Cores were described in terms of the following parameters:

- Rock type
- Colour
- Grain size
- Sorting
- Mineral content
- Sedimentary structures
- Secondary structures

All the core trunks were photographed using a digital camera. The purpose was to have a detailed record of the cores for datum referencing and archiving. The photographs are also used to describe additional features missed during core description, especially with relation to the other interpretations. The core data were transferred from the field notes to standard core logging results (Appendix C) generated by an Excel-based software developed by the research team.

In terms of fracture orientation, there are thr
namely bedding fractures with a plunge of 15°
steep fractures (>60°). During the core logging
fractures was counted. The frequency plots of the

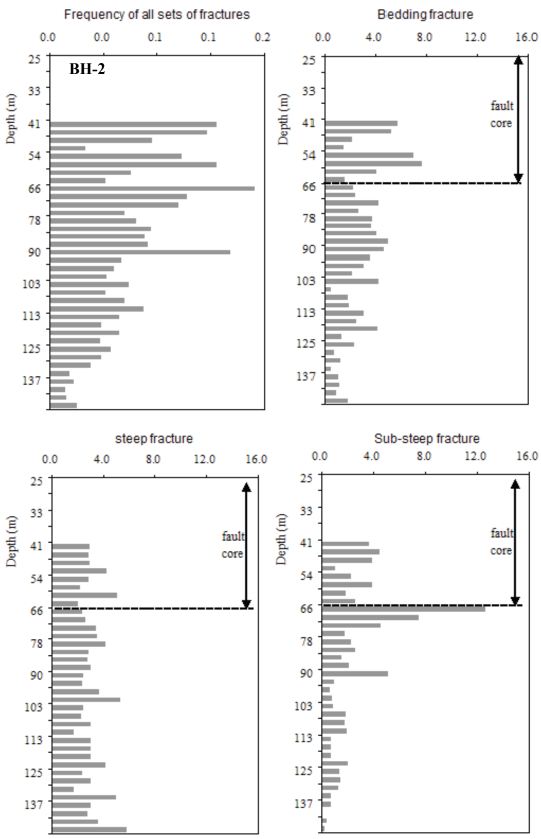


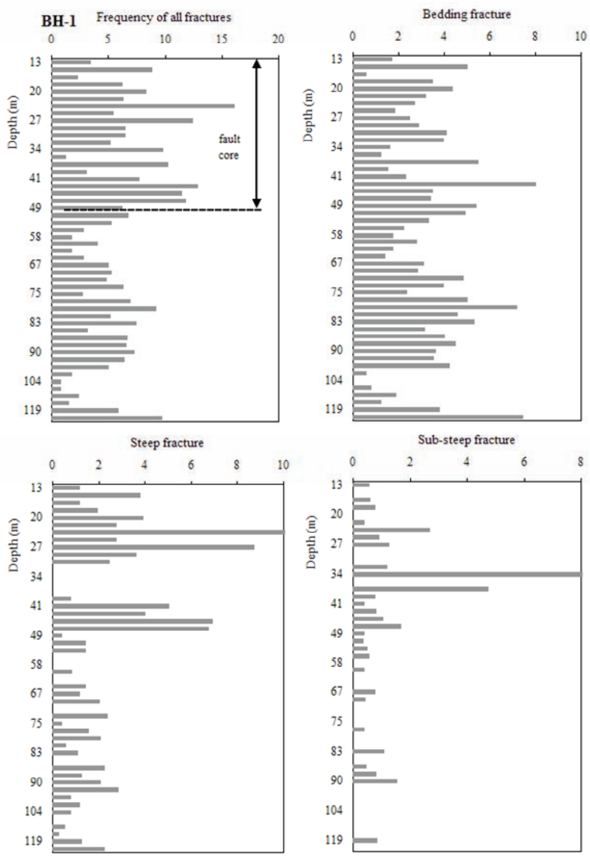


**Fig. 4-4** Fracture frequency plots against depth

1 and BH-2 with a logging interval of 1~4 m are shown in Fig. 4-4. The top cut-off of BH-2 is 40 m because it is extremely difficult to capture the fracture data in the highly fractured and weathered fault core at shallower depths. In general the spatial correlation of fracture density is very weak, especially in the BH-1. In BH-2 the density of both bedding and sub-steep fractures appears to decrease with depth, especially the fractures below the fault core zone. In contrast, the steep fractures in both BH-1 and BH-2 are not substantially depleted with depth; in BH-2 it shows a uniform spatial distribution of the steep fractures. These observations are consistent with the results from core sample study on hydraulically active fractures in the Rietfontein deep borehole where the steep fractures become dominant in the deeper zone.

#### 4.2.3.2 Surface geophysical logs

Among the non-invasive geophysical techniques, the radon emanation method is an effective tool to detect the concentration of groundwater (Levin, 2000). This method is based on the nuclear disequilibrium process of the isotopes of the uranium family of which the radioactive decay series by alpha recoil process is from $^{234}U$ through $^{230}Th$ and $^{226}Ra$ to $^{222}Rn$. Because uranium in groundwater is soluble under oxidizing conditions, the distribution and magnitude of the radioactivity of the U family consequently reflects the groundwater concentration in the aquifer. Therefore the radon isotope $^{222}R$ is often employed as a natural groundwater tracer, and is particularly useful for indicating open fractures in a fractured rock aquifer.

A series of soil and water $^{222}Rn$ measurements on the surface were carried out. Using the alpha card instrument, $^{222}Rn$ was stripped from the air pumped from subsurface soil or from the bubble of water and measured in a gas proportional counter. This count is termed pulse number in the alpha card instrument, from which the concentration of the radon gas can be estimated:

$$C_{Rn} = J \cdot N_{RaA} \tag{4-1}$$

where $C_{Rn}$ is the concentration of Rn, $N_{RaA}$ the pulse number measured, and J is the coefficient of Rn concentration, a constant fixed by the measuring equipment.

The in-situ operation procedure of the alpha card equipment has been discussed in detail by Wu et al (2003). In order to have comparable results, measuring operations are classified into four categories, i.e. soil radon anomaly, soil radon background value, borehole water and stream water radon concentrations (Table 4-3). For the measurement of radon gas in soil, the measuring probe needs to reach a depth of more than 0.5 m to access the subsurface air. Fig. 4-5 shows the measuring points, the coordinates of which were captured by GPS equipment. At these points, pulse number data were collected to represent the radon concentration.

Table 4-3 shows that the observed radon pulse number of groundwater ($N_{RaA}$=30~69) is much higher than that of stream water ($N_{RaA}$=6~15). This also confirms the basis of radon gas concentration for the characterization of groundwater distribution in the fractured rocks. In the soil radon measurements (Fig. 4-5), relatively higher pulse numbers mostly fall in the east side of the stream. Especially to the east of BH-2 and BH-4 where the Peninsula sandstone is exposed, most of the pulse numbers of $^{222}Rn$ are above 50, in which the highest ($N_{RaA}$=90~107) occur between BH-3 and BH-5 distributed at the northeast corner of the measuring area. In comparison, the pulse number on the west side of the stream, where the Nardouw sandstone is exposed, is much lower with an average of 17.7 and range of 3 to 36. These values are the same as the background values. In the central fault core zone, the majority of the pulse numbers fall in the range of 20 to 40. These values possibly represent the radon concentration of the shallow regolith aquifer because the pulse number of the water from BH-4 is 40.

Thus it can be seen that $^{222}$Rn data are useful indicators of groundwater concentration in the relatively shallow zones such as that of the regolith aquifer and the Peninsula aquifer. In

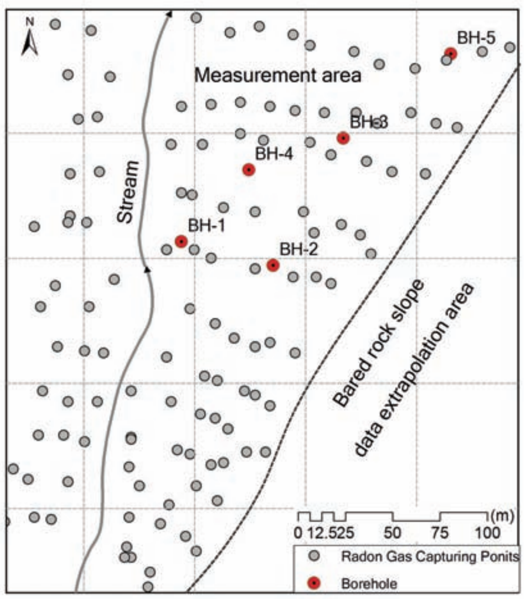


**Fig. 4- 5 Measuring points for the collection of radon ($^{222}$Rn) gas emanating from subsurface water**

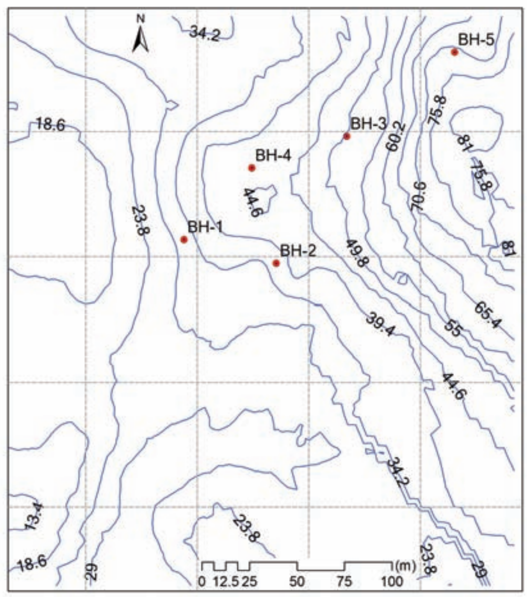


**Fig. 4- 6 Contour map of pulse number anomaly for radon ($^{222}$Rn)**

fractured rocks like the Peninsula sandstone, the uneven distribution of pulse numbers might be another indication of the anisotropic feature of open fractures and subsequently the groundwater concentration in this aquifer. In the Nardouw sandstone, the lower pulse number is perhaps attributed to the deep seated artesian flow and the mostly closed fractures in the shallow zone.

**Table 4-3 Statistic of the $^{222}$Rn pulse number from different sources**

| $^{222}$Rn pulse number | Soil anomaly | Soil background | Groundwater | Stream water |
|---|---|---|---|---|
| maximum | 107 | 23 | 69 | 17 |
| Minimum | 3 | 7 | 30 | 6 |
| Average | 33.5 | 12.1 | 37.8 | 10.7 |
| Standard deviation | 22.6 | 6.1 | 19.6 | 4.5 |

#### 4.2.3.3 Surface fracture measurements

On both the Peninsula and the Nardouw sandstone outcrops facture data were gathered on orientation, length, spacing, and aperture. The methods of measurement and the data statistics have been discussed in Chapter 3. According to their orientation, 334 measured fractures were put in four categories. The statistics of basic elements are listed in Table 4-9 and all the measured data are listed in Appendix D. Fig. 4-7 shows the orientation distribution of the fractures, in which gently-dipping bedding fractures have a orientation range of 14°~28°/69°~125° (dip angle/dip azimuth, set 1). The other three categories are 38°~89°/192°~233° (set 2), 67°~89°/123°~169° (set three) and 70°~89°/235°~317° (set 4). Although the fracture densities are different, the orientation results are broadly comparable with that of the core samples. Fractures of set 2 may account for the sub-steep fractures in the core samples, but the other two sets of fractures are mixed.

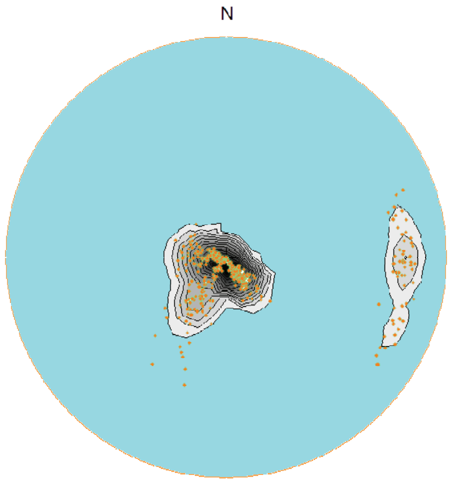


**Fig. 4- 7** Orientation distribution of fractures measured at the site

### 4.2.4 Hydraulic properties

Single packer tests with an interval of 6 m were done on BH-1 and BH-2 during the process of core drilling. A 24-hour pumping test on the existing borehole BH-5 was carried out in May 2006. A 24-hour pumping test was conducted at percussion hole BH-3 in November 2006.

#### 4.2.4.1 Packer tests

Almost all the hydraulic tests conducted in the TMG aquifers so far are pumping tests. No records of packer tests for hydrogeological exploration in the TMG aquifers can be found, except a few from dam foundation investigations (Rosewarne, 2002). Generally the hydraulic parameters estimated from pumping tests represent parameters at a scale of tens of metres, while packer tests can only be used to estimate such parameters at a scale of a few metres (Nestev et al., 2004).

In order to evaluate the hydraulic conductivity of the TMG sandstones at a relative small scale (in comparison with pumping tests), packer tests on the two core boreholes were completed using a single packer with an interval of 6 m. Packer tests for the whole borehole length of BH-2 was carried out, while for the inclined borehole BH-1 only half of the borehole was packer tested because the normal coring drilling was replaced with wire line drilling after this hole was diverted at a shale band at 140 m below surface.

For the hydraulic tests, the injection pressure in a packer was changed in steps from 350-700-1050-700-350 kPa below the depth of 40 m. Hydraulic conductivity (*K*) was calculated by the following formula suggested by Moye (1967, cited by Park et al., 2002):

$$K = \frac{q}{HL}\left[\frac{1}{2\pi}\left(1 + \ln\left(\frac{1}{r_w}\right)\right)\right] \quad (4\text{-}2)$$

where $q$ is flow rate ($m^3/s$), $H$ is total working pressure (m), $L$ the packer interval (m), and $r_w$ borehole diameter (m).

The mean value of each interval test based on equation (4-2) is taken to be the hydraulic conductivity for that interval. Hydraulic conductivity against borehole depth plots in Fig. 3-33 shows that the *K* value varies widely from $1.11\times10^{-6}$ to $2.35\times10^{-9}$ m/s (average $2.15\times10^{-7}$ m/s) in BH-1 and from $1.25\times10^{-6}$ to $7.25\times10^{-10}$ m/s (average $9.73\times10^{-8}$) in BH-2. These *K* values are one to two orders of magnitude less than those from dam investigations ($1.97\times10^{-6}$ to $8.1\times10^{-7}$ m/s, Rosewarne, 2002).

In the top portion of the boreholes near the fault zone, the *K* values vary a lot and are higher than those at the lower portion of the boreholes. Below the depth of 60 m in BH-1 and 80 m in BH-2 the variation of *K* values becomes stable and the *K* values gently decrease with depth in both boreholes. Note that there are many test intervals without water strikes and therefore K=0. The variation in conductivity at depth for both these hole reveals a general trend of reduction in hydraulic conductivity as has been discussed in Chapter 4. This suggests that the majority of fractures may be closed in the deeper part of crust (Goodman, 1974).

#### 4.2.4.2 Pumping tests

Twenty-four hour pumping tests were done at BH-5 and BH-3. The observed drawdown of the constant discharge rate pumping test at the BH-5 is plotted in Fig. 4-8 (Appendix E). Using the Cooper-Jacob method for radial flow, the estimated later-time *T* value is $7.1\times10^{-5}$ $m^2/s$ (6.1 $m^2/d$) and the corresponding *K* value is $4.2\times10^{-7}$ m/s ($3.6\times10^{-2}$ m/d).

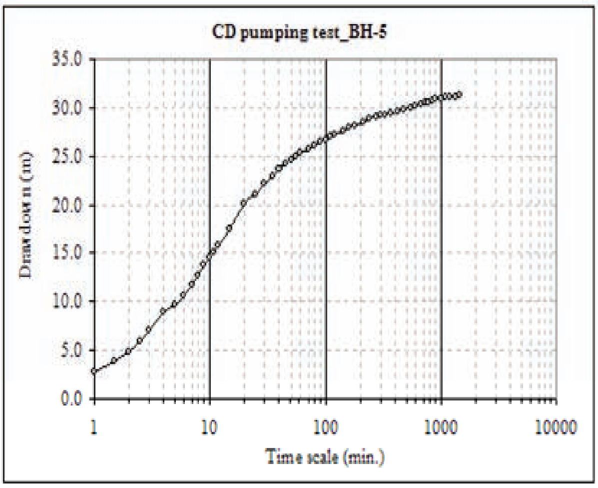


**Fig. 4-8** Constant discharge ($q$=1.3 *l/s*) pumping test at BH-5

Similarly, the *T* value estimated for the BH-3 is $1.7\times10^{-4}$ $m^2/s$ (14.7 $m^2/d$) and the K value is $8.8\times10^{-7}$ m/s ($7.6\times10^{-2}$ m/d); while the T value derived from drawdown recovery is $8.0\times10^{-5}$ $m^2/s$ (6.9 $m^2/d$).

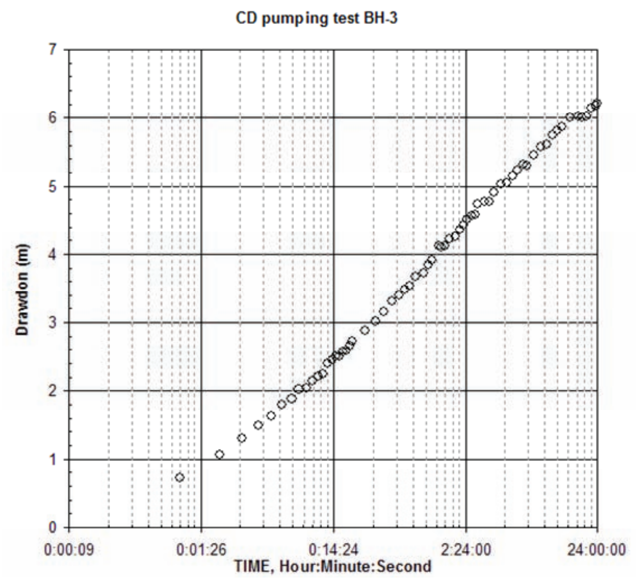


**Fig. 4-9** Constant discharge (q=1.8 l/s) pumping test at BH-3.

During the pumping test at the BH-3, the surrounding boreholes BH-1, BH-2, BH-4, and BH-5 were monitored. The artesian flow rate at the BH-1 was manually measured; while the water levels in the pumping hole and the other boreholes were automatically recorded by Diver well pressure loggers. To avoid the turbulence flow that may affect the reading at the pumping hole, the Diver was installed to a depth of 20 m below the pump inlet. Water levels in each borehole were regularly checked after the pumping test commenced; and continued after pumping ceased until recovery was 95% of the initial rest water level.

It was interesting to find that only BH-5 had a sharp response to the pumping hole. The first drawdown observed at BH-5 was 3 minutes after the pumping started, whereas it was 5 minutes at BH-2 before drawdowns were observed. Fig. 4-10 shows the final drawdown at the pumping and monitoring boreholes, together with the distance between these holes. The maximum drawdown in BH-2 is merely 0.6 m which seems to be on the boundary of the depression cone. Monitoring data also show that there is no discernible response at BH-1 and BH-4 to pumping at BH-3.

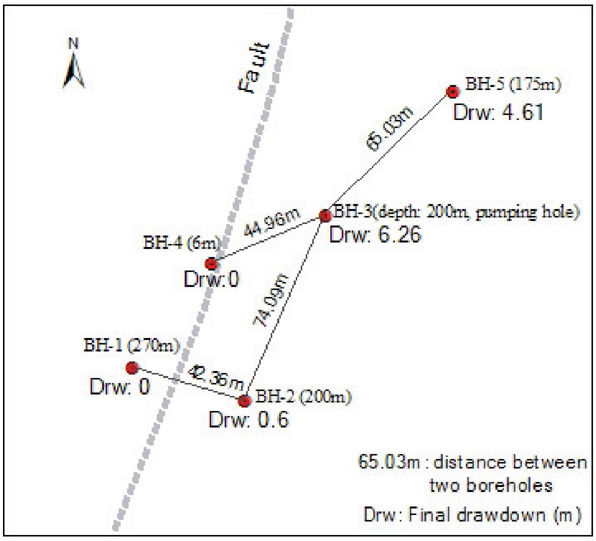

**Fig. 4-10** Map showing the final drawdowns, and distance between boreholes

This aquifer response to external stress reflects endemic anisotropic features at a site scale in which the uneven drawdown distribution is governed by various-scale fracture networks. Because of this many of the existing interpretation techniques may possibly have a limited applicability to the estimation of the aquifers' hydraulic properties. In this case, for example, the Cooper-Jacob method derived from the Theis theory regarding the aquifer as an isotropic medium is thought unsuitable for interpreting the pumping test data gathered from such aquifer that is bounded by a fault acting as a groundwater barrier. Therefore image well method (Ferris et al., 1962) is introduced to the estimation of the hydraulic properties. The effect of the drawdown of the image well can be expressed by:

$$s = \frac{Q}{4\pi T}[W(u_1) + W(u_2)] \qquad (4\text{-}3)$$

At large times the well function of the pumping hole ($W(u_1)$) and image well ($W(u_2)$) both tend to be less than 0.01. The Eq. (4-3) can therefore be represented using the Cooper-Jacob formula, where

$$s = 0.366\frac{Q}{T}\log\frac{2.25Tt}{r_w \cdot r_m S} \qquad (4\text{-}4)$$

in which $r_w$ is the radius of the pumping well and $r_m$ is the distance from the pumping well to the image well. [The other symbol meanings are the same as those of Eq. (3-10)]. The distance from BH-3 to the fault is 18 m and that of the BH-5 is 30 m. The calculated $T$ and $K$ values are much lower than those estimated by standard radial flow methods (Table 4-4).

**Table 4-4** Hydraulic properties from pumping tests at the Gevonden site

| Hydraulic properties | Borehole BH-3 drawdown | | | Borehole BH-5 drawdown | |
|---|---|---|---|---|---|
| | Radial flow | | Image well | Radial flow | Image well |
| | Withdraw | Recovery | Withdraw | Withdraw | Withdraw |
| $T$ (m$^2$/s) | 1.7×10$^{-4}$ | 8.0×10$^{-5}$ | 4.5×10$^{-4}$ | 7.1×10$^{-5}$ | 1.2×10$^{-4}$ |
| $K$ (m/s) | 8.8×10$^{-7}$ | 4.0×10$^{-7}$ | 1.8×10$^{-6}$ | 4.2×10$^{-7}$ | 7.9×10$^{-7}$ |

### 4.2.5 Fracture network model (FNM)

#### 4.2.5.1 Natural fracture network

As previously mentioned the groundwater in the BH-2, BH-3, and BH-4 is connected. In order to have a better understanding of such hydraulic connections, a generated fracture network is used. Based on the fracture data measured on the surface, the method of fracture realization is the same as what has been discussed in Chapter 3 and parts of the results of this site have already been presented there.

Fig. 4-11 shows another two plan views of the generated fractures on the profiles of N10E – S190W and N40E – S225W. Fracture networks on the both profiles reveal the similar geometric pattern to those previously discussed. However, in the two generated networks, not only do fractures occur in the form of blocks of interconnected fractures, but also one well-connected fracture cluster at each network appears to break through both side of the study domain. The first profile seems to be dominated by bedding and relatively gentle dipping fractures, whereas in the later steep fractures, together with the gentle-dipping ones, allow the well connected clusters to extend vertically.

It can be seen that the generated fractures on the profile trending SE-NW only produce small blocks of interconnected fractures. Thus, if there is a preferential flow path in the fracture rocks, this flow path should have a trend of NE-SW. The distribution of soil radon pulse numbers seems to support this inference, since the highest pulse numbers are concentrated to the northeast.

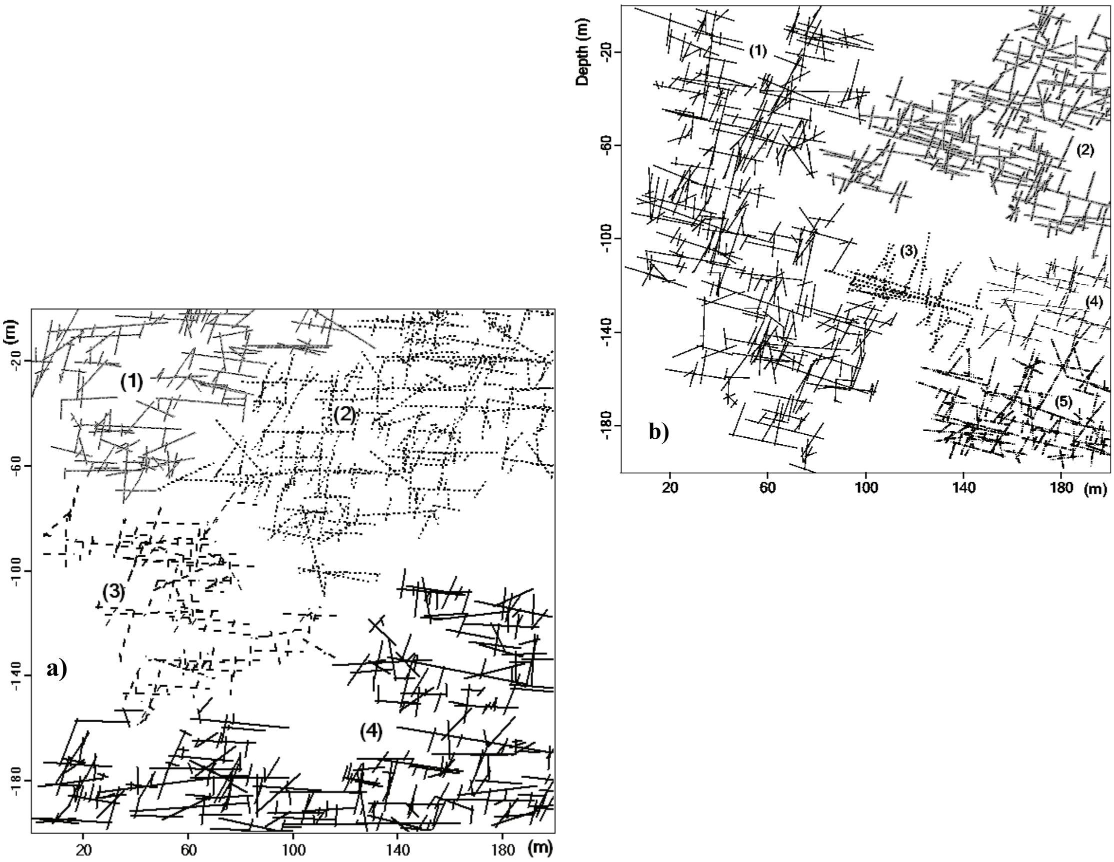


**Fig. 4-11** Plan views of interconnected fracture blocks generated with the data derived from field measurement on profiles: a) profile of N10E-S190W, b) profile N45E-S225W

#### 4.2.5.2 Discrete fracture model

There are many uncertainties in both the estimation and application of hydraulic properties of fractured rocks, simply as a result of their anisotropic characteristics. For this reason anisotropic hydraulic properties have been widely studied. Based on the Theis well function, Heilweil and Hsieh (2006) were able to develop a simplified Papadopoulos method to characterize directional transmissivity. Zhang et al. (1996) used hydraulic tensor methods to estimate the permeability of fracture network with constant apertures. Based on stochastic fracture realization, a discrete fracture network (DFN) model is often used to calculate the equivalent permeability of fractured rock through percolation theory (Baghbanan and Jing, 2007) or the hydraulic conductivity tensor approach (Min et al., 2004). Most of these studies are dealing the 2-D groundwater problem from different perspectives. It should be note that, when using stochastic DFN models to study the 2-D groundwater problem, a spatial projection of the fracture data is required. For example, in a 2-D plane, all the fractures are commonly assumed to have a vertical plunge because only the fracture strikes can be used to represent the fracture orientations. Thus the estimated hydraulic conductivity $K_x$ and $Ky$ can be representative.

For the calculation of equivalent hydraulic conductivity on the 2-D profiles in this study, the tensor method as presented Chapter 3 is used. Fracture data with dip directions, dip angles and length, are extracted from the four interconnected blocks as shown in Fig. 4-11a. Using the central coordinate, the spacing of each fracture is defined as the average distance to its adjacent fracture; and this process can be automatically completed by a VBA subroutine in the ArcGIS software. In this study a constant aperture ($b$=0.15 mm) and constant $JRC$ ($JRC$=0.18) are applied, which are the average of the four sets of fractures listed in Table 3-11. Therefore it is possible to calculate the $K$ values for each fracture block by the superposition of each fracture at the block. The computed results listed in Table 4-5 show that the average $K$ value based on Eq. (3-25) is $1.11\times10^{-5}$ m/s. This value appears to be the higher than the results of hydraulic tests. This is attributed to the projection of fractures on the profile resulting in the intensification of fracture density and accordingly the spacing between fractures. Therefore, these $K$ values on the 2-D plan can only be regarded apparent hydraulic conductivity but not equivalent hydraulic conductivity.

In a fractured rock aquifer, only a few fractures form part of the flow system (Witherspoon, 2000; Shapiro et al., 2007). This point is supported by the results shown in Fig. 4-12 where the major interconnected fractures in the 3-D DFN model are presented. Fig. 4-12a is the 3-D visualization of total fractures generated based on the data listed in Appendix D. The interconnection analysis of these fractures is performed by a 3-D face model developed in Microsoft Excel. As a result, Fig. 4-12b presents three major blocks comprising interconnected fractures, with fracture numbers of 2, 18, and 6 from the top to the bottom. The block with the interconnected fractures accounts for just 2.4% of total fractures generated. This suggests that the majority of fractures are not necessarily involved in a flow system in fractured rocks. Provided that all of the 18 fractures are open and have the same constant aperture and constant JRC as the above mentioned, and using the hydraulic tensor model, the calculated directional $K$ results for the 3-D problem are listed in Table 4-5. The average $K$ of $1.22\times10^{-8}$ m/s falls roughly in the same range of those from packer and pumping tests.

**Table 4-5 Computed equivalent K values for fracture blocks of interconnected fractures for both 2-D and 3-D analyses**

| | Fracture block | Hydraulic conductivity (m/s) | | | | | | |
|---|---|---|---|---|---|---|---|---|
| | | Principle *K* | | | | Axial *K* | | |
| | | Average | $K_{p1}$ | $K_{p2}$ | $K_{p3}$ | $K_x$ | $K_y$ | $K_z$ |
| 2-D | Block1 | 1.57E-05 | 2.36E-05 | 1.92E-05 | 4.46E-06 | 9.03E-06 | 1.46E-05 | 2.36E-05 |
| | Block2 | 1.33E-05 | 2.00E-05 | 1.64E-05 | 3.62E-06 | 6.70E-06 | 1.33E-05 | 2.00E-05 |
| | Block3 | 1.03E-05 | 1.54E-05 | 1.33E-05 | 2.19E-06 | 1.07E-05 | 1.54E-05 | 1.41E-06 |
| | Block4 | 5.01E-06 | 7.51E-06 | 7.05E-06 | 4.58E-07 | 1.54E-05 | 1.41E-06 | 7.51E-06 |
| 3-D | 18 fractures in a block | 1.22E-08 | 1.70E-08 | 1.60E-08 | 6.65E-09 | 9.55E-09 | 3.25E-08 | 1.65E-08 |
| | Dip direction(°) | | 210.8 | 69.1 | 128.4 | | | |
| | Dip angle(°) | | 24.3 | 60.0 | 16.4 | | | |

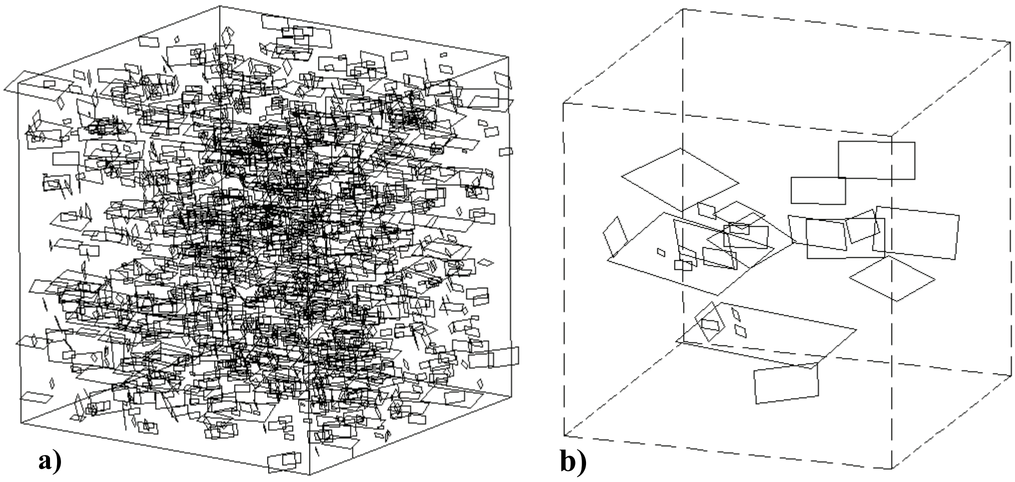


**Fig. 4-12** Fracture generated based on the data derived from surface measurements at the Gevonden site (SE views). a) fracture generated with the domain size of 200×200×200 $m^3$; b) Three major blocks of interconnected fractures are revealed

## *4.3 Kammanassie area*

### 4.3.1 Introduction to the area

The Klein Karoo area comprises a broad valley surrounded by Outeniqua, Swartberg, Kammanassie, and Rooiberg Mountains. The Kammanassie Mountains are located in the eastern section of the Klein Karoo area (Kotze, 2002) and has been part of the KKRWSS (Klein Karoo Rural Water Supply Scheme). Abstraction has been ongoing for about fifteen years. The Toorwater hot spring issuing in the vicinity of the Cango fault is situated on the northeast of Kammanassie Mountains. Some 30 km to the west of Oudtshoorn, the Calitzdorp hot spring occurs at the foothills of Rooiberg Mountains, and may indicate a regional groundwater flow regime.

The Kammanassie Mountains comprise three blocks of TMG window areas or Peninsula outcrops that are actually the core area of the Kammanassie mega-anticline, surrounded by Nardouw and Cedarberg rocks (Fig. 4-13). The whole study area can be regarded as an intermediate groundwater flow regime, where the contacts with Nardouw and Bokkeveld Group act as flow boundary. Three local flow regimes can be identified in the window areas, mainly bounded by the Cedarberg Shale aquitard. Groundwater has been extracted from both the Peninsula and Nardouw Aquifers.


**Fig. 4-13** Simplified Geology map of Kammanassie Mountains

Thirteen main production boreholes have been established for the KKRWSS, 4 in the Peninsula Formation and 9 in Nardouw Group. The associated abstraction and water level data are available. Some other production boreholes in this area are privately owned and mostly situated in Nardouw outcrop. Monitoring boreholes and data are also available. It can be observed, from borehole location map, that most of the boreholes were drilled in fault zones or the contacts between Nardouw Subgroup and Bokkeveld Group.

Previous studies have been re-evaluated and provide the basis for this study. A 3-D model of the Kammanassie area was generated, with the aim of improving the understanding of the conceptual hydrogeological model. A numerical groundwater flow modeling was established for the Vermaaks Window area (Peninsula outcrop in the western plunge of Kammanassie anticline, see Fig. 4-13 and 4-14) to simulate the effects of groundwater abstraction on the Peninsula Aquifer. An inverse simulation was also performed in order to calibrate the relative recharge rates and aquifer properties.

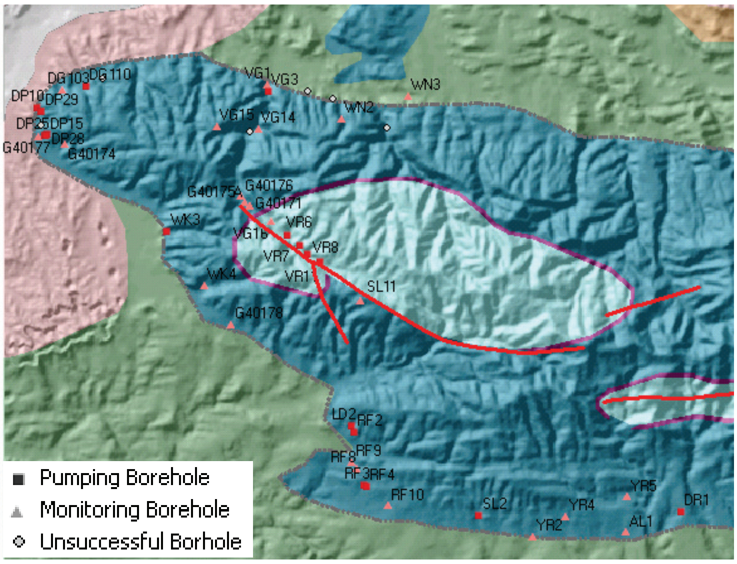


**Fig. 4-14** Borehole location map of Kammanassie Mountains

### 4.3.2 Introduction to 3-D models

An ideal conceptual hydrogeological model for fractured rock aquifers should demonstrate the settings and fabric of the groundwater regimes and should present groundwater circulation characteristics under natural and stressed conditions. It usually requires basic information such as geological data, fracture properties, and aquifer test and monitoring results to construct the hydrogeological model.

A 3-D model can create a virtual reality. It gives a perspective view from surface to subsurface of the earth, which is not possible with a 2-D map, and can make it easier to perceive the spatial relationship between geological formations and groundwater circulation. No true 3-D subsurface models were created previously for the TMG area except some geological cross sections and surface models interpolated from borehole logging data. This may be because the construction of 3-D models is difficult without dedicated software.

With such a thick sequence of target formations buried below the ground, it becomes crucial to build a 3-D model in TMG area to reveal the groundwater storage and subsurface flow regime. In this study an initial 3-D model was built for Kammanassie Mountains.

#### 4.3.2.1 Process of 3-D model construction

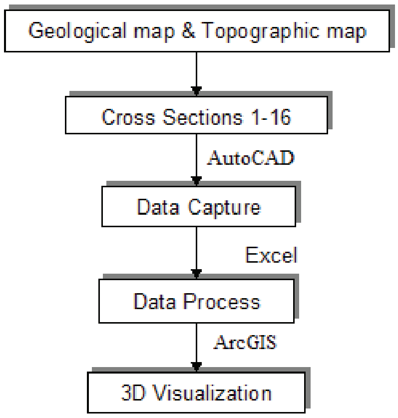


**Fig. 4-15** Flow chart of the construction of the 3-D model

Cross sections have been compiled, based on geological studies of the area, to reveal the deeper – predominately TMG – aquifer. The process of 3-D model construction is schematically depicted in Fig. 4-15. Information from both geological maps and topographical maps, i.e. surface elevation, top and bottom elevation for specific formations, were captured for each cross section (Fig. 4-16). These cross sections were then digitized in AutoCAD. Thereafter the elevation data for each geological formation are captured manually for these cross sections and input to Excel, where the data were processed to be compatible with ArcGIS. The 3-D model of Kammanassie Mountains was then constructed using the 3-D analyst extension of ArcGIS and VBA programming.

The accuracy of the 3-D model is highly dependent on the accuracy of the source data which have been captured. The aim of the 3-D model is to improve the understanding of the conceptual hydrogeological model in the study area.

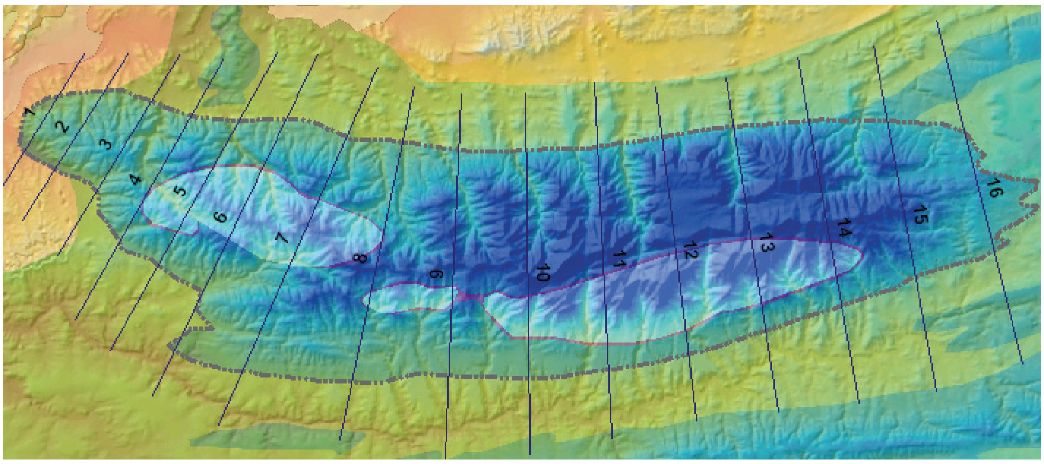


**Fig. 4-16** Cross sections (1-16) of Kammanassie Mountains

#### 4.3.2.2 Results of 3-D Visualization

Fig. 4-17 shows the 3-D Kammanassie Mountains model displayed with a vertical exaggeration of 6. The left shows the distribution of these cross sections. It can be seen that the Kammanassie mega anticline is plunging in both the eastern and western directions. The

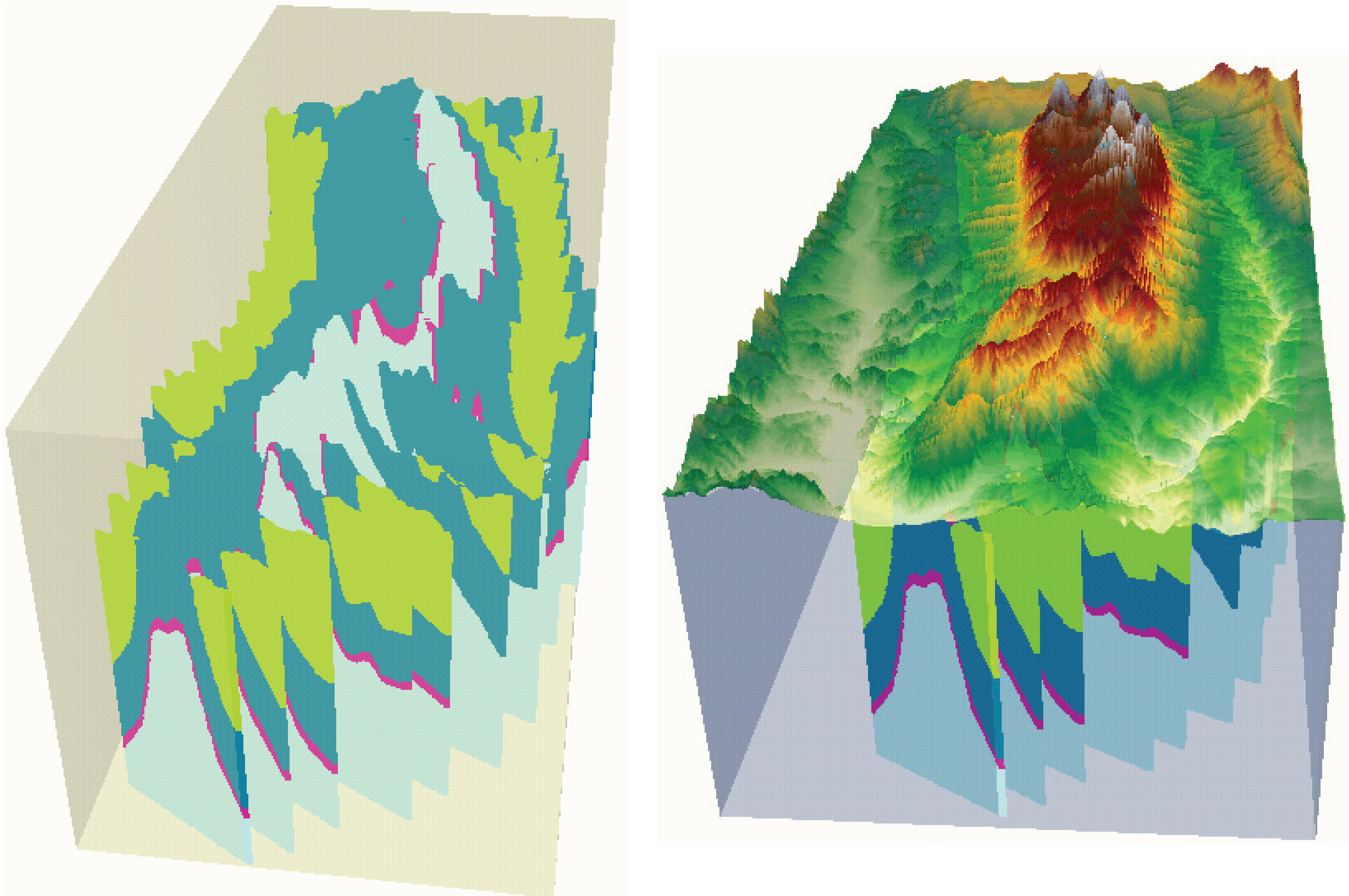

**Fig. 4-17** 3-D model of Kammanassie Mountains. Left: Distribution of the 16 cross sections; Right: DEM overlying on the cross sections

Peninsula Aquifer (Fig. 4-18) comprises two thirds of the total thickness of the TMG (1800 m to 2150 m) and the outcrops of Peninsula Formation form the recharge areas. The Nardouw Aquifer with a thickness of 500-1000 m is compartmented by the Kammanassie mega anticline. The Cedarberg Formation forms an aquitard between the Peninsula and Nardouw aquifers.

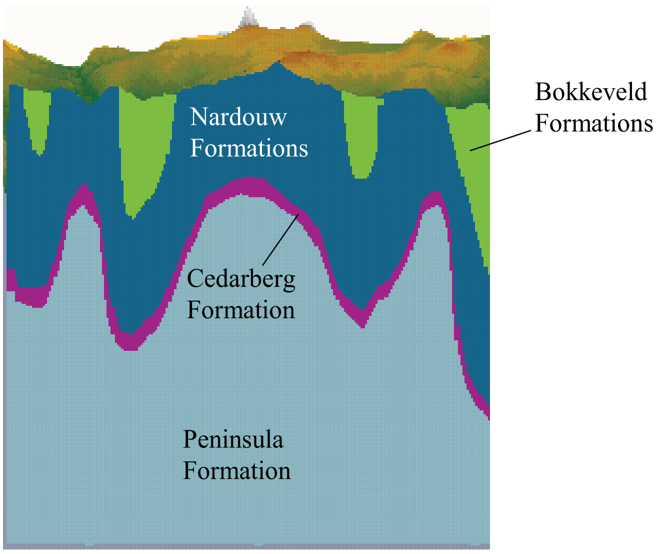


**Fig. 4-18** Cross Section 16 on the east of the Kammanassie Mountains

The figure on the right in Fig. 4-17 presents a whole picture of the study area, incorporating both the surface topography and the subsurface stratigraphy. The DEM distinctly shows the surface hydrogeological features. Tributary streams develop from the mountainous area and flow northward to the Olifants River or southward to the Kammanassie River. Considering the surface topography and the stratigraphy, high groundwater yields would be expected at great depths. However, so far no borehole has reached the deep (usually much greater than 500 m) buried TMG groundwater in the wide river valley areas. Except for inferences from the existing hot springs and conceptual models, there is no incontrovertible evidence of the bigger groundwater circulation at depth. Groundwater exploitation is still limited to the local or intermediate regime, usually targeting strongly fractured zones along the faults. The contact zone between the target aquifer (TMG) and adjacent aquitard (Cedarberg Formation or Bokkeveld Formations) is another common choice in borehole siting.

### 4.3.3 Groundwater flow regimes

Because of lack of data, the regional groundwater flow can only be assumed, using a schematic section to illustrate the postulated regional groundwater flow directions. The Cango fault in the north of Kammanassie Mountains is usually regarded as an impervious boundary for regional flow. Groundwater recharge via the Swartberg Mountains is assumed to flow to the Karoo area to the north. The groundwater flow direction matches the configuration of Peninsula aquifer, which is elevated in the mountainous area and depressed sharply in the intermontane area where Bokkeveld Group outcrops. More data are needed to verify the postulated regional flow.

By combining the 3-D model with borehole water levels, the intermediate and local groundwater flow regimes could be preliminarily described. On an intermediate scale, like that of the Kammanassie Mountains, groundwater recharge mainly takes place in the higher altitude areas where more precipitation occurs. Recharge areas include Peninsula outcrop areas and part of the Nardouw outcrop areas. Groundwater recharge reaches the groundwater storage through fracture networks including the unsaturated infiltration zone between groundwater level and the surface. Because of the direct infiltration, the groundwater level in the recharge areas is higher and then flows to the lower altitude areas.

A postulation made here is that the lower limit of intermediate groundwater flow depth is in accordance with the hydrological system on the same scale, which means in practice that the intermediate flow regime occurs between the groundwater levels in recharge areas and the water stages in the adjacent Olifants and Kammanassie Rivers. This postulation is consistent with the borehole water level distribution in this area and does not contradict previous inferences (Wu, 2005). According to this postulation, the lowest water stage of the two rivers in the study area (350 m a.m.s.l.) is assumed to be the lower limit of intermediate groundwater flow. The upper flow limit according to borehole water levels is about 1000 m a.m.s.l.

The Vermaaks Window area is regarded as a local flow regime according to the surface geological evidence and borehole water level distribution. Though the groundwater flow in the Vermaaks Window area may be impacted by surface topographical features, the dominant hydrogeological controls are the hydraulic boundaries of the Cedarberg Aquitard and the Vermaaks River fault.

## 4.4 Groundwater flow simulation

Since the local flow regime has been determined and the initial values of model parameters could be extracted from the borehole data in Vermaaks Window area, the numeric groundwater flow model can be constructed for this area. Firstly the past conditions are used to calibrate the model parameters and then the calibrated parameters are introduced into the model to predict the aquifer response to the recommended pumping scenarios. The water budgets associated with the modeling scenarios are expected to form the basis of the groundwater resource allocation in this area. To simplify the problem, the assumption is made that the aquifer is a continuous porous medium and the fracture networks are averaged to an equivalent isotropic hydraulic conductivity. The Cedarberg aquitard is modeled as a groundwater flow boundary, which surrounds the modeling area except where the Vermaaks River fault cuts cross. The steady-state groundwater flow is simulated using PMWIN (Chiang and Kinzelbach, 2001).

### 4.4.1 Model configuration and preprocess

#### 4.4.1.1 Model configuration

The modeling area is shown in Fig. 4-19. The size of the rectangle area is 14000 m (west-east) by 6500 m (north-south) or 91 $km^2$. The active area is about 47.34 $km^2$. The rectangle area is discretized into square grids with 140 columns and 65 rows, as shown in Fig. 4-20. After several model trials with different settings of model layers, only one layer is involved and modeled as confined/unconfined with variable transmissivity. Both transmissivity and storage coefficients are set as "calculated" rather than "user specified" to take into account the uncertainties in the variation of water levels. The top elevation of the layer is derived from the DEM and the bottom is set at the lower limit of the local flow regime (400 m a.m.s.l.).

The interaction between the Vermaaks River and groundwater has not been modeled with the RIVER Package, because only the upper reaches of Vermaaks River are included in the modeling area, and these are ephemeral. According to the borehole water levels (652~656 m a.m.s.l.) and the elevation of the river bed (minimum of 675 m a.m.s.l.) derived from the DEM, it can be assumed that the Vermaaks River has no direct hydraulic interaction with the main groundwater system being studied. Other intermittent rivers mainly interact with the shallow water in the weathered zone.

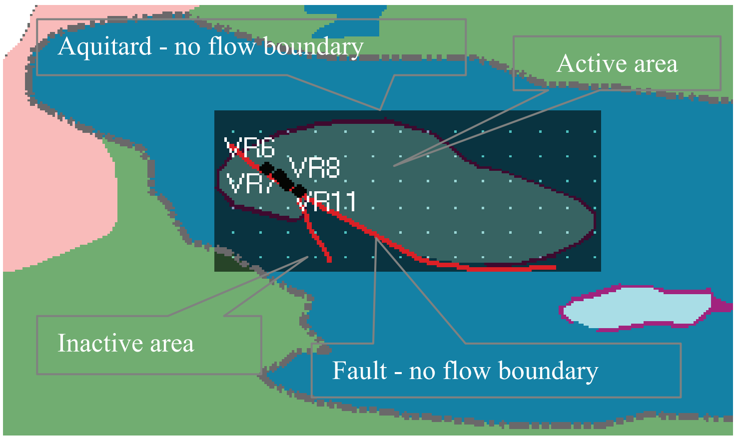


**Fig. 4-19 Modeling area of Vermaaks Window**


**Fig. 4-20 Model grid in PMWIN and observation boreholes (Coordination System is WGS_1984_UTM_Zone_34S)**

Averagely recharge rate for the whole year is set by the RECHARGE package since there is not a distinctive bimodal seasonal cycle of rainfall in this area. Four zones of groundwater abstraction representing the abstraction boreholes VR6, VR7, VR8 and VR11 are set using the WELL Package. For the past 10 years (1993 to 2002) actual pumping rates are modeled, from which the parameters could be calibrated, and then they are used to model the planned scenarios.

#### 4.4.1.2 Data preprocessing

Most of the data preprocessing was done in ArcGIS and Excel, automated with VBA programming, including discretization and assigning parameters. All the programming scripts were compiled in-house. The procedures are described in the following steps:

*Step 1*. Determination of model area in GIS

An initial estimate of the size of the model area was made, then the number of the columns and rows of the grids be used for modeling was designed, after which a rectangle polygon covering the model area was created as a shape file in ArcMap.

*Step 2*. Discretization of the model area in GIS

The polygon from in step 1 was discretized using a VBA script, named "DividePolygonForFreeSize" in ArcMAP. The user selects a polygon that needs to be discretized using a selection tool, then runs the script (Fig. 4-21). Two input boxes prompt the user to input the number of columns and rows for the selected polygon. Then the discretization process is implemented.

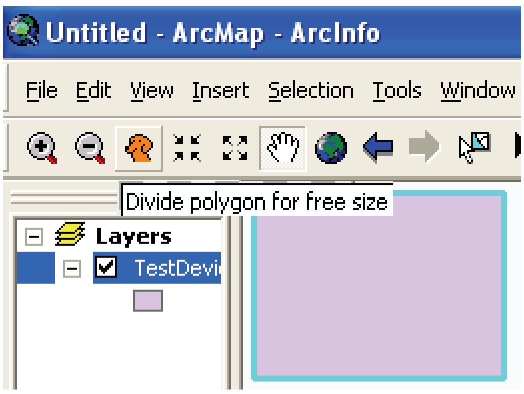


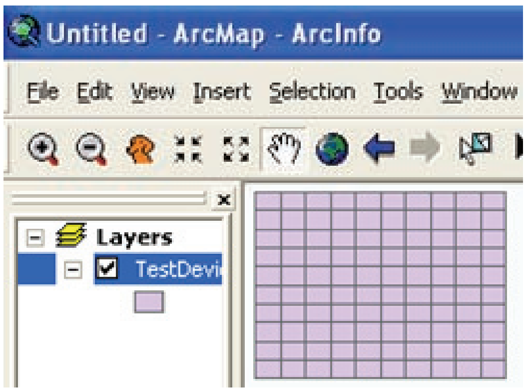


**Fig. 4-21** Automatic discretization of model area in ArcMap. Left: Polygon preparation, Right: Discretization result (10 Rows by 10Columns).

*Step 3.* Determination of the row and column number for each grid in GIS

The discretized grids in step 2 need to be indexed with column and row numbers before they can be used in MODFLOW. Initially this was planned to be an integral part of step 2. However it was found that this was not time-effective since the number of rows and columns vary during discretization, and that separate indexing was a better option. Therefore another script, named “CalculateColAndRow”, based on the topology relationship of these grids was created to index the grids. The sequence of numbers was designed to coincide with MODFLOW, in which the number of columns increases from left to right, and the number of rows from top to bottom. Two fields named “Column” and “Row” were added to the attribute table with the corresponding number for each grid.

*Step 4*. Setting elevations in GIS

A script named “ExtractValueToPolygon” was compiled to extract surface elevation values for each grid from the DEM of modeling area. Bottom elevations for each layer can also be extracted if a raster file of the bottom elevation is available. This is usually associated with very well studied areas. Two methods of extraction were considered: one was that the elevation value at the center of each grid is extracted to represent the elevation for that grid, the other one is that the elevation values are extracted for the four corners of the grid and then averaged for that grid. The second method may be more accurate but at the cost of a fourfold increase in processing time.

*Step 5*. Assigning parameter value in GIS

Almost all the model parameters can be assigned in GIS, including boundary conditions, top and bottom elevation for each layer, initial hydraulic heads, and aquifer properties. The most frequently used function in this step is the spatial selection, which is embedded in ArcMap. For example, the active cells, inactive cells or fix-head cells can be decided using a series of spatial selection.

Some data cannot be prepared just by spatial selection and then assigning value. The WELL package in MODFLOW requires the wells’ position (row and column), pumping layers and pumping rate for each layer. The spatial selection can only deal with the first parameter. The others need to be managed in step 6.

*Step 6*. Preparation of input files for PMWIN in Excel

If all the spatial parameter values for each cell have been assigned in GIS, the attribute table of the target shape file can be exported as a dbf file or text file to Excel. If the number of cells exceeds 66536(the maximum rows for Excel) Microsoft Access should be selected as the processing software. A VBA script named “TransferData” was compiled to transfer the cells into the MODFLOW compatible format for each parameter. Fig. 4-22 shows an example of the data format before and after the transfer.

As for the "WELL" data as mentioned in the previous step, only the column and row number can be decided in GIS. Additional processing is required. First the pumping rate for each well was calculated for each modeling layer. Then another data transfer script "TransferData2" was used to transfer the wells into MODFLOW compatible format for each layer.

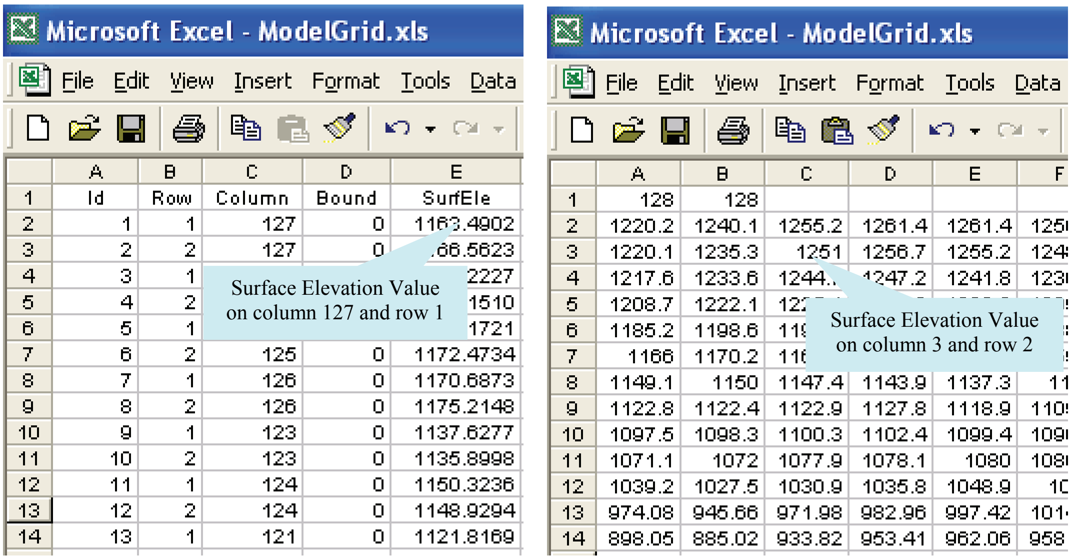


**Fig. 4-22** Data transferred from the GIS attribute table data to PMWIN compatible format. Left: Original data; Right: Data after the transfer

After all the data are converted to the MODFLOW compatible format, the parameter values will be assigned to each grid in PMWIN. The flow chart of the data preprocessing for groundwater flow modeling is showed in Fig. 4-23. Some of the procedures used here can also be applied elsewhere. For example the discretization of polygons has also been applied in the study of the fracture connectivity combined with other scripts compiled in ArcGIS.

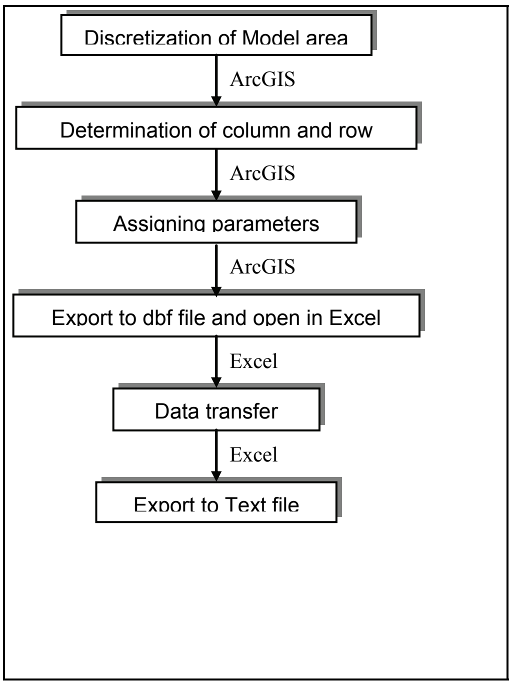


**Fig. 4-23** Flow chart of data preprocessing for the groundwater flow modeling.

### *4.4.2 Model Parameters and inputs*

The parameters and inputs used in modeling are discussed as follows:

- <u>*Aquifer Parameters*</u>

The type 3 model layer with varied transmissivity in MODFLOW requires the following aquifer parameters to be specified: horizontal hydraulic conductivity, specific storage (for transient-state simulation), effective porosity and specific yield (for transient-state simulation). The initial values are assigned and input to the model, as listed in Table 4-6. The associated Min and Max values are used as lower and upper limits in model calibration.

**Table 4-6 Initial Aquifer Parameter values**

| Aquifer Parameter | Initial Value | Min | Max |
|---|---|---|---|
| Horizontal hydraulic conductivity (m/s) | $8\times10^{-7}$ | $1.0\times10^{-8}$ | $1.0\times10^{-5}$ |
| Horizontal hydraulic conductivity (m/s) (Vermaaks River Fault zone) | $8\times10^{-6}$ | $1.0\times10^{-8}$ | $1.0\times10^{-5}$ |
| Specific storage | $5.5\times10^{-6}$ ($m^{-1}$) | $1.0\times10^{-7}$ | $1.0\times10^{-5}$ |
| Effective porosity | 0.2‰ | | |
| Specific yield | 2‰ | 0.1‰ | 5‰ |

- <u>*Recharge*</u>

Recharge estimations vary a lot among different researchers. The existing estimated recharge values, and the modeled recharge values for the Vermaaks Window area are listed in Table 4-7. The estimated recharge values range between 1.65% and 14% in the modeling area. Including the higher elevation Peninsula outcrops, the MAP for the area is about 600 mm. Therefore, according to the existing estimates, the Vermaaks Window area is recharged by an amount of some $0.4752\times10^6$ $m^3$ to $4.032\times10^6$ $m^3$ every year. Recharge is another model parameter that is calibrated by the model.

**Table 4-7 The existing recharge estimation values and the modeling values for Vermaaks Window area**

| Area ($km^2$) | MAP (mm) | Type | | Recharge | | | | Ref. |
|---|---|---|---|---|---|---|---|---|
| | | | | Rate | (mm/yr) | ($10^6$ $m^3$/yr) | (m/sec) | |
| 48 | 600 | Existing estimation | Min | 1.65% | 9.9 | 0.48 | $3.14\times10^{-10}$ | Wu (2005) |
| | | | Max | 14% | 84 | 4.03 | $2.66\times10^{-9}$ | Kotze (2002) |
| | | Numerical model | Initial | 0.05 | 30 | 0.3 | $9.51\times10^{-10}$ | |
| | | | Min | 0.05% | 3.15 | 1.44 | $1.00\times10^{-10}$ | |
| | | | Max | 15.77% | 94.61 | 4.54 | $3.00\times10^{-9}$ | |

- *Abstraction*

Abstractions from the existing four boreholes are modeled using the WELL package in MODFLOW. Initially the 10-year pumping regime (1993 to 2002) listed in Table 4-8 was modeled with the water level at the end of the modeling period as observations. The borehole abstractions are calculated based on the pumping conditions, as shown in Table 4-9. To simplify the modeling, total yearly abstractions ($Mm^3$/yr) are averaged to mm/s though the abstraction may be different from month to month. It is assumed that for a long span of 10 years could the seasonal variations could be ignored.

**Table 4-8 Borehole abstractions (m3/s) for the modeling area for the years 1993 to 2002**

| No | Column | Row | 1993 | 1994 | 1995 | 1996 | 1997 |
|---|---|---|---|---|---|---|---|
| VR6 | 20 | 24 | -4.0523E-03 | -3.8904E-03 | -2.0870E-03 | -3.0275E-03 | -2.6940E-03 |
| VR7 | 24 | 28 | -3.6954E-03 | -5.9480E-03 | -5.1282E-03 | -4.8249E-03 | -7.5320E-03 |
| VR8 | 27 | 31 | -2.9828E-03 | -2.8650E-03 | -1.2650E-03 | -7.4566E-04 | -2.8752E-03 |
| VR11 | 31 | 33 | -2.2668E-03 | -2.2784E-03 | -1.7634E-03 | -1.7203E-03 | -3.0801E-03 |
| **No** | **Column** | **Row** | **1998** | **1999** | **2000** | **2001** | **2002** |
| VR6 | 20 | 24 | -3.5484E-03 | -3.9768E-03 | -4.2554E-03 | -3.9410E-03 | -3.1020E-03 |
| VR7 | 24 | 28 | -1.0415E-02 | -9.8977E-03 | -8.8610E-03 | -8.1413E-03 | -8.3293E-03 |
| VR8 | 27 | 31 | -2.3928E-03 | -3.0538E-03 | -3.2614E-03 | -3.0640E-03 | -2.5312E-03 |
| VR11 | 31 | 33 | -3.4527E-03 | -7.2501E-04 | -8.0134E-04 | -2.1976E-03 | -2.9492E-03 |

**Table 4-9 Pumping conditions and associated water levels of the boreholes for 1993-2002**

| Year | VR6 | | | VR7 | | | VR8 | | | VR11 | | | Total abstraction |
|---|---|---|---|---|---|---|---|---|---|---|---|---|---|
| | Abstraction | | Water level | Abstraction | | Water level | Abstraction | | Water level | Abstraction | | Water level | |
| | ($m^3$/yr) | (*l/s*) | mamsl | ($m^3$/yr) | (*l/*sec) | mamsl | ($m^3$/yr) | (*l/*sec) | mamsl | ($m^3$/yr) | (*l/s*) | mamsl | (*l/s*) |
| 1993 | 127794 | 4.052 | 675.3 | 116539 | 3.695 | 674.69 | 94066 | 2.983 | 678 | 71485 | 2.267 | 676.7 | 12.997 |
| 1994 | 122688 | 3.89 | 671.9 | 187577 | 5.948 | 674.3 | 90351 | 2.865 | 674.35 | 71851 | 2.278 | 675.32 | 14.981 |
| 1995 | 65816 | 2.087 | 669.6 | 161723 | 5.128 | 670.4 | 39894 | 1.265 | 671.1 | 55610 | 1.763 | 671.2 | 10.243 |
| 1996 | 95475 | 3.027 | 675.89 | 152159 | 4.825 | 677.19 | 23515 | 0.746 | 677.15 | 54251 | 1.72 | 677.28 | 10.318 |
| 1997 | 84958 | 2.694 | 665.78 | 237528 | 7.532 | 664.34 | 90673 | 2.875 | 665.76 | 97133 | 3.08 | 663.2 | 16.181 |
| 1998 | 111903 | 3.548 | 661.5 | 328435 | 10.415 | 661.22 | 75459 | 2.393 | 662.82 | 108883 | 3.453 | 662.4 | 19.809 |
| 1999 | 125411 | 3.977 | 659.43 | 312134 | 9.898 | 659.68 | 96305 | 3.054 | 661.13 | 22864 | 0.725 | 663.12 | 17.654 |
| 2000 | 134199 | 4.255 | 657.83 | 279441 | 8.861 | 657.16 | 102850 | 3.261 | 664.14 | 25271 | 0.801 | 658.74 | 17.178 |
| 2001 | 124284 | 3.941 | 657.82 | 256745 | 8.141 | 657.53 | 96626 | 3.064 | 660.12 | 69303 | 2.198 | 658.68 | 17.344 |
| 2002 | 97826 | 3.102 | 657.11 | 262673 | 8.329 | 656.88 | 79823 | 2.531 | 657.75 | 93007 | 2.949 | 656.32 | 16.911 |

- *Boundary conditions*

It is assumed that under natural conditions, the inflow to the system is rainfall percolation to the saturated zone (recharge) and the outflow from the system is groundwater discharge from the spring 051 located on the western boundary. As is known from the observed data, spring 051 has dried up as a result of groundwater levels declining with pumping. Therefore in the simulation of pumping conditions in this area (transient state simulation), spring 051 could not be assumed to be a constant head boundary. Under such condition the outflow from the system is the well abstraction. Also, from the distribution of initial heads it may be inferred that the eastern boundary of the modeling area – the furthest from the pumping zone – is hardly influenced by the abstraction. The imposition of a no-flow boundary around the modeling area would imply that the groundwater flow system within the modeling area is relatively independent. This simplifies the modeling but ignores any possible groundwater/stream water interactions, as well as ignoring groundwater exchanges with adjacent aquifers. To take these factors into account, a general head boundary is specified on the eastern boundary of the modeling area to allow for the communication between the local groundwater flow system and external systems. The hydraulic head on the boundary is specified as the initial head and the hydraulic conductance can be calibrated by inverse modelling.

- *Time periods*

Ten time periods are used to simulate 10 years (1993 to 2002) and 12 steps representing 12 months are included in each period in the model calibration process. Both the steady-state and transient-state were simulated and finally it is decided that steady-state was more applicable to the modeling area because of a relatively consistent recharge and yearly abstraction. The Model used for prediction is also simulated for 10 years.

- *Initial hydraulic heads*

Though actual hydraulic heads are not a prerequisite in MODFLOW for steady-state simulations, to improve the representivity of the numerical model, the simulation of actual conditions was attempted. However, actual hydraulic heads are not generally available. Although several boreholes were drilled along the Vermaaks River valley, they could not be interpolated and extrapolated for the whole area. Therefore a pre-model run on a steady-state was executed for 5 years to simulate the pre-pumping conditions. Initial hydraulic heads for the pre-model were derived from DEM except where there were borehole water levels. The rest borehole water levels before 1993 were used and specified as constant heads. No abstraction and recharge was imposed with a view to simulating the natural water balance

The resulting hydraulic heads of the pre-model (Fig. 4-24) are assumed to be the initial hydraulic heads for the simulation.

- *Boreholes and observations*

Besides the four pumping boreholes, borehole VG16 served as monitoring hole and has been monitored on a regular basis. The water level data of VG16 are available for the modeling periods. The water levels of the four pumping boreholes are also used as observations. Their coordinates and corresponding hydraulic heads are input for the model calibration. The location of the observation boreholes is showed in Fig. 4-20.

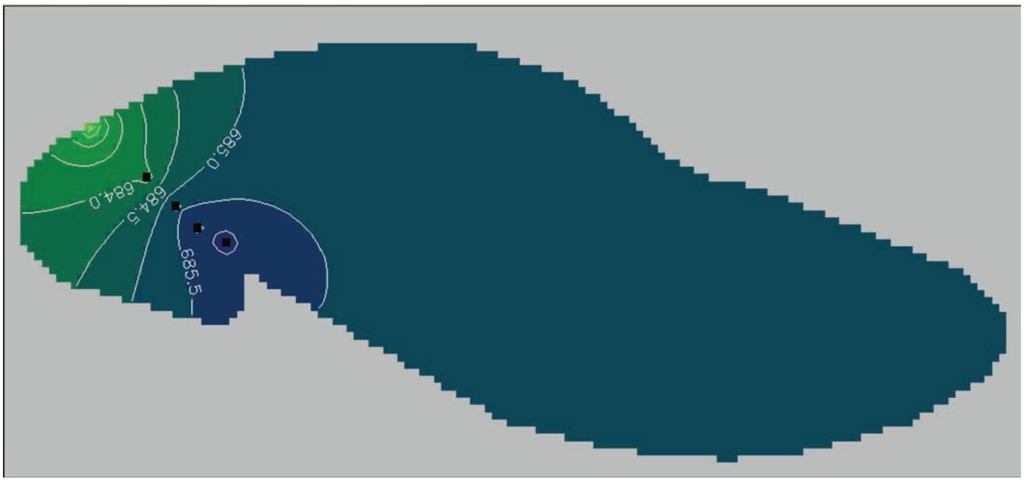


**Fig. 4-24 Initial hydraulic heads in the modeling area**

#### *4.4.3 Model Calibration*

Model calibration is carried out by the inverse model PEST (Doherty et al., 1994) which is incorporated in PMWIN. Because the steady-state simulation type is selected, only two parameters, namely recharge and horizontal hydraulic conductivity, are calibrated in the inverse model. Their initial values, and possible range (minimum and maximum values) have been given in Tables 4-6 and Table 4-7. Table 4-10 lists the simulated water levels at the observation wells, as well as the difference between the simulated and observed values. It can be seen that the simulated water level is generally lower than the observed ones, except for VR11. Calibrated parameter values are shown in Table 4-11 at a 95% confidence interval.The estimated hydraulic conductivity and the hydraulic conductance of the General Head Boundary are all higher than the initial value, but the calibrated recharge is much lower than the initial one. The contour maps of simulated hydraulic heads and drawdown for December of 2002 using calibrated model parameters are showed in Fig. 4-25 (a) and (b).


(a) Simulated hydraulic heads in 2002.12

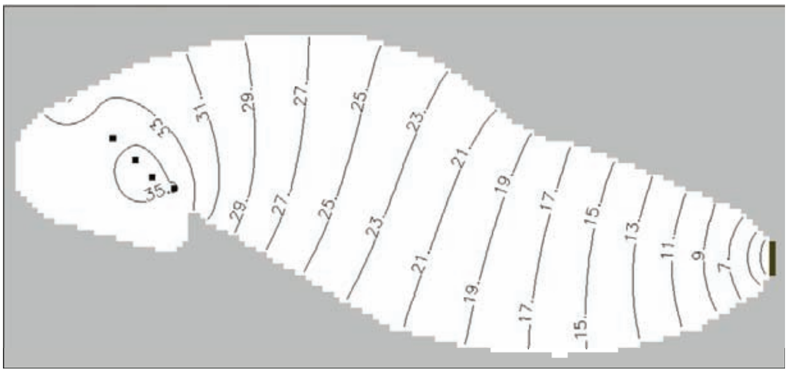


(b) Simulated drawdown in 2002.12

**Fig. 4-25** Contour map for pumping scenario1

**Table 4-10** Comparison of measured water level and simulated water level in Dec, 2002

| Borehole | Initial WL (mamsl) | Observed Result WL (mamsl) | Simulated Result WL (mamsl) | Error (m) |
|---|---|---|---|---|
| VG16 | 683 | 656.450 | 653.031 | 3.419 |
| VR6 | 683.66 | 654.400 | 652.196 | 2.204 |
| VR7 | 685.60 | 653.870 | 651.642 | 2.228 |
| VR8 | 686.20 | 654.820 | 652.689 | 2.131 |
| VR11 | 686.50 | 652.270 | 653.731 | -1.461 |

**Table 4-11** Calibrated model parameters and their confidence limits

| Model Parameters | Initial Value | Estimated Value | 95% percent confidence limits | |
|---|---|---|---|---|
| | | | Lower limit | Upper limit |
| Recharge (m/s) | $9.5\times10^{-10}$ | $5.01\times10^{-11}$ | $2.366046\times10^{-11}$ | $1.056615\times10^{-10}$ |
| Hydraulic conductivity (m/s) | $8\times10^{-7}$ | $7.2\times10^{-6}$ | $5.111307\times10^{-6}$ | $1.013505\times10^{-5}$ |
| Hydraulic conductivity (m/s) Vermaaks River Fault Zone | $8\times10^{-6}$ | $1\times10^{-5}$ | $3.616345\times10^{-6}$ | $2.361634\times10^{-5}$ |
| GHB Hydraulic Conductance ($m^2$/s) | $2.9\times10^{-4}$ | $2.69\times10^{-3}$ | $1.872598\times10^{-6}$ | $3.86708\times10^{-1}$ |

It is surprising that the calibrated recharge of $5.01\times10^{-11}$ m/s is extremely low compared with the previous estimations. It is equivalent to 0.27% of the MAP (600 mm) and the annual recharge volume amounts to about 77200 $m^3$. The water budget shows that only 14% of the abstraction (out-flow) is balanced by recharge (in-flow), accounting for the continuously declining water levels and the induced recharge.

The calibrated recharge should not necessarily be regarded as the actual recharge that takes place in this area because there are a number of assumptions which may simplify the system and introduce inaccuracies to the model. Most of the previous estimates are crosschecked and it was found that the different demarcation of the flow regime may account for the large variety of the estimations. The estimation given by Kotze (2002) was an averaged value of all the previous results obtained from different methods. The flow regime defined in the different methods may range from the weathered zone to the intermediate groundwater circulation system. Usually if the flow regime is limited to the saturated zone, the recharge estimation only considers the infiltration that reaches the groundwater storage, and therefore tends towards a relatively small value. The estimation in this study and those used hydrochemistry methods fall in this case. On the other hand, if the flow regime not only includes the saturated zone but also the shallow unsaturated zone, the recharge estimation tends to be relatively high. The baseflow method, earth model, and soil method fall in this case.

According to the water level in the boreholes, the groundwater abstraction in the modeling area is clearly from the saturated zone. Therefore the estimation of recharge should be accordingly made only for the saturated zone to ensure the proper evaluation of the sustainable yield of the aquifer through utilizing boreholes. Based on these considerations and an integrated consideration of the previous estimates, it is suggested that the Peninsula groundwater recharge is in the range of 0.2% to 2% of the rainfall, which amounts to about 57600 ~ 576000 $m^3$ per year or a continuous boreholes yield of 1.83 to 18.3 *l/s*. The upper limit of this range is probably still too high because the groundwater level has declined by some 30 m with a continuous abstraction rate of less than 18 *l/s* (average 15.36 *l/s*, ranging from 10.2-19.8 *l/s*) in the years of 1993 ~ 2002. From this point of view, the groundwater of Peninsula Window area has been overexploited with the pumping rate near the upper limit of the recharge rate.

### *4.4.4 Model prediction and sustainable yield of model area*

The calibrated model parameters are used in the model prediction for another 10 years from 2003 to 2012. Firstly the three scenarios of pumping schedule listed in Table 6-3 are simulated and then the pumping rates of the existing boreholes are calibrated by the inverse model PEST.

Figs. 4-26 ~ Fig. 4-28 shows the contour map of simulated hydraulic heads and drawdown of the three scenarios. Because the total pumping rate is the same (18 *l/s*) in all the scenarios, the general distributions of the hydraulic heads and the drawdown are similar to each other. The averaged drawdown of the modeling area is about 22.9 m for each scenario. It appears highly likely that a 10-year-drawdown at this pumping rate would induce many problems including insufficient water supply, deterioration of borehole efficiency, negative environmental impacts, and so on. Therefore the sustainable yield of the boreholes is simulated inversely using the previously calibrated parameters with the given drawdown in the 5 boreholes (VG16, VR6~VR11) as constraints. According to the pumping test, VR7 is the most efficient borehole of the four in Vermaaks Wellfield; therefore it is assumed that the abstraction is solely from borehole VR7. Three levels of drawdown (1 m, 5 m, and 10 m) in the 5 observation boreholes affected by the pumping in VR7 are simulated to derive the optimized pumping rate of VR7 for each drawdown level. The optimized values are modified to integer values and then the groundwater flows are simulated directly with the integer value of pumping rate. The optimized pumping rate of VR7 and the relevant integral values together with the resultant averaged drawdown from the direct model are listed in Table 4-12.

**Table 4-12** Drawdown and pumping rate of VR7

| Observation Drawdown[1] (m) | Pumping Rate (l/s) | | Averaged Drawdown[4] (m) |
|---|---|---|---|
| | Optimized[2] | Integer[3] | |
| 1 | 2.26 | 2 | 0.045 |
| 5 | 4.23 | 4 | 2.758 |
| 10 | 6.61 | 7 | 6.980 |

Notes:
1) Observation Drawdown: the drawdown is input into the inverse model as observation values;
2) Optimized: the optimized pumping rate of borehole VR7 from the inverse model;
3) Integer: the integral value of the optimized pumping rate of borehole VR7;
4) Averaged Drawdown: the averaged drawdown in the modeling area derived from the direct model using the integral pumping rate values.

Figs. 4-29 ~ Fig. 4-31 shows the contour map of simulated hydraulic heads and drawdown of the direct model with the integer pumping rates of VR7. As can be clearly seen, if the pumping rate is 2 *l/s*, the averaged drawdown of the model area is close to 0 after 10 years of abstraction. Therefore the sustainable yield should be 2 *l/s* or a little higher than that, e.g. 2.4 *l/s*, equaling to the recharge rate in this area on a continuously pumping basis. The pumping rate of 4 *l/s* will probably lead to an averaged drawdown of 2.758 m after 10 years, which may not cause serious problems as described before. Compared with the current pumping rate of the wellfield, a rate of 7 *l/s* might still be acceptable, although the possibility that it may induce problems cannot be ruled out.


(a) Simulated hydraulic heads in 2012.12

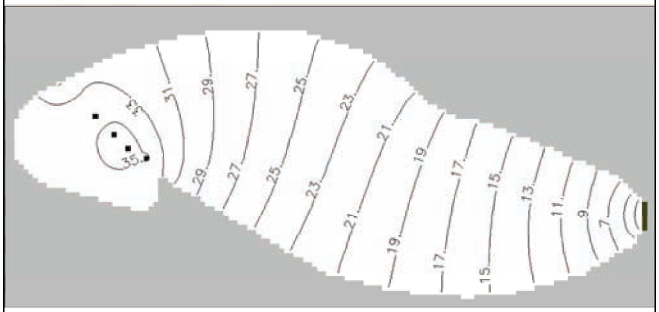


(b) Simulated drawdown in 2012.12

**Fig. 4-26 Contour map of pumping scenario1**

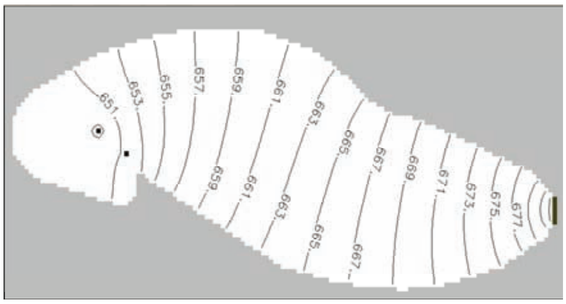


(a) Simulated hydraulic heads in 2002.12

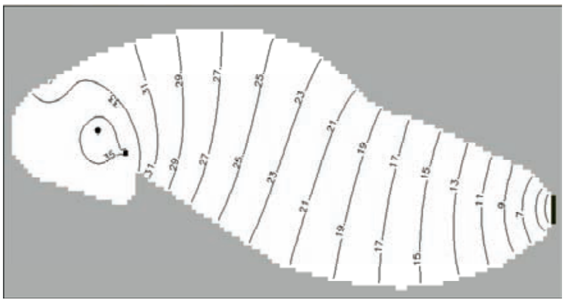


(b) Simulated drawdown in 2002.12

**Fig. 4-27 Contour map of pumping scenario2**


(a) Simulated hydraulic heads in 2012.12

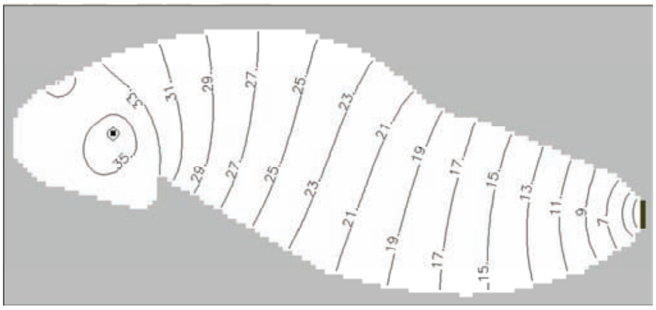


(b) Simulated drawdown in 2012.12

**Fig. 4-28 Contour map of pumping scenario3**

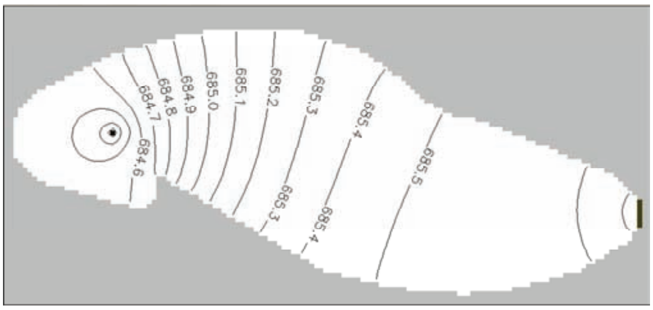


(a) Simulated hydraulic heads in 2012.12

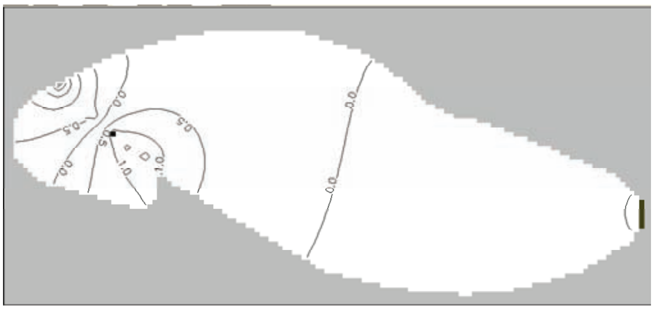


(b) Simulated drawdown in 2012.12

**Fig. 4-29 Contour map of the groundwater flow simulation from 2003.1 to 2012.12**
**(Pumping Rate=2 l/s, Averaged Drawdown=0.045 m)**

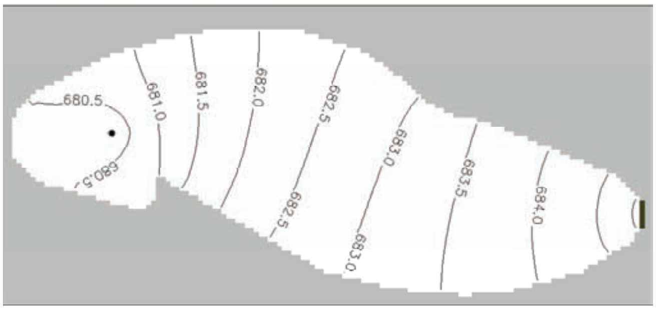


(a) Simulated hydraulic heads in 2012.12

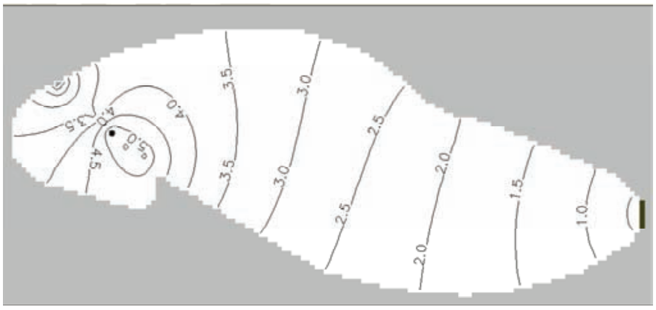


(b) Simulated drawdown in 2012.12

**Fig. 4-30 Contour map of the groundwater flow simulation from 2003.1 to 2012.12 (Pumping Rate=5 l/s, Averaged Drawdown=2.758 m)**

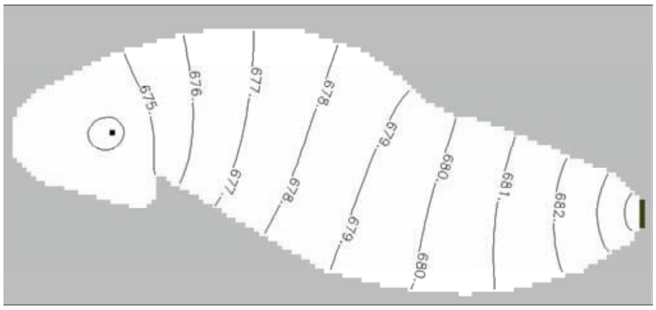


(a) Simulated hydraulic heads in 2012.12

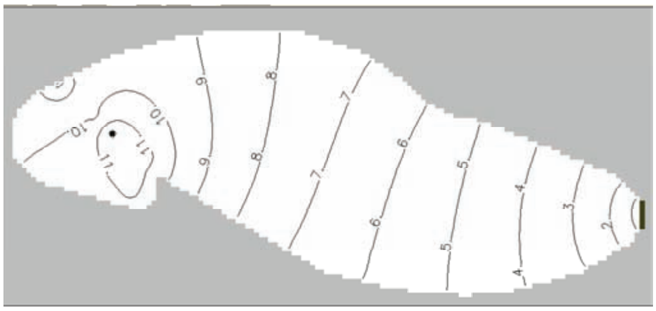


(b) Simulated drawdown in 2012.12

**Fig. 4-31 Contour map of the groundwater flow simulation from 2003.1 to 2012.12 (Pumping Rate=7 l/s, Averaged Drawdown=6.980 m)**

# 5. Regional Groundwater Resource Evaluation

## 5.1 Introduction

The opportunities for the additional utilization of surface water resources are limited in the TMG area and the construction of new large dams may result in serious environmental problems since most of the mountain areas along Cape Fold Belt belong to a diverse but threatened floral kingdom and are ecologically sensitive (Hartnady and Hay, 2002). It has been suggested that the TMG aquifer system has the potential to become a major source of bulk water supply in the Western and Eastern Cape provinces. However the lack of proper resource estimation, and the practical difficulties involved in investigating this aquifer system impedes the optimal exploration and exploitation of the aquifers. Moreover, it is extremely difficult to characterize the fractured rock aquifers due to the complexity of their geometric and hydraulic properties.

It is also difficult to transfer the knowledge gained from local level studies to regional level resource evaluation. At times an incorrect assessment of local aquifer parameters has lead to the failure of water supply schemes (Jolly, 2002). To be a viable source of bulk water supply the TMG aquifers must bridge the gap between increasing water demand and the limited existing surface water resources in a sustainable manner. Therefore the regional evaluation of TMG groundwater resources is of foremost importance in the context of integrated water resources utilization and management. The quantitative estimations of TMG groundwater recharge, storage and discharge are presented in this chapter based on the data processing and analyses largely carried out on GIS platform on a regional scale, from which the sustainable yield of TMG aquifer is recommended.

## 5.2 Data availability

All climate data are obtained from WR90, the project "Surface Water Resources of South Africa 1990" funded by the South Africa Water Research Commission (Midgley et al., 1994). The project started in January 1990 and ended in 1994, and it yielded a wealth of information on surface water resource, including precipitation, evaporation, stream flow, land cover, water use and hydrological analysis, which is either adopted or adapted in this study.

Borehole data for the current study were largely extracted from NGDB (National Groundwater Database), including elevation, geological borehole logging, hydrogeological parameter estimates (very few), water level and pumping test data. References related to the TMG studies since 1935 have been critically reviewed and the data were captured.

### *5.2.1 The study area*

TMG outcrop area is estimated at 37,000 km$^2$. The study area is usually limited to the area of 80,000 km$^2$ along the Cape Fold Belt (Fortuin, 2004). However, the TMG extends to a large extent underneath the Karoo basin to the north. To study the TMG aquifers properly as a unique groundwater circulation system independent from other systems such as the Bokkeveld Group and Karoo Super Group, it is necessary to expand the study area to include not only the outcrop but also the area where the TMG underlies younger rocks. The area is bounded by the zero-thickness deposit of TMG in the north, and coastlines in the west, south, and east. The revised study area of 248,400 km$^2$ where the TMG can be found within South Africa was demarcated using GIS techniques. TMG outcrop accounts for 14.91% of the whole study area. Most of the TMG strata are exposed on the mountainous areas along the Cape Fold Belt from Vanrhynsdorp in the northwest to Wellington and Worcester in the south, and to Port Elizabeth in the east.

### *5.2.2 Topographic data*

Topographic data include the point elevation data and contours as shape files. The DEMs of the study area are constructed from these data using TopoGrid function on an ArcInfo workstation (ESRI, 1996). The elevation for the study area ranges from 0 m to 2200 m and most of the TMG exposed in the mountainous area have an elevation of greater than 1000 m.

### *5.2.3 Geologic Data*

The lithostratigraphic and structural information for the study area is mainly extracted from the digital geology map available from WR90 database, calibrated with geological map sheets (1:250,000 scale). Both the printed maps and the digital map provide abundant data for the studies of cross sections and further generation of isopach and isobath maps of TMG, which is essential for storage calculation.

### *5.2.4 Climatic and hydrologic data*

Climatic and hydrologic data includes precipitation, stream flow, water-holding capacity and evapotranspiration data, which is used in the groundwater recharge and discharge estimation. It is generally accepted that the recharge of TMG aquifers mainly takes place in the outcrop areas (Wu, 2005).

### 5.2.4.1 Precipitation

Precipitation data from 1920 to 1989 are given in two forms, monthly average percentage for each hydro-zone and monthly observation data from rainfall stations. To make sure the study is on a mean annual basis, it is preferable to use the monthly average percentage data together with the isolines of mean annual precipitation (MAP) to obtain the monthly precipitation data for the study area.

The MAP in the TMG outcrop areas ranges from 100 mm to 1500 mm (fig. 5-1). There are 81 rainfall zones identified in the TMG outcrop areas (Fig. 5-2), which means that there are 81 rainfall patterns with different monthly percentages of MAP appearing in the area. The monthly percentages of some rainfall zones are listed in Table 5-1. The resultant spatial distribution of monthly precipitation for the outcrop area can be derived by intersecting the two maps in GIS.

**Table 5-1** Monthly percentage for rainfall zones in TMG outcrop area (%)

| Rainfall zone | OCT | NOV | DEC | JAN | FEB | MAR | APR | MAY | JUN | JUL | AUG | SEP |
|---|---|---|---|---|---|---|---|---|---|---|---|---|
| E1C | 5.64 | 4.03 | 2.74 | 1.77 | 2.45 | 3.21 | 8.05 | 13.80 | 19.09 | 15.30 | 15.59 | 8.34 |
| E1D | 5.05 | 4.17 | 2.91 | 1.72 | 2.37 | 3.58 | 8.06 | 13.64 | 20.58 | 15.18 | 15.03 | 7.72 |
| G1A | 6.14 | 4.16 | 2.93 | 2.58 | 2.64 | 3.29 | 8.00 | 14.35 | 17.42 | 15.27 | 14.33 | 8.90 |
| G4C | 7.38 | 4.82 | 3.27 | 3.44 | 3.63 | 4.11 | 7.87 | 12.59 | 15.77 | 14.20 | 13.77 | 9.18 |
| H2 | 6.60 | 5.43 | 3.21 | 3.11 | 4.15 | 4.66 | 8.20 | 11.94 | 17.34 | 13.70 | 14.04 | 7.64 |
| H4C | 8.09 | 7.87 | 4.24 | 4.58 | 5.76 | 6.90 | 10.34 | 10.06 | 11.11 | 10.09 | 12.59 | 8.38 |
| H6A | 6.37 | 5.10 | 2.59 | 2.47 | 2.63 | 3.37 | 7.12 | 12.87 | 17.22 | 15.55 | 15.69 | 9.02 |
| H8A | 9.67 | 9.74 | 6.08 | 7.02 | 8.10 | 9.90 | 9.58 | 8.11 | 6.67 | 7.30 | 9.51 | 8.31 |
| J1D | 6.90 | 7.81 | 5.47 | 5.44 | 6.60 | 8.57 | 10.21 | 10.43 | 11.75 | 9.62 | 10.36 | 6.84 |
| J3F | 8.30 | 9.76 | 6.77 | 6.21 | 8.61 | 9.97 | 9.88 | 8.98 | 7.28 | 7.80 | 8.58 | 7.86 |
| K1 | 9.62 | 9.82 | 6.50 | 7.49 | 7.79 | 10.25 | 9.15 | 8.04 | 6.66 | 7.05 | 9.01 | 8.61 |
| K3 | 9.64 | 9.94 | 8.49 | 8.88 | 8.76 | 10.76 | 8.11 | 7.10 | 5.33 | 6.11 | 8.03 | 8.85 |
| K9B | 9.76 | 9.48 | 6.71 | 6.96 | 6.72 | 9.47 | 7.78 | 9.02 | 7.14 | 8.42 | 9.27 | 9.26 |
| L8D | 9.27 | 9.01 | 7.12 | 6.98 | 8.08 | 10.78 | 7.75 | 8.95 | 6.51 | 7.66 | 8.63 | 9.25 |
| M1A | 10.49 | 10.79 | 7.63 | 7.30 | 8.27 | 11.23 | 8.81 | 7.21 | 5.49 | 6.63 | 7.11 | 9.03 |

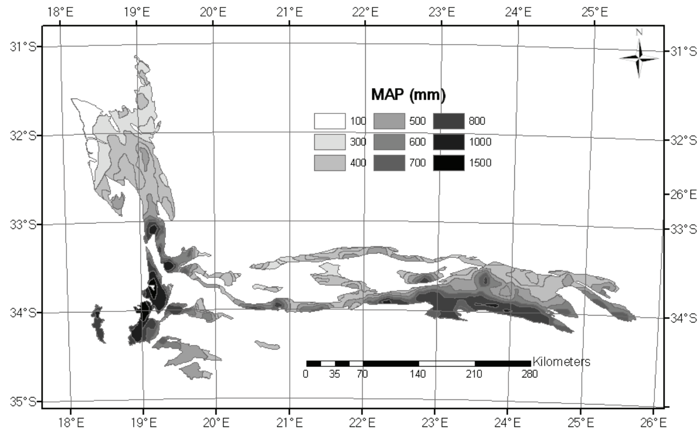


**Fig. 5-1** MAP for the TMG outcrop areas

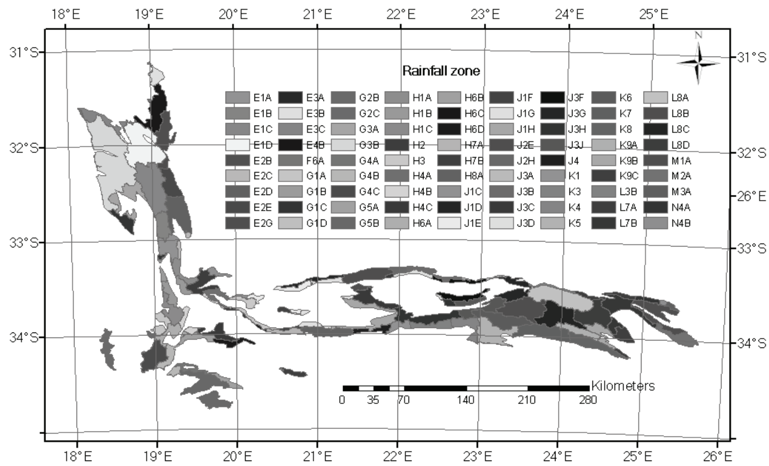


**Fig. 5-2** Rainfall zones for the TMG outcrop areas

### 5.2.4.2 Stream flow data

Stream flow data throughout the country are available in WR90 (Midgley et al., 1994) and have been pre-processed for more reliable analysis. The distribution of Mean Annual River flow (MAR) in the TMG outcrop areas is shown in Fig. 5-3. This data set is also stored in two forms: monthly flow on gauge station and naturalized monthly stream flow in the quaternary catchments. The latter is selected in the study. Based on the concept that stream flow is composed of baseflow and surface runoff, a digital recursive filter method is used for baseflow separation.

**Table 5-2** Typical Values (m) for Soil-water Parameters by Texture (after ASCE, 1990)

| Texture Class | Field Capacity | Wilting Point | Available Capacity |
|---|---|---|---|
| Sand | 0.12 | 0.04 | 0.08 |
| Loamy Sand | 0.14 | 0.06 | 0.08 |
| Sandy Loam | 0.23 | 0.10 | 0.13 |
| Loam | 0.26 | 0.12 | 0.14 |
| Silt Loam | 0.30 | 0.15 | 0.15 |
| Silt | 0.32 | 0.15 | 0.17 |
| Silty Clay Loam | 0.34 | 0.19 | 0.15 |
| Silty Clay | 0.36 | 0.21 | 0.15 |
| Clay | 0.36 | 0.21 | 0.15 |

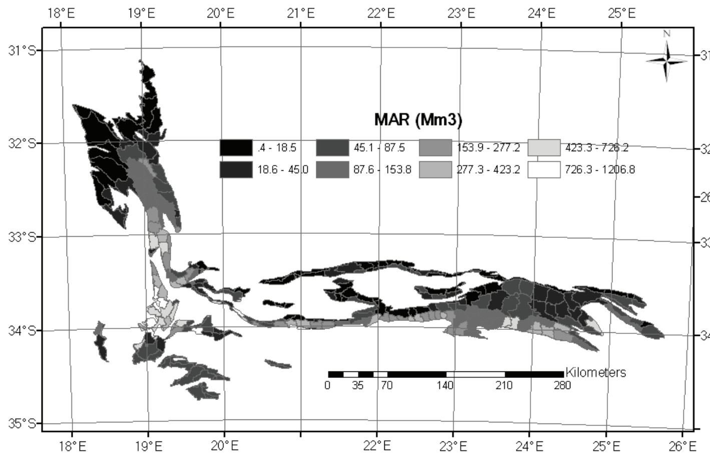


**Fig. 5-3** MAR for the TMG outcrop areas

### 5.2.4.3 Water-holding capacity data

Water-holding capacity data is usually required in soil water balance calculations. Global estimates of "plant-extractable water capacity" are available on a 0.5° grid (Dunne and Wilmot, 1996). One reason for developing this global database was to eliminate the need for assuming spatially invariant plant-extractable water capacity in soil-water balance computations made over large areas. Information about sand, clay, organic content, plant rooting depth, and horizon thickness are used to estimate the plant-extractable water capacity. Table 5-2 gives some typical values of available water-holding capacity for the most common texture classes. In the current study, we take the global estimates as a reference due to the low precision of the 0.5° grid and the irregular shape of the study area.

The soil map provided by WR90 shows 82 soil types throughout the country. The soil types were analyzed in terms of features that are most likely to influence hydrological response, i.e. depth of soil, soil texture, and slope. In the TMG outcrop area 18 soil types are included

(Fig. 5-4). The water-holding capacity data for study area is derived from the combined analysis of the local soil map and global soil map.

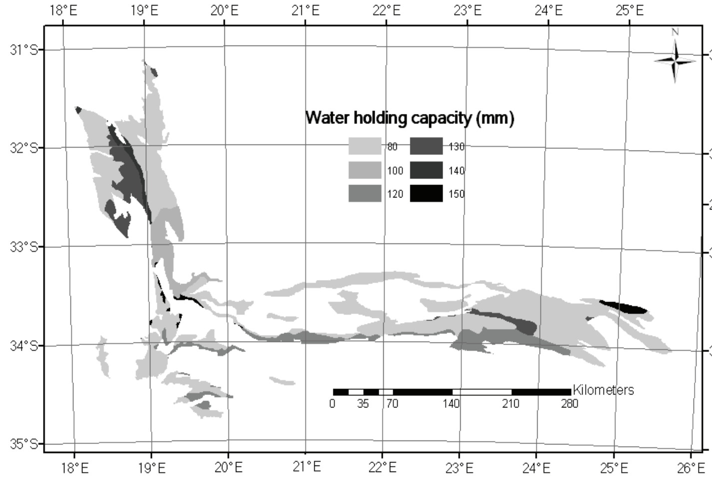


**Fig. 5-4** Water holding capacity of TMG outcrop areas

#### 5.2.4.4 Evapotranspiration

Evapotranspiration is the largest component of water balance estimates (Connelly et al., 1989). Although it includes evaporation from soils and plant transpiration, a common function is applied to calculate these two components combined.

*Pan Evaporation (ET)* data in WR90 is interpolated for each location based on data from major regional centres. It is given in the same form as precipitation data and the same approach is adopted to derive the monthly pan-evaporation data as a percentage of MAE for each evaporation zone (listed in Table 5-3), from which the mean monthly evaporation can be determined and used for estimates of potential evaporation in the soil-water balance calculations. The distribution of MAE, the evaporation zones and the vegetation types in the

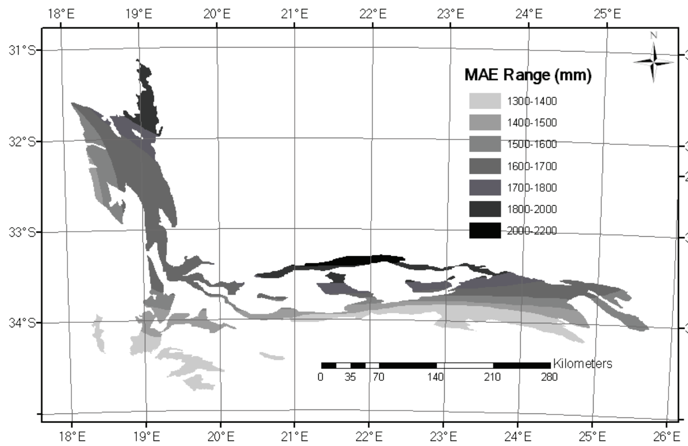


**Fig. 5-5** MAE for the TMG outcrop areas

TMG outcrop areas are showed in Fig. 5-5, Fig. 5-6 and Fig. 5-7 respectively.

*Potential evapotranspiration (PET)* is defined as the total of moisture evaporated from the soil surface and transpired by the plant roots when there is an unlimited water supply. Factors such as temperature, sunlight hours, wind, humidity and atmospheric pressure and the vegetation type affect the potential evapotranspiration. The simplest way to estimate PET is:

$$PET = ET * Pan\ Factor * Crop\ factor \quad (5\text{-}1)$$

Where *Pan Factor* is the ratio of open water evaporation or catchment transpiration to Pan Evaporation. Pan factors vary with location and season. *Crop factor* is the coefficient expressing the proportion of open water evaporation transpired by a crop under the same energy gradient, varying with stage of growth, plant type, plant density, sunlight, wind and soil conditions (Patterson, 2002). The Pan factors (Table 5-4) and Crop factors (Table 5-5) for each vegetation type in the study area are listed below (Midgley et al., 1994).

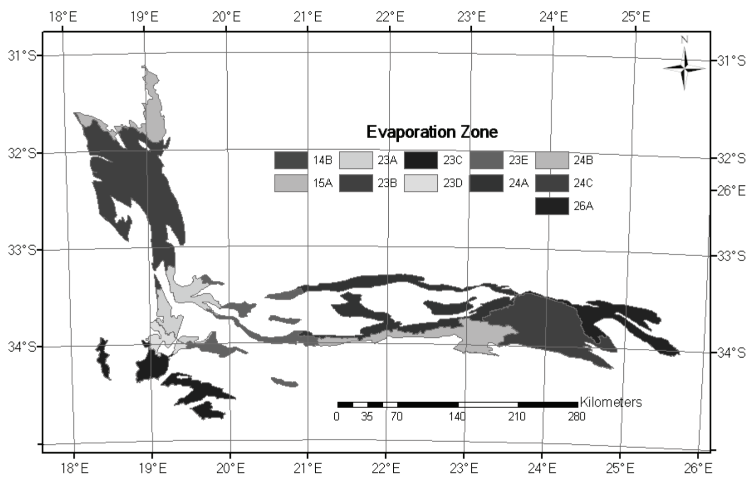


**Fig. 5-6** Evaporation Zones for the TMG outcrop areas

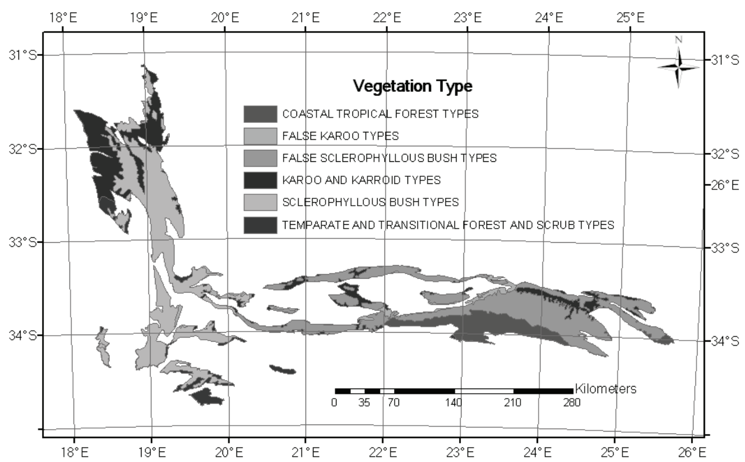


**Fig. 5-7** Vegetation types for the TMG outcrop areas

**Table 5-3** Monthly evaporation percentages for the TMG evaporations zones

| Evaporation zone | OCT | NOV | DEC | JAN | FEB | MAR | APR | MAY | JUN | JUL | AUG | SEP |
|---|---|---|---|---|---|---|---|---|---|---|---|---|
| 14B | 9.58 | 11.40 | 12.32 | 12.64 | 10.23 | 9.57 | 6.92 | 5.41 | 4.76 | 4.52 | 5.53 | 7.12 |
| 15A | 9.21 | 11.38 | 13.37 | 14.22 | 11.48 | 10.38 | 6.69 | 4.63 | 3.47 | 3.62 | 4.77 | 6.78 |
| 23A | 9.19 | 11.46 | 14.11 | 14.78 | 12.40 | 11.16 | 7.05 | 4.34 | 2.94 | 2.96 | 3.83 | 5.78 |
| 23B | 8.67 | 12.08 | 14.83 | 15.09 | 12.45 | 11.51 | 7.06 | 4.00 | 2.62 | 2.55 | 3.57 | 5.57 |
| 23C | 8.76 | 12.23 | 14.38 | 14.73 | 12.43 | 10.86 | 6.76 | 3.90 | 3.00 | 3.32 | 3.90 | 5.73 |
| 23D | 8.77 | 12.40 | 15.47 | 16.12 | 13.44 | 11.29 | 6.12 | 3.24 | 2.40 | 2.21 | 3.24 | 5.30 |
| 23E | 9.65 | 12.36 | 14.97 | 14.98 | 11.88 | 9.81 | 6.36 | 3.91 | 2.69 | 2.94 | 4.09 | 6.36 |
| 24A | 9.31 | 11.56 | 13.89 | 14.21 | 11.62 | 10.18 | 6.77 | 4.51 | 3.30 | 3.50 | 4.68 | 6.47 |
| 24B | 9.21 | 10.91 | 13.29 | 12.96 | 10.16 | 8.77 | 6.59 | 5.41 | 4.95 | 5.06 | 5.92 | 6.77 |
| 24C | 9.19 | 11.10 | 13.74 | 13.97 | 11.09 | 9.72 | 6.91 | 4.85 | 3.95 | 3.94 | 4.87 | 6.67 |
| 26A | 9.51 | 11.23 | 13.45 | 13.79 | 11.06 | 9.54 | 6.92 | 4.88 | 3.54 | 3.83 | 5.23 | 7.02 |

**Table 5-4** Pan factors for open water evaporation and catchment evapotranspiration

| | OCT | NOV | DEC | JAN | FEB | MAR | APR | MAY | JUN | JUL | AUG | SEP |
|---|---|---|---|---|---|---|---|---|---|---|---|---|
| Lake evaporation | 0.81 | 0.82 | 0.83 | 0.84 | 0.88 | 0.88 | 0.88 | 0.87 | 0.85 | 0.83 | 0.81 | 0.81 |
| Catchment evapotranspiration | 0.80 | 1.00 | 1.00 | 1.00 | 1.00 | 1.00 | 1.00 | 1.00 | 1.00 | 0.80 | 0.80 | 0.80 |

**Table 5-5** Crop factors for vegetation types

| Vegetation type | Crop factors | | | | | | | | | | | |
|---|---|---|---|---|---|---|---|---|---|---|---|---|
| | OCT | NOV | DEC | JAN | FEB | MAR | APR | MAY | JUN | JUL | AUG | SEP |
| Costal Tropical Forest | 0.67 | 0.69 | 0.75 | 0.75 | 0.75 | 0.74 | 0.69 | 0.61 | 0.56 | 0.40 | 0.51 | 0.60 |
| Inland Tropical Forest | 0.73 | 0.78 | 0.78 | 0.78 | 0.78 | 0.75 | 0.70 | 0.65 | 0.50 | 0.40 | 0.55 | 0.65 |
| BushVeld | 0.51 | 0.56 | 0.59 | 0.59 | 0.59 | 0.58 | 0.50 | 0.44 | 0.32 | 0.27 | 0.35 | 0.45 |
| False Bushveld | 0.48 | 0.58 | 0.60 | 0.62 | 0.62 | 0.58 | 0.53 | 0.38 | 0.25 | 0.20 | 0.23 | 0.35 |
| Karoo and Karroid | 0.41 | 0.46 | 0.50 | 0.50 | 0.50 | 0.48 | 0.46 | 0.37 | 0.25 | 0.20 | 0.22 | 0.33 |
| False Karoo | 0.36 | 0.45 | 0.50 | 0.50 | 0.50 | 0.46 | 0.36 | 0.26 | 0.21 | 0.20 | 0.20 | 0.27 |
| Temperate and Transitional Forest and Scrub | 0.58 | 0.61 | 0.61 | 0.61 | 0.60 | 0.60 | 0.57 | 0.46 | 0.36 | 0.29 | 0.36 | 0.48 |
| Pure Grassveld | 0.43 | 0.56 | 0.62 | 0.62 | 0.62 | 0.55 | 0.43 | 0.28 | 0.20 | 0.20 | 0.20 | 0.27 |
| False Grassveld | 0.53 | 0.65 | 0.73 | 0.73 | 0.73 | 0.67 | 0.61 | 0.43 | 0.24 | 0.20 | 0.27 | 0.41 |
| Fynbos | 0.60 | 0.60 | 0.60 | 0.60 | 0.55 | 0.55 | 0.55 | 0.45 | 0.40 | 0.20 | 0.35 | 0.50 |
| False Fynbos | 0.55 | 0.55 | 0.55 | 0.55 | 0.55 | 0.50 | 0.50 | 0.40 | 0.35 | 0.20 | 0.35 | 0.50 |

*Actual evapotranspiration (AET)* Water is not always readily available for evapotranspiration. Over many rural surfaces there are times, notably on a summer afternoon, when the soil and plants are incapable of moving water to the surface ready for evaporation or transpiration as fast as the atmosphere can do the evaporation. Bare soil surfaces begin to dry out and plants begin to wilt. Their rate of evapotranspiration is termed actual evapotranspiration, which will be less than the potential evapotranspiration. Many investigators have used a soil-moisture extraction function or coefficient of evapotranspiration, *f*, which relates the actual rate of evapotranspiration to the potential rate of evapotranspiration based on some function of the current soil moisture content and the water-holding capacity (Haan, 1972)

$$AET = f * PET \tag{5-2}$$

$$f = \mathrm{wc} / \mathrm{wc}^* \tag{5-3}$$

Where $f$ is the function in which the ratio of evapotranspiration to potential evapotranspiration is proportional to the current moisture level. It has been applied when budgeting with monthly climate values and is used in this study (Shuttleworth, 1993 and Dingman, 1994). This function predicts lower evapotranspiration rates than a function with a breakpoint that may offset (to some degree) the low rainfall intensities resulting from the use of monthly averaged rainfall. *wc* denotes the current soil water moisture *and wc** the water holding capacity.

### *5.2.5 Borehole information from NGDB*

#### 5.2.5.1 Borehole distribution and usability

A total of 35151 boreholes drilled in the TMG area were identified from the NGDB and these TMG-related boreholes were carefully sorted out, based on their locations, drilling depth, geological formations, hydrological characteristics, and so on. The procedure carried out is summarized as follows:

- As the statistics of borehole discharge rate will be used in the quantification of the regional discharge of the TMG aquifer, boreholes without information on discharge rate are excluded
- For the convenience of the study, boreholes are grouped into outcrop-boreholes and non-outcrop-boreholes. Boreholes located on the TMG outcrop area are termed outcrop-boreholes, while the remainder are called non-outcrop-boreholes
- Three subgroups of outcrop-boreholes are identified: Nardouw, Peninsula and Piekenierskloof. There are 1139 boreholes drilled on the outcrops of Nardouw, 622 on the outcrops of Peninsula and 209 on the outcrops of Piekenierskloof
- Though most of the boreholes were drilled in the non-outcrop area of TMG, because of the limited depth of these boreholes, almost all of them don't penetrate the TMG, and are therefore are irrelevant to this study. A thorough filtering according to their geological

logging information together with their location, revealed that for boreholes located in the non-TMG outcrop area, only 173 penetrated the Nardouw and 50 the Peninsula. Most of the non-TMG outcrop boreholes were drilled in the contact zones of TMG and the adjacent Cedarberg Formation or Bokkeveld Group.

Fig. 5-8 shows the spatial distribution of the sorted TMG-related boreholes, and their depth statistics are listed in Table 5-6. The water level data for all these boreholes are unevenly distributed both spatially and temporally and can not be used in the regional resource evaluation. However local analysis in some specific areas can be performed if the water level data in those areas are adequate. The discharge rates of the boreholes are used in the regional groundwater discharge estimation.

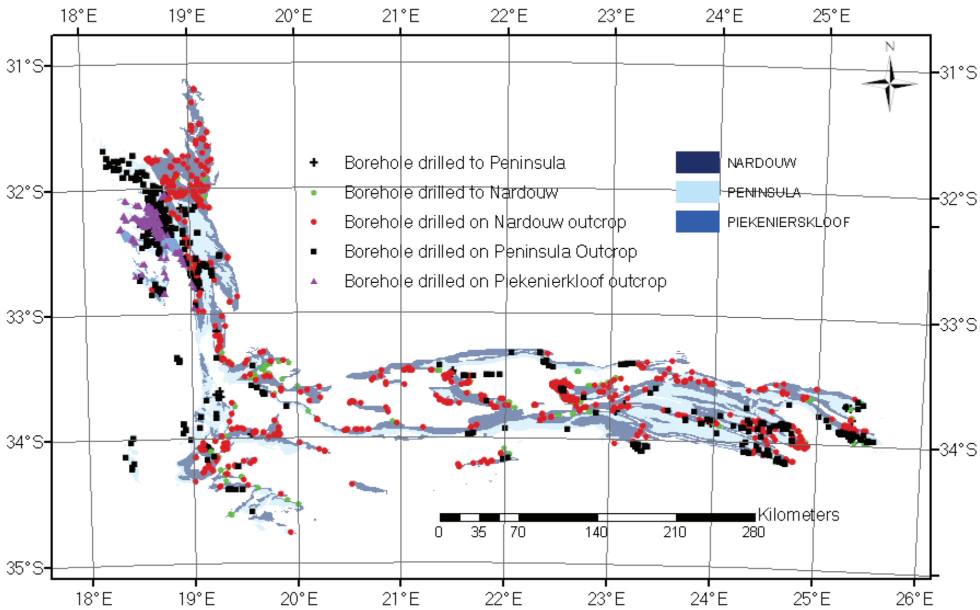


**Fig. 5-8** The spatial distribution of TMG-related boreholes

**Table 5-6** Depth statistics of TMG related boreholes

| **TMG related Boreholes** | | **Number** | **Percentage on depth range** | | | | | | |
|---|---|---|---|---|---|---|---|---|---|
| | | | <50 | 50-100 | 100-200 | 200-300 | 300-500 | >500 | Unknown |
| Outcrop | Nardouw | 1139 | 20.9% | 38.7% | 28.9% | 4.7% | 0.2% | 0.2% | 6.4% |
| | Peninsula | 622 | 14.6% | 32.6% | 41.3% | 2.7% | 0.3% | 0.0% | 8.4% |
| | Piekenierskloof | 209 | 14.4% | 31.1% | 36.4% | 1.0% | 0.0% | 0.0% | 17.2% |
| Non Outcrop | Nardouw | 173 | 0.0% | 55.5% | 37.0% | 7.5% | 0.0% | 0.0% | 0.0% |
| | Peninsula | 50 | 0.0% | 6.0% | 82.0% | 6.0% | 4.0% | 2.0% | 0.0% |
| Sum | | 2193 | 16.4% | 36.9% | 35.0% | 4.1% | 0.3% | 0.1% | 7.3% |

#### 5.2.5.2 Springs issuing from TMG

A lot of springs issue from the TMG. Meyer (2002) contributed a detailed description and classification of these springs. According to the mode of occurrence, three types of springs were identified: shallow circulating springs, lithology controlled springs and fault controlled springs. In the TMG area, 501 springs are identified with a depth of "0.01 m" in the National Groundwater Database (NGDB, 2005) in TMG area, among which 103 springs located in the TMG outcrop area are assumed TMG-related (Fig. 5-9). Because of the lack of attribute descriptions for these springs, it is difficult to classify them into the abovementioned three types.

#### 5.2.5.3 Hot springs

Due to their specific hydrogeological significance the eleven more important and well-known fault controlled hot springs are separately discussed here. It is interesting that these springs are distributed along the Cape Fold Belt and form a distinctive curvature (Fig. 5-9). Five hot

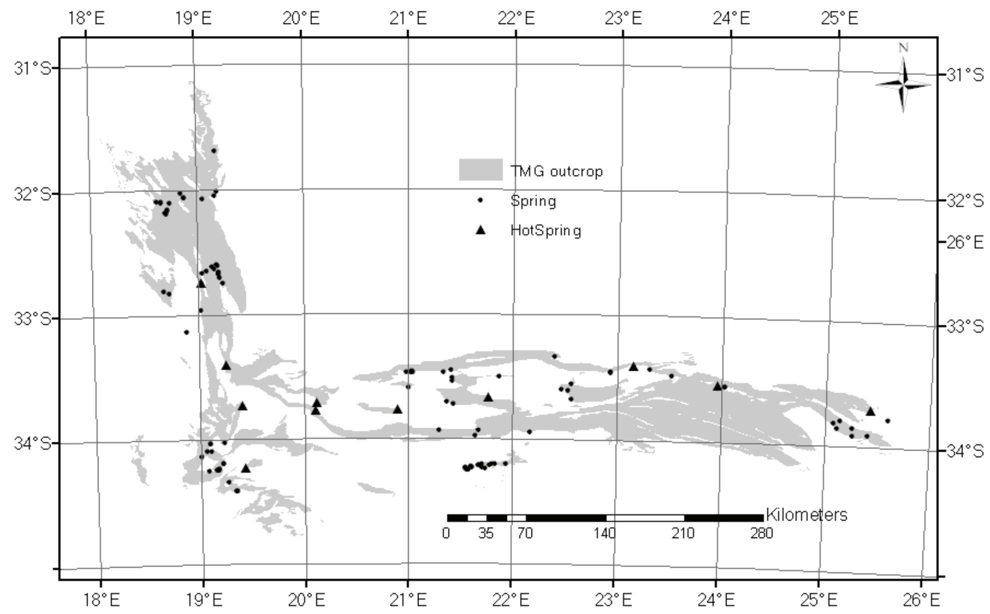


**Fig. 5-9** Spatial distribution of TMG-related springs and hot springs.

springs are located in the limited syntaxis domain, which may indicate more intensive and deeper fracturing in that domain. The main characteristics of these springs are listed in Table 5-7.

**Table 5-7** Main information of TMG-related hot springs (After Meyer, 2002)

| Name | Temp (°C) | Yield (l/s) | Cond. (mS/m) | Probable depth of circulation (m) | Classification of thermal water | Geological setting |
|---|---|---|---|---|---|---|
| The Baths | 43 | 29 | 8 | 2000 | Hyperthermal | Situated on the western limb of a deep syncline on the contact with the Cedarberg Shale Formation. |
| Goudini | 40 | 11 | 7 | 1700 | Thermal | Situated on a NNW-striking fault near the contact with Bokkeveld group shale. |
| Brandvlei | 64 | 127 | 8 | 3600 | Hyperthermal | Situated on a NE-striking fault, close to the contact with Bokkeveld Group shale |
| Caledon | 37 | 9 | 20 | 1600 | Thermal | Situated on an E-striking fault against Bokkeveld Group shale. |
| Avalon | 43 | 38 | 11 | 2000 | Hyperthermal | E-striking fault, Nardouw sandstones faulted against Bokkeveld Group shale. |
| Baden | 38 | 37 | 10 | 1500 | Thermal | Ill-defined E-striking fault in Nardouw sandstones on the contact with Bokkeveld shales. |
| Warmwater-berg | 45 | 9 | 26 | 2100 | Hyperthermal | NE-striking fault. Nardouw Subgroup sandstone faulted against Bokkeveld Group shale. |
| Calitzdorp | 50 | 8 | 31 | 2500 | Hyperthermal | NE-striking fault. Nardouw Subgroup sandstone faulted against Bokkeveld Group shale. |
| Toverwater | 44 | 11 | 15 | 2000 | Hypothermal | E-striking Cango fault. Peninsula Formation sandstone faulted against Enon Formation (Uitenhage Group) conglomerate. |
| Studtis | 24 | 31 | 18 | 480 | Hypothermal | NE-striking fault. Nardouw Subgroup sandstone faulted against Bokkeveld Group shale. |
| Uitenhage | 23 | 45 | 34 | 400 | Hypothermal | ESE-striking fault in Peninsula Formation sandstone, on or close to the contact with Kirkwood Formation (Uitenhage Group). Yield fluctuates in accordance with abstraction from aquifer. |
| | | | | | | |

## 5.3 Demarcation of confined and unconfined aquifers

Whether the TMG aquifer is confined or not deserves clarity. It is incorrect to classify an aquifer as the confined aquifer only because water level rises up after it gets struck. The rise of water level is a necessary condition  for a confined aquifer but not sufficient condition for an aquifer being termed the confined. In fact rise up of water level is an innate hydraulic behaviour of fractured rock aquifers, especially in the TMG. As the confining units in the TMG suffer from fault displacement, both confined and unconfined aquifers could be demarcated according to their geological settings even at a regional scale.

Basically the TMG distribution area can be divided into TMG outcrop areas and non-TMG outcrop areas. In TMG outcrop areas, the subdivision of Nardouw outcrop and Peninsula outcrop is applied. In Nardouw outcrop areas, the Nardouw aquifer can be considered to be an unconfined aquifer while the Peninsula is confined by the overlying Cedarberg Aquitard. In the Peninsula outcrop areas where the Cedarberg formation has been denuded, the Peninsula aquifer becomes unconfined. In non-TMG outcrop areas, both the Nardouw and the Peninsula are overlain by Bokkeveld Group, therefore both the Peninsula and Nardouw can be regarded as confined aquifer system because overlying Gydo Formation at the base of the Bokkeveld is usually regarded as an aquitard. This delineation is schematically depicted in Fig. 5-10.

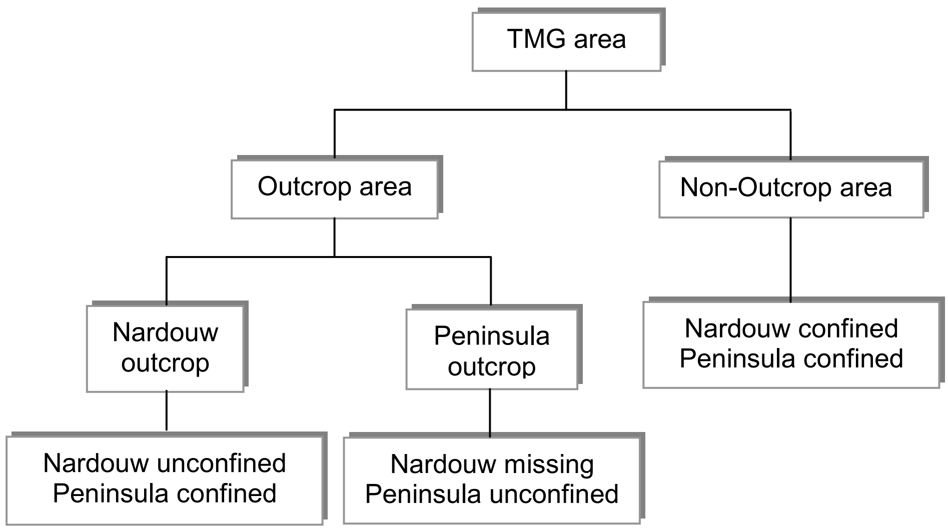


**Fig. 5-10** Demarcation of confined and unconfined aquifers in the TMG area

## *5.4 Recharge estimation*

It is assumed that only the TMG outcrop area can receive the precipitation as recharge area for the TMG aquifers. This probably does not seem to introduce significant error for groundwater recharge estimation in the whole TMG area since hydraulic connections seldom occur between TMG and other geologic formations. Hence only the TMG outcrop areas are selected as the study area in recharge estimation.

Several approaches have been applied in the recharge estimation in TMG areas, many of which were conducted on local scales or at field sites. The soil water balance method is a commonly used and effective method to estimate groundwater recharge on a regional scale (Barringer and Lilburne, 1999; Reed et al., 1997). Based on physical conceptual model the soil water balance method simulates the hydrological procedures involved in a soil water budget using a knowledge of the relationship of the components that participate in these processes. The components commonly include precipitation, actual evapotranspiration, runoff, soil moisture and recharge. Regarding the relationships between these components, a simplified empirical function or formula usually provides a reasonable solution for large-scale estimations. Soil water balance is seldom used in TMG area because the TMG rocks are characterized by a thin overlying soil layer or bare outcrops and fractured sandstone. This study however attempts to apply the soil water balance method toget a regional coverage of recharge estimation. With limited knowledge of the hydraulic dynamic processes in the fractured rock zone, this study only considers the hydrological process in the upper soil zone, rather than the recharge process as a whole. Thus  the estimated result could be more accurately regarded as recharge potential or an upper limit of the actual recharge. The term surplus or infiltration other than recharge is used to denote this value – the surplus of soil water that could percolate further to the bedrock.

### *5.4.1 Model Description*

A simple algorithm is used to predict soil water storage, evaporation, runoff, and soil water surplus in this model. Surplus is precipitation that does not evaporate or remain in soil storage or runoff by surface flow or sub-surface flow. It is the water quantity that infiltrates into the bedrock under the soil layer when the soil is saturated with water, after which it will be redistributed in the rock system, some percolates into the groundwater, some forms lateral flow (interflow) and flow out of the aquifer along fractures. The conservation of mass equation for soil water can be written as follows (Reed et al., 1997):

$$\frac{\partial w}{\partial t} = P - E - R - S \quad (5\text{-}4)$$

In Equation (5-4), $S$ stands for soil water surplus, $P$ precipitation, $E$ evaporation, $R$ surface runoff, $w$ soil moisture, and $t$ time. Snowmelt was not considered in these computations because of the shortage of data.

### *5.4.2 Soil water balance modeling*

The procedure for computing soil water storage is described by Equation (5-5) below (Reed et al., 1997):

$wc_i=wc_{i-1}+P_i-R_i-f_{i-1}PET_i$ if $wc_i < wc^*$

$S_i = wc_i - wc^*$ and set $wc_i = wc^*$ *if* $wc_i > wc^*$ (5-5)

Where $wc_i$ is the current soil moisture, $wc_{i-1}$ is the soil moisture in the previous time step (month), $P_i$ precipitation, $R_i$ runoff, $PET_i$ potential evapotranspiration, $S_i$ the surplus in a given month, $f$ the soil-moisture extraction function and $wc^*$ the water-holding capacity. When evaluating Equation (5-5), if $wc_i$ drops below zero, then $wc_i$ is set equal to 0.01; if $wc_i > wc^*$, then the surplus for that month is $wc_i-wc^*$ and $wc_i$ is set equal to $wc^*$. The soil-moisture extraction function $f=wc/wc^*$ was used for this study.

If the initial soil moisture is unknown, which is typically the case, a balancing routine is used to force the net change in soil moisture from the beginning to the end of a specified balancing period (12 months) to zero. In this study the initial soil moisture is set to the water holding capacity, and budget calculations are made up to the time period ($N+1$). The initial soil moisture at time 1 ($wc_1$) is then set equal to the soil moisture at time $N+1$ ($wc_{N+1}$) and the budget is re-computed until the difference ($wc_1$ - $wc_{N+1}$) is less than a specified tolerance. The flow chart of the computation is showed in Fig. 5-11.

In this study, in order to be consistent with the recorded data, October is set as the initial time step and the first month that the computing starts with. Therefore the soil moisture in October is set to the water holding capacity. Equation (5-5) is programmed in Excel to calculate other months' water surplus or infiltration. Each month's soil moisture as well as surplus is calculated with the previous month's soil moisture content and the current month's precipitation, runoff, actual evapotranspiration, and so on. The algorithm of Equation (5-5) is an iteration process.

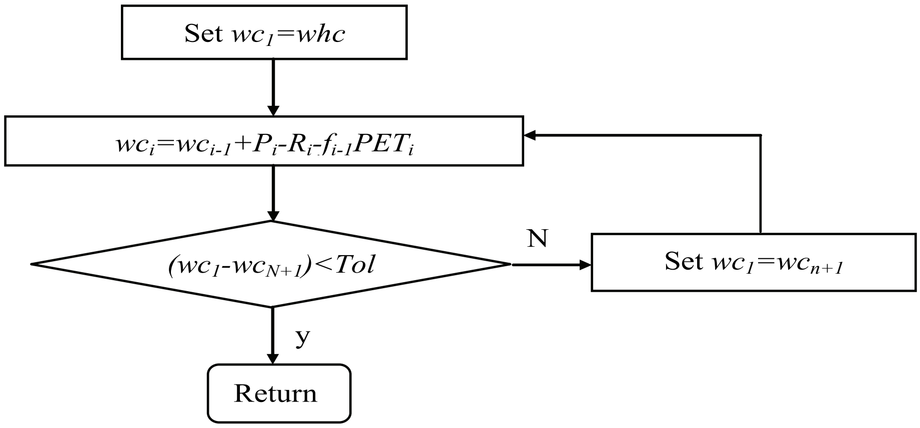


**Fig. 5-11** Flow chart of soil water balance computation

### *5.4.3 Data processing*

The source data layers used in the GIS are listed in Table 5-8. The input maps, i.e. Rainfall, Evaporation, Soil and Runoff, were derived by integrating relative data layers. Then the four maps were overlaid to generate an initial map, in which the TMG outcrop areas are divided into thousands of hydrologically equivalent polygons. Each polygon is homogeneous and unique. The attribute table of the initial map was exported to Excel, and then the soil water balance calculation described in section 4.3.2 was performed by executing the subroutine "CalculateSoilWater" compiled in VBA and embedded in Excel. From this monthly soil water, surplus, actual evapotranspiration for each polygon was calculated. After this calculation the results were exported from Excel to ArcGIS and linked to the initial map. The final maps were compiled from the calculated results of soil water, surplus and actual evapotranspiration. The procedures are summarized by a flow chart as Fig. 5-12.

**Table 5-8** Source data layers for recharge estimation

| Item | Data layer | File Type |
|---|---|---|
| Rainfall | Rainfall isolines (MAP) | shape file |
| | Rainfall zone | shape file |
| | Rainfall monthly percentage table | .dbf table |
| Evaporation | Evaporation isolines (MAE) | shape file |
| | Evaporation zone | shape file |
| | Evaporation monthly percentage table | .dbf table |
| | Vegetable | shape file |
| | Crop factor | .dbf table |
| Soil | Soil properties | shape file |
| Runoff | Runoff zone and value (MAR) | shape file |
| | Runoff monthly percentage table | .dbf table |

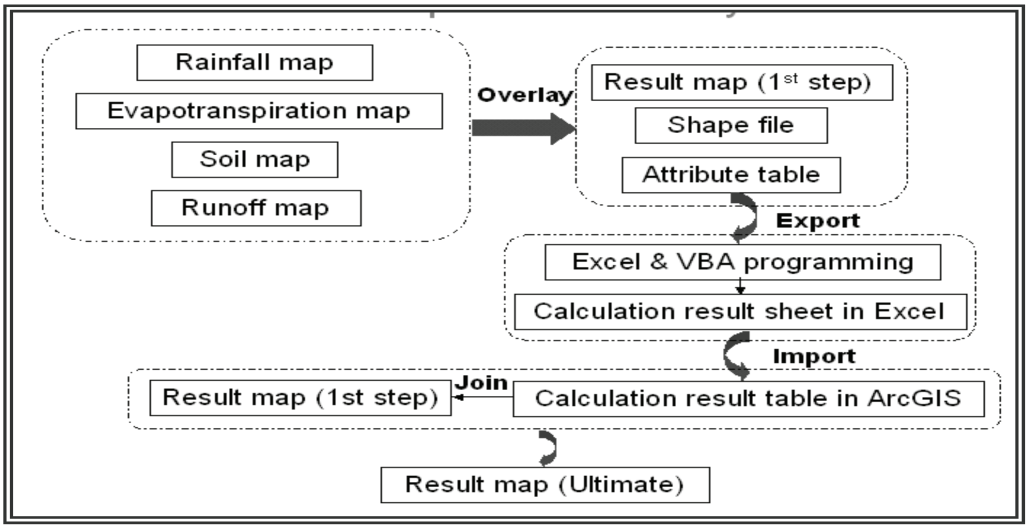


**Fig 5-12 Flow chart of data processing**

### *5.4.4 Results and discussion*

The results from the soil water balance modeling are monthly values of surplus from October to September. The maps show mean annual surplus (mm) and mean annual surplus rate (percentage of MAP) for TMG outcrop areas, as shown in Fig. 5-13, and Fig. 5-14. The modeling results are also summarized by quaternary catchment in Appendix G. The calculated total soil water surplus (the upper limit of recharge volume) is about $4.36\times10^{9}$ $m^3$ per annum, and the mean annual surplus in TMG outcrop areas is calculated as 115 mm. This value is large when compared with some of previous research results**.** This may be because the hydrological processes in the rock system are not taken into account in this model. Interflow could be a significant part of water balance in some cases. With the baseflow separation method, interflow can not be separated from the total stream flow successfully. Therefore the entire water surplus from soil to the underlying TMG rocks is calculated out as potential recharge capacity or an upper limit of recharge in this area.

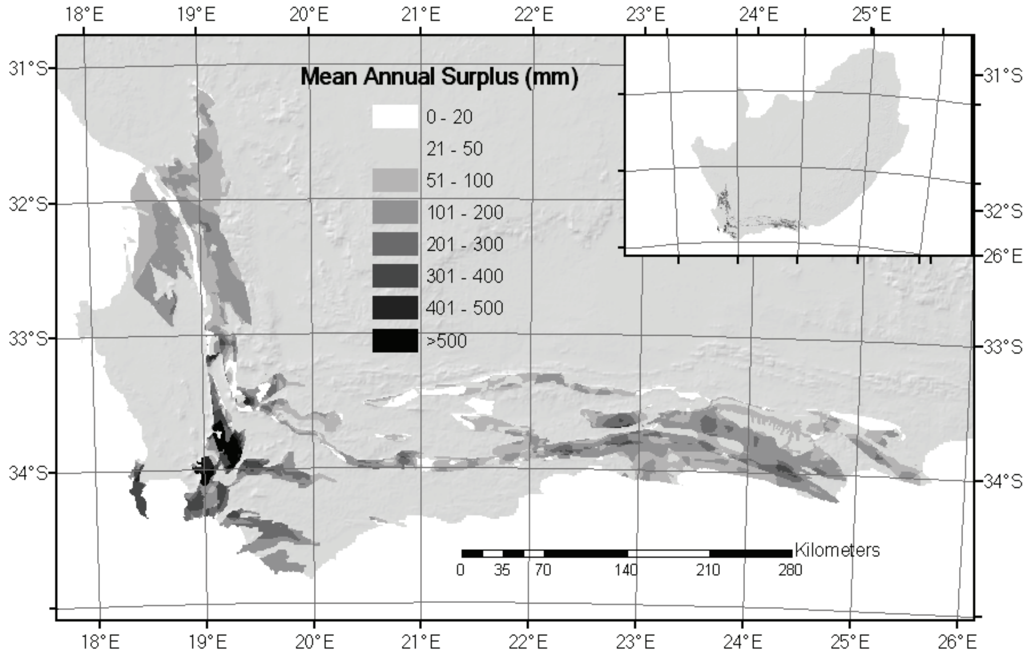


**Fig. 5-13** Mean annual surplus (mm) for the TMG outcrop area

Alternative recharge estimates in the TMG outcrop areas derived from integrated approaches were made by Wu (2005). These estimates can be used to calibrate the present estimates and help to determine an acceptable recharge quantity for this study. Wu (2005) estimated that the recharge volume is about $1.12\times10^9$ $m^3$ per annum and the mean annual recharge in TMG outcrop area is 29.74 mm.

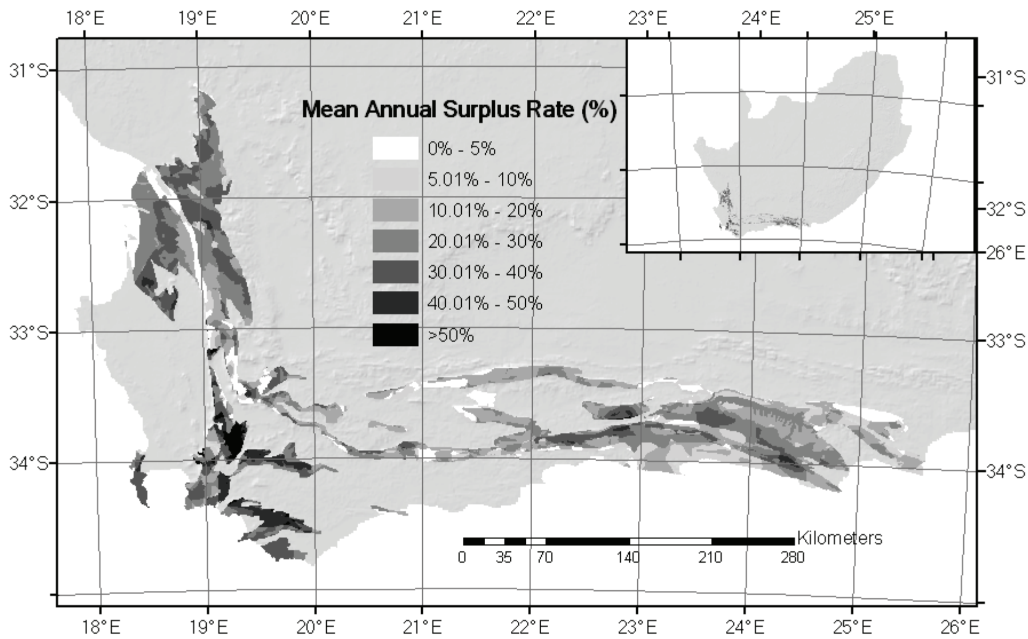


**Fig. 5-14** Mean annual surplus rate (%) for TMG outcrop area

## *5.5 Storage capacity estimation*

In this study the storage capacity of the TMG is classified into total groundwater capacity, usable groundwater capacity and available groundwater capacity according to the groundwater depth and the exploitation techniques required to utilize the water. This classification is shown in Fig. 5-15. Usable storage refers to stored groundwater that can be technically and economically extracted. Available storage is defined as the volume of an aquifer that is unsaturated and capable of storing additional groundwater.

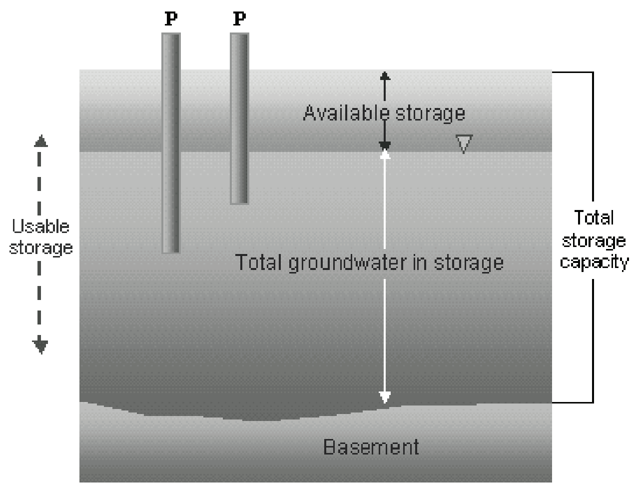


**Fig. 5-15** Total storage capacity, usable storage capacity and available storage capacity

### *5.5.1 Storativity of TMG aquifers*

Storativity is the general term for specific yield and storage coefficient for the unconfined and confined aquifers, respectively. In most of the TMG studies, storativity, instead of specific yield or storage coefficient, is commonly used to describe the aquifer storage properties.

The storativity of fractured rock aquifer is scale-dependent. On a microscopic scale, the storativity can be estimated by core sample porosity, which accounts for the storativity of both fractures and rock matrix at scales of less than one metre. Very few porosity analyses of the TMG core samples have been carried out (Table 3-5). These result shows that the porosity of the TMG sandstones ranges from 1.0~3.6% with an average of 2.5. These values greatly depend on laboratory methods used and the handling of core samples. Other factors influencing the measurement of the porosity is the stress release of the core samples, which may mask the variation of in-situ porosity with depths.

On a macroscopic or site scale, storativity values are usually derived from pumping test analyses. The storativity values derived from pumping tests may account for the aquifer porosity at a scale of several metres to a hundred metres. However groundwater flow in the fractured rock is mostly controlled by fracture characteristics, such as orientation, density, aperture, and connectivity. In terms of fracture extension and connection, Woodford (2002) stated that storativity of a fracture in a pumping process is complex and varies spatially and temporally. When the piezometric-level is above the fracture, the confined storage coefficient may be applied to the fracture while the unconfined specific yield applies to the dewatered fracture. Table 3-6 lists storativity estimates from some representative pumping tests conducted in the TMG aquifers. These pumping test results yield a storativity with values ranging widely from $1\times10^{-4}$-$1.2\times10^{-2}$ which are about two to three orders of magnitude less than those obtained from core samples.

The storativity values estimated from pumping tests generally use the late drawdown data, where the elastic release stage is assumed to be over and fractures are assumed the main conduits to deliver flow into boreholes and the matrix porosity can be ignored. A simple way to estimate the porosity of TMG aquifers can be carried out by fracture measurement and statistics. The fracture measurements may be conducted on the surface of outcrop or on a rock block which has moved from its original position. A lot of fracture measurements have been done in various outcrop areas of the TMG, such as Table Mountain, Rawsonville and Montague. A wide porosity range from 0.041% to 0.52% was derived from these measurements. Note that the values of porosity are in the same range as those from pumping tests. An example of such measurement is introduced here. A rock block (Fig. 5-16) found in Kirstenbosch, Cape Town, and identified to be a boulder that fell down from the famous Table Mountain of Peninsula Formation nearby, contained four sets of fractures.

**Fig. 5-16** A rock block of Peninsula Formation at Kirstenbosch

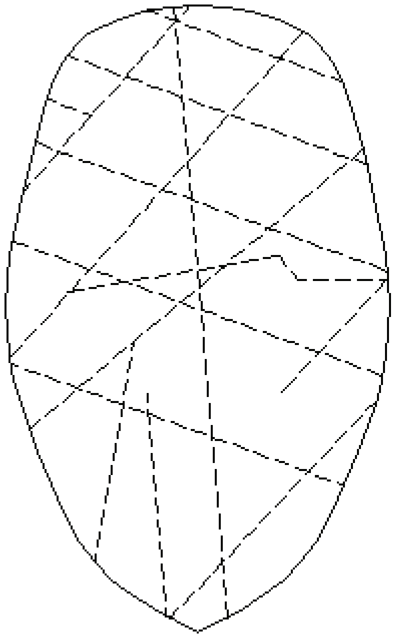

**Fig. 5-17** The fracture tracement of the rock block

The geometric size of the rock block is as follows:

S (Surface Area) = 3.397 $m^2$, and

D (Average Thickness) = 0.423 m,

from which, the volume of the rock could be calculated as V=S*D=1.438 $m^3$.

In this case only the visible fractures can be measured for the computation of the porosity. The surface fracture tracement of the rock block is shown in Fig. 5-17. Fracture porosity is defined as the ratio of total volume of fractures at the measurement scale to the volume of the rock mass. In general the porosity of a rock mass is the sum of fracture porosity and rock matrix porosity:

$$Nt = Nf + Nm(1-Nf) \tag{5-6}$$

Where Nt, Nf, and Nm stand for total porosity, fracture porosity, and rock matrix porosity, respectively.

In this case, the rock matrix porosity is approximated to 0 since the primary interstice between the sand grains have been cemented. The orientation, spacing and aperture of the four sets of fractures are measured and listed in Table 5-9. The corresponding porosity is calculated from these measurements and also listed in Table 5-9. A total porosity of 0.041% is finally arrived at for this rock block.

**Table 5-9** Fracture measurements, statistics and derived porosity of the block

| Sets | Orientation | Spacing (m) | Aperture (mm) | Porosity |
|---|---|---|---|---|
| Set 1 | 290°~320° | 7.437 | 0.08 | 1.751E-04 |
| Set 2 | 40°~50° | 4.793 | 0.08 | 1.129E-04 |
| Set 3 | 350°~20° | 4.5643 | 0.05 | 6.717E-05 |
| Set 4 | 70°~90° | 1.280 | 0.15 | 5.652E-05 |
| Total | | | | 4.117E-04 |

On a microscopic scale, the aperture of a fracture is proportional to fracture length (Zimmermann et al., 2003). However, on a macroscopic or a regional scale, the relationship between fracture aperture and fracture length follows a power law with an exponent of 0.3~0.5 (Liu and Bodvarsson, 2001):

$$B = c \cdot L^{d}$$

where B = fracture aperture, L = trace length, and *c* and *d* are constants. These relationships between fracture length and aperture imply that the porosity of a fractured rock may decrease dramatically from a small scale to a large scale.

In this study $ETM^{+}$ imagery was used for the interpretation of lineaments, considered to be the surface reflection of subsurface fracture systems (Fig. 3-10). The remote sensing study area extended over 80.25 $km^2$ and 888 fractures with various lengths were mapped using ArcGIS. To calculate the fracture apertures, the constants *c* and *d* are specified as $1.01\times10^{-4}$ and 0.42 respectively, based on the fracture statistics. As a result, the apparent porosity of the area is $1.24\times 10^{-8}$.

On a regional scale, Weaver (2002) stated that there are no confining units in the TMG, excluding local conditions where Bokkeveld shale or Cedarberg shale overlies the TMG. The available water from the TMG is a combination of both storage coefficient and specific yield (Sc + Sy) with spatial variations. At a regional scale, the demarcation of aquifers described in Section 5.3 was applied for the assignment of storativity values, (specific yield is assigned to the unconfined aquifers and storage coefficient to the confined aquifers).

Though in most of the previous studies Peninsula and Nardouw Aquifers are not differentiated clearly when evaluating the hydrogeological parameters, significant differences between them do occur. The Peninsula Aquifer usually outcrops at higher altitudes and is separated from the Nardouw by the Cedarberg Formation. The Peninsula receives more precipitation and therefore more direct recharge. Groundwater flow paths and residence times are shorter, providing low EC groundwater. By comparison the Nardouw receives less direct rainfall recharge and groundwater has longer travel-times and therefore a higher EC. The Peninsula Aquifer has a lower shale content and is much more fractured than the Nardouw and the flow system is therefore more dynamic, i.e. more active flow circulation and recharge and less blocking of permeability from the products of shale weathering. Such differences can also be reflected in storativity of the two aquifers. Considering these differences, an assumption of 30% reduction in storativity is applied to Nardouw Aquifer compared to Peninsula Aquifer.

No conclusive or consistent values of storativity of the TMG aquifers can be determined, which is a common difficulty encountered in regional studies because the storativity values are scale-dependent. However a range of values can be selected based primarily on previous research. A range of $10^{-3}$ to $10^{-5}$ is selected for the storage coefficient of the confined Peninsula Aquifer, and a range of $5\times10^{-3}$ to $1\times10^{-4}$ is assigned to the specific yield of unconfined Peninsula Aquifer (Table 5-10). These value ranges are generalized from previous studies, which have not taken into consideration the effect of depth on the storage of TMG aquifers. Three scenarios (low, medium and high storage coefficient or specific yield) for the TMG storage capacity estimations will be conducted based on these values.

**Table 5-10** Recommended storativity values for the TMG aquifers

| Aquifer Type | Range | Storativity | |
|---|---|---|---|
| | | **Specific yield (Unconfined)** | **Storage coefficient (Confined)** |
| Nardouw | Low | 7E-5 | 7E-6 |
| | Medium | 3.5E-4 | 7E-5 |
| | High | 3.5E-3 | 7E-4 |
| Peninsula | Low | 1E-4 | 1E-5 |
| | Medium | 5E-4 | 1E-4 |
| | High | 5E-3 | 1E-3 |

### *5.5.2 Thickness and regional distribution of TMG aquifers*

Besides storativity, the thickness and spatial distribution of the TMG rocks is needed for groundwater storage capacity evaluation. In this study, because of a scarcity of sub-surface geological information, the determination of aquifer thickness was done using the following procedures:

1) *Construct cross sections*

The purpose of the cross sections is to visualize, analyze and measure the variation in depth, thickness and altitude of the different formations of the Table Mountain Group (TMG) over the Cape Fold Belt. Regionally the key rocks that control the TMG aquifer systems are the Peninsula and Cedarberg Formations and the overlying Nardouw Subgroup.

Generally the TMG is strongly compartmentalized by faults or fault zones created in the Palaeozoic and reconstructed during the Mesozoic tectonics. As a result two major regional faults – the Worcester and Kango faults – control the TMG distribution to a large extent. Eight geological profiles were therefore selected across these structures (Fig. 5-18, Fig. 5-19 and Table 5-11) to encompass the variation in lithology and thickness of the TMG as well as the structural complexity of the Cape Fold Belt. Meanwhile 21 smaller cross sections were located over the TMG to represent the geology in some typical domains.

Very few boreholes penetrated the main aquifers in the TMG outcrop areas, or reached the TMG in Karoo areas, which makes it difficult to accurately determine the top or bottom of the TMG layers and check the accuracy of layer locations on maps of the cross sections.

Most of the work was done manually by capturing and reading the coordinates and elevation of the intersection points of cross section lines and the geological formations. Then the original coordination data and the relevant geological data were input into AutoCAD and the cross sections were constructed in CAD format.

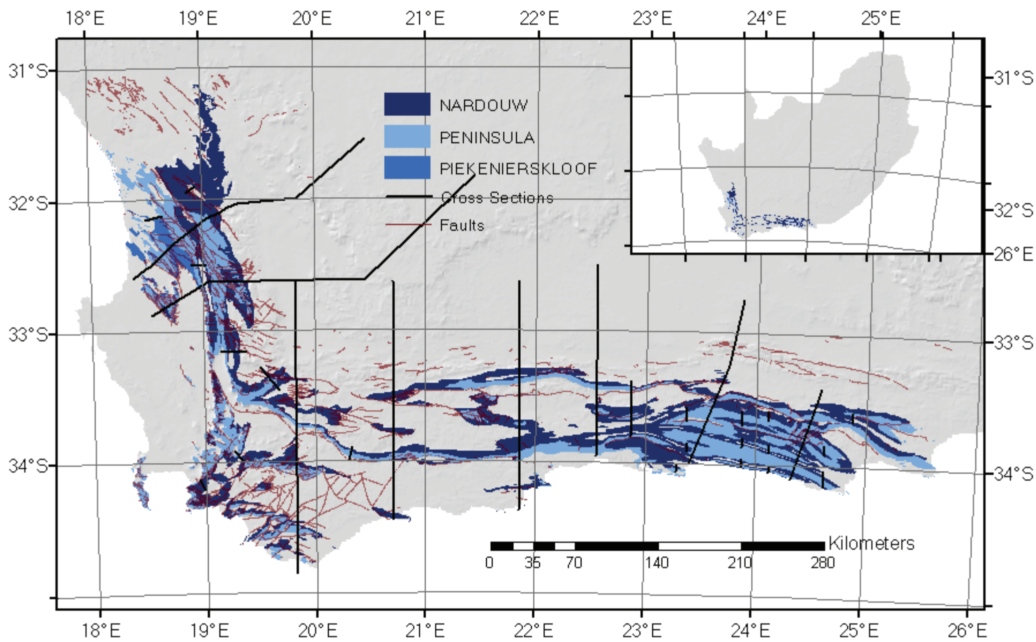


**Fig. 5-18** Location of cross sections in the TMG area

**Table 5-11 Locations of Vertex along main Cross section lines**

| Cross section | Vertex on section line | Coordinate | | Cross section | Vertices on section line | Coordinate | |
|---|---|---|---|---|---|---|---|
| | | E (°) | S (°) | | | E (°) | S (°) |
| 01 | 1 | 18.3884 | -32.6094 | 02 | 1 | 18.5389 | -32.8833 |
| | 2 | 18.5000 | -32.5275 | | 2 | 19.0544 | -32.6233 |
| | 3 | 18.5380 | -32.5000 | | 3 | 20.4542 | -32.6167 |
| | 4 | 18.7500 | -32.3464 | | 4 | 21.4389 | -31.8264 |
| | 5 | 18.8852 | -32.2500 | 03 | 1 | 19.8333 | -34.8333 |
| | 6 | 19.0000 | -32.1667 | | 2 | 19.8333 | -32.6667 |
| | 7 | 19.0709 | -32.1383 | 04 | 1 | 20.7000 | -34.4667 |
| | 8 | 19.1791 | -32.1105 | | 2 | 20.7000 | -32.6167 |
| | 9 | 19.2236 | -32.0771 | 05 | 1 | 21.8500 | -34.3708 |
| | 10 | 19.3320 | -32.0481 | | 2 | 21.8500 | -32.6333 |
| | 11 | 19.5000 | -32.0339 | 06 | 1 | 22.5500 | -32.5000 |
| | 12 | 19.7500 | -32.0106 | | 2 | 22.5500 | -33.9500 |
| | 13 | 19.8611 | -32.0000 | 07 | 1 | 23.3893 | -34.0000 |
| | 14 | 20.0000 | -31.8961 | | 2 | 23.7500 | -33.2500 |
| | 15 | 20.1947 | -31.7500 | | 3 | 23.8083 | -33.0000 |
| | 16 | 20.2500 | -31.7081 | | 4 | 23.8661 | -32.7500 |
| | 17 | 20.4552 | -31.5530 | 08 | 1 | 24.3216 | -34.1025 |
| | | | | | 2 | 24.5869 | -33.4167 |

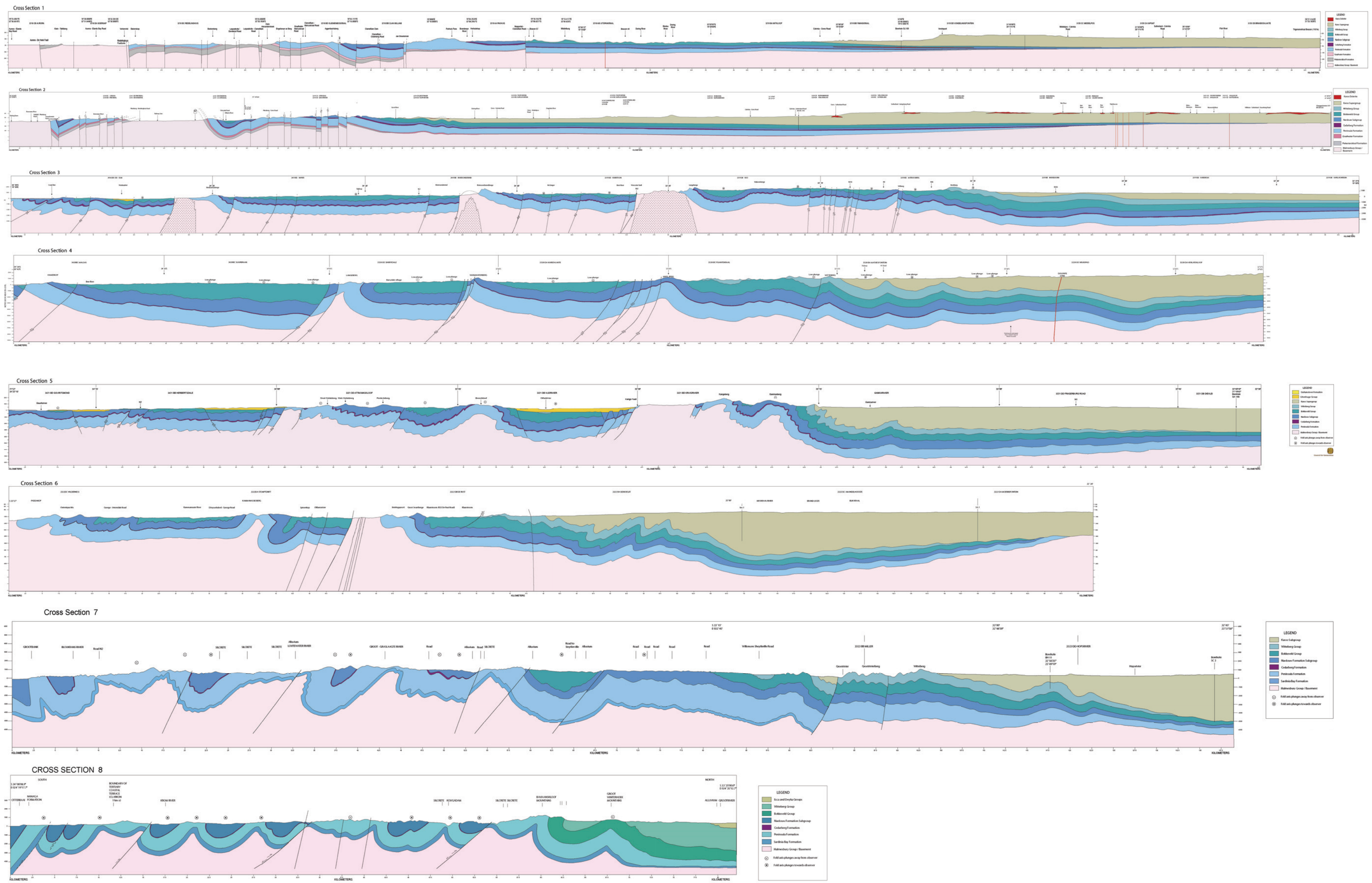


**Fig. 5-19** Main cross sections (1- 8) through TMG area (completed by CGS, 2004)

*2) Data capture of cross sections*

The reliability of the source data and the experience of the hydrogeologist are critical when interpreting the geological map. Each cross section was processed in the following way: vertical lines are made on the start location, the end location of the section and the structural change locations (e.g. the start, end, and axis of fold, fault and etc) along the section and then the control elevations (top elevation and bottom elevation) of each typical layers on each location are recorded. Point data with the top and bottom elevation through out the TMG are obtained for each typical layer.

Typical layers only involve the two main aquifers (Nardouw aquifer and Peninsula aquifer), the Cedarberg aquitard, and the TMG basement. The resultant control elevation layers include the top elevation of the Nardouw aquifer, the bottom elevation of the Nardouw aquifer, the top elevation of the Peninsula aquifer, the bottom elevation of the Peninsula aquifer and the top elevation of the TMG basement. The point data are input into the interpolation software Surfer 7.0 to create the primary contours, from which the evenly and densely distributed point data are derived for the next step. Interpolation processes invariably introduce mistakes. Before the next procedure, the data are calibrated and corrected according to the spatial relationship between the typical layers, e.g. on each point, the top of Nardouw should not be lower than bottom of Nardouw, and so on.

*3) Creation of TMG isobaths and isopachs*

The evenly and densely distributed point data – the result of previous procedure – were input into ArcGIS, in which the grid for each layer can be produced by using the spatial analyst extension. Other processes included removing the non-TMG deposit area for all layers except the top of TMG basement, and removing the Peninsula outcrop area for the top and bottom of the Nardouw. Isobaths of the typical layers were created by the resultant grid maps, based on which the isopachs of the typical layers were created using the raster calculation function in ArcGIS spatial analyst.

Due to the limitation of data sources and the interpolation techniques, errors may be produced in any of the above-mentioned procedures. Therefore more data sources are needed to calibrate the results.

In general the study of cross sections, isobaths and isopachs of TMG is essentially a regional scale analysis, through which an initial graphic visualization and understanding of the TMG aquifers, geological nature, and spatial relationships may be formed. Hydrogeologically, the results (Fig. 5-20 to Fig. 5-27) carried out provide a basic overview of the TMG aquifer systems.

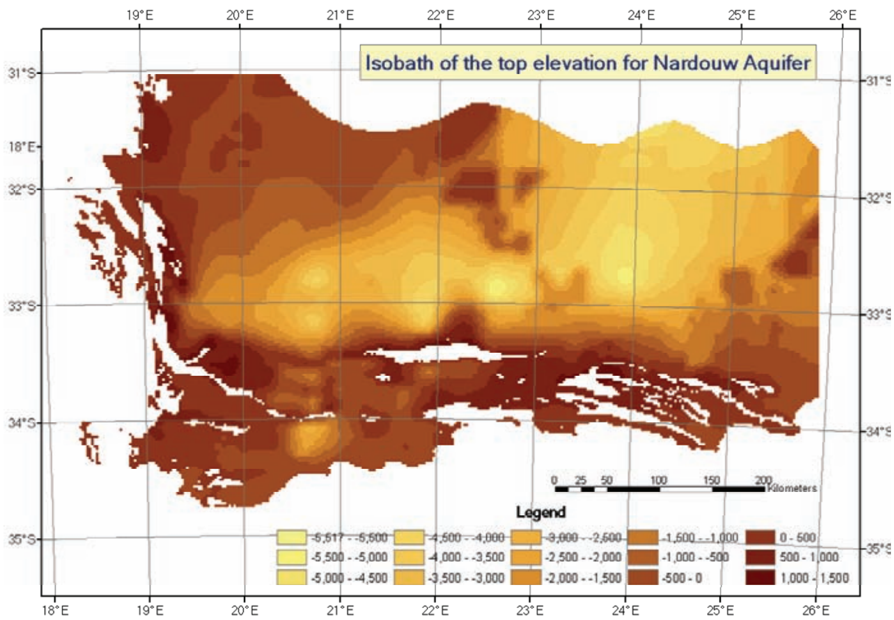


**Fig. 5-20** Isobath of the top of the Nardouw Aquifer

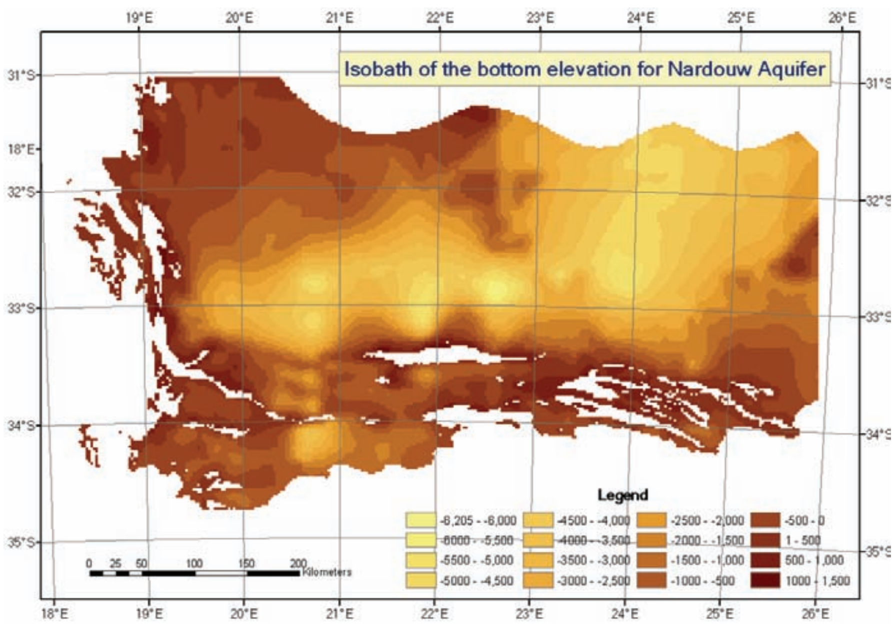


**Fig. 5-21** Isobath of the bottom of the Nardouw Aquifer

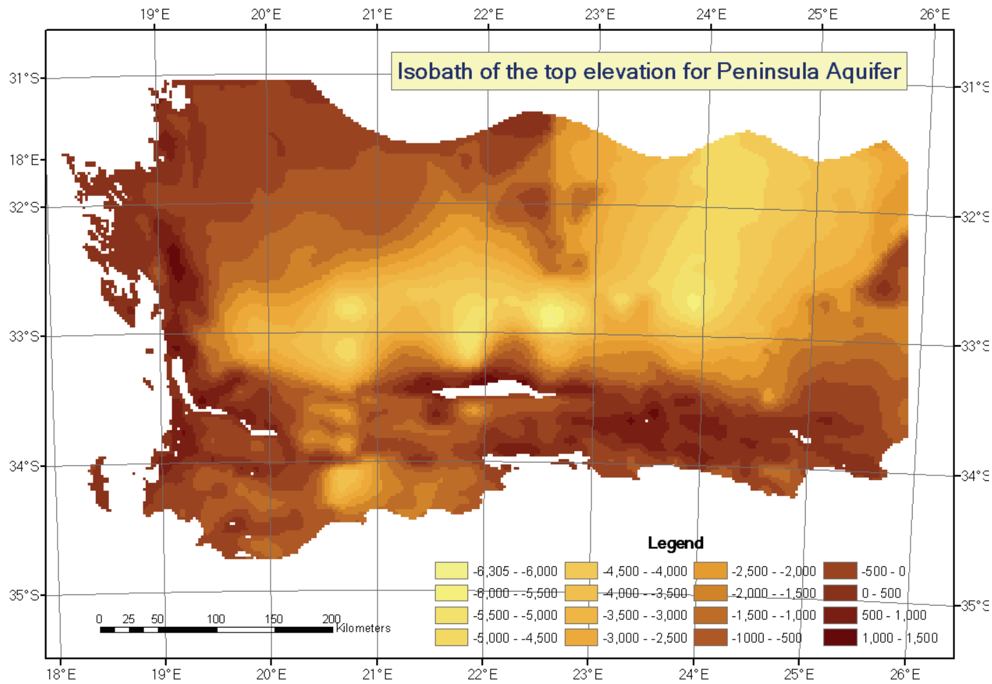


**Fig. 5-22** Isobath of the top of the Peninsula Aquifer

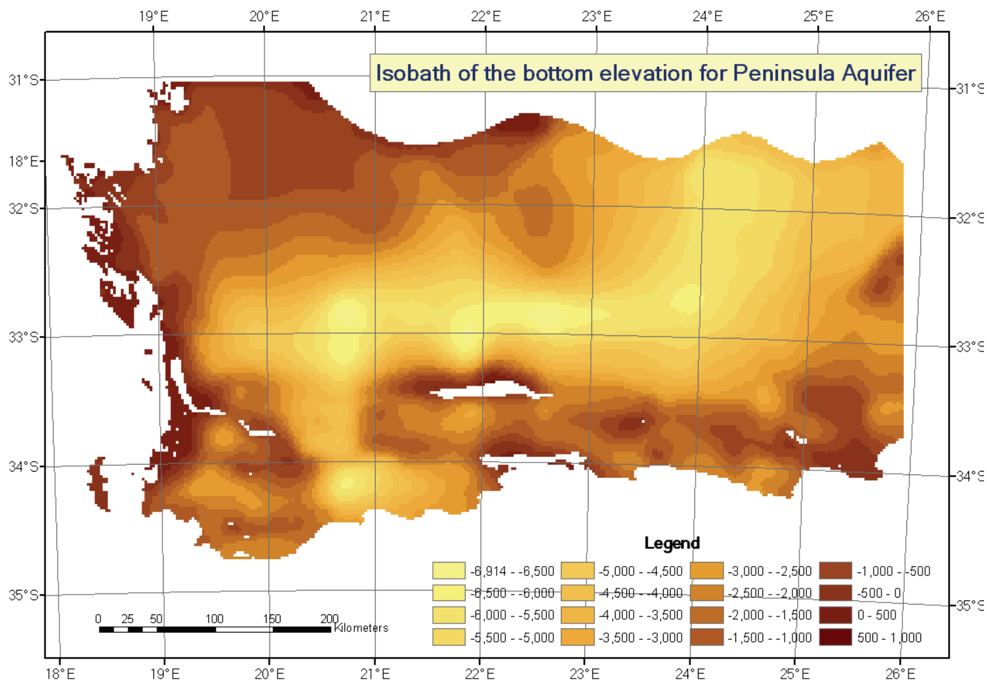


**Fig. 5-23** Isobath of the bottom of the Peninsula Aquifer

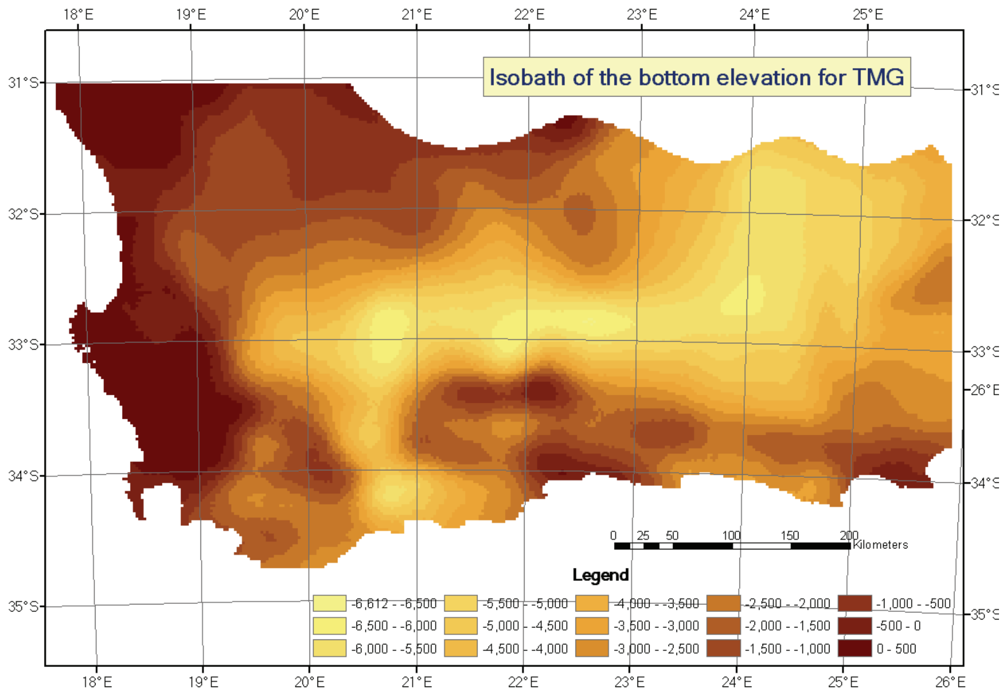


**Fig. 5-24** Isobath of the bottom of the TMG

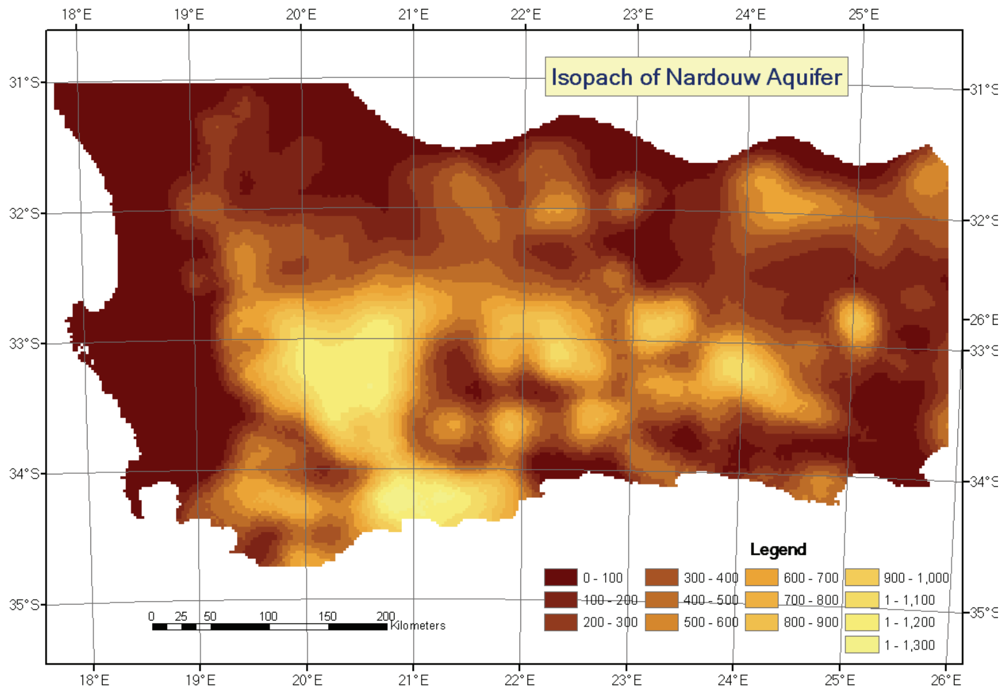


**Fig. 5-25** Isopach of the Nardouw Aquifer

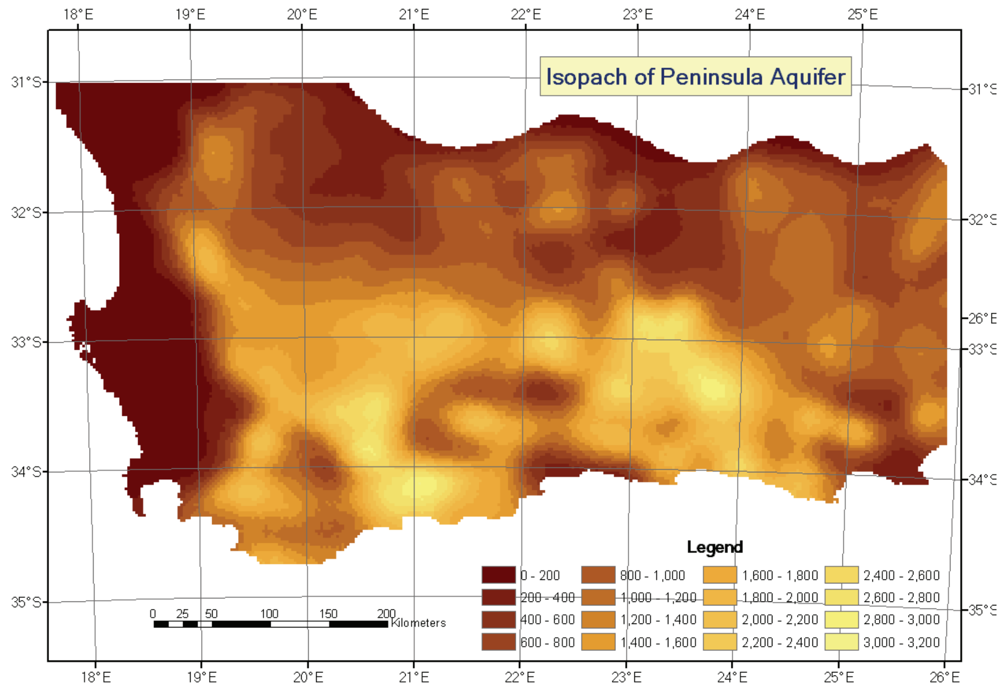


**Fig. 5-26** Isopach of the Peninsula Aquifer

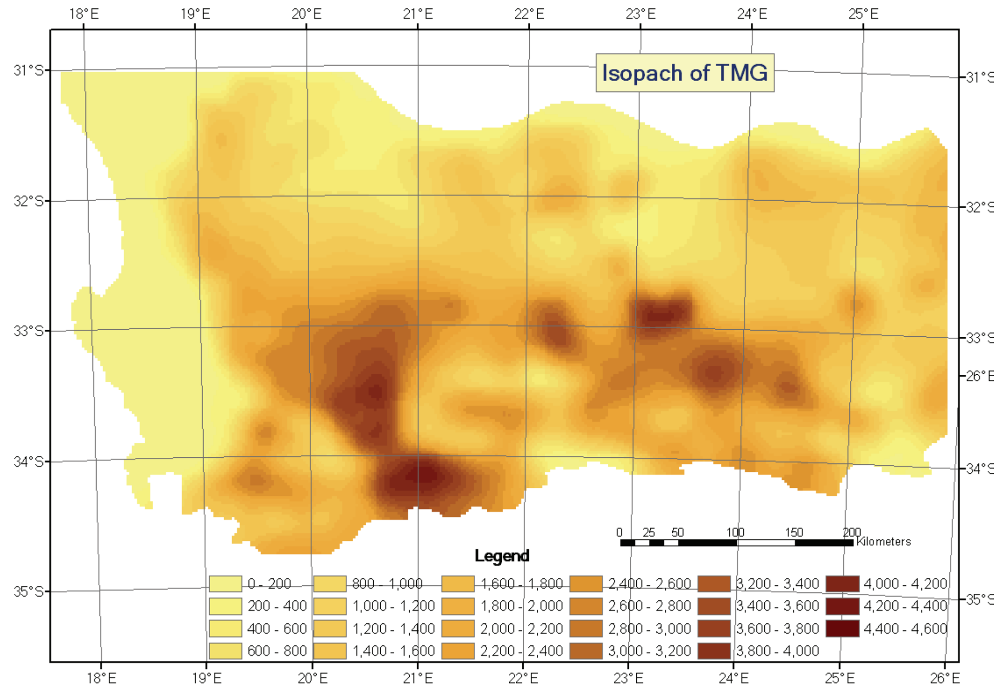


**Fig. 5-**27 Isopach of the TMG Aquifer

### *5.5.3 Total groundwater storage capacity estimation*

The total groundwater storage capacity is constant, and is dependent on the geometry and hydrogeological characteristics of the aquifer(s). Due to incomplete information about the groundwater storage properties, it is difficult to perform a precise evaluation of the total storage capacity of TMG aquifers In this section, based on the assumed specific yield and storage coefficient, and the results of the isobaths and isopachs derived in previous section, the total storage capacity is calculated for 3 scenarios with high, medium and low storativity values. The estimates are listed in Table 5-12.

**Table 5-12 Estimation of total storage capacity for the TMG aquifers**

| Unit: $m^3$, % of Aquifer Volume | | | Outcrop (Unconfined) | | Non-outcrop (Confined) | | Total | |
|---|---|---|---|---|---|---|---|---|
| **Nardouw Aquifer** | Aquifer Volume | | 6.4E+12 | | 7.1E+13 | | 7.8E+13 | |
| | Total storage capacity | Low | 4.5E+08 | 0.007% | 5.0E+08 | 0.001% | 9.5E+08 | 0.001% |
| | | Medium | 2.3E+09 | 0.036% | 5.0E+09 | 0.007% | 7.2E+09 | 0.009% |
| | | High | 2.3E+10 | 0.359% | 5.0E+10 | 0.070% | 7.2E +10 | 0.092% |
| **Peninsula Aquifer** | Aquifer Volume | | 1.8E+13 | | 2.2E+14 | | 2.4E+14 | |
| | Total storage capacity | Low | 6.4E+08 | 0.004% | 2.2E+09 | 0.001% | 2.9E+09 | 0.001% |
| | | Medium | 3.2E+09 | 0.018% | 2.2E+10 | 0.010% | 2.6E+10 | 0.011% |
| | | High | 3.2E+10 | 0.178% | 2.2E+11 | 0.100% | 2.6E+11 | 0.108% |
| **Total** | Aquifer Volume | | 2.4E+13 | | 2.9E+14 | | 3.2E+14 | |
| | Total storage capacity | Low | 1.1E+09 | 0.005% | 2.7E+09 | 0.001% | 3.8E+09 | 0.001% |
| | | Medium | 5.5E+09 | 0.023% | 2.7E+10 | 0.009% | 3.3E+10 | 0.010% |
| | | High | 5.5E+10 | 0.229% | 2.7E+11 | 0.093% | 3.3E+11 | 0.103% |

### *5.5.4 Usable storage capacity estimation*

Usable storage capacity is defined as the amount of groundwater of suitable quality that can be technically and economically extracted from the storage. It is computed by multiplying the average storativity of the aquifer by the volume of the aquifer to a specific depth that is considered the technical and economical limit for exploitation. The usable storage may change because of changes in economic and technical conditions.

In present study, considering the current situation of drilling techniques, the following limitations are set to be the limits of the usable storage capacity. First, the TMG aquifer storage capacity in the Karoo area (which is located in the north part of study area) is excluded because boreholes have rarely reached the TMG rocks, which are deeply buried (>3000 m below sea level). Then three scenarios: maximum borehole depths of 250 m, 350 m and 500 m (below ground level), are used to calculate the useable storage capacity. The calculation results are listed in Table 5-13, Table 5-14 and Table 5-15.

**Table 5-13 Estimation of usable storage capacity (500 m below surface)**

| 500 m below surface Unit: $m^3$, % of Aquifer Volume | | | Outcrop (Unconfined) | | Non-outcrop (Confined) | | Total | |
|---|---|---|---|---|---|---|---|---|
| Nardouw Aquifer | Aquifer Volume | | 3.3E+12 | | 6.0 E+12 | | 9.2E+12 | |
| | Usable storage capacity | Low | 2.3E+08 | 0.007% | 4.2E +07 | 0.001% | 2.7E+08 | 0.003% |
| | | Medium | 1.1E+09 | 0.033% | 4.2E +08 | 0.007% | 1.6E+09 | 0.017% |
| | | High | 1.1E+10 | 0.333% | 4.2E+09 | 0.070% | 1.6E+10 | 0.174% |
| Peninsula Aquifer | Aquifer Volume | | 2.9E+12 | | 3.7E +12 | | 6.6E+12 | |
| | Usable storage capacity | Low | 2.9E+08 | 0.010% | 3.7E +07 | 0.010% | 3.3E+08 | 0.005% |
| | | Medium | 1.5E+09 | 0.052% | 3.7E +08 | 0.052% | 1.8E+09 | 0.027% |
| | | High | 1.5E+10 | 0.517% | 3.7E+09 | 0.517% | 1.8E+10 | 0.273% |
| Total | Aquifer Volume | | 6.2E+12 | | 9.6E+12 | | 1.5E+13 | |
| | Usable storage capacity | Low | 5.2E+08 | 0.008% | 7.9E+07 | 0.001% | 6.0E+08 | 0.004% |
| | | Medium | 2.6E+09 | 0.042% | 7.9E+08 | 0.008% | 3.4E+09 | 0.023% |
| | | High | 2.6E+10 | 0.419% | 7.9E+09 | 0.082% | 3.4E+10 | 0.227% |

**Table 5-14 Estimation of usable storage capacity (350 m below surface)**

| 350 m below surface Unit: $m^3$, % of Aquifer Volume | | | Outcrop (Unconfined) | | Non-outcrop (Confined) | | Total | |
|---|---|---|---|---|---|---|---|---|
| Nardouw Aquifer | Aquifer Volume | | 2.4E+12 | | 3.6E+12 | | 6.0E+12 | |
| | Usable storage capacity | Low | 1.7E+08 | 0.007% | 2.5E+07 | 0.001% | 1.9E+08 | 0.003% |
| | | Medium | 8.3E+08 | 0.035% | 2.5E+08 | 0.007% | 1.1E+09 | 0.018% |
| | | High | 8.3E+09 | 0.346% | 2.5E+09 | 0.069% | 1.1E+10 | 0.183% |
| Peninsula Aquifer | Aquifer Volume | | 1.7E+12 | | 1.8E +12 | | 3.4E+12 | |
| | Usable storage capacity | Low | 1.7E+08 | 0.010% | 1.8E +07 | 0.001% | 1.9E+08 | 0.006% |
| | | Medium | 8.5E+08 | 0.050% | 1.8E +08 | 0.010% | 1.0E+09 | 0.029% |
| | | High | 8.5E+09 | 0.500% | 1.8E+09 | 0.100% | 1.0E+10 | 0.294% |
| Total | Aquifer Volume | | 4.1E+12 | | 5.4E+12 | | 9.4E+12 | |
| | Usable storage capacity | Low | 3.3E+08 | 0.008% | 4.3E+07 | 0.001% | 3.8E+08 | 0.004% |
| | | Medium | 1.7E+09 | 0.041% | 4.3E+08 | 0.008% | 2.1E+09 | 0.022% |
| | | High | 1.7E+10 | 0.415% | 4.3E+09 | 0.080% | 2.1E+10 | 0.223% |

**Table 5-15 Estimation of usable storage capacity (250 m below surface)**

| 250 m below surface Unit: $m^3$, % of Aquifer Volume | | | Outcrop (Unconfined) | | Non-outcrop (Confined) | | Total | |
|---|---|---|---|---|---|---|---|---|
| Nardouw Aquifer | Aquifer Volume | | 1.7E+12 | | 2.2E+12 | | 3.9E+12 | |
| | Usable storage capacity | Low | 1.2E+08 | 0.007% | 1.6E +07 | 0.001% | 1.3E+08 | 0.003% |
| | | Medium | 5.8E+08 | 0.034% | 1.6E +08 | 0.007% | 7.4E+08 | 0.019% |
| | | High | 5.8E+09 | 0.341% | 1.6E+09 | 0.073% | 7.4E+09 | 0.190% |
| Peninsula Aquifer | Aquifer Volume | | 9.9E+11 | | 8.9E +11 | | 1.9E+12 | |
| | Usable storage capacity | Low | 9.9E+07 | 0.010% | 8.9E +06 | 0.001% | 1.1E+08 | 0.006% |
| | | Medium | 4.9E+08 | 0.049% | 8.9E +07 | 0.010% | 5.8E+08 | 0.031% |
| | | High | 4.9E+09 | 0.495% | 8.9E+08 | 0.100% | 5.8E+09 | 0.305% |
| Total | Aquifer Volume | | 2.6E+12 | | 3.1E+12 | | 5.8E+12 | |
| | Usable storage capacity | Low | 2.1E+08 | 0.008% | 2.5E+07 | 0.001% | 2.4E+08 | 0.004% |
| | | Medium | 1.1+09 | 0.042% | 2.5E+08 | 0.008% | 1.3E+09 | 0.022% |
| | | High | 1.1E+10 | 0.423% | 2.5E+09 | 0.081% | 1.3E+10 | 0.224% |

### *5.5.5 Available storage capacity estimation*

Available storage capacity is defined as the volume of an aquifer that is partially saturated at a local scale and capable of storing additional groundwater. It is computed as the product of the empty volume of the aquifer and the average specific yield of the unsaturated part of the aquifer. The available storage will vary with the amount of groundwater taken out of storage and with recharge. The total groundwater in storage will change inversely as the available storage changes.

In the present study, the unsaturated zone of the TMG aquifer is assumed to be limited to the unconfined TMG area where TMG rocks outcrop. There is no reliable information available to determine the elevation difference between the top of the aquifer and the potentiometric surface on a regional scale. Nevertheless Hartnady and Hay (2002) pointed out that it might be in the order of a hundred metres over a wide area. Consequently an elevation difference of 100 m between the top of aquifer and the groundwater level is used to estimate the available storage capacity for the unconfined part of the TMG aquifers (Table 5-16).

**Table 5-16 Estimation of available storage capacity of TMG aquifers**

| Unit: $m^3$, % of Aquifer Volume | | ***Nardouw Aquifer*** | | **Peninsula Aquifer** | | **Total** | |
|---|---|---|---|---|---|---|---|
| **Available storage capacity** | **Aquifer Volume** | 1.7E+12 | | 2.2E+12 | | 3.9E+12 | |
| | **Low** | 1.2E+08 | 0.007% | 2.2E+07 | 0.001% | 1.4E+08 | 0.004% |
| | **Medium** | 5.8E+08 | 0.034% | 2.2E+08 | 0.010% | 8.1E+08 | 0.021% |
| | **High** | 5.8E+09 | 0.341% | 2.2E+09 | 0.100% | 8.1E+09 | 0.208% |

### *5.5.6 Storage capacity relative to sea level*

A significant part of groundwater in TMG aquifers may be stored below sea level in the deeply buried, confined TMG aquifers. In this study, based on the estimates of isobaths and isopachs for the TMG aquifers, the storage capacity related to sea level (above sea level and below sea level) is calculated using the raster calculation function of the spatial analyst extension in ArcGIS. The calculation method is illustrated in Table 5-17 using the Nardouw Aquifer as an example. The storage capacity of Peninsula Aquifer related to sea level was estimated the same way.

**Table 5-17 The calculation basis of TMG storage capacity related to sea level**

| **Relationship between TopNar, BotNar and SL** | | **Volume above sea level** | **Volume below sea level** |
|---|---|---|---|
| TopNar is higher than SL | BotNar is higher or equal to SL | (TopNar-BotNar) * Grid Area | 0 |
| | BotNar is lower than SL | (TopNar-0) * Grid Area | (0-BotNar) * Grid Area |
| TopNar is lower or equal to SL | | 0 | (TopNar-BotNar) * Grid Area |

Note: TopNar is elevation of the top of Nardouw Aquifer, BotNar is elevation of the bottom of Nardouw Aquifer, SL is sea level and Grid Area is the area of each grid of the raster file, i.e. 100 m $\times$ 100 m =10000 $m^2$.

The results are listed in Table 5-18. From Table 5-18 it can be observed that the estimated groundwater storage capacity below the sea level is about 5 to 10 times more than that of the above the sea level.

**Table 5-18 Estimation of storage capacity related to sea level**

| Unit: $m^3$, % of Aquifer Volume | | | Above sea level | | Below sea level | | Total | |
|---|---|---|---|---|---|---|---|---|
| Nardouw Aquifer | Aquifer Volume | | 1.1E+13 | | 6.6E+13 | | 7.7E+13 | |
| | Groundwater storage capacity | Low | 4.5E+08 | 0.004% | 4.9E+08 | 0.001% | 9.4E+08 | 0.001% |
| | | Medium | 2.2E+09 | 0.020% | 4.9E+09 | 0.007% | 7.2E+09 | 0.009% |
| | | High | 2.2E+10 | 0.200% | 4.9E+10 | 0.074% | 7.2E+10 | 0.094% |
| Peninsula Aquifer | Aquifer Volume | | 9.8E+12 | | 2.3E+14 | | 2.4E+14 | |
| | Groundwater storage capacity | Low | 5.9E+08 | 0.006% | 2.4E+09 | 0.001% | 3.0E+09 | 0.001% |
| | | Medium | 2.9E+09 | 0.030% | 2.4E+10 | 0.010% | 2.7E+10 | 0.011% |
| | | High | 2.9E+10 | 0.296% | 2.3E+11 | 0.100% | 2.6E+11 | 0.108% |
| Total | Aquifer Volume | | 2.0E+13 | | 3.0E+14 | | 3.2E+14 | |
| | Groundwater storage capacity | Low | 1.0E+09 | 0.005% | 2.9E+09 | 0.001% | 3.9E+09 | 0.001% |
| | | Medium | 5.2E+09 | 0.026% | 2.9E+10 | 0.010% | 3.4E+10 | 0.011% |
| | | High | 5.2E+10 | 0.260% | 2.8E+11 | 0.093% | 3.3E+11 | 0.103% |

### *5.5.7 Change in storage*

The calculation of change in storage can reflect the hydrologic trends in a groundwater basin or region over time. If the change in storage is quite small over a specific period, the basin is essentially in equilibrium under current conditions. Groundwater budgets are the most reliable way to estimate the change of storage, however this method is usually limited by the availability and accuracy of data. An alternative and simpler way is to determine the average change in groundwater elevation over the study area or groundwater catchment, and then multiply the elevation change by the area and the average storativity. The choice of time interval of groundwater elevation change is case specific, but a one-year cycle is usually adopted. Although the change in storage calculation is a relatively quick and inexpensive method of observing changes in the groundwater system, the groundwater budget method is preferable if data are available. Usually on a regional scale, the regional groundwater flow is assumed to be in steady-state and change in storage is taken as zero, which is the case in the TMG aquifer systems.

## 5.6 Groundwater discharge estimation

Groundwater discharge from TMG aquifers includes natural discharge and exploitation. Natural groundwater discharge occurs through stream baseflow, spring flow, evaporation, leakage to adjacent aquifers and discharge to the sea. The latter two discharges are difficult to estimate in this study due to insufficient subsurface geological information. The first four components of natural groundwater discharge, plus exploitation are quantitatively estimated using existing data.

### *5.6.1 Baseflow*

It is well known that baseflow can be separated from the stream flow by analyzing the stream hydrographs. However it is still open to debate how much of the baseflow is actually derived from groundwater and how much is derived from interflow through the unsaturated zone. For a regional estimation, it is not always feasible to distinguish the groundwater component of baseflow. Rather baseflow can be regarded as the upper limit of groundwater discharge from the aquifers. Of the baseflow separation techniques, the digital recursive filtering method was applied to determine the baseflow estimates for the TMG aquifers. Only the stream flow in outcrop areas were taken into account. In the non-outcrop areas, because the TMG aquifers are mostly deeply buried, flow is assumed to have no interaction with TMG aquifers.

The baseflow calculation results from Chapter 7 are used in this section. The total annual baseflow volume in TMG outcrop area was estimated to be $1.08\times10^9$ $m^3$ /yr.

### *5.6.2 Spring flow*

Meyer (2002) generalized three types of springs related to TMG according to their mode of occurrence: shallow circulating springs, lithology controlled springs, and fault controlled springs. Because of the special hydrogeological significance of the fault-controlled springs, they were separated from the first two types and their contribution to groundwater discharge from the TMG were estimated separately. 501 springs can be identified on NGDB in the TMG area, of which 103 are recognized as TMG-related springs according to their geographical relationship with TMG. The total yield of the 103 springs amounts to 141 *l*/s or $4.45\times10^6$ $m^3$/yr.

### *5.6.3 Thermal spring*

The notable 11 hot springs are unquestionably the discharge from the deep zone of TMG aquifers. The detailed information of these springs is listed in Table 5-7, in which the average yield of each is included. Therefore the total yield of these hot springs might be a good estimation of the deep zone discharge. The total yield of the 11 hot springs is about 355 *l*/s or $1.12\times10^7$ $m^3$/yr.

### *5.6.4 Borehole yield*

The boreholes yields were estimated by summing the discharge rates of the TMG-related boreholes found on the NGDB. If there were more than one record of the discharge rate, the latest one is used. The estimation results are listed in Table 5-19. The result shows that the biggest component of borehole yield is from the unconfined Nardouw Aquifer, i.e. 3139.76 *l/s* or $9.902\times10^{7}$ $m^3$/yr. The abstraction from the confined TMG aquifers only accounts for around 13.6% of the total abstraction, which reflects the fact that there are still technical limitations regarding the drilling of boreholes in the confined TMG aquifers.

**Table 5-19 Borehole yield estimation of TMG aquifers**

| | **Nardouw Aquifer** *l/s* ($10^6$ $m^3$/yr) | **Peninsula Aquifer** *l/s* ($10^6$ $m^3$/yr) | **Piekenierskloof Aquifer** *l/s* ($10^6$ $m^3$/yr) | ***Sum of TMG Aquifers*** *l/s* ($10^6$ $m^3$/yr) |
|---|---|---|---|---|
| **Unconfined** | 3139.76 (99.02) | 1107.59 (34.93) | 951.35 (30) | 5198.7 (163.94) |
| **Confined** | 686.37 (21.65) | 130.47 (4.11) | | 816.84 (25.76) |
| **Total** | 3826.13 (120.65) | 1238.06 (39.04) | 951.35 (30) | 6015.54 (189.71) |

## *5.7 Discussion regarding groundwater storage and discharge*

### *5.7.1 Demarcation of groundwater types in the TMG aquifers for water supply purposes*

In the previous sections, the dynamic groundwater resource quantification of the TMG aquifer systems was discussed and the related components such as groundwater recharge, storage and discharge were estimated using different approaches. These estimations were made by assuming the TMG aquifers form an independent groundwater system, and ignoring the possible influence of adjacent aquifers and sea impacts on TMG aquifers.

The estimated value ($3.3\times10^{10}$ $m^3$) of the total TMG storage capacity is so big that it is about 30 times the estimated recharge ($1.12\times10^{9}$ $m^3$/yr).

The groundwater of the TMG aquifers mainly discharges as baseflow, springs, hot springs, and borehole abstraction. To a certain extent, these discharges constitute a valuable resource in the TMG area, and can be used by different groundwater users, subject to legal, environmental and other restraints. Due to the specific spatial distribution of the TMG, the mechanism and quantity of groundwater discharges to the sea is unknown

With respect to the inland TMG groundwater, discharge via hot springs represents that part of water issuing from the deep circulation, while groundwater discharge to streams, springs, and boreholes largely accounts for the water at relatively shallow circulation. So far there are no consistent criteria to subdivide groundwater into deep and shallow flows because the demarcation may vary greatly with the scale of problems studied. In the case of the TMG aquifers, the deepest known circulation limit of groundwater can perhaps be represented by the Brandvlei hot spring with a circulation depth of 3600 m (Meyer, 2002). If the maximum depth at which water is stored in the TMG is also in the order of 3600 m, then the total storage capacity of $3.3\times10^{10}$ $m^3$ in the TMG aquifers would be overestimated.

By considering the aquifer distribution and the currently technical ability to exploit groundwater resources through boreholes in the TMG, the critical depth of 350 m is taken as the limit of shallow flow. Accordingly, the aquifer storage capacity of the shallow zone is $1.29\times10^9$ $m^3$, taking into account the storage capacity values in the zones above 350 m and above 100 m.

### *5.7.2 Groundwater discharge from TMG aquifers*

Strictly speaking, evapotranspiration is an important part of groundwater natural discharge in most cases. However in the TMG area the regional depth to the groundwater table is in the order of hundreds of metres (Hartnady and Hay, 2002), which gives no chance for discharge via evapotranspiration. It is possible that the estimated discharge items, i.e. baseflow, spring flow, hot spring and borehole yields, are not accurate enough as a results of the limited source data. However, the estimated results listed in Table 4-20 provide a quantitative insight into the component and magnitude of outflow ($1.29\times10^9$ $m^3$/yr) of the TMG aquifers. These values are not fixed, but vary with the influence of climate (recharge by precipitation), human activities (development of more pumping wells), and other factors.

Other processes that can not be properly estimated at this stage include leakage to the adjacent non-TMG aquifers and groundwater discharge to the sea along the coast. About 211 km of coastline mainly distributed along the east and south coast has a direct contact with TMG outcrops. Assuming the precipitation within 300 m of the coastline is able to discharge to the sea, and the average recharge rate is 50 mm/yr (equivalent to medium level of recharge estimation), the recharge-discharge volume is calculated at $3.17\times10^6$ $m^3$, which approximates 1.67% of the total borehole yields given in Table 5-20. Groundwater may also discharge to the sea through fracture networks at greater depths below sea level but the quantification of this part of groundwater discharge is beyond the scope of the current study. However, taking into account the coastline (Fig. 5-28), groundwater discharge to the sea can be estimated (Table 5-20).

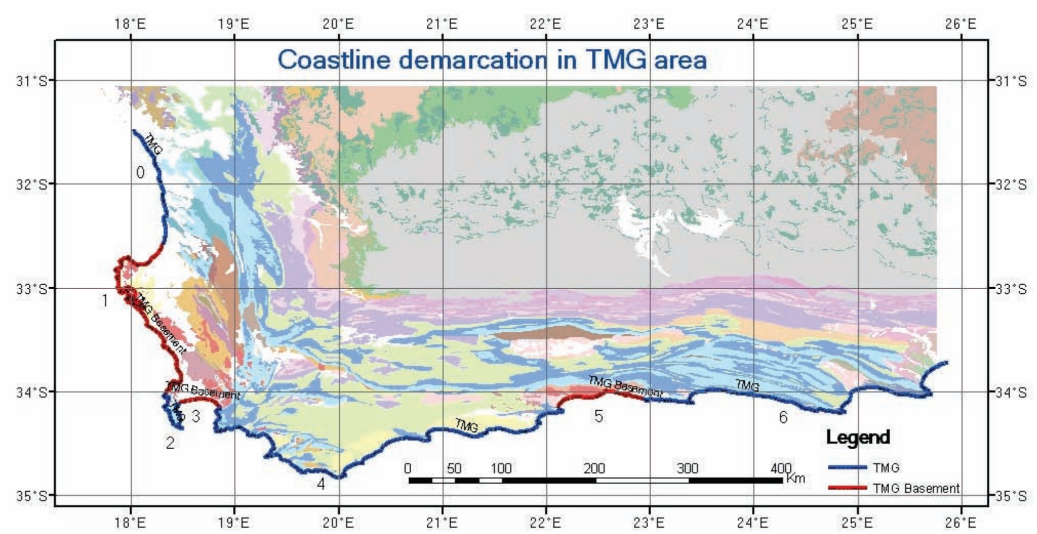


**Fig. 5-28** Coastline of the TMG – a length of 11309 km

**Table 5-20 Discharge estimates of TMG aquifers**

| Items | Discharge rate (*l/s*) | Discharge rate ($m^3$/yr) |
|---|---|---|
| Base flow | 34340.9 | 1.08E+09 |
| Spring flow | 141.0 | 4.45E+06 |
| Hot spring flow | 355.0 | 1.12E+07 |
| Borehole yield | 6015.5 | 1.90E+08 |
| Discharge to the sea | 101.0 | 3.17E+06 |
| Sum | 40953.4 | 1.29E+09 |

### *5.7.3 Groundwater budget on a regional scale*

In the hydrologic cycle, groundwater is a renewable resource ultimately fed by precipitation. Meteoric water goes into aquifers as natural recharge and groundwater exits from them as natural discharge. The system can be assumed to be in a naturally steady state before any development, and recharge is balanced by natural discharge, i.e. evaporation, baseflow, springs, aquifer leakage, and so forth. When a pumping process is imposed on an aquifer or aquifers, the natural balance is disturbed and it begins to evolve towards a new steady state. This state is achieved when the abstraction of the wells is balanced by increased recharge, decreased natural discharge, or the combination of the two. The sum of the diverted discharge and induced recharge is called the "capture" of the wells. At a basin scale, the sustainable yield can be determined by the capture when no further withdrawals from aquifer storage are made and no unmanageable or intolerable effects have been created. Usually a groundwater budget is needed for catchment management, which analyzes a groundwater catchment's inflows and outflows to determine the change in groundwater storage. Alternatively, if the change in storage is known, the value of one of the inflows or outflows could be determined. A detailed groundwater budget can provide understandings of the physical processes affecting storage in the catchment, which cannot be reflected in the simple calculation of change in storage. The basic equation of a groundwater budget can be expressed as:

INFLOWS – OUTFLOWS = CHANGE IN STORAGE (5-7)

Inflows include:

- natural recharge from precipitation;
- seepage from surface water;
- human activities inducing recharge;
- subsurface inflows from other catchments or aquifers.

Outflows include:

- discharge to surface water bodies and springs;
- extraction by wells;
- evapotranspiration; and
- subsurface outflow to other catchment or aquifers.

Groundwater budgets can be useful tools to understand and manage a catchment. A detailed groundwater budget requires subsurface exploration and monitoring over a series of years; the collection of field data is time-consuming and expensive. Consequently, detailed budgets are not available in most cases, especially on a regional scale like the TMG area. An initial groundwater budget for the TMG aquifer system is shown in Table 5-21. Because this study is on a multi-year averaged basis, the item of change in storage is approximated to zero in the budget. Recharge by precipitation is the only item of inflow and others are ignored. With regard to the outflows, the baseflow component is estimated as the upper limit of groundwater discharge to streams. Evaporation loss, discharge to the sea and outflows are ignored, which may be fruitfully evaluated by future research. Most of the main components are included in the budget. The recharge quantity is about $1.12\times10^9$ m$^3$, which is considered to be balanced by the summed outflows of $1.29\times10^9$ m$^3$, allowing for the imprecision introduced by the data sources and the ignored items.

**Table 5-21 Groundwater budget for TMG aquifer systems**

| Groundwater Budget | Items | Quantity ($m^3$/yr) |
|---|---|---|
| **Inflows (Recharge)** | Precipitation | 4.4E+09 (Upper limit) |
| | | 1.12E+09 (Wu, 2005) |
| | Other sources | ? |
| **Outflows (Discharge)** | Base flow (Upper limit) | 1.08E+09 |
| | Spring flow | 4.45E+06 |
| | Hot spring flow | 1.12E+07 |
| | Borehole yield | 1.90E+08 |
| | Discharge to the sea | 3.17E+06 |
| | Other sources | ? |
| | Sum | 1.29E+09 |
| **Change in storage** | | ≈ 0 |

An accurate evaluation of the sustainable yield of the TMG aquifers could not be made from the existing knowledge and information, but some scenarios can be proposed. On a regional scale the sustainable yield can be determined by the long-term mean annual recharge or natural baseflow. According to the recharge estimation, together with the baseflow estimation in Table 5-21, a sustainable yield of no more than $1.0\times10^9$ $m^3$/year (or <35515 l/s) is proposed for groundwater exploitation of the TMG aquifers. If this is correct, the present exploitation could be expanded to about 5 times the current level with well-planned abstraction schemes. This is just a general guide, and doesn't necessarily mean that if the total abstraction from TMG aquifer is less than $1.0\times10^9$ $m^3$/year, there will be no adverse impacts on the regional groundwater level or the environment.

On specific sites or local groundwater catchments, both the local groundwater-dependent ecosystems and the regional groundwater levels should be carefully monitored to prevent any adverse impacts by over-exploitation. It is also important is that the sustainable yield should not be regarded as a fixed value, but can be adjusted on a seasonal basis according to the actual conditions within the limitations of a long-term scheme. This is particularly important in the light of climate change.

## *5.8 Groundwater quality*

Generally speaking, TMG groundwater is of excellent quality with a very low salinity due to the inert nature of the rock, mountainous terrain, and locally high rainfall. Bacteria and nitrate are seldom concentrated in the TMG groundwater except where the groundwater has been polluted by localized sources. The electrical conductivity (EC) is usually less than 100 mS/m and most falls in the range of 20 to 50 mS/m, which makes the groundwater from the TMG aquifer suitable for most purposes (Smart and Tredoux, 2002).

With regard to hydrochemical problems, corrosivity may arise from the softness, poor buffering capacity and acidic nature of the TMG groundwater. This problem can be avoided by appropriate water pumping and transportation equipment. Another problem is the presence of ferrous iron, prevalent in the Nardouw Formation and also found in the Peninsula Formation to a limited extent. It can result in problems like borehole clogging. The situation is more serious when associated with sulphate. So far the Fe occurrence is only partially understood. Research is needed to identify its formation processes and the development of suitable prevention or mitigation measures. The pollution of TMG groundwater is very limited at present, owing to the difficult access of the mountainous TMG terrain and therefore relative lack of anthropogenic activity. However in the light of possible future development of this resource, measures should be in place to ensure the quality of this precious resource.

# 6. Groundwater and Surface Water Interaction

## 6.1 Introduction

Currently, more research focus is oriented towards the important issue of water exchange between groundwater and surface water. Concerns of water availability as well as ecologic concerns drive this interest. This section mainly deals aspects pertaining to the implementation of new National Water Act in South Africa. In this legislation the ecological reserve represents flow requirements for aquatic ecosystems. A quantified assessment of groundwater – surface water (GW-SW) interactions is required for the determination of baseflow proportion in the stream and the minimum in-stream flow requirements (IFR) for ecological health, after which a water allocation can be made (Xu et al., 2002).

The GW-SW interaction is controlled by the positions of the surface water bodies relative to the groundwater levels, the characteristics of their beds and underlying materials, and their climatic setting (Winter et al., 1998). Water exchange across the surface water –groundwater interface has been explored in some detail in the past decade, with most studies focused on streams (Jones and Mulholland, 2000). The interactions of groundwater with lakes, wetlands, estuaries, and oceans are also recognized as important processes (Mortimer et al., 1999; Fraser et al., 2001; Moore, 1999; Basu et al., 2001).

Knezek and Krasny (1990) stated that groundwater runoff or baseflow assessment is the best way to estimate regional groundwater resources. With regard to resource evaluation, GW-SW interactions can occur in both directions. On the one hand groundwater can be recharged from surface water, i.e. losing streams or river leakage. On the other hand, groundwater can discharge to surface water, i.e. stream baseflow (Lerner, 2005). The interaction between groundwater and streams is ubiquitous in the TMG outcrop areas. The picture depicted in Fig. 6-1 is taken from a ready-made groundwater supply site in the TMG outcrop area. The bedrock is Nardouw Formation. The stream is perennial, which implies its source includes stable groundwater discharge from the TMG aquifer. The stream

**Fig. 6-1** A GW-SW interaction in the TMG outcrop area

flows into a mountainous lake, the leakage of which could be the recharge source of the lower-lying TMG aquifers.

In this chapter the basic concepts of groundwater and surface water interaction are introduced and then the groundwater and surface water interaction related to TMG aquifers is studied. The focus is stream baseflow analysis, from which the value of mean annual baseflow is estimated as one component of groundwater discharge from the TMG aquifers.

## 6.2 Basic concepts of groundwater and surface water interaction

Groundwater-surface water interaction may occur at various zones in the hydrological cycle. As rain or snow falls to the earth's surface, some water may enter the soil and infiltrate deeper to reach groundwater. When the groundwater level is higher than the surface water stage, groundwater will discharge to the surface through wells, springs and marshes.

The United States Geological Survey (Winter et al., 1998) has described a conceptual landscape to define the most common types of groundwater and surface water interaction. The following types of terrain are defined: mountainous, river valleys, coastal, glacial, dune, and karts. Descriptions of typical interactions are presented in Winter et al., 1998. A simple introduction of the mountainous terrains and river valleys is quoted here.

In mountainous terrains, usually in the inter-storm or snowmelt periods, mountainous streams are sustained by groundwater discharge from the adjacent aquifer, whereas during the storms the surface runoff quickly flows to the streams (Fig. 6-2). Mountainous stream flow is composed of overland flow on the hill slope, interflow from the unsaturated zone and groundwater discharge from groundwater storage. Their respective proportions of flow depend on climatic and geologic factors.

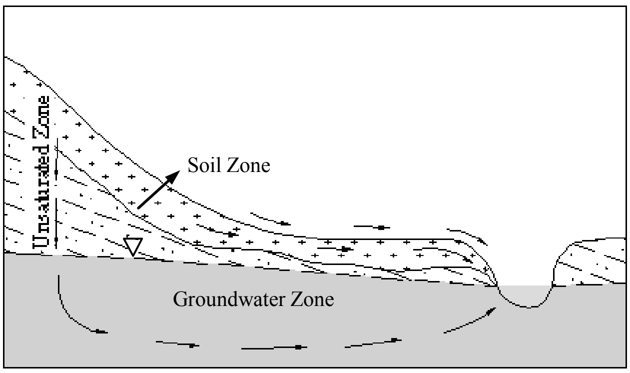

**Fig. 6-2** Groundwater and surface water interaction in Mountain terrain (after Winter et al., 1998)

In a river valley terrain, the extent of interaction between groundwater and surface water depends on the scale of the river. Similar to the mountainous terrain, climatic factors, i.e. storm induced flooding and evapotranspiration, and

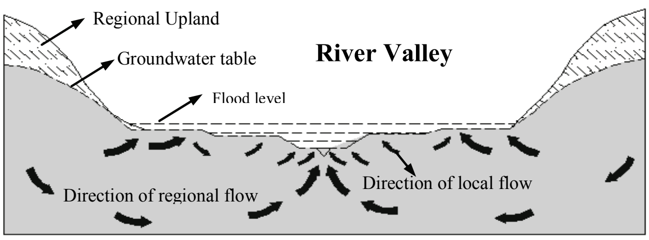

**Fig. 6-3 Groundwater** and surface water interaction in River Valley terrain (after Winter et al., 1998)

geologic factors, i.e. the riverbed deposits, also play a role in the process of water exchange in river valley terrain. As would be expected, small streams usually receive groundwater discharge from local flow systems, which are limited and highly seasonal. As for broad river valleys or flood plains, groundwater discharge from regional flow systems may flow to the river or the flood plain. The occurrence of fault lines may also create areas where significant exchanges between surface water and groundwater occur. Fig. 6-3 shows the interaction type of groundwater and surface water in river valley terrain.

In South Africa, especially in the TMG area, GW-SW interaction involves streams more than other surface water bodies like lakes and wetlands. The interaction between groundwater and streams depends on their relative water levels. Four basic types of streams can be identified according to the relative elevation of the water level in the stream to that of the water table of the groundwater. The four types of streams are:

1) Gaining streams: Streams gain water from groundwater through the streambed when the groundwater table adjacent to the streambed is greater than the water level in the stream

2) Losing streams: Streams lose water to groundwater by outflow through the streambed when the elevation of the water table is lower than the water level in the stream

3) Detached streams: For some streams in more arid region, the GW-SW interaction becomes quite inactive.

4) Intermittent streams: In some instances a stream may take on different characteristics during different seasons. In wet seasons or flood seasons, the water table rises up to the base of the stream and the stream may become a gaining stream. After the wet season, as the water table declines, the stream may attain a losing character.

The quantification of GW-SW interactions in streams has been studied using different approaches for specific sites, quaternary catchments or a single hydrological event (Smakhtin, 2001; Linsley et al., 1958; Farvolden, 1964; Rorabaugh, 1964; Halford and Mayer, 2000 Rutledge, 1993; Mayer and Jones, 1996). Based on a hydrogeomorphological understanding, Xu et al. (2002) propose an empirical approach to estimate the IFRs, which combines both the hydrogeomorphological typing of the streams and quantitative baseflow separation, and thus makes the estimation more realistic. However for a regional study like the TMG area, it is impossible to investigate each individual stream and assign the most reasonable quantification algorithm to derive the groundwater discharge to the streams. Empirical methods are needed to perform the estimation in a batch-calculation way, where different parameters could be set to allow for the different hydrogeological and hydrometeorological settings of the streams.

## 6.3 The interaction between groundwater and streams related to TMG aquifers

From the discussion of groundwater discharge estimation in the previous chapter, it is clear that baseflow, which is assumed to be the upper limit of the groundwater discharge to stream flow, accounts for the largest proportion of the existing groundwater discharge components. It is estimated that there is – at most – 1.1 billion $m^3$ of groundwater discharge to stream flow from the TMG aquifers each year.

### *6.3.1 Periodicity of stream flow and long-term trends*

#### 6.3.1.1 General climate change and periodicity of stream flow in South Africa

Flow in streams is not invariable for the whole year because it may be a quick response to a short rainfall event as we can usually see directly. There is also the seasonality of the stream flow under seasonal weather variations. Expand the view to a long history of the stream flow, and variability can also can be found in the medium-term and long-term trends.

Meyer (2005) has made a comprehensive review on the issue of climate change in Southern Africa. The ancient climate (during the Pleistocene and Holocene) cycles and the climatic variations during the last 200 years are summarized in his report. The major wet and dry phases in the Kalahari are listed in Table 6-1.

Meyer (2005) mentions that various rainfall cycles have been noted from the perspective of groundwater in South Africa, including cycles of 18-years, 10.5-years and also the smaller cycles of 3.5 or 2.3 years.

#### 6.3.1.2 TMG-related rainfall zones and stream flow gauge stations

In WR90 (Midgley et al., 1994), 448 rainfall zones are demarcated throughout the country, and the representative rainfall histories were compiled for each zone. The rainfall zones are built up by congregating quaternary catchments that have similar rainfall characteristics. The TMG outcrop areas are located in 83 of these rainfall zones.

Only 17 stream flow gauge stations with monthly flow records are located in the TMG outcrop areas. A further filtering has been carried out to these gauge stations by overlying river and TMG outcrop maps on the gauge-station location map to check what kind of hydraulic relationship between the streams and TMG aquifers were likely. The GIS analysis shows that 13 of these gauge stations have full relationship with TMG because the gauged part of the streams is almost entirely located within the TMG outcrop areas. Three of the stations are identified to be partially related to TMG aquifers with only part of the gauged catchment located on TMG outcrop areas. One station was found with no hydraulic relationship with the TMG and was left out of the study.

**Table 6-1** Major wet and dry phases in the Kalahari during the 19th century and for South Africa in general for the 20th century (after Meyer, 2005)

| Major wet periods | Major drought periods | Probable regional extent |
|---|---|---|
| 1816/17 | | Southern Kalahari |
| | 1820-1822 | Cape. Dry period of below normal rainfall. |
| | 1820-1827 | Southern Kalahari plus parts of the former Eastern Cape* |
| 1829/1830 | | Southern Kalahari plus adjacent parts of South Africa* |
| | 1831-1835 | Southern Kalahari plus parts of the former Eastern Cape* |
| | 1844-1851 | Entire Kalahari plus adjacent parts of Angola and Zambia* |
| 1851/52 | | Entire Kalahari plus large areas of South Africa |
| | 1857-1865 | Middle and Southern Kalahari plus much of South Africa, with drought punctuated by widespread wetter conditions in 1863/64* |
| 1863/64 | | Southern Kalahari plus areas of former Eastern Cape |
| 1874/75 | | Middle and Southern Kalahari plus large areas of South Africa* |
| | 1877-1886 | Entire Kalahari plus parts of South Africa |
| 1889-1991 | | Middle and Southern Kalahari plus large areas of South Africa* |
| | 1894-1899 | Entire Kalahari plus large areas of neighbouring South Africa |
| 1899/1900 | | Middle and Southern Kalahari plus adjacent parts of South Africa |
| | 1905/06-1915/16 | Southern Africa |
| 1916/17-1924/25 | | Southern Africa |
| | 1925/26-1932/33 | Southern Africa |
| 1933/34-1943/44 | | Southern Africa |
| | 1944/45-1952/53 | Southern Africa |
| 1953/54-1961/62 | | Southern Africa |
| | 1962/63-1970/71 | Southern Africa |
| 1971/72-1980/81 | | Southern Africa |
| | 1982/83-1992/93 | Southern Africa |
| 1993/94-2002/3 | | Southern Africa* |

The types of the gauged streams (perennial or non-perennial) are also available from the associated attributes of the stream map and they can also be calibrated with the rainfall records on these gauge stations. The spatial distribution of the 16 TMG-related gauge stations (Fig. 6-4) covers virtually the whole TMG area and can therefore be assumed to be representative. Table 6-2 lists the basic information on these gauge stations.

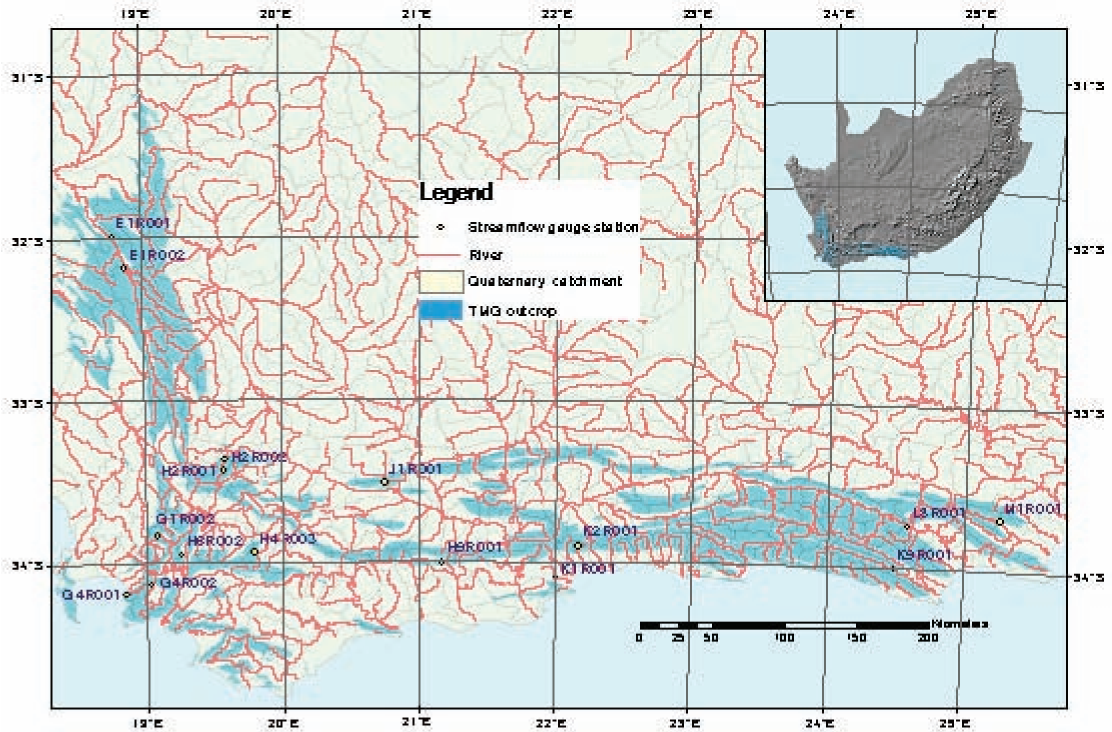


**Fig. 6-4** Spatial distribution of TMG-related river flow gauge stations with data records

**Table 6-2** Information re stream flow gauging stations in TMG outcrop areas

| Station No. | Rainfall zone | MAP (mm) | Gauged area (km$^2$) | Gauged QCat(s) | MAR (Mm$^3$) |
|---|---|---|---|---|---|
| E1R001 | E1D | 250 | 2769 | E10A-E10J & Part of E10K | 396.1 |
| E1R002 | E1C | 350 | 2033 | E10A-E10G | 395.8 |
| H2R001 | H2 | 600 | 139 | H20C & Part of H20D | 19.5 |
| H2R002 | H2 | 600 | 80 | H20C | 5.5 |
| G1R002 | G1A | 1000 | 86.2 | Part of G10B | 69.3 |
| G4R001 | G4C | 900 | 66.8 | Part of G40A | 43.8 |
| G4R002 | G4C | 900 | 63 | Part of G40C | 54.7 |
| L8R001 | L8D | 400 | 3887 | L81A-L81D & L82A-L82H | 187.1 |
| K9R001 | K9B | 700 | 357 | K90A-K90B | 53.4 |
| K1R001 | K1 | 400 | 100 | Part of K10B | 2.4 |
| K2R001 | K3 | 700 | 16.8 | Part of K20A | 3.7 |
| H4R003 | H4C | 400 | 54 | Part of H40K | 2.8 |
| H6R002 | H6A | 1000 | 50 | Part of H60C | 23.9 |
| J1R001 | J1D | 300 | 757 | J12G | 3.5 |
| H9R001 | H8A | 600 | 37 | Part of H90B | 9.5 |
| M1R001 | M1A | 600 | 265 | M10A | 16.0 |

### 6.3.1.3 Long-period trends of rainfall and stream flow in the TMG outcrop areas

To indicate the condition of climatic cycles in TMG area, the rainfall history expressed by a spatially-averaged percentage of annual rainfall of the abovementioned 15 rainfall zones from 1920 to 1989 and the relevant smoothed rainfall (averaged by 5 years continuously) are depicted by Fig. 6-5. It is difficult to recognize the abovementioned wet or dry periods from this graph, probably because less statistic techniques are used to summarize the cycle. However it is clear that the rainfall periodicity does exist. It can be confirmed from the linear trend line of the spatially averaged rainfall that the rainfall in this area was not undergoing a long-period decline. On the contrary it shows a slight increase (slope K=0.0941) with time.

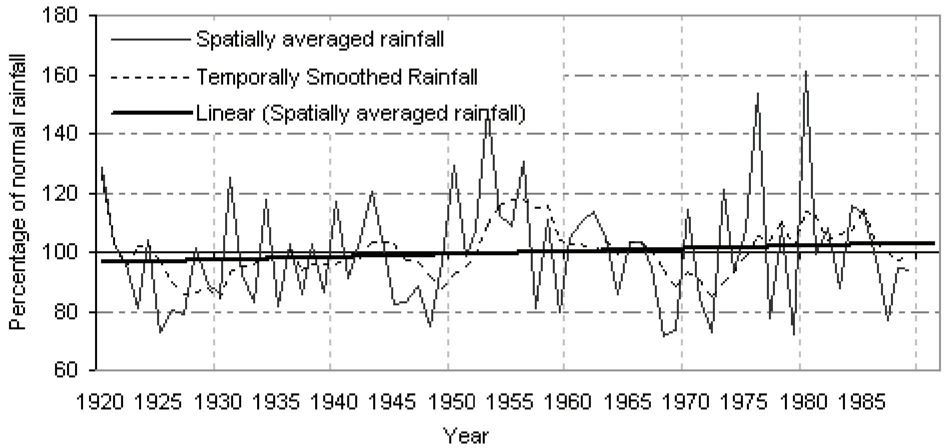


**Fig. 6-5** Spatially averaged and temporally smoothed rainfall in the TMG outcrop area

The stream flow variations are mainly attributed to the climate changes. The hydrograph of a specific stream flow gauge station usually mirrors the rainfall at that same site. The monthly stream flow records and rainfall records from 1920 to 1989 for station E1R001 is plotted in Fig. 6-6 to depict this phenomenon. The study of the periodicity of the rainfall could be applied to the stream flow in most cases. Alexander (1995, 2002) analyzed South African stream flow data and confirmed a 19 to 21 year periodicity in both rainfall and stream flow records.

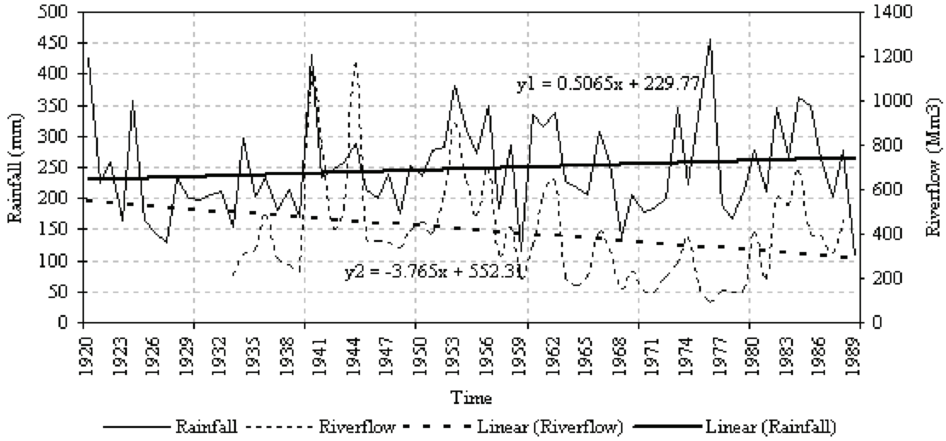


**Fig. 6-6** Annual rainfall and river flow records and their trend lines of river flow gauge station E1R001

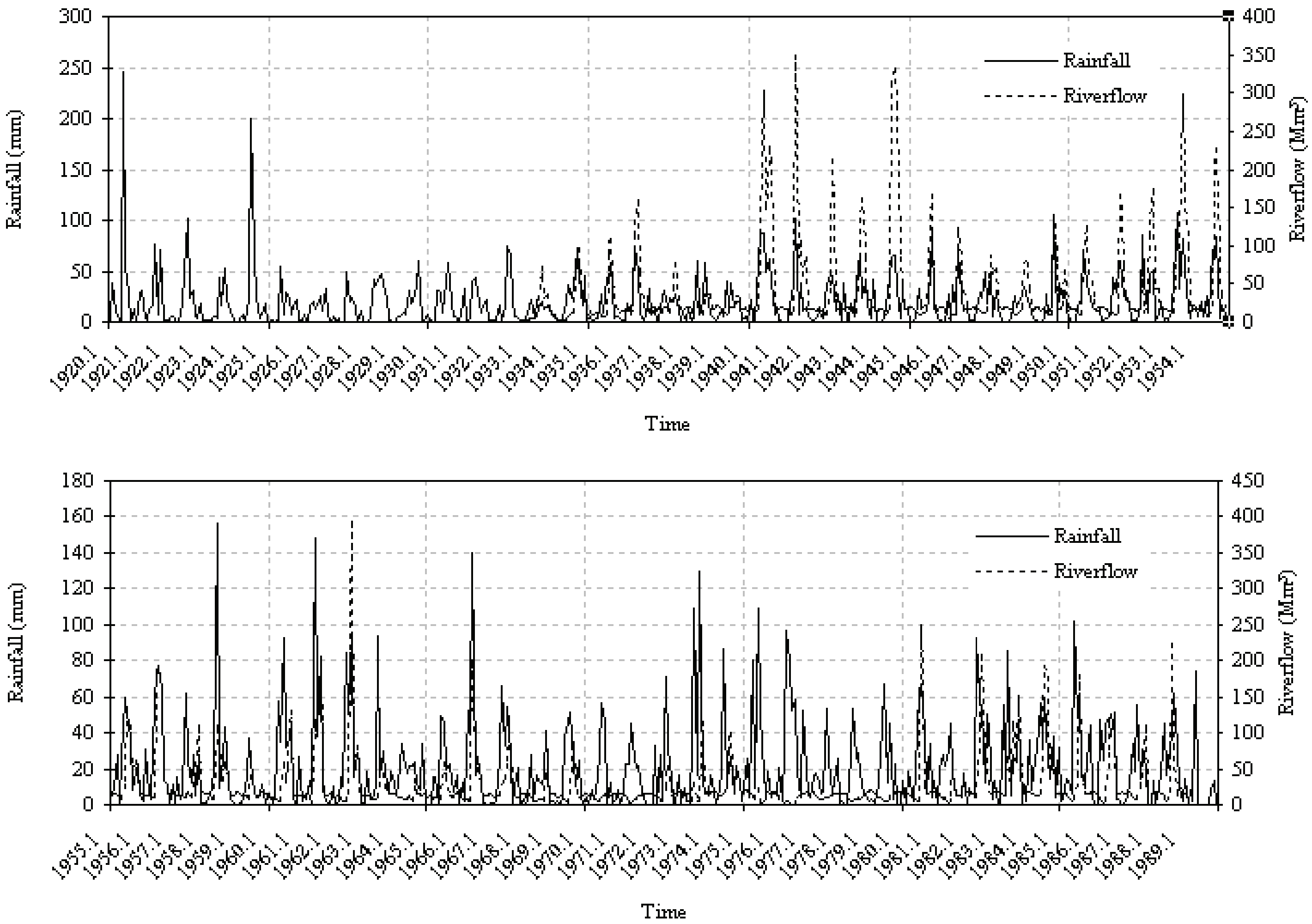


**Fig. 6-7** Monthly stream flow and rainfall records from 1920 to 1989 on station E1R001

The annual rainfall and stream flow records for 1920 to 1989 for the 16 stream flow gauge stations located in TMG outcrop areas were analyzed graphically. The chart of E1R001 is shown in Fig. 6-7 as an example. Blank spaces indicate that some or part of the stream flow data are missing. The relationships between the rainfall and stream flow are presented explicitly and both of their linear trend lines are added to the charts to illustrate their respective long-period trends. These data are summarized for each stream flow gauge in Table 6-3.

**Table 6-3** Summary of long-period trends of rainfall and stream flow for 16 stream flow gauge stations in the TMG outcrop area

| Station No. | Rainfall | | Stream flow | | Region |
|---|---|---|---|---|---|
| | Trend | Slope (k) | Trend | Slope (k) | |
| E1R001 | Inc. | 0.5065 | Dec. | -3.765 | West |
| E1R002 | Inc. | 1.1102 | Dec. | -1.9074 | West |
| G1R002 | Inc. | 1.2861 | Dec. | -0.2722 | West |
| G4R001 | Inc. | 1.8289 | Dec. | -0.1784 | West |
| G4R002 | Inc. | 1.8289 | Dec. | -0.1771 | West |
| H4R003 | Inc. | 0.5585 | Dec. | -0.454 | West |
| J1R001 | Inc. | 0.1675 | Dec. | -0.0361 | West |
| H2R001 | Inc. | 2.0226 | Inc. | 0.4932 | Middle |
| H2R002 | Inc. | 2.0226 | Inc. | 0.095 | Middle |
| H6R002 | Inc. | 0.8843 | Inc. | 1.2175 | Middle |
| H9R001 | Inc. | 1.1384 | Inc. | 0.1687 | Middle |
| K1R001 | Inc. | 1.0768 | Inc. | 0.0649 | Middle |
| L8R001 | Dec. | -1.1995 | Dec. | -1.1842 | East |
| K9R001 | Dec. | -1.3838 | Dec. | -0.8023 | East |
| K2R001 | Dec. | -0.0524 | Inc. | 0.0009 | Middle |
| M1R001 | Dec. | -0.1559 | Inc. | 0.0626 | East |
| *Inc. = Increasing, Dec. = Declining | | | | | |

Table 6-3 also lists the long-period trend of rainfall and stream flow for the 16 stream flow gauge stations together with the linear slope k derived from the chart. An evaluation with three rankings of “Good”, “Medium” and “Poor” on the stream flow data is performed based on the length and the continuity of the records. Most of the data are ranked as “Good” and “Medium” while only 3 of them are ranked as “Poor” due to less than 10 years’ record length. The relative location of each gauge in TMG area is also listed in the table to indicate the locality of rainfall and stream flow pattern. It can be observed that in the west and middle regions of the TMG outcrop area, where the winter rainfall pattern prevails, the long-period trend of rainfall shows a slight increase. In the east region where rain fall occurs in both summer and winter, the rainfall was undergoing a progressive decline.

Furthermore, in the winter rainfall region, the stream flow presents two different trends. In the west region of TMG outcrop area, the stream flow shows a progressive decline, even though there was an increase in rainfall. In the middle region, however, both the stream flow and the rainfall increased. A possible explanation to this phenomenon may be that there was more groundwater abstraction in the west region of TMG area than the middle region during the study period.

From Fig. 4-8 (distribution map of the TMG-related boreholes), it can be seen that the distribution of the boreholes in the west region is much denser than that in the middle region. However most of these boreholes were constructed after 1989 which means they cannot affect the stream flow trends.

### *6.3.2 Baseflow*

#### 6.3.2.1 Stream hydrographs

A stream hydrograph is made up of several components, which normally include direct precipitation, overland flow (surface runoff), and baseflow (both interflow and groundwater discharge). The concept of baseflow is understood differently by hydrologists and hydrogeologists (Chapman, 1999). Surface hydrologists usually identify baseflow as the low amplitude and high frequency flow events, based on which, baseflow separation techniques are used to separate the baseflow component from the stream hydrograph. However, the origins and the mechanisms of the generation of water are seldom considered in their techniques. Hydrogeologists often take baseflow as the groundwater contribution to the stream and it provides an approach to estimate the related recharge, discharge and dynamic storage of groundwater.

#### 6.3.2.2 Baseflow separation

Many of the hydrograph separation approaches try to distinguish between rapidly occurring overland flow, slower-moving interflow, and even slower-moving groundwater discharge (Freeze, 1972a). However the interflow component is not easy to separate quantitatively and can usually only be illustratively depicted on the graph. In some cases the interflow component is overlooked to simplify the separation process. Freeze (1972b) concluded that overland flow can become a significant stream flow component only on convex hill slopes that feed deeply incised channels. Generally the separated baseflow cannot be arbitrarily regarded as the groundwater discharge but just the upper limit of it, especially in the mountainous catchments. A lot of separation techniques have been reviewed (Nathan et al., 1990; Tallaksen, 1995; Boughton, 1998; Xu et al., 2002; Eckhardt, 2004). These methods can generally be summarized into two groups, viz. “event-based separation methods” and “continuous separation techniques” (Smakhtin, 2001).

***Event-based baseflow separation methods***

Usually the event-based separation methods focus on separating baseflow from a flood hydrograph and are aimed at the estimation of the surface runoff component of the flood. In most of the literature the flood event is regarded as single rainfall event. However, it could be a hydrologic event of various magnitudes to meet different study needs. For example, a quick response of a stream flow to rainfall may be studied on a daily or an hourly scale, while for the unevenly distributed monthly stream hydrograph, storm flow or surface runoff dominate the stream flow and high discharge months may also be characterized by a specific hydrological event in a broad sense.

The event-based separation methods are generalized by McCuen (2004):

- *Constant-discharge* – start at the beginning of rising limb of the hydrograph; draw a horizontal line until it intersects the recession curve. This is based on the assumption that the baseflow remains constant. It is easy to perform, but ignores the fact that baseflow could increase following a storm event
- *Constant-slope* – start at the beginning of the rising the limb, draw an upward sloping line to the inflection point on the recession limb. The inflection point on the recession limb is taken to be the end of surface runoff, and the time from the end of the rainfall event to the inflection point is the watershed’s “time of concentration”. The problem is that it can be difficult to exactly determine the inflection because of the noisiness of field data. A widely used empirical relationships can be applied to determine the inflection point: $T = A^{0.2}$, where T is days from peak to inflection point, and $A$ is basin area
- *Concave* – extend the pre-storm recession trend (linearly) until the time of the peak (tp), then draw an upward sloping line to the inflection point

***Continuous baseflow separation methods***

The continuous separation method is designed to distinguish baseflow components from stream hydrograph for a longer period, for instance one year or more, or for the entire period of observations. The rationale behind the continuous separation techniques is that the baseflow characteristics may provide a qualitative or quantitative understanding of the interaction between groundwater and stream flow. The easiest method of this type of techniques is the “local minimum method”, which mainly deals with the daily stream flow data. Other methods of continuous separation techniques are mostly digital filter methods. Normally a filtering procedure is employed to disintegrate the stream flow time series into quick flow and baseflow. Several digital filter methods and their applications have been reported, including the BFLOW filter (Lyne and Hollick, 1979), Eckhardt filter (Eckhardt, 2004), smoothed minima method (FREND, 1989), recursive digital filter (Nathan and McMahon, 1990) and various others (Sittner et al., 1969; Birtles, 1978; Boughton, 1988; Smakhtin, 1993; Sloto, 1996).

Another notable method in this category is the hydrogeomorphological approach proposed by Xu et al. (2002). The hydrogeomorphological typing is used to guide a process of separating groundwater discharge time series from hydrographs.

It is not realistic to apply event-based baseflow separation methods to a regional-scale study such as this. Among the continuous baseflow separation methods, the local minimum method is more suitable for the daily flow data. As the stream flow data are stored on monthly basis in WR90, the recursive digital filter method was selected for this study because of both the availability of data and the successful experience of applying this method in South Africa (Smakhtin, 2001; Hughes et al., 2003).

***Recursive digital filter method and its application in the TMG outcrop areas***

Both the daily and monthly stream flow time series are appropriate for baseflow separation, whilst the former simulates the baseflow response on a more detailed basis better. Daily data series are not always available or are cumbersome to deal with even when available. In South Africa, all the stream flow data have been arranged in monthly series on a regional scale in the WR90 study. Therefore a suitable technique for monthly baseflow separation was required. One of the abovementioned continuous baseflow separation techniques, the recursive digital filter method was selected for this study. The method originates from signal analysis and was first used in hydrology by Nathan et al. (1990). It has been widely used with monthly stream flow data for South African streams and catchments and yields satisfactory results when compared with that of daily data (Smakhtin, 2001; Hughes et al., 2003). The algorithm of this method is:

$$q_m=\alpha q_{m-1}+\beta(1+\alpha)(Q_m-Q_{m-1}) \quad (6\text{-}1)$$

$$QB_m=Q_m-q_m \quad (6\text{-}2)$$

Where:

q is part of the monthly flow that can be attributed to high-flow events or runoff,

Q is total monthly flow (original stream flow time series),

QB is part of the total monthly flow which could be attributed to baseflow,

$\alpha$ is a filter parameter,

m is the index of the current month in a time series, and

m-1 is the index of the previous month.

Hughes et al. (2003) set $\beta$ in the range of $0<\beta<0.5$. However in the application of this method, was found that parameter $\alpha$ was flexible enough and has almost the same efficacy to control the shape and the volume of the separated baseflow. Hence the $\beta$ parameter is fixed to 0.5 in present study and only the parameter $\alpha$ is adjusted to simulate the baseflow separation process.

No one has tried to imbue the recursive digital filter method with hydrological meaning and the opinion is held that it is a purely empirical method and not based on any real knowledge of the hydrological processes (Hughes et al., 2003).

When assigning the filtering parameter values for $\alpha$, Smakhtin (2001) recommend that a starting point of 0.925 is applicable for most of the monthly baseflow separations in regions where MAPs range from 600 to 1100 mm in South Africa. He suggested that for semi-arid and arid regions with MAPs less than 600 mm, the filter value can be increased by about 2% and in regions where MAP is over 1100 mm, the filter value can be decreased by 2%. These recommendations may be used for reference but should not be applied mechanically. Almost all of the TMG outcrop areas are mountainous and have quite thin soil layers, which gives suggests that more surface runoff will occur than in other geological with the same rainfall MAPs. In other words, baseflow could be less than expected. This is supported by observing the peak time of rainfall and stream flow on the same chart. On each of the existing studied 11 gauging stations, the peak value of rainfall and stream flow occurs in the same month in more than 90% of the observation years. In less than 10% of the years do the peak values of stream flow lag behind the peak month of rainfall.

The estimate of the filtering parameter $\alpha$ should therefore be modified when applied to TMG outcrop areas because of the effects of geomorphology and surface soil layer. Another modification is to change the threshold value of MAP of 1100 mm to 1000 mm because the rainfall differences between regions are not sufficiently delineated in the existing rainfall isoline map in WR90. In terms of Smakhtin's recommendations, in this study an increase of 0.04 was added to the parameter $\alpha$ to account for the geological and geomorphological characteristics of TMG outcrop areas impacted on baseflow. The values of $\alpha$ were set to range from 0.945 to 0.985 according to the different MAP values.

With the recursive digital filter method, low-frequency baseflow can be separated from the stream flow by analyzing the stream flow hydrographs. How much groundwater has actually contributed to the baseflow is still a question, although baseflow is usually arbitrarily equated to groundwater discharge in practice. At this stage, especially for a regional estimation, it is not realistic to differentiate the interflow and groundwater components of baseflow; rather baseflow can be regarded as an upper limit estimation of groundwater discharge derived from stream flow.

For the estimation of total baseflow related to TMG aquifers, the assumption is made that all the streams located on the TMG outcrop areas have a losing characteristic. Only streams flowing across the outcrop areas are taken into account, while on the non-outcrop areas, because of TMG aquifers are mostly deep buried, the stream flow is assumed to have no interaction with TMG aquifers but rather with the overlying layers, i.e. Bokkeveld Group.

The monthly stream flow data for each quaternary catchment in South Africa has been reconstructed from 1920 to 1989 in WR90, providing an ideal basis for this study. The same technique is also applied to the data series from stream flow gauging stations with the aim of validating the results derived from the quaternary catchments baseflow separation for some catchments. The manipulation of baseflow separation for quaternary catchments includes the following procedures:

- Prepare the quaternary catchment map with the attributes of "MAR" (Mean Annual River flow) for TMG outcrop areas in GIS.
- The simulated or reconstructed monthly stream flow history data for each quaternary catchment in TMG outcrop areas are extracted from WR90, which provides the original stream flow data input for the baseflow separation process.
- By programming the separation technique described by Equation (6-1) in Excel, monthly baseflow volumes for each quaternary catchment in TMG outcrop areas are successfully simulated. The annual baseflow volume is obtained by adding the monthly volumes for each quaternary catchment.

- The ultimate result of annual baseflow separation is linked to the quaternary catchment map in GIS and the spatial distribution map of baseflow is generated based on the linked attribute fields.

Fig. 6-8 and Fig. 6-9 show the spatial distributions of baseflow in the TMG outcrop areas units of $10^6$ m$^3$ and mm respectively. The results of annual baseflow volume for quaternary catchments in TMG outcrop areas are listed in Appendix H. The total annual baseflow volume in TMG outcrop area was estimated to be $1082.97 \times 10^6$ m$^3$/yr or 34340.89 *l/s*. Table 6-4 lists the baseflow separation result for each gauge station and the BFI (Baseflow Index) is given as well.

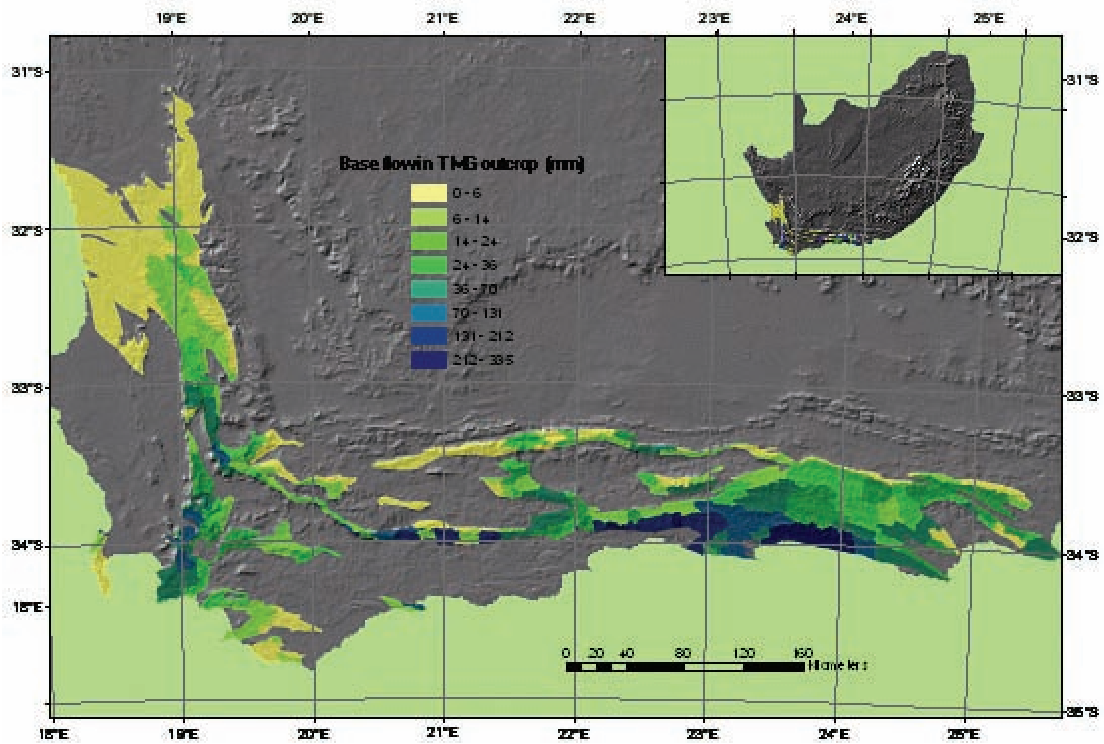


**Fig. 6-8** Spatial distribution of Mean Annual Baseflow (mm) in the TMG outcrop areas

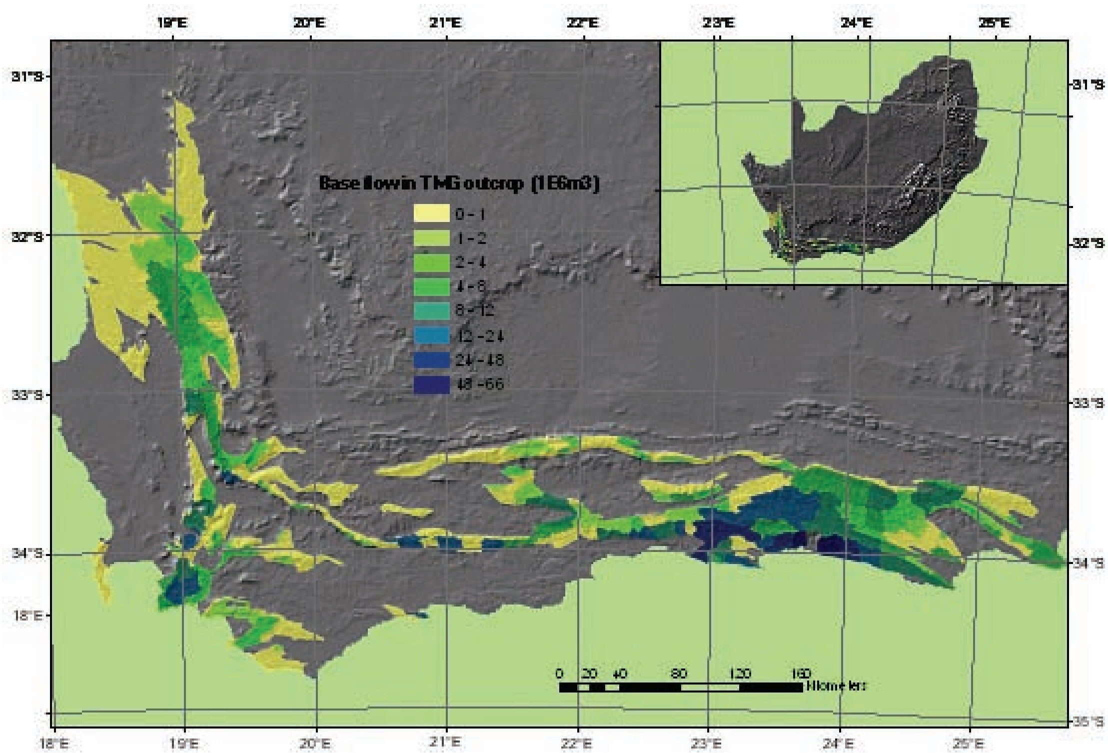


**Fig. 6-9** Spatial distribution of Mean Annual Baseflow (Mm$^3$) in the TMG outcrop areas

**Table 6-4 Baseflow separation results of the stream flow gauge stations related to TMG**

| Station No. | MAP (mm) | Parameter *a* | MAR (Mm$^3$) | MAS (Mm$^3$) | MAB (Mm$^3$) | BFI (%) |
|---|---|---|---|---|---|---|
| E1R001 | 250 | 0.985 | 396.1 | 286.6 | 109.5 | 27.6 |
| E1R002 | 350 | 0.985 | 405.5 | 363.3 | 42.2092 | 10.4 |
| H2R001 | 600 | 0.965 | 19.5 | 16.0 | 3.5 | 17.8 |
| H2R002 | 600 | 0.965 | 5.6 | 4.7 | 0.9 | 15.6 |
| G1R002 | 1000 | 0.945 | 71.3 | 51.0 | 20.3 | 28.5 |
| G4R001 | 900 | 0.965 | 43.8 | 36.2 | 7.5 | 17.2 |
| G4R002 | 900 | 0.965 | 54.7 | 41.6 | 13.1 | 23.9 |
| L8R001 | 400 | 0.985 | 187.1 | 153.6 | 33.6 | 17.9 |
| K9R001 | 700 | 0.965 | 53.4 | 44.0 | 9.4 | 17.6 |
| K1R001 | 400 | 0.985 | 2.4 | 2.3 | 0.1 | 4.8 |
| K2R001 | 700 | 0.965 | 3.8 | 2.7 | 1.2 | 30.3 |
| H4R003 | 400 | 0.985 | 2.8 | 2.7 | 0.1 | 4.8 |
| H6R002 | 1000 | 0.945 | 27.0 | 22.3 | 4.7 | 17.5 |
| J1R001 | 300 | 0.985 | 3.5 | 3.4 | 0.1 | 3.9 |
| H9R001 | 600 | 0.965 | 10.1 | 7.3 | 2.8 | 27.9 |
| M1R001 | 600 | 0.965 | 16.0 | 12.9 | 3.1 | 19.3 |

MAR: Mean Annual River flow;
MAS: Mean Annual Surface runoff;
MAB: Mean Annual Baseflow;
BFI: Baseflow Index, the ratio of baseflow to total stream flow.

For the convenience of this study, only those stations that gauge the whole quaternary catchment(s) were selected for the calibration of the baseflow separation results, including E1R002, H2R002, L8R001, K9R001, and M1R001. The comparison is shown in Table 6-5.

**Table 6-5 Baseflow separation results of stream gauge station and Quaternary catchment**

| Station No. | Gauged QCat(s) | QCat(s) MAP Range (mm) | QCat(s) MAR ($Mm^3$) | QCat(s) MAB ($Mm^3$) | QCat(s) BFI (%) |
|---|---|---|---|---|---|
| E1R002 | E10A-E10G | 400-1000 (350) | 404.0 (395.8) | 77.0 (42.2) | 19.1 (10.4) |
| H2R002 | H20C | 500-700 (600) | 3.6 (5.5) | 0.7 (0.9) | 18.7 (15.6) |
| L8R001 | L82H | 400-800 (400) | 189.0 (187.1) | 46.2 (33.6) | 24.4 (17.9) |
| K9R001 | K90A-K90B | 700-800 (700) | 56.0 (53.4) | 13.9 (9.4) | 24.9 (17.6) |
| M1R001 | M10A | 400-600 (600) | 16.0 (16.0) | 2.7 (3.9) | 16.7 (19.3) |
| * Values in brackets are data derived from corresponding gauge stations. | | | | | |

Theoretically, the Baseflow Indexes (BFIs) derived from the quaternary catchments and from the corresponding gauge stations are supposed to be the same. However, as shown in Table 6-5, differences do exist. This may partially be attributed to the original data. A more important reason is the different MAP values used as reference to decide the value of parameter $\alpha$ in the process of the baseflow separation. Taking gauge station E1R002 as an example, the MAP value 350 mm is used in terms of the corresponding rainfall zone, accordingly the lowest $\alpha$ value of 0.985 is used to simulate the baseflow from which the BFI of 10.4% is obtained. On the other side, the gauged station E1R002 gauges the quaternary catchments from E10A to E10G, which span a region with MAP values ranging from 400 to 1000 mm. A range of $\alpha$ value from 0.945 to 0.985 was used for the baseflow separation of these quaternary catchments based on their MAP values. And obviously this resulted in the BFI derived from E10A to E10G being higher than that from the E1R002 station. As another example of gauge station versus quaternary catchment differences, the baseflow separation results from the stream gauge station L8R001 and from the quaternary catchment L82H are plotted with the total stream flow in Fig. 6-10 and Fig. 6-11.

From this analysis of baseflow separation results from both gauge stations and quaternary catchments and their comparison, it can be concluded that the latter is more suitable and reliable for a regional evaluation in that the data from the quaternary catchments have been spatio-temporally averaged and smoothed, and are consequently more representative. The data from the stations are more specific and suitable for site study.

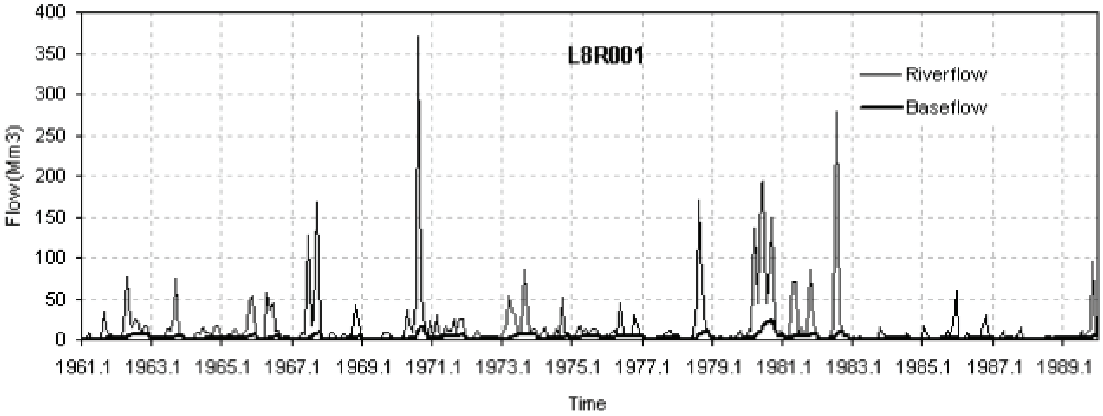


**Fig. 6-10** Baseflow separation result for stream gauge station L8R001

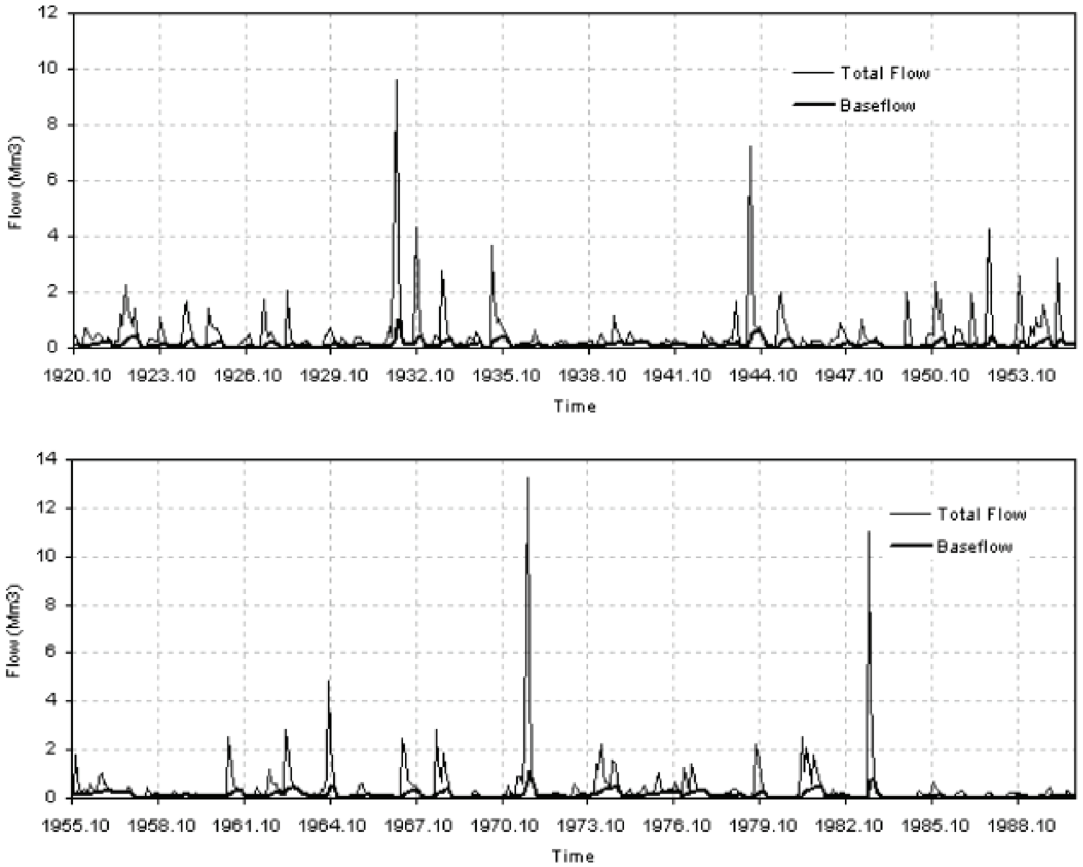


**Fig. 6-11** Baseflow separation result for quaternary catchment L82H

### 6.3.2.3 Baseflow recession

If a long enough history of stream flow data in a catchment is available on a detailed basis, another analysis – baseflow recession – can be performed to estimate groundwater discharge or recharge for the catchment. It can be observed from the stream hydrographs in the previous section, that during dry weather, water stored in the catchment is depleted by groundwater drainage and evapotranspiration. These processes occur at various rates in different times and space, and are therefore difficult to quantify. On a typical stream hydrograph, after a critical time following a precipitation event when overland flow and interflow are no longer contributing to stream flow, the hydrograph of a stream will typically decay exponentially. Discharge during the decay period is composed entirely of groundwater contributions as the stream drains water from the groundwater storage. This discharge during the decay period is termed baseflow recession. For a specific catchment, the baseflow recession is a function of the overall topography, drainage patterns, soils, and geology of the catchment.

Tallaksen (1995) contributed a detailed review on recession analysis traced back to studies of Boussinesq in 1877 and Maillet in 1905. The review summarizes and exemplifies the application of recession analysis in many aspects of water resource planning and management, such as low flow forecasting, mathematical modeling, hydrograph analysis, frequency analysis, indexing the storage capacity of the catchment, and so on. The analytical expression, derivation of the characteristic recession, optimization of parameters and time variability in recessions are also reviewed. Though Tallaksen's review covered a wide area of baseflow recession analysis, its application to the quantification of recharge or dynamic storage of groundwater was not discussed. In this section, the most commonly used baseflow recession expression is presented and applied to one of the quaternary catchments in TMG outcrop area to estimate the recharge quantity.

Theoretically, the slope of baseflow recession is supposed to be constant for a given catchment and independent of the magnitude of precipitation events or peak flow. However in practice this condition can rarely be met because the recession is also influenced by the variability of evapotranspiration. Here we assume that the hydrograph of a stream at the times when all groundwater discharge to the stream is contributed by groundwater will decay following an exponential law. Thus baseflow recession is described by:

$$Q = Q_0 e^{-kt} \tag{6-3}$$

where $Q$ is the flow at some time $t$ after recession has started, $Q_0$ is the flow at the start of baseflow recession, $k$ is the recession constant for the basin, and $t$ is time.

At the beginning of recession $t$=0 and $Q$=$Q_0$, the recession constant $k$ can be expressed as:

$$k = -\left(\frac{1}{t}\right)\ln\left(\frac{Q}{Q_0}\right) \tag{6-4}$$

Where $k$ is a number larger than 0 and less than 1. It will be the large for flat recessions (close to 1), and the small (close to 0) for steep recessions. Usually karstified terrains have flat recessions because much of the drainage occurs in the subsurface, while granitic terrains have steep recessions.

Baseflow recession curve can be used as an effective tool to estimate groundwater recharge, discharge and dynamic storage (Wittenberg, 1999; Peters, 1994). The following procedures are involved:

1) A logarithmic, multi-year baseflow recession curve is used for the analysis. The slope of the recession curve (which should be a straight line) is the recession constant. Then the recession expression becomes:

$$Q = \frac{Q_0}{10^{t/t_1}} \tag{6-5}$$

where $Q_0$ is the discharge at time $t$=0, $t_1$ is the time 1 log cycle later (or the time that takes the baseflow to go from $Q_0$ to 0.1 $Q_0$), and $t$ can be any time during the recession. In the case of $t$=$t_1$, Equation (6-5) becomes:

$$Q = \frac{Q_0}{10} \tag{6-6}$$

2) The total volume of baseflow discharge regarding a recession can be calculated by integrating (5-6) over the times of interest

$$V = \int_{t_0}^{t} Q dt = -\frac{Q_0 t_1 / 2.3}{10^{t/t_1}}\Bigg|_{t_0}^{t} \tag{6-7}$$

Where $t_0$ is the starting time of interest, the other denotations are as above.

3) To calculate total potential baseflow discharge for a complete groundwater recession (for the first year of the selected continuous multi-years, or year 1), let $t_0$ equals zero and $t$ equals infinity, Equation (6-7) can be simplified to

$$V_{tp1} = \frac{Q_0 t_1}{2.3} \tag{6-8}$$

Where $V_{tp1}$ is the total potential groundwater discharge. This volume is defined as the total volume of groundwater that would be discharged during an entire baseflow recession if the depletion could proceed continuously. This is an ideal condition and in physical circumstance the recession is usually interrupted by the next precipitation event before the entire potential groundwater discharge is depleted. This volume can also be regarded as the total volume of water in storage at the beginning of the recession.

4) Calculate the discharge that actually takes place during a baseflow recession.

$$V_t = \frac{V_{tp}}{10^{t/t_1}} \tag{6-9}$$

In this equation the time $t$ represents the duration of the actual entire recession from the start to the end, and the potential discharge is greater than actual discharge.

5) Calculate the remaining potential groundwater discharge at the end of the recession for the first year.

$$V_r = V_{tp1} - V_t \tag{6-10}$$

6) Calculate the potential discharge $V_{tp2}$ for the second year (year 2), and then subtract the actual discharge (year 1) from the potential discharge of year 2. The difference describes the groundwater recharge to the basin between the two recessions.

$$R = V_{tp2} - V_t \tag{6-11}$$

7) The above steps can be done continuously for the selected multiple years to calculate the recharge for each year.

This method has been automated in Excel. Initially it was intended to apply the method to the whole history of stream flow records (monthly baseflow data from 1920 to 1989) for all of the quaternary catchments in TMG outcrop to simulate the recharge for a continuous 70 years period. Unfortunately a considerable time variation in the baseflow recession was found for most of the catchments. According to Tallaksen's review (1995), the variation is not only dependent on physical factors like climate influence, but also on the recession model and calculation procedures selected. In other word, variability may occur by using a fixed recession equation to simulate a wide range of flow records. To minimize the uncertainty of the model, more work is needed to select appropriate recession equations for different periods of flow records based on their characteristics

Climate influence on the recession includes recharge from precipitation or snowmelt and losses from evapotranspiration – these were assumed zero during the recession calculation process. Possible solutions to the problem of the evapotranspiration loss have been investigated (Farvolden, 1963; Tschinkel, 1963; Reigner, 1966 and Weisman, 1977).

Besides the prevailing climate influences, the previous weather conditions before the start of recession and aquifer types can also influence the time variation of the baseflow recession. The spatial variability of storm response in larger catchments may lead to the distribution pattern of flow paths in the catchment, which in turn influences the drainage pattern

(Laurenson, 1961). Also the occurrence of different types of aquifers or the anisotropy of the specific aquifer adds even more to the variability of the recession results.

Considering these factors, several periods in the quaternary catchment G40A (Fig. 6-12) were selected to implement the baseflow recession analysis because the time variation of the recession during these periods is relatively smaller. The monthly baseflow series of several hydro-years, including 1928 to 1930, 1963 to 1966 and 1985 to 1987, were chosen to estimate groundwater recharge.


**Fig. 6-12** The location of quaternary catchment G40A

The quaternary catchment G40A is located near the southeast of Cape Flats, and covers 71.5 km$^2$ in surface area. Its northwest boundary is the Hottentots Holland Mountain. The whole catchment is controlled by a syncline striking E20°N, in which the exposed bedrock, from the centre to the margins comprises the Bokkeveld, Nardouw Subgroup, and Peninsula Formation. The Steenbras River develops along the axis of the syncline.

The baseflow recession calculation for catchment G40A was done as follows:

(1) 1928 to 1931 (Figure 13)

In November 1928, the baseflow discharge reached its highest value and from this month, the baseflow recession started. The average discharge of this month is 0.569 m$^3$/s ($Q_0$), which is averaged from the monthly value. According to the recession chart and calculations, it takes about 2.616 months to decrease to the amount of $Q_0/10$. Therefore the potential baseflow discharge at the start of the recession is:

$$V_{tp(1928.11)} = \frac{Q_0 \cdot t_1}{2.3} = \frac{0.569 \times 2.616 \times 30d \times 24h \times 3600s}{2.3} = 1.68 \times 10^6 m^3$$

After 4 months, in March of 1929, the baseflow discharge reached the minimum value of 0.023 $m^3$/s, the baseflow recession stopped and the recharge started. The actual baseflow discharge during this recession period can be calculated:

$$V_{t\ (1928.11\text{-}1929.3)} = \frac{V_{tp(1928.11)}}{10^{t/t_1}} = \frac{1.6784 \times 10^6}{10^{4/2.616}} = 0.05 \times 10^6 m^3$$

Then the remaining potential baseflow discharge can be calculated:

$$V_{r(1928)} = V_{tp(1928.11)} - V_{t(1928.11-1929.3)} = 1.6784 \times 10^6 - 0.0497 \times 10^6 = 1.63 \times 10^6 m^3$$

The next baseflow recession started from October of 1929, with a potential discharge ($V_{tp(1929.10)}$) of $1.6693 \times 10^6 m^3$. Then the recharge from March of 1929 to October of 1929 is:

$$R_{(1929.3-1929.10)} = V_{tp(1929.10)} - V_{r(1928)} = 1.6784 \times 10^6 - 1.6287 \times 10^6 = 0.04 \times 10^6 m^3$$

The calculations were continued to derive the recharge for the successive years in this period. The results are:

$$R_{(1930.2-1930.11)} = V_{tp(1930.11)} - V_{r(1929)} = 2.0477 \times 10^6 - 1.6199 \times 10^6 = 0.43 \times 10^6 m^3$$

$$R_{(1931.3-1931.11)} = V_{tp(1931.11)} - V_{r(1930)} = 2.8639 \times 10^6 - 1.8747 \times 10^6 = 0.99 \times 10^6 m^3$$

(2) 1963 to 1966 (Figure 14)

$$R_{(1964.3-1964.11)} = V_{tp(1964.11)} - V_{r(1963)} = 2.2898 \times 10^6 - 1.8804 \times 10^6 = 0.41 \times 10^6 m^3$$
$$R_{(1965.1-1965.11)} = V_{tp(1965.1)} - V_{r(1964)} = 2.3418 \times 10^6 - 1.8012 \times 10^6 = 0.54 \times 10^6 m^3$$
$$R_{(1966.2-1966.10)} = V_{tp(1966.10)} - V_{r(1965)} = 2.8502 \times 10^6 - 2.1110 \times 10^6 = 0.74 \times 10^6 m^3$$

(3) 1985 to 1987 (Figure 15)

$$R_{(1985.2-1985.10)} = V_{tp(1985.10)} - V_{r(1984)} = 2.6589 \times 10^6 - 1.9248 \times 10^6 = 0.73 \times 10^6 m^3$$

$$R_{(1986.1-1986.10)} = V_{tp(1986.10)} - V_{r(1985)} = 2.5786 \times 10^6 - 2.4324 \times 10^6 = 0.15 \times 10^6 m^3$$

$$R_{(1987.3-1987.10)} = V_{tp(1987.10)} - V_{r(1986)} = 2.9211 \times 10^6 - 2.5360 \times 10^6 = 0.39 \times 10^6 m^3$$

The results of the above calculations indicate that the recharge values derived from the baseflow recession vary a lot from year to year. This reflects the fact that the groundwater recharge, in the form of difference between potential and actual groundwater discharge, is definitely influenced by climate changes, both over long periods and seasonally. Based on the recession analysis, taking 0.5 $Mm^3$ as an approximately averaged value of groundwater recharge, the annual recharge is calculated to be 7 mm/year for the catchment, which account for 0.7% of the MAP.

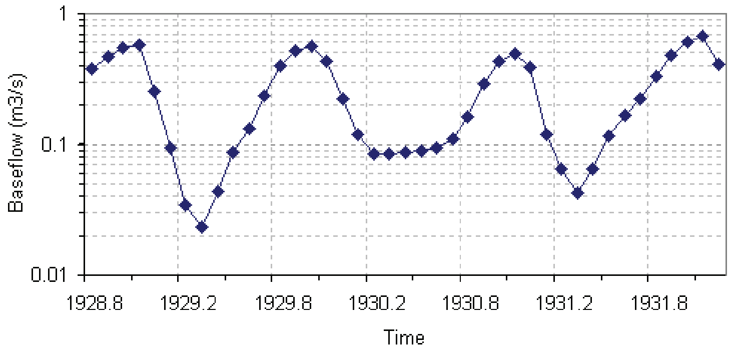


**Fig. 6-13** Baseflow recession for G40A (1928-1931)

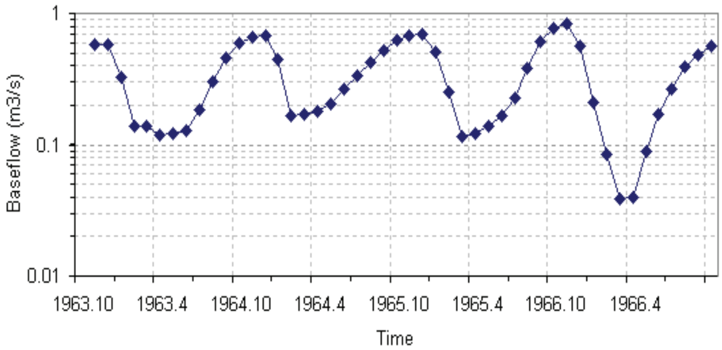


**Fig. 6-14** Baseflow recession for G40A (1963-1966**)**

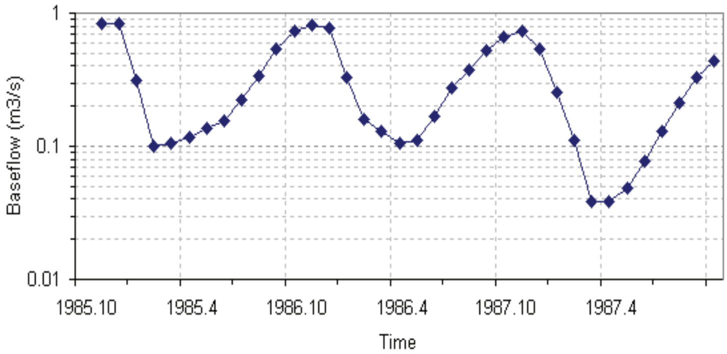


**Fig. 6-15** Baseflow recession for G40A (1985-1987)

The baseflow recession approach for G40A could not be extrapolated to the other TMG-related catchments to estimate groundwater recharge to or discharge from the TMG aquifers.

The baseflow recession of a catchment is dominated by the processes of infiltration, runoff, soil moisture movement and other hydrological processes, all of which have a close relationship with the size, shape, soils, sediment, bedrock, vegetation and topography of the catchment. Even in the G40A catchment, it is difficult to be certain that the derived groundwater recharge and discharge are truly representative of TMG conditions since the stream has hydraulic contact with other aquifers as well. Also, in most cases, surface water catchments don't coincide with the groundwater catchments, although in practice such assumptions are usually made for the convenience of the study.

# 7. Conclusions and Recommendations

## *7.1 Conclusions*

On a regional scale, the TMG Aquifer is both a heterogeneous and anisotropic entity, and a fractured rock aquifer system with unique features regarding its stratigraphy, structure, and geomorphology. It is compartmentalized into various hydrogeological units, bounded by large faults, lithologies, and topographies. Various-scale TMG aquifers are the fortuitous combination of stratigraphic, tectonic, geomorphologic and climatic features. The establishment of hydrogeological units, associated subunits, and the analysis of aquifer types provide a regional view of the aquifer system and boundary conditions in the vast area, which forms the initial conceptual models for the aquifers in a regional scale. Much more commonly encountered problem in the TMG aquifer is how to conceptualize the aquifer media to meet the understanding of many site-specific problems and from which perform a proper analysis and a sound estimation of the aquifer properties. The discussion of the TMG aquifer types raises the necessity of the aquifer media study, especially the study of fractured media which shows prominence in controlling groundwater in the TMG aquifers. Based on the study and subsequent understanding of fracture networks, it is possible to propose the conceptual model both for fault and relatively small-scale fractured media, which has rarely been done for the TMG aquifers.

Based on previous information and present study, estimated results of the aquifers' hydraulic properties fall in a wide range of values which reveal big differences between different sites of an area and in different well bores of a site.

**Aquifer media**

Based on previous studies and current researches, the characterization of the TMG fractured media on regional and local scales has been performed, through the interpretation of existing geological data and remote sensing imagery, the study of core samples, and the analysis of fracture field measurement data, from which an initial conceptual model of fracture network is developed. This model can help to have a better understanding of the TMG fractured rock media and can be applied to the quantification of aquifer properties.

According to the experience of groundwater development in the TMG area, fault structures have attracted much attention in the development of wellfields for water supply. Most of the fault zones developed in the TMG sandstones and siltstones are evidenced to have been recemented and act as aquicludes. Based on the study of fault architecture, a conceptual model of the fault zone is adapted, which stresses that fracture zones at both walls of a fault core may become a particular interest of borehole siting; this suggests that the groundwater occurrence and flow path are dominated by fractures or fracture network.

In the context of hydrogeological setting, it is better to classify fractures in the TMG aquifers into two categories of the open and closed than conventional classes based on the mode of rock deformation. To investigate such types of fractures, a case study on core sample fractures in an 800-m deep borehole at the Rietfontein site is then introduced. Data from field fracture measurement, and fracture core samples and coating scanning are comparatively analyzed, which yield the results in the distribution of orientation, and the variations both fracture density and fracture coating intensity at depth. These results are informative for the characterization of the TMG fracture media; in particular the analysis of fracture coating, which has never been done in the TMG, discloses a mode of hydraulically active fractures at depth.

For the study of a regional problem, remote sensing can be an effective tool, especially when incorporating with GIS technique. For the characterization of fractures on a regional scale, lineaments captured from imagery often provide a crucial clue on the interpretation and analysis of fractured rocks. Using Landsat ETM$^+$ imagery, a quantitative analysis is carried out through the VBA subroutine developed in the software ArcMap to determine the distributions of lineament orientations and lengths in seven domain areas, from which a universal lognormal distribution of lineament length is established. This distribution pattern can be introduced to the smaller-scale fracture systems, especially where difficulty is encountered on the weathered grounds to have sufficient trace-length data to represent the statistic population.

For the site-specific groundwater problems, because the existing data for characterizing fractured rocks of the TMG are very limited, field measurements on fracture elements are carried out over the sandstone outcrops at selected sites. Based on statistic features and distribution pattern of the fracture elements, fractures on both 2D plan and profiles, and in 3D domains are generated using random processes, from which the connectivity is qualitatively examined. These results commonly show that the interconnected fractures collectively exhibit a mode of separated and anisotropic fracture blocks (networks). Such connectivity pattern is thought to be general in the TMG sandstones, especially where the TMG rocks are exposed and not confined by overlaying geological formations. Because the basic data is measured at different structural domain and lithologies, the generated results and subsequent fracture connectivity is accordingly representative. In order to verify the validity of the generated fracture blocks, a case study is briefly carried out in the Boschkloof site, from which some of the field observations of groundwater phenomena can be explained by the models.

**Hydraulic properties**

To characterize storage and flow of groundwater in the TMG aquifers, it is most important to study their hydraulic properties, including porosity and storativity, and transmissivity and hydraulic conductivity. However, uncertainty associated with estimation of these parameters always exists through different approaches.

There are two major ways to determine aquifer storativity, one is through the porosity estimation of rock formation and the other is derived from pumping tests. Laboratory test of rock samples, field measurement of rock blocks, derivation of pumping test data, and the interpretation of geophysical data and remote sensing, yield a wide range of porosity values, from which the scale-dependency of the porosity is revealed and discussed. The conversion of the porosity to aquifer storativity requires a proper estimate of bulk modulus of the rock mass; in this regard, there is still a large amount of work to be done in the field of hydrogeology in South Africa.

In terms of aquifer permeability, most of transmissivity results of the TMG aquifers have been derived from hydraulic tests, especially the pumping tests that have yielded a wide range of the transmissivity values form 9 to 400 $m^2/d$ which leads to draw a brief conclusion that the TMG aquifers are highly anisotropic both in regional and local scales. Furthermore, the applicability of the interpreted results is also discussed through the analysis of four types of familiar drawdown observed in the TMG aquifers. It is observed that both drawdown-based and model-based interpretations of hydraulic tests need to be reconciled with the geological observations, especially in the TMG aquifers where boreholes are mostly sited to be close to hydrogeological boundaries such as fault structure and lithological contacts.

Because the hydraulic conductivity (*K*) of the TMG aquifers is mainly controlled by fractures or fracture network, a new tensor approach is proposed. For the prediction of hydraulic properties of the anisotropic TMG aquifers, fundamental principles of *K* tensor and some problems with their application to groundwater flow are discussed. It is observed that the *K* value tends to be higher than that of hydraulic tests because the data sets measured on surface are often overestimated with respect to the fracture apertures even by means of scientific sampling and statistical methods. It is also pointed out that different types of *K* values derived from *K* tensor approach have different meanings physically, although they are related. For the use of calibration coefficient of roughness $C_{er}$, it is recommended that Lomize's model be used for microscopic fractures and Barton's model for relative macroscopic ones.

The results are compared with those from field tests and in turn the tensor model is calibrated to meet the changes in fracture features and fracture setting conditions, from which a depth model of $K$ is accordingly proposed and comparatively studied with the data from hydraulic tests.

The derivation of negative exponential form of hydraulic aperture is based fundamentally on rock mechanics by considering both fracture roughness and stress conditions. Comparing with the results from hydraulic tests at three sites, it is found that the $K$ values estimated through the tensor model may represent that of a relatively small scale in meters; and this scale is dependent on the size of fractures collectively measured. Using this calibrated model it is possible to calculate the hydraulic conductivity at depth, by assuming that the rock masses in an aquifer are subjected to lithostatic pressure. The computed results show that the reduction of $K$ over depths roughly follows a negative exponential law with different exponents. This is also confirmed by the results of packer tests conducted in the Gevonden site and can be compared with that of Snow (1969). The tensor model provides a scientific tool to simulate the hydraulic conductivity of the TMG aquifers both on the surface and at depth.

Due to the complexity of geometric and hydraulic properties of the TMG aquifers, the study of site-specific groundwater problem is of greatly hydrogeological significance; especially the study regarding aquifer's hydraulic properties.

In order to have a better understanding of the common aquifer type, fault bounded aquifer in the TMG, together with the study of aquifer properties, a site with a five-borehole network was established. Multidisciplinary approaches to the field investigation were employed, including borehole coring and logging, field geophysical survey, field fracture measurement, in-situ identification and examination of groundwater behavior, and hydraulic tests. The results obtained from these methods were comparatively analyzed, from which an initial conceptual model was proposed and presented on a plan view. As more information is gained from the analytical results, it is realized that the groundwater in the fractured aquifer is actually not flowing through a geological continuum. Large variation of the aquifer responses to hydraulic tests shows a great deal of difficulty in determining the aquifer's hydraulic properties represented by the $T$ and $K$. In other word, it is extremely difficult, through hydraulic tests, to give a sound estimate then to tell how much the aquifer's transmissivity or the aquifer's hydraulic conductivity is. This is due to the anisotropic features embedded in the fractured rocks and the scale-dependent aquifer properties in the TMG.

Therefore the hydraulic conductivity tensor method is reused to estimate the anisotropic *K* values. Based on the FDN models, current problem of 2D fracture network is discussed. Because groundwater in the fractured rocks is actually 3D problem, a 3D FDN model is developed, which shows that only 2.4% of bulk fractures at the measurement scale would be actively involved in the groundwater flow system. The *K* value for this site is estimated to be in the order of magnitude of $10^{-8}$ m/s, which is perhaps not the ultimate estimate, but it helps to get the understanding to a 3D reality.

**Groundwater resource estimation**

So far there are only some rough estimates on the groundwater resource of TMG aquifers on a regional basis. An assessment on this resource is very necessary for the realisic utilization and management of it. Based on data and information available, groundwater recharge, storage and discharge of TMG aquifers are quantitatively evaluated. Sustainable yield is discussed according to the groundwater budget.

Groundwater recharge potential is estimated using the soil water balance approach and the calculated result is soil water surplus, which can be regarded as the upper limit of groundwater recharge. The calculated total soil water surplus or the upper limit of recharge volume is about $4.36\times10^9$ $m^3$ per annum, and the mean annual soil water surplus in TMG outcrop area is 115.38 mm. The estimates by Wu (2005) is used as a calibration of the current result in this study.

The isobaths and isopachs are generated for the whole TMG area, which is used for the storage capacity estimation of TMG aquifers. The storativity values are generalized from the various studies, including three scenarios, i.e. low, medium and high. The total groundwater storage capacity is estimated as $3.3\times10^{10}$ $m^3$ with the medium storativity values. By taking into account the current technical feasibility of groundwater exploitation in the TMG aquifers, the usable storage capacity is evaluated with three scenarios presented by the exploitation depth of 250 m 350 m and 500 m, with the amount of the storage capacity estimated at $1.3\times10^9$ $m^3$, $2.1\times10^9$ $m^3$ and $3.4\times10^9$ $m^3$, respectively. Available storage capacity is estimated as $8.06\times10^8$ $m^3$, which stands for the storage capacity of the unsaturated zone.

A sum of $1.29\times10^9$ $m^3$/yr is estimated as the groundwater discharge from TMG aquifers, in which baseflow is separated from the stream flow data, and accounts for the biggest part of TMG groundwater discharge.

According to primary groundwater budget carried out, it is thought that the inflows and outflows are basically balanced out with a possible imprecision. A sustainable yield of no more than $1.0\times10^9$ $m^3$/year (or <35515 l/s) is proposed for the groundwater exploitation of TMG aquifers based on the groundwater budget. The existing exploitation could be expanded accordingly.

As the most common type of groundwater/surface water interaction in TMG area, stream-aquifer interaction is quantitatively analyzed for the TMG-related hydrological catchments. A digital recursive filtering method is adopted to separate the baseflow component from the monthly stream flow data, in which parameters are adjusted according to the hydrogeological characteristics of TMG aquifers. A total of $1.08\times10^9$ $m^3$ /yr is derived as the upper limit of the TMG groundwater discharge via streams considering the occurrence of interflow and the hydrodynamic changes of the interaction of groundwater and surface water. The results are summarized in terms of quaternary catchments for the convenience of study.

The baseflow recession analysis is also carried out on the quaternary catchment G40A. The groundwater recharge and discharge in other catchments could be estimated by this way. Unfortunately because of the relatively high data requirements, this analysis could not be extended to the whole TMG area.

The response of TMG aquifer to pumping in Kammanassie Mountains is studied by groundwater flow modeling. The Kammanassie Mountains has been part of the KKRWSS. Due to the incomplete understanding of the conceptual hydrogeological model and inaccurate water balance calculation, the groundwater off the Kammassie wellfield has been overexploited and pumping schedule has been adjusted 5 times to compensate for the continuous lowering of water level in Vermaaks River catchment. Based on the existing data, including hydrogeological setting, rainfall and river flow, borehole and monitoring and abstraction data, Vermaaks River wellfield is selected to simulate the groundwater flow in Peninsula Aquifer. An inverse model is carried out first to calibrate the essential model parameters such as recharge, hydraulic conductivity, and etc from which an optimized recharge value of 0.26% of MAP is derived from the inverse model. With the consideration of the previous estimates, the groundwater recharge in Vermaaks Window is estimated in the range of 0.2~2% of the MAP, equaling to 1.8 mm to 18 mm. More inverse models should be developed by setting different drawdown levels. The model results imply that the sustainable yield in Vermaaks River wellfield may be as little as 2.0 *l/s*. The model results also indicate that the implementation of higher pumping rate to the Vermaaks River wellfield can cause the lowering of groundwater level. Thus the overabstraction should consider the rest of the aquifer for the recovery of water level in a long-term operation.

The vast distributed and highly fractured nature of TMG has posed a lot of problems to be resolved, like data collection, statistics and analysis. The restrictions to the study may result from data deficiency, spatial variety, and difficulties in data processing, all of which could impede the sensible understanding of the hydrogeological model, and concequently the reasonable assessment of the aquifer.

Most of the work in this study has been done in ArcGIS Desktop system. AutoCAD and Excel are also relied on to conduct part of the figure and data processing. Especially the second development with VBA (Visual Basic for Applications) embedded in these softwares has made a lot of impossibilities of the work into realities. Some genearl approaches, like 3D model construction and the data preprocessing for PMWIN are developed and can be applicable to other analog studies.

3D visualization is very difficult to be accomplished by the normal implementation in ArcGIS. Only the surface of the geological layers could be displayed as the DEM, which is called 2.5D – between 2D and 3D. With some scripts compiled with VBA, the true 3D model of the subsurface can be constructed and visualized to help to understand the conceptual hydrogeological model. This approach can be adapted in other similar studies.

Another integrated approach in the data preprocess is adapted for the groundwater modeling using PMWIN. GIS data are not compatiable with the present edition of PMWIN, which is inconvenient for the modeling since in most cases the spatial data are stored in GIS format. In this study some scripts are developed in ArcGIS, making the model discretization, boundary setting and parameter assignment easily available with the spatial function and then they can be transferred to PMWIN through Excel. This approach successfully links GIS to MODFLOW, makes the groudnwater flow modeling much easier, especially in the procedure of data preprocessing.

## 7.2 Recommendations

Based on this study, a number of areas for future and further research on the TMG aquifers are suggested:

Because of the complexity of geometric and hydraulic properties of the TMG aquifers, and no relevant data to support the large-scale study on the aquifer properties, more research projects focusing on site-specific study need to be encouraged. Data collected for such study may focus on the consideration of problems of scale-dependency and uncertainty of aquifer properties.

In South Africa, lithologic and stratigraphic studies have been completed in great detail. However, for sustainable development and management of groundwater in fractured rock aquifers, tremendous efforts still need to be made in the study of geological structure, fault structure in particular.

For the estimation of aquifer storage, storativity and porosity are two critical parameters. The former can be estimated from many pumping tests conducted in the area, but the uncertainty of the parameter suggests its limited applicability. Using porosity to estimate storativity, the mechanical properties of rock mass should be predetermined. This requires a lot of laboratory and in situ rock mass tests to be done.

So far there is not yet an effective method to perform a sound estimate for the hydraulic properties like T and K of a fractured rock aquifer. This estimation requires a lot of efforts in the characterization and conceptualization of fractured rocks. For this reason, a multidisciplinary approach is suggested for the study of hydraulic properties in a fractured rock aquifer.

Any model-based or drawdown curve-based studies for pumping test data need to add the field observations on groundwater behavior and geological investigation especially the geological structure.

Numerical modeling should be very carefully used in evaluation groundwater problems in the fractured rock aquifers, because it is in most cases very difficult to determine the boundary conditions, the anisotropic feature of the aquifer body, water body (stream, lake, and so on), and structural and lithologic boundaries.

The methodologies used in the groundwater resource evaluation may be improved to be more adaptive to the TMG fractured rock aquifer system, including the definition and classification of groundwater resources, methods of investigations, management of the resource, dynamics of groundwater recharge, storage and discharge, transition between shallow groundwater and deep groundwater, determination of aquifer parameters, and groundwater dependent ecosystem, etc.

Comprehensive groundwater resource evaluation entails various approaches including both quantity and quality aspects, with a specific consideration of flow characteristics in fractured rock aquifers.

The continuous accumulation of basic data and information can always benefit a study. More case studies in TMG area should be conducted with a focus on the spatial distribution of the groundwater resource and flow charateristics. In addition, the groundwater monitoring network should be optimised, in conjunction with surface water monitoring if and where necessary, and focused on the water quantity, quality, water level, abstraction rate and etc.

The study of sustainable yield or sustainable yield is a primary concern for groundwater resource evaluation and development. As the estimation of sustainable yield can be based on the study of recharge, baseflow, numerical model or hydraulic test interpretation etc, it is recommended that these methods be jointly used for the applicable sustainable yield estimates, which are of significance in the scale of wellfield or water supply scheme. On the regional scale, the estimated sustainable yield results should be allocated to each basin for the convenience of water resource planning and management.

# References


Alexander WJR (1995). Floods, Droughts and climate change. S. Afr. Jnl. Science, 91, 403-408.

Alexander WJR, 2002, Climate change – the missing links. In: Science in Africa – Africa's First On-Line Science Magazine, Sept. 2002. Department of Civil and Biosystems Engineering, University of Pretoria, South Africa.

Alley WM, Reilly TE and Franke OL, 2001, Sustainability of Ground-Water Resources, U.S. Geological Survey Circular 1186.

Andersen NJB and Ainslie LC, 1994, Neotectonic reactivation – an Aid to the Location of Ground Water, Afr Geo Rev, 1: 1-10.

Andreoli MAG, Doucoure M, and Van Bever Donker J, 1996, Neotectonics of Southern Africa – a review, Africa Geoscience Review, Vol.3, No.1: 1-16.

Andreoli MAG, Doucoure M, Van Bever Donker J, Faurie JN, and Fouché J, 1995, the Ceres-Prince Edward Fabric (CPEF): an Anomalous Neotectonic Domain in the Southern Sector of the African Plate, in Centennial Geocongress (1995)-Extended Abstract Vol.I (Batton JM and Copperthwaite eds.), ISBN: 0-620-19031-0:434- 437.

Arnold JG and Allen PM, 1999, Automated methods for estimating baseflow and ground water recharge from stream flow records. Journal of the American Water Resources Association, 35(2), 411-424.

ASCE, 1972, Groundwater Management, Manual Engineering Practice 40: 216.

ASCE, 1990, Evapotranspiration and Irrigation Water Requirements (eds: Jensen ME, Burman RD and Allen RG, ASCE Manuals and Reports on Engineering Practice No. 70.

Baghbanan A and  Jing L, 2007, Hydraulic properties of fractured rock masses with correlated fracturelength and aperture, International Journal of Rock Mechanics & Mining Sciences, V44: 704-719.

Bandis SC, Lumsden AC and Barton NR, 1983, Fundamentals of Rock Joint Deformation, International Journal of Rock Mechanics and Mining Science, Geomechanics, 20(6): 249-268.

Barringer J and Lilburne L, 1999, Scale Issues in Developing Regional-Scale Soil Water Balance Surfaces, Proceeding on The 11th Annual Colloquium of the Spatial Information Research Centre, University of Otago, Dunedin, New Zealand

Barton NR, Bandis SC and Bakhtar K, 1985, Strength, Deformation and Conductivity Coupling of Rock Joints, International Journal of Rock Mechanics and Mining Sciences, 22(3): 121-140.

Basu AR, Jacobsen SB, Poreda RJ, Dowling CB and Aggarwal PK, 2001 Science, 293 (5534): 1470-1473.

Bear J and Verruijt A, 1987, Modeling groundwater flow and pollution, D. Reidel Publishing Co.: 140-155.

Bird P, Ben-Avraham Z, Schubert G, Andreoli MAG, and Viola G, 2006, Patterns of stress and strain rate in the southern Africa, Journal of Geophysical Research V.111, B08402, doi: 10.1029/2005JB003882, 2006.

Birtles AB, 1978, Identification and separation of major base flow components from a stream hydrograph. Water Resour. Res. 14 791- 803.

Boughton WC, 1988, Partitioning stream flow by computer. Inst. Eng. Civ. Eng. Trans. CE30 (5) 285-291.

Boulton AJ, 2000, River ecosystem health down under: assessing ecological condition in riverine groundwater zones, Ecosyst. Health (6): 108-118.

Brace WF, 1984, Permeability of crustalline rocks: New in situ measurements. J. Geophys. Res. (89): 4327-4330.

Bradbury KR and Muldoon MA, 1994, Effect of fracture density and anisotropy on delineation of wellhead protection area in fractured-rock aquifers, Applied Hydrogeology, 3/94: 17-23.

Bredenkamp DB, Botha LJ, Van Tonder GJ and Van Rensburg HJ, 1995, Manual on Quantitative Estimation of Groundwater Recharge Aquifer Storativity. Pretoria: Water Research Commission. TT 73/95.

Bressan, M.A. and Anjos C.D., 2003 Techniques of remote sensing applied to the environmental analysis of part of an aquifer located in the São José Dos Campos region SP, Brazil, Environmental Monitoring and Assessment, 84: 99-109.

Broquet CAM, 1992, The sedimentary record of the Cape Supergroup: A review. In: De Wit MJ and Ransome IGD (editors) Inversion Tectonics of the Cape Fold Belt, Karoo and Cretaceous of Southern Africa, Balkema, Rotterdam: 159-183.

Brown SR, 1987, Fluid flow through rock joints: the effects of surface roughness, Journal of Geophysical Research, 92B: 1337-1347

Caine JS, Evans JP and Forster CB, 1996, Fault zone architecture and permeability structure, Geology 24:1025-1028.

California Department of Water Resource, 2003, California's Groundwater – Bulletin 118, Update 2003, pp: 93

Cavrilenko P and GueGuen Y, 1998, Flow in Fractured Media: a Modified Renormalization Method, Water Resource Research, Vol.34: 177-191.

Chapman T, 1999, A comparison of algorithms for stream flow recession and baseflow separation, Hydrological Processes (13): 701-714.

Charles EF, 1988, Determination of fracture aperture Multi-trecer Approach, A Report Submitted to he Department of Petroleum Engineering of Stanford University.

Chevallier, L., 1999, Regional structural geological interpretation and remote sensing Little Karro, WRC Project: K8/324.

Chiang WH, Kinzelbach W (2001) 3D groundwater modeling with PWWIN, Springer, Berlin: 346pp.

Ciriacy-Wantrup SY (1952) Resource Conservation Economics and Policies, Brkeley, California. University of California Press: 28 pp.

Connelly RJ, Abrams LJ and Schultz CB (1989). An Investigation into Rainfall Recharge to Ground Water, Report No. 149/1/89, Water Research Commission, Pretoria.

Cook PG, 2001, A Guide to Regional Ground Water Flow in Fracture Rock Aquifers, CSIRO Land and Water, Glen Osmand, Australia: 115pp.

De Beer, CH, 2002, the Stratigrapgy, Lithology and Structure of the Table Mountain Group, In (Petersen K and Parsons R editors eds.): A Synthesis of the Hydrogeology of the Table Mountain Group- Formation of a Research Strategy, WRC Report No. TT 158/01: 9-18.

Degnan, J.R., Clark, S.F. and Jr., 2002, Fracture-correlated lineaments at Great Bay, Southwestern New Hampshire, USGS open-file report, 02-13, 14pp.

Department of Water Affairs & Forestry (2002) Utilization and availability of water –Profile of water management in Berg, Breede, Gouritz, Olifants/Doring Water Management Areas, DWAF.

Department of Water Affairs and Forestry (1993) A review of the groundwater resource of the Western Cape. Prepared by G. Dyke of Ninham Shand (Pty) Ltd, in association with BKS Inc., as part of the Western Cape System Analysis. DWAF Report No. P G000/00/2591: 71 & appendices.

Dingman SL (1994) Physical Hydrology, Prentice Hall, Inc., Englewood Cliffs, NJ, 1994.

Doherty J, Brebber L, and Whyte P (1994) PEST model-independent parameter estimation: Watermark Computing, Corinda, Australia, 122pp.

Domenico PA and Schwartz FW, 1990, Physical and Chemical Hydrogeology, Jhon Wiley & Sons: pp824.

Dreuzy JR, Davy P, and Bour O, 2000, Percolation parameter and percolation-threshold estimates for three-dimensional random ellipses with widely scattered distributions of eccentricity and size, Physical Review, Vol.62, No.5: 5948-5952.

Drury SA, Peart RJ and Deller ME, 2001, Hydrogeological potential of major fractures in Eritrea, Journal of African Earth Sciences, 32: 163-177.

Dunne KA and Willmott CJ (1996) Global Distribution of Plant-extractable Water Capacity of Soil International Journal of Climatology (16): 841-859

Du Toit AL, 1954, The geology of South Africa (3rd edn.), Oliver and Boyd, London, 611pp.

Eckhardt K (2004) How to Construct Recursive Digital Filters for Baseflow Separation. Accepted for Hydrological Processes.

ESRI, Environmental Systems Research Institute (1996) Topogrid Reference. Within ArcInfo workstation System Documentation.

Evans WR, and Cook PG (2002) What is sustainable yield for Australia's groundwater systems? In: Balancing the Groundwater Budget, International Association of Hydrogeologists' Groundwater Conference, Darwin, May 2002.

Ewer, FK, 1985, Rock Grouting with emphasis on dam sites, Springer-Verlag, PP: 175-188.

Farvolden RN (1963) Geological controls on ground-water storage and base flow. J. Hydrol., 1: 219-249.

Farvolden RN (1964) Geologic controls on groundwater storage and base flow. J. Hydrol. 1 219-250.

Ferris JG, Knowless DB, Brown RH, and Stallman RW, 1962, Theory of Aquifer Tests, US geological Survey, Water Supply Paper No. 1536E: 174pp.

Fisher AC (1981) Resource and Environmental Economics, Cambridge Surveys of Economic Literature, Cambridge, Cambridge University Press.

Fortuin M, Woodford AC, Rosewarne PN, and Low AB, 2004, Identification and prioritization of type areas for detailed research in terms of the regional variability of the groundwater and ecological characteristics of the Table Mountain Group aquifer systems, SA WRC Report, No.1332/1/04: 13-18.

Fouché, K.J., Bate, K.J and Van der Merwe, R., 1992, Plate tectonic setting of the Mesozoic Basins, southern offshore, South Africa: A review. In: M.J. De Wit and I.G.D. Ransome eds, Inversion tectonics of the Cape Fold Belt, Karoo and Cretaceous Basins of Southern Africa.

Fraser CJD, Roulet NT and Laffleur M (2001) Groundwater flow patterns in a large peatland, Journal of Hydrology, 246: 142-154.

Freeze RA (1972a). Role of subsurface flow in generating surface runoff: 1. Upstream source areas. Water Resources. Res., 8, pp. 609-623.

Freeze RA (1972b). Role of subsurface flow in generation surface runoff: 2. Upstream source areas. Water Resources Res., 8, pp. 1272-1283.

Freeze RA and Cherry JA (1979) Groundwater. Prentice Hall Inc., New Jersey, 604pp.

FREND (FLOW REGIMES FROM EXPERIMENTAL AND NETWORK DATA) (1989) I: Hydrological Studies. II: Hydrological Data. Wallingford, UK.

Friese AEW, 2007, Neotectonics of southern Africa: nature, origin and consequence, in Andreoli MAG and Cichowicz A eds., Neotectonics and Mining Seismology- is a Relationship Possible. Seismology Workshop on 8th May 2007, Council for Geoscience, Pretoria: 11-14.

Goodman RE, 1974, the Mechanical Properties of Joints, Proc 3rd Int. Congr., Int. Soc. Rock Mechanics, Vol.I:127-140.

Gutman G and Rukhovetz L, Towards Satellite-Derived Global Estimation of Monthly Evapotranspiration Over Land Surfaces, Adv. Space Res. (18): 67-71.

Haan CT (1972) A water yield model for small watersheds. Water Resources Research 8(1): 58-69.

Hälbich IW and Cornell DH, 1983, Metamorphic history of the Cape Fold Belt, in: Sohnge APG and Hälbich IW (eds), Geodynamics of the Cape Fold Belt, Spec. Publ. geol. Soc. S. Afr., 12: 131-148.

Hälbich IW, 1983, A tectogenesis of the Cape Fold Belt, in: Sohnge APG and Hälbich IW (eds), Geodynamics of the Cape Fold Belt, Spec. Publ. geol. Soc. S. Afr., 12: 165-175.

Hälbich IW and Greef GJ, 1995, Final report on a structural analysis of the west plunge nose of the Kammanassie anticline, Technical report to SA DWAF.

Halford KJ and Mayer GC (2000) Problems associated with estimating groundwater discharge and recharge from stream-discharge records. Ground Water 38 (3).

Halihan T, Love A, and Sharp J M, 2005, Identifying Connections in a Fractured Rock Aquifer Using ADFTs, GROUND WATER, Vol.43, No.3: 327-335.

Harbaugh AW, McDonald MG (1996) User's documentation for Modflow-96, an update to the US Geological Survey modular finite-difference groundwater flow model. Open-File Report 96-845, US Geological Survey: 56pp.

Hartnady CJH and Hay ER (2001) Use of structural geology and remote sensing during the hydrogeological exploration of the Olifants and Doring river catchments. Kevin Pietersen and Roger Parsons (Editors) (2002) A synthesis of the Hydrogeology of the Table Mountain Group-Formation of a Research Strategy, WRC Report NO. TT 158/01, January 2002, (IBSN 1 86845 804 0), Water Research Commission.

Hartnady CJH and Hay ER (2002) Deep Artesian Groundwater Exploration in the Greater Oudtshoorn District for Bulk Water Supply (DAGEOS). "Groundwater Divison, western Cape Conference: Tales of a hidden treasure; Somerset West, 16 Sept. 2002. 53-58.

Hartnady CJH and Hay ER (2002) Potential of Table Mountain Group Aquifers and integration into catchment water management, In: A Synthesis of the Hydrogeology of the Table Mountain Group- Formation of a Research Strategy (Pertersen K and Parsons R editors), WRC Report, No.TT 158/01: 242-248.

Hartnady CJH and Hay ER, 2000, Reconnaissance Investigation into the Development and Utilisation of Table Mountain Group Artesian Groundwater, Using the E10 Catchment as a Pilot Study Area. Final Report to Department of Water Affairs and Forestry by Umvoto Africa/SRK Consulting Joint Venture.

Hartnady CH and Hay ER, 2002a, Fracture system and attribute studies in Table Mountain Group groundwater target generation, A Synthesis of the Hydrogeology of the Table Mountain Group-Formation of a Research Strategy, WRC Report No. TT 158/01, Pretoria: 89-94.

Hartnady CH and Hay ER, 2002b, Boschkloof Groundwater Discovery, *In* (*Petersen K and Parsons R eds.*): *A Synthesis of the hydrogeology of the TMG Formation of a research strategy*, WRC Report No. TT 158/01: 168-177.

Hartnady CH and Hay ER, 2002c, Experimental deep drilling At Blikhuuis, Oloifant River Valley, Western Cape: Motivation, Setting and current progress, WRC Report No. TT 158/01, Pretoria: 192-197.

Heilweil VM and Hsieh PA, 2006, Determining Anisotropic Transmissivity Using a Simplified Papadopulos Method, Ground Water, V.44, No.5:749 -753.

Hill RS, 1988, Quaternary Faulting in the South-eastern Cape Province, Southern Africa Journal of Geology, 91(3): 399-403

Horne R, 1995, Modern well test analysis, 2nd edn. Petroway, Inc., Palo Alto.Hughes DA and Munster F (1999) Hydrological Information and Techniques to Support the Determination of Water Quantity Component of the Ecological Reserve for Rivers. WRC Report No 867/3/99.

Hsieh PA and Neuman SP, 1985, Field Determination of the 3-Dimension Hydraulic Conductivity Tensor of Anisotropic Media, 1, Theory, Water Resources Research, 21(11): 1655-1665.

Hsieh P, 2000, A Brief Survey of Hydraulic Tests in Fractured Rocks, *in* (*Faybishenko B, Witherspoon PA, and Benson SM eds*): *Dynamics of Fluids in Fractured Rock*, AGU, Washington DC: 59-72.

Hughes DA, Hannart P and Watkins D (2003) Continuous baseflow separation from time series of daily and monthly stream flow data. Water SA 29 (1) 43-48.

Issar AS, 1995, On the regional hydrogeology of South Africa. Unpublished Report No. 3 to Directorate Geohydrology, DWAF: 39.

Jaeger C, 1979, Rock Mechanics and Engineering, Cambridge University Press: 161-178.

Jia H, 2007, Groundwater Resource Evaluation in Table Mountain Group Aquifer Systems, PhD thesis, University of the Western Cape: 75-79.

Johnson MR (1991) Sandstone petrography, provenance and plate tectonic setting in Gondwana context of the Cape-Karoo Basin, S. Afr. J. Geol., 94:137-154.

Jolly JL (2002) Sustainable use of Table Mountain Group Aquifers and problems related to scheme failure, In: A Synthesis of the Hydrogeology of the Table Mountain Group-Formation of a Research Strategy (Pertersen K and Parsons R editors), WRC Report, No.TT 158/01: 108-111.

Jones JA, Mulholland PJ (2000) Streams and Groundwater, Academic Press, San Diego, CA

Karasaki K, Freifeld B., Cohen A., Grossenbacherb K., Cook P., Vasco D., 2000, A multidisciplinary fractured rock characterization study at Raymond field site, Raymond, CA, Journal of Hydrology, V236 (2000): 17-34.

Knezek M and Krasny J (1990) Natural groundwater resources mapping in mountainous areas of the Bohemian Massif (Czechoslovakia), Mem 22nd. I.A.H. Congr. Lausanne

Kok TS (1992) Recharge of springs in South Africa. GH Report 3748. DWAF.

Koch, M. and Mather, P.M., 1997, Lineament mapping for groundwater resource assessment: a comparison of digital synthetic aperture (SAR) imagery and stereoscopic large format camera (LFC) photographs in the Red Sea Hills, Sudan, International Journal of Remote Sensing, 18: 1465-1482.

Kotze JC (2002a) Hydrogeology of the Table Mountain Sandstone aquifer – Klein Karoo. Unpub. PhD Thesis.

Kotze JC, 2002b, Towards a management tool for groundwater exploitation in the Table Mountain sandstone fractured aquifer, WRC report No.: 729/1/02.

Kotze JC (2000) Modeling of Groundwater Flow in the Table Mountain Sandston Fractured Aquifer in the Little Karoo Region of South Africa. WRC Project No K5/729.

Kresic, N., 1995, Remote sensing of tectonic fabric controlling groundwater flow in Dinaric Karst, Remote Sensing and Environment, 53: 85-90.

Kulatilake PHSW and Panda B.B., 2000, Effect of rock block and joint geometry on jointed rock hydraulics and REV, ASCE J. Engrg. Mech., 126(8): 850-858.

Kulatilake P, Jeong-gi Um, Wang M, Escandon R and Narvaiz, J, 2003, Stochastic fracture geometry modeling in 3-D including validations for a part of Arrowhead East Tunnel, California, USA, Engineering Geology, V.70 (2003): 131-155.

Kulatilake PHSW and Panda BB, 2000, Effect of Rock Block and Joint Geometry on Jointed Rock Hydraulics and REV, ASCE J. Engrg. Mech., 126(8): 850-858.

Lamb R and Beven K (1997) Using interactive recession curve analysis to specify a general catchment storage model, Hydrology and Earth System Sciences (1): 101-113.

Laurenson BE (1961) A study of hydrograph recession curves of an experimental catchment, J. Inst. Eng. Aust., 33: 253-258.

Lee CH (1915) Determination of safe yield of underground reservoirs of the closed basin type. Trans Am Soc Civil Engineers (78):148-151

Lerner DN (2005) Surface Water – Groundwater Interactions in the Context of Groundwater Resources. Yongxin Xu and Hans E. Beekman (Editors). Groundwater Recharge Estimation in Southern African. IBSN 92-9220-000-3: 90-107

Levin M, 2000, the Radon Emanation Technique as a Tool in Ground Water Exploration, Borehole Water J, 46: 22-26.

Lin L and Xu Y, 2006, A tensor approach to the estimation of hydraulic conductivities in Table Mountain Group aquifers of South Africa, Water SA, Vol.32, No. 3: 371-378.

Lin L, Jia H, & Xu Y, 2007, Fracture network characteristics of a deep borehole in the Table Mountain Group (TMG), South Africa, Hydrogeology Journal, Vol.15, No7: 1231-1437.

Linsley RK, Kohler MA and Paulhus JLH (1958) Hydrology for Engineers. New York, McGraw-Hill.

Lowe PD and Goyder J (1983) Environmental Groups in Politics, Resource management series (6). London, Allen & Unwin.

Lomize GM, 1951, Filtrasia v treshinovatykh porodakh (flow in fractured rocks), Gosudastvennoe Energetitcheskoe Izdatelstvo, Moskva-Leningrad.

Louis C, 1974, Introduction to Rock Hydraulic, Bureau Researches Géologiques et minières, Orleans France: III (4): 283-356.

Lyne VD and Hollick M (1979) Stochastic Time-variable Rainfall-Runoff Modeling. Hydro. And Water Resour. Symp. Institution of Engineers Australia, Perth. Pp. 89-92.

Mabee, S.B., Hardcastle, K.C., Wise, D.W., 1994, A method of collecting and analyzing lineaments for regional-scale fractured bedrock aquifer studies, Ground Water, 32: 884-894.

Maclear LGA (1996) The geohydrology of the Swartkops River basin – Uitenhage Region, Eastern Cape. Unpublished MSc dissertation. University of Cape Town, Cape Town.

Manual (1983) Manual on water supplying hydrogeology – Volume 3: Groundwater resource evaluation, Geology Press of China: 695pp.

Marmonier P, (2000) Subterranean Ecosystems, Wilkens H, Culver DC, Humphreys WF (Eds), Ecosystems of the World (30), Elsevier, Amsterdam: 513-531.

Mayer GC and Jones LE (1996) SWGW – A Computer Program for Estimating Groundwater Discharge to a Stream Using Stream flow Data. USGS WRI 96-1071.

Maclear LGA, 2001, The hydrogeology of the Uitenhage Artesian Basin with reference to the Table Mountain Group Aquifer, Water SA, Vol. 27 No. 4: 499-505.

Margolin G, Berkowitz B, and Scher H, 1998, Structure, Flow, and Generalized Conductivity Scaling in Fracture Networks, Water Resour Res, 34:2103-2121.

McCarthy T and Rubidge B, 2005, the Story of Earth and Life, a South African Perspective on a 4.6-billion-year Journey, New Holland Publishing (South Africa): 184-211.

McCuen RH (2004) Hydrologic Analysis and Design, 3rd ed., Prentice Hall, Upper Saddle River, New Jersey, 07458.

Meinzer OE (1923, The occurrence of groundwater in the United States with discussion of principles. US Geological Survey Water Supply Papers, v(489)

Meyer PS, 1998, 1999, 2001, An explanation of the 1:500 000 general hydrogeological map of Cape Town 3317, Port Elizabeth 3324, Oudtshoorn 3320, Department of Water Affairs and Forestry.

Meyer R (2005) Analysis of Groundwater level time series and the relation to rainfall and recharge WRC Report, No.1323/1/05.

Meyer PS, 2002, Springs in the Table Mountain Group, with Special Reference to Fault Controlled Springs, In (Petersen K and Parsons R eds.): A Synthesis of the hydrogeology of the TMG Formation of a research strategy, WRC Report No. TT 158/01: 224-229.

Midgley DC, Pitman WV and Middleton BJ (1994) Surface Water Resources of South Africa 1990, Volumes I to VI. WRC Reports, No. 298/1.1/94 to 298/6.1/94.

Min KB, Jing L and Stephansson, 2004, Determining the equivalent permeability tensor for fractured rock masses using a stochastic REV approach: Method and application to the field data from Sellafield, UK, Hydrogeology Journal, 12:497-510.

Mintz Y and Walker GK (1993) Global Fields of Soil Moisture and Land Surface Evapotranspiration Derived from Observed Precipitation and Surface Air Temperature J. Applied. Meteor. (32): 1305-1334.

Moore, WS (1999) The subterranean estuary: a reaction zone of ground water and seawater, Mar. Chem. 65:111-125.

Mortimer RJG, Krom MD, Boyle DR and Nishri A (1999) Use of a high-resolution pore-water gel profiler to measure groundwater fluxes at an underwater saline seepage site in Lake Kinneret, Israel, Limnology and Oceanography, 44 (7): 1802-1809.

Mourzenko VV, Thovert J-F, and Adler PM, 1998, Percolation and conductivity of self-affine fractures, Physical Review, Vol.59, No.4: 4266 -4284.

Mulhall MJ and Demicco PM (2004) Evaluation of groundwater resources of the Sourland Mountain region of the central New jersey, Technical Report for Sourland Smart Growth Project: 90pp.

Murray EC, 1996, Guidelines for Assessing Borehold Yields in Secondary Aquifers, Unpublished M.Sc.Thesis, Univ. of Rhodes, Grahamstown.

Nakhwa RA and Xu Y (2005) Evaluation of water supplies from the Table Mountain Group Aquifer – a brief overview. Biennial Groundwater Conference, Pretoria.

Nathan RJ and Mcmahon TA (1990a) Estimating low flow characteristics in ungauged catchments. Water Res. Manage. 6: 85-100.

Nathan RJ and Mcmahon TA (1990b) Evaluation of automated techniques for base flow and recession analyses. Water Resour. 26: 1465-1473.

National Research Council, 1996, Rock fractures and fluid flow: contemporary understanding and applications, National Academy Press, Washington DC: 29-35.

NGDB, National Groundwater Database (2005) Department of Water Affairs and Forestry, Pretoria, computer database.

Nestev M, Savard MM, Lapcevic P, Lefebvre R, and Martel R, 2004, Hydraulic Properties and Scale Effects Investigation in Regional Rock Aquifers, South-Western Quebec, Canada, Hydrogeology Journal, 12:257-269.

Newton AR, Shone RW, and Booth PWK, 2006, the Cape Fold Belt, (in Johnson MR, Anhaeusser CR and Thomas RJ eds.) the Geology of South Africa, the Geological Society of South Africa, Pretoria: 521-530.

Odling NE, 1997, Scaling and connectivity of joint systems in sandstones from western Norway, Journal of Structural Geology, Vol.19, No.10: 1257-1271.

O'Leary, D.W., Friedman, J.D. and Pohn, H.A., 1976, Lineament, linear, lineation: some proposed new word standards for old terms, Geological Society of American Bulletin, 87: 1463-1469.

Olsson R and Barton NR, 2001, An Improved Model for Hydraulic Coupling During Shearing of rock Joints, International Journal of Rock Mechanics & Mining Science, 38(2000): 317-329.

Paces JB, Newmark LA, Marshall BD, Whelan JF, and Peterman ZE, 1996, Ages and origins of subsurface secondary minerals in the Exploratory Studies Facility, Milestone Rep. 3GQH450M, USGS, Denver, 1996.

Park BY, Kim KS, Kwon S, Kim C, Bae DS, Hartley LJ, and Lee HK, 2002, Determination of the hydraulic conductivity components using a three-dimensional fracture network model in volcanic rock, Engineering Geology, 66 (2002): 127-141.

Parsons R (2002) Recharge of Table Mountain Group aquifer systems. IN: A synthesis of the Hydrogeology of the Table Mountain Group-Formation of a Research Strategy: 97-102.

Partridge TC and Maud RR, 1987, Geomorphic evolution of Southern Africa since the Mesozoic, South African Journal of Geology, V.90:179-208.

Patir C and Cheng HS, 1978, An Average Flow Model fro Determining Effects of Three-dimension Roughness on Hydrodynamic Lubrication, ASME J Lobr Techno, 100(1): 12~17.

Patterson RA (2002) Evapotranspiration Bed Designs for Inland Areas. Environment & Health Protection Guidelines. Technical Sheet Reference No. 05/15. March 2002.

Petersen K and Parsons R, 2002, A Synthesis of the Hydrogeology of the Table Mountain Group- Formation of a Research Strategy, WRC Report No. TT 158/01.

Peters NE (1994) Hydrologic Processes. In: Biogeochemistry of Small Catchments-A Tool for Environmental Research (eds: MoldanB and Cerny J). Prepared by Scientific Committee on Problems of the Environment (SCOPE). Published by John Wiley & Sons Ltd, ISBN 0-471-93723-1: 207-228

Pollard DD and Aydin A, 1988, Progress in understanding jointing over the past one hundred years, Geological Society of America Bulletin, 100, 1181-1204.

Pyray-Nolte LJ, Montemango CD, and Notle DD, 1997, Volumetric Imaging of Aperture Distribution in Connected Fracture Networks, Geophysical Research Letter, Vol.24,No.18: 2343-2346.

Ransome IGD and de Wit MJ, 1992, Preliminary Investigation into a Microplate Model for the South Western Cape, in de Wit MJ and Ransome IGD eds: Inversion Tectonics of the Cape Fold Belt, Karoo, and Cretaceous Basins of Southern Africa, Balkema, Royyerdam, Holland: 257- 266.

Reed SM, Maidment DR and Patoux J (1997) Spatial Water Balance of Texas, CRWR Online Report 97-1.

Rees J (1985) Natural Resources: Allocation, Economics, and Policy, Methuen & Co Ltd, New York (ISBN:0416320007): 449 pp.

Renard P,  2005, The future of hydraulic tests, Hydrogeology Journal,  3:259-262.

Reigner IC (1966) A method of estimating stream flow loss by evapotranspiration from the riparian zone. For. Sci., 12(2): 130-139.

Rodell, M. and Famiglietti, J.S., 2002, The potential for satellite-based monitoring of groundwater storage changes using GRACE: the High Land Plains aquifer, Central US, Journal of Hydrology, 263: 245-256.

Rorabaugh MI (1964) Estimating Changes in Bank Storage and Groundwater Contribution to Stream flow. Int. Assoc. of Sci. Hydrol. Publication 63 432-441.

Rosenberry DO, Striegl RG, Hudson DL (2000) Plants as indicators of focused ground water, Ground Water (38): 296-303.

Roswarne PN, 1990, Groundwater Resource Evaluation at St Francis Bay: Project Review, SRK Report No. 171719/5: 35pp.

Rosewarne P (2002a) Hydrogeological characteristics of the Table Mountain Group aquifers, In: A Synthesis of the Hydrogeology of the Table Mountain Group- Formation of a Research Strategy (Pertersen K and Parsons R editors), WRC Report, No.TT 158/01: 33-44.

Rosewarne P (2002b) Potential of Table Mountain Group Aquifers and integration into catchment water management, In: A Synthesis of the Hydrogeology of the Table Mountain Group- Formation of a Research Strategy (Pertersen K and Parsons R editors), WRC Report, No.TT 158/01: 241-242.

Rosewarne P (2004) Table Mountain Group Aquifer wellfield development-an overview. SRK Report (occasional report).

Rosewarne PN, 1993a, St Francis bay Groundwater Monitoring Final Report, SRK Report No.171719/M6.

Rosewarne PN, 1993b,Ceres Groundwater Investigation Phase 2: Borehole Sitin, SRK Report No.197759/1.

Rust, IC, 1967. On the sedimentation of the Table Mountain Group in the Western Cape Province: D.Sc. thesis, Geology Department, University of Stellenbosch (unpublished), 110 pp.

Rust, IC, 1973. The evolution of the Palaeozoic Cape basin, southern margin of Africa in The Ocean Basins and Margins, Volume 1. The South Atlantic (A.E.M. Nairn and F.G. Stehli, eds.), Plenum, New York: 247-276.

Rutledge AT (1993) Computer programs for describing the recession of ground-water discharge and for estimating mean ground-water recharge and discharge from stream flow records. Ground Water 32 (2) 180-189.

Rutqvist J and Stephansson O, 2003, the Role of Hydromechanical Coupling in Fracture Rock Enginnering, Hydrogeology Journal, 11(2003): 7-40.

Sander, P., Cheskey, M.M. and Minor, T.B., 1996, Groundwater assessment using remote sensing and GIS in a rural groundwater project in Ghana: lesson learned, Hydrogeology Journal, 4(3): 40-49.

Sander, P., Minor, T.B. and Chesley, M.M., 1997, Groundwater exploration based on lineament analysis and reproducibility tests, Ground Water, 35: 888-894.

Schowengerdt, R., Babock, EM, Ehtridge, L. and Glass, CE, 1979, Correlation of geologic structure inferred from computer enhanced Landsat imagery with underground water supplies in Arizana, Satellite Hydrology AWRA: 387-397.

Serzu MH, Kozak ET, Lodha GS, Everitt RA, Woodcock DR (2004) Use of borehole radar techniques to characterize fractured granitic bedrock at AECL's Underground Research Laboratory, Journal of Applied Geophysics, 55 (2004): 137-150.

Sharp JM, Banner JL (2000) The Earth Around Us: Maintaining a Livable Planet, Schneiderman JL (Ed), Freeman, New York: 154-165.

Shapiro AM, Hsieh PA, Burton WC, and Walsh GJ, 2007, Integrated Multi-Scale Characterization of Ground-Water Flow and Chemical Transport in Fractured Crystalline Rock at the Mirror Lake Site, New Hampshire, in Subsurface Hydrology: data Integration for Properties and Processes, Geophysical Monograph Series 171: 201-225.

Shuttleworth JW (1993) Evaporation, in Handbook of Hydrology, Maidment DR (Editor), McGraw-Hill Inc.

Sittner WT, Schauss CE and Monro JC (1969) Continuous hydrograph synthesis with an API-type hydrologic model. Water Resour. Res. 5 1007-1022.

Smakhtin VU (2001) Estimating continuous monthly baseflow time series and their possible applications in the context of the ecological reserve. Water SA 27 (2) 213-217.

Smakhtin VU and Hughes DA (1993) The application of automated procedures for low-flow analysis of South African rivers. Proc. of the 6th S. Afr. Natl. Hydrol. Symp. Pietermaritzburg, South Africa. Vol 1 329-336.

Smart MC and Tredoux G, 2002, Groundwater quality and fitness for use, A Synthesis of the Hydrogeology of the Table Mountain Group-Formation of a Research Strategy, WRC Report No. TT 158/01, Pretoria: 118-123.

Snow DT, 1968, Hydraulic characteristics of fractured metamorphic rocks of the Front Range and implications to the Rocky Mountain Arsenal well, Colorado School of Mines Quarterly, v. 63, no.1.

Snow DT, 1969, Anisotropic Permeability of fractured media, Water Resource research, 5(6): 1273-1298.

Sloto RA and Crouse MY (1996) HYSEP: A Computer Program for Stream flow Hydrograph Separation and Analysis. U.S. Geological Survey Water-Resources Investigations Report 96-4040. 46 pp.

Sophocleous M and Devlin JF (2004). Discussion on The water budget myth revisited: Why hydrogeologists model. Ground Water 40, no. 4: 340-345. Ground Water 42(4): 618-618.

Stone AW and Lindley SAJ (1994), Wetlands and groundwater in the United States, American Ground Water Trust, Dublin.

Tallaksen L (1995) A review of baseflow recession analysis, Journal of Hydrology (165): 349-370.Talobre J, 1957, Rock Mechanics, Paris.

Thamn AG (1993) Lithostratigraphy of the Piekenierskloof Formation (Table Mountain Group), South Africa Committee for Stratigraphy, Lithostratigraphy series, 27:8pp.

Tian K, 1988, An almost developed Technique of karst collapse prevention during mine drainage, Proceedings of the IAH 21st Congress, Vol.21, Part 2.

Thompson ME and Brown SR, 1991, The effect of anisotropic surface roughness on flow and transport in fractures, Journal of Geophysical Research, 96B: 21923-21932.

Titus R, Adams S and Xu Y, 2002, The Sandveld Core, Report prepared for the Department of Water Affairs and Forestry: Directorate Geohydrology, South Africa.

Todd DK (1980) Groundwater Hydrology, Second Edition, John Wiley and Sons, New York: 353-376.

Tschinkel HM (1963) Short-term fluctuation in stream flow as related to evaporation and transpiration. J. Geophys. Res., 68(24): 6459-6469.

Umvoto, 2003, Task 1 Report – Hydrogeological Reconnaissance for Table Mountain Group Aquifer Feasibility study and Pilot Project, Report to City of Cape Town: 121pp.

United States Geological Survey, (1998), Ground Water and Surface Water A Single Resource, US Geological Survey Circular 1139.

Van Tonder G, Bardenhagen I, Riemann K, Bosch KRJ, Dznanga P, and Xu Y, 2002, Manual on Pumping Test Analysis in Fractured-rock Aquifers, WRC Report No. 1116/1/02: 12-27.

Van Tonder GJ, Botha JF and Van Bosch J, 2001, A Generalized Solution for Step-drawdown Tests Including Flow Dimension and Elasticity, Water SA, Vol. 27 No. 3: 345-354.

Van Tonder G and Xu Y (1999) The Flow-Characteristic method of analyzing pumping-tests. Pump Test workshop held February 1999, CSIR, Stellenbosch.

Vegter JR, 2001, Groundwater development in South Africa and an Introduction to the Hydrogeology of Groundwater Regions, SA WRC Report, No.TT 134/00: 60-70.

Vegter JR (1995a) An Explanation of a Set of National Groundwater Maps. WRC Report TT74/95, Water Research Commission, Pretoria.

Vegter JR (1995b) Groundwater resources of South Africa. An explanation of a set of National Groundwater maps. WRC Report No. TT 74/95. Water Research Commission, Pretoria.

Velde B, 1984, Electron microprobe analysis for clay minerals, Clay minerals, 19(1984): 243-247.

Vogel RM and Kroll CN (1996) Estimation of Baseflow Recession Constants, Water Resources Management (10): 303-320.

Wang HF and Anderson MP (1982) Introduction to Groundwater Modeling, Finite Difference and Finite Element Methods, W.H. Freeman and Company: 237pp.

Wang M, Kulatilake PHSW, Um J and Narvaiz J, 2002, Estimation of REV size and three-dimensional hydraulic conductivity tensor for a fractured rock mass through a single well packer test and discrete fracture fluid flow modelling, International Journal of Rock Mechanics & Mining Sciences, 39 (2002): 887-904.

Waters, P.G., Smart, P.L. and Osmaston, H., 1990, Application of remote sensing to groundwater hydrology, Remote Sensing Review, 4: 223-264.

Weaver JMC (2000) Deep flowing groundwater in the Table Mountain Group Quartzite, Groudwater: past achievements and future challenges. Proc. XXX IAH Congress, Cape Town.

Weaver JMC (2002) Potential of Table Mountain Group Aquifers and integration into catchment water management, In: A Synthesis of the Hydrogeology of the Table

Mountain Group- Formation of a Research Strategy (Pertersen K and Parsons R editors), WRC Report, No.TT 158/01: 249-255.

Weaver JMC and Talma AS (1999a) Field Studies of Chlorofluorocarbons (CFCs) as Groundwater Dating Tool in Fractured Rock Aquifers. Report 731/1/99 Water Research Commission.

Weaver JMC, Talma AS and Cavé LC (1999b) Geochemistry and Isotopes for Resource Evaluation in the Fractured Rock Aquifers of the Table Mountain Group. WRC Report 481/1/99, Water Research Commission, Pretoria.

Weaver JMC, Rosewarne P, Hartnady CJH and Hay ER, 2002, Potential of Table Mountain Group Aquifers and integration into catchment water management, *In* (Petersen K and Parsons R *eds*.): *A Synthesis of the Hydrogeology of the Table Mountain Group- Formation of a Research Strategy*, WRC Report, No.TT 158/01: 242-248.

Weisman RN (1977) The effect of evapotranspiration on stream flow recession. Hydrol. Sci. Bull.; XXII(3-9): 371-377.

Witherspoon PA, 2000, Investigations at Berkeley on Fracture Flow in Rocks: From the Parallel Model to Chaotic Systems, *in* (*Faybishenko B, Witherspoon PA, and Benson SM eds*): *Dynamics of Fluids in Fractured Rock*, AGU, Washington DC: 1-58.

Winter TC, Harvey JW, Franke OL and Alley WM (1998), Ground Water and Surface Water A Single Resource, US Geological Survey Circular 1139.

Witherspoon PA, Wang JCY, Iway K, and Gale JE, 1980, Validity of the cubic law for fluid flow in a deformable rock fracture. Water Resources Research, 16-6: 1016-1024.

Wittenberg H (1999a) Baseflow recession and recharge as nonlinear storage process, Hydrological Processes (13): 715-726.

Wittenberg H and Sivapalan M (1999b). Watershed groundwater balance estimation using streamflow recession analysis and baseflow separation. J. Hydrology, 219(1-2): 20-33.

WMO (1997) Comprehensive Assessment of the Freshwater Resources of the World, ISBN: 91 88714 45 4. World Meteorological Organization, Geneva, Switzerland.

Woodford AC, 2002, Interpretation and Applicability of Pumping-tests in the Table Mountain Group Aquifers, *In* (Petersen K and Parsons R *eds*.): *A Synthesis of the Hydrogeology of the Table Mountain Group- Formation of a Research Strategy*, WRC Report, No.TT 158/01: 71-84.

Woodford AC and Chevallier L, 2002, Regional characterization and mapping of Karoo fractured aquifer systems – an integration approach using geographical system and digital image processing, SA WRC technical report, No. 653/1/02: 40-55.

Wu Y, 2005, Groundwater Recharge estimation in Table Mountain Group Aquifer Systems with a Case Study of Kammanassie Area.PhD Thesis, University of the Western Cape: 52-61.

Wu Y, Wang W, Xu Y, Liu H, Zhou X, Wang L and Titus R, 2003, Radon concentration: A tool for assessing the fracture network at Guanyinyan study area, China, Water SA, Vol.29 No.1: 49-53.

Xu Y, Wu Y, and Duah A, 2007, Groundwater Recharge Estimation of Table Mountain Group Aquifer Systems with Case Study, WRC Report No. 1329/1/07: 9-19.

Xu Y and Beekman HE (2003). A Box model for estimating recharge-The RIB Method. Yongxin Xu and Hans E. Beekman (Editors). Groundwater Recharge Estimation in Southern African. IBSN 92-9220-000-3: 83-88.

Xu Y, Titus R, Holness SD, Zhang J and Van Tonder GJ (2002): A hydrogeomorphological approach to quantification of groundwater discharge to streams in South Africa. Water SA 28(4): 375-380.

Xu Y, Wu Y and Titus R (2002) Influence of the Vermaaks Wellfield Abstraction on Groundwater Levels and Streams in Vicinity. Report prepared for Bellville Branch of the Department of Water Affairs and Forestry.

Zhang X, Sanderson DJ, Harkness RM, and Last NC, 1996, Evaluation of the 2-D Permeabilitty Tensor for Fractured Rock Masses, International Journal of Rock Mechanics and Mining Sciences, Vol.33, No.1:17-37.

Zektser IS (2000) Groundwater and the Environment, Applications for the Global Community, Lewis Publisher: 1-28.

Zimmermann EW (1951) World Resources and Industries. Revised Edition. New York, Harper.

Zimmermann G, Burkhardt H and Engelhard L (2003) Scale Dependence of Hydraulic and Structural Parameters in the Crystalline Rock of the KTB, Pure appl. Geophys. 160 (2003): 1067-1085.

Плтников HA (1959) Classification and calculation of groundwater storage for water supply (in Chinese), Geology Press of China: 127pp.

# Appendix A CROSS-SECTIONS

**Chevallier, L**

**Council for Geosciences, Western Cape**

## REGIONAL STRUCTURE AND LOCATION OF CROSS SECTIONS

The aim of the cross sections is to visualize, analyse and measure the variation in depth, thickness and attitude of the different formations of the Table Mountain Group (TMG) all over the Cape Fold Belt. The Table Mountain Group, i.e. the hydrogeological target of interest, comprises of the Piekenierskloof, Graafwater, Sardinia Bay, Peninsula, Cedarberg (including the Pakhuis) Formations and the overlying Nardouw Subgroup.

The TMG is very compartmented by extension faulting created during Mesozoic rifting and it is not possible to represent all the variations in detail inside each block. However two major regional faults i.e. the Worcester fault and the Kango fault control the attitude and outcrops of the TMG to a very large extent. Eight geological profiles were therefore selected across these structures (**Figure 1**). Their location was chosen so that they encompass the variation in lithology and thickness of the Table Mountain Group as well as the structural complexity of the Cape Fold Belt.

Faulting along these major fault zones is in many cases found to be within a severely brecciated fractured zone. Cementation of this breccia may however render these fault zones less permeable for water storage and movement, except in those cases of faults which may have been subject to neotectonic reactivation in places such as the Kango Fault.

The Kango-Baviaanskloof fault appears to have been re-activated during the Tertiary Period in a number of places east of Oudtshoorn (Hill, 1988). Preliminary fieldwork along Profile 7 suggests a similar style of reactivation. Only 600 m due east of the section line, a silcrete capping on a remnant of the Cretaceous land surface overlying both the Peninsula Formation of the TMG and the Enon Formation of the Uitenhage Group appears to have been down-faulted by several metres (33º30'42.5"S, 023º42'53.5"E). Follow up fieldwork is required to more accurately determine the amount of displacement and age of deformation. Resolution of slip direction may also contribute to determining the stress field leading to the fracturing, and hence selection of preferred lineaments for groundwater targeting.

Sections 1 and 2 run across the western branch of the Cape Fold Belt. The area is characterised by a thickening of the TMG in the north-northwest-trending Clanwilliam Trough, and by the presence of the Piekenierskloof (fluvial environment with conglomerate) and Graafwater (tidal environment with shale) Formations below the Peninsula Formation. Lateral lithofacies changes occur in these two basal formations. They also thin out towards the East and disappear at the syntaxis.

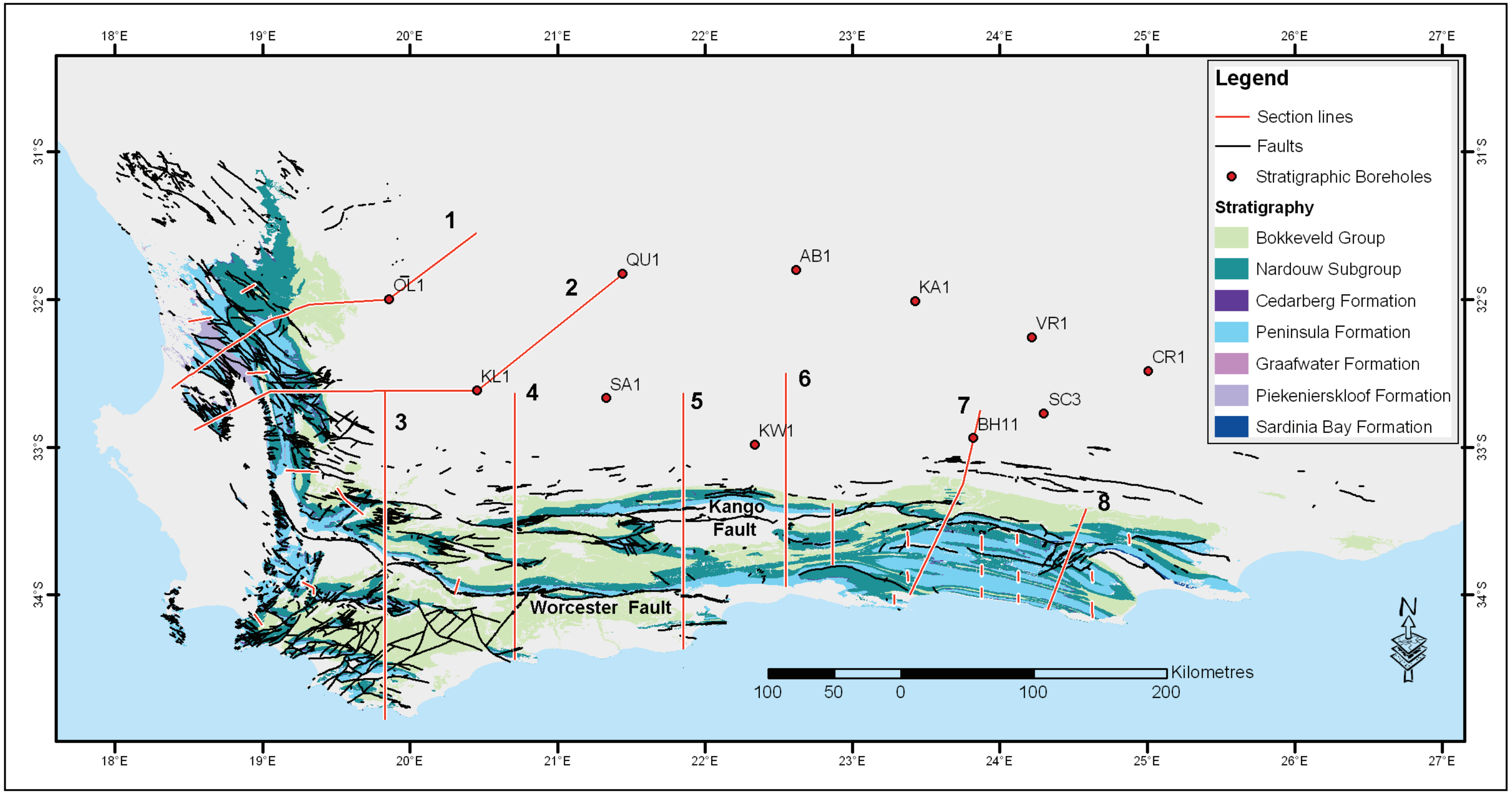


**Figure 1: Map of the Cape Fold Belt showing the Formations of the Table Mountain Group and the location of the geological cross sections**

Section 3 runs through the syntaxis, the most complex part of the Cape Fold Belt where fold interferences (E-W and N-S trending) are numerous. The section was chosen to run at right angle to the main structures (major faults). There is no Piekenierfloof or Graafwater Formations at the base of the sequence and the Peninsula Formation rests directly on the basement.

Sections 4, 5 and 6 were selected across the southeastern branch of the Cape Fold Belt perpendicular to the E-W trending synclines and anticlines. In that part of the belt the Peninsula Formation rests on the Malmesbury Group, basement in this area.

Sections 7 and 8 cut through the most eastern part of the Cape Fold Belt where the TMG sequence outcrops the most. The Sardinia Bay Formation (part of the TMG succession in the East) is present below the Peninsula Formation. This formation is composed of phyllite and metasediments (fluvial to shallow marine environment).

In addition 21 smaller sections were drawn in between major profiles. This was done to provide extra control points on the depth of the geological contacts. The extra sections were chosen in areas where the TMG outcrops the most, like the eastern belt, the syntaxis and the Western branch. In the southern branch only two sections were done, one across the Kammanassie Mountains east of section 6 and another one between section 3 and 4.

## DESCRIPTION OF INDIVIDUAL CROSS SECTIONS

The profiles were constructed using the unpublished 1: 50 000 geological field sheets, which allowed estimations of thicknesses to be made from the disposition of stratigraphic boundaries. The structure was determined from the distribution of strikes and dips, fold axes and faults. Thicknesses were also taken from Rust (1967, 1973), Theron and Loock (1988), Theron and Johnson (1991), Johnson et al. (1999) and SACS (1980). The field sheets that were used to draw the sections are shown on **Figure 2**. Several stratigraphic boreholes drilled by Soekor (Winter H.de la R. and Venter, 1970) were also used to complete these sections under the Karoo Sequence.

The geological profiles are shown on **Figure 3**.

### Profile 1

Profile 1 trends northeast and east-northeast across the strike of the Table Mountain Group from 32°36'34"S, 18°23'18"E near Aurora to 31°33'11"S, 20°27'19"E' northeast of Middelpos. It spans the central and north-eastern part of the 3218 Clanwilliam sheet, the extreme south-eastern part of the 3118 Calvinia sheet and the south-western part of the 3120 Williston sheet. The stratigraphy indicated on the profile consists of basement (Malmesbury Group in the southwest overlain by Klipheuwel Group in the extreme southwest and Namaqua Metamorphic Province in the northeast), the Piekenierskloof, Graafwater, Peninsula and Cedarberg Formations (Pakhuis Formation included), the Nardouw Subgroup,

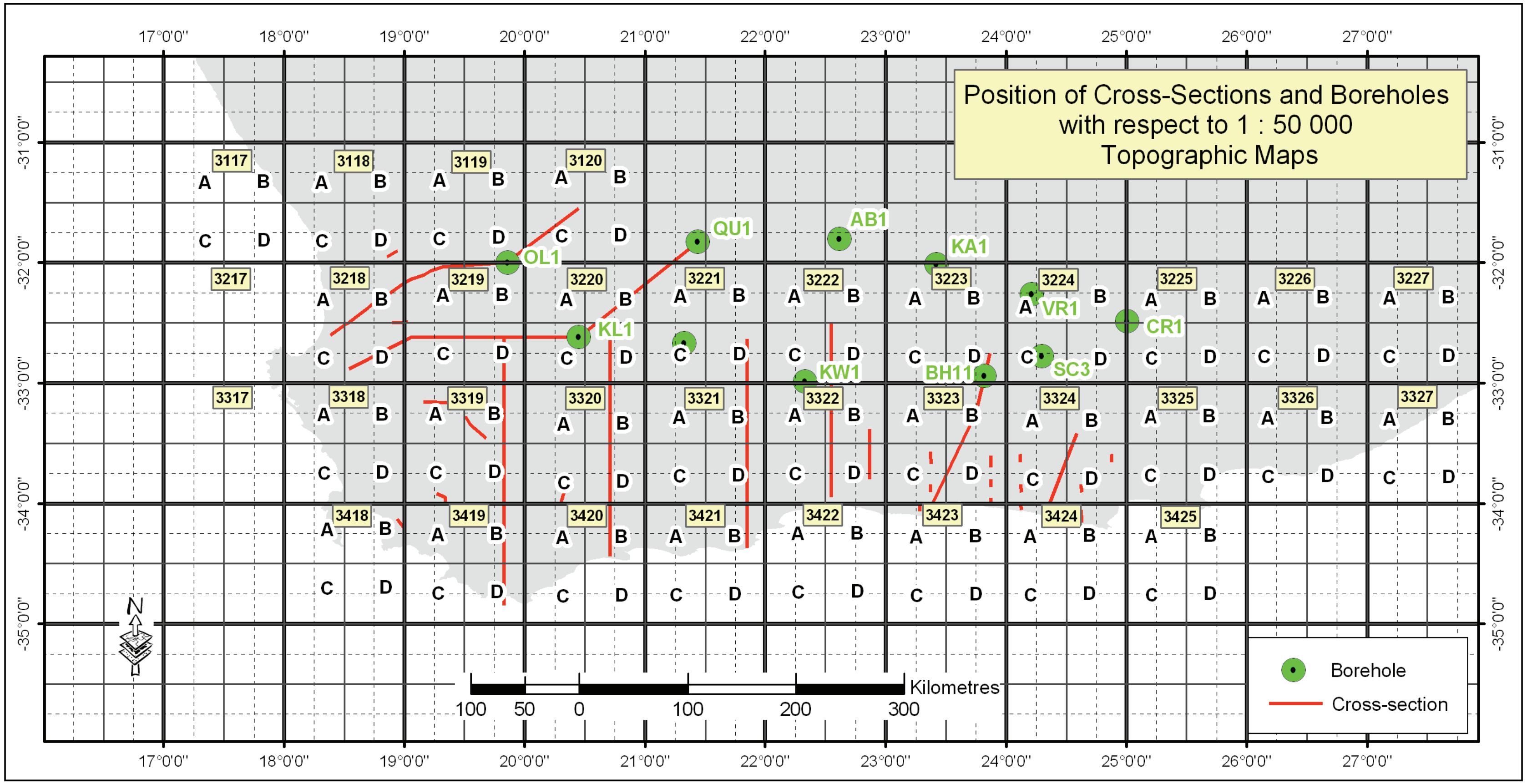


Figure 2: 1:50 000 Field sheets used to draw the geological profiles.

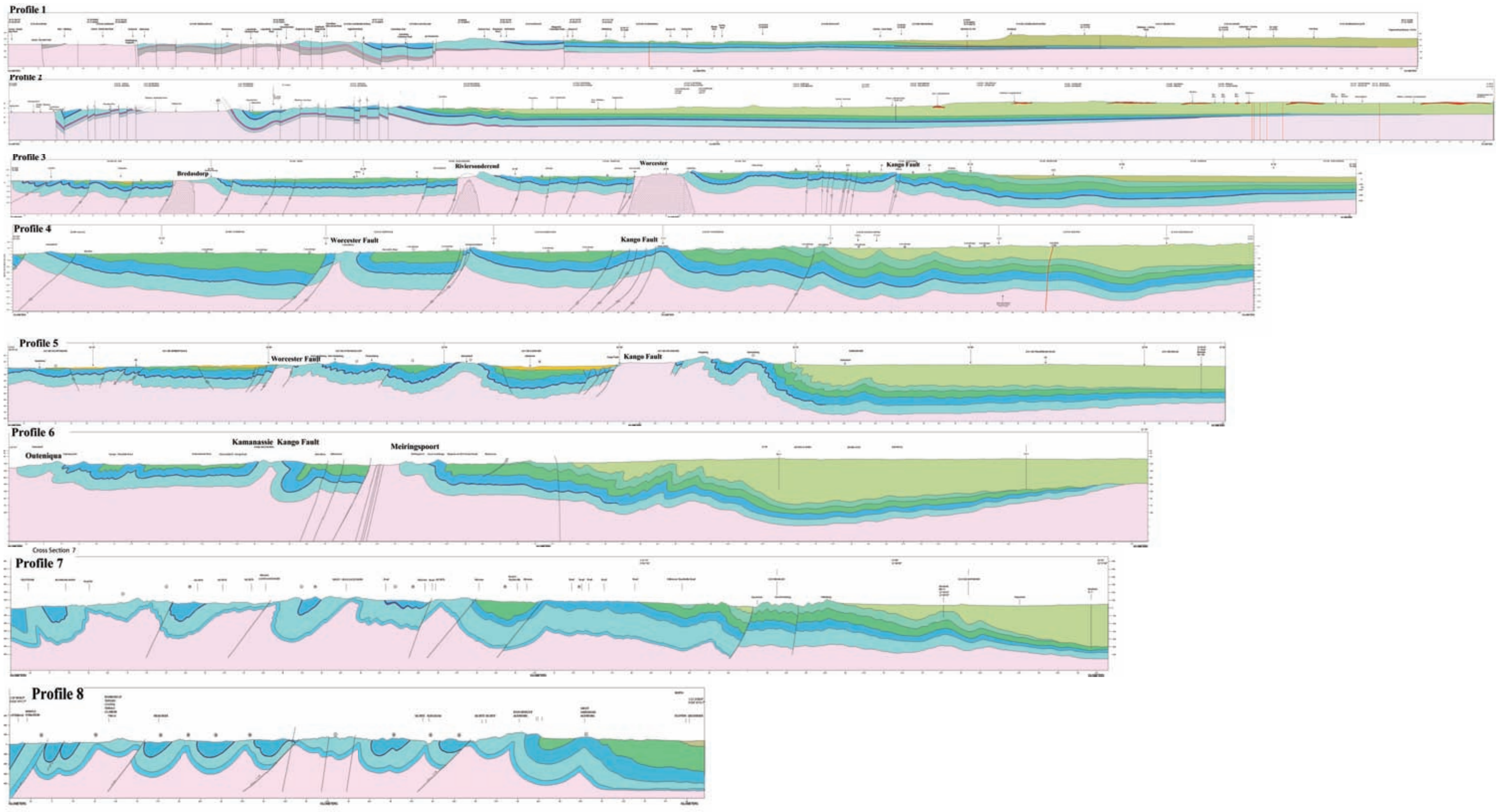


*Figure 3 : Geological profiles across the Cape Fold Belt. See Figure 1 and 2 for location.*

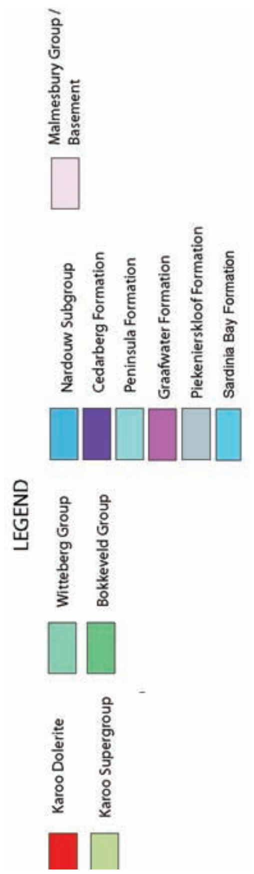
LEGEND
Karoo Dolerite
Karoo Supergroup
Witteberg Group
Bokkeveld Group
Nardouw Subgroup
Cedarberg Formation
Peninsula Formation
Graafwater Formation
Piekenierskloof Formation
Sardinia Bay Formation
Malmesbury Group / Basement

the Bokkeveld Group and the Karoo Supergroup (made up of the Dwyka, Ecca and Beaufort Groups) and including the Karoo dolerite.

Southwest of longitude 19°30'E, the Table Mountain Group varies in thickness from 1000 m to 3300 m with the latter occurring in a graben southwest of Clanwilliam. There is a progressive north-easterly thinning away from the Clanwilliam Trough and an overburden of Bokkeveld Group up to 500 m thick. One deep borehole, OL1/69 drilled at 32°00'S,19°51'40"E, provided thickness control of the Table Mountain Group beneath an overburden of Bokkeveld Group and Karoo Supergroup.

***Four structural compartments can be defined along the profile from West to East:***

1- A small graben containing outliers of Piekenierskloof and Graafwater Formations. This graben is more developed on profile 2.

2- A series of gently-dipping strata, folded into a series of broad (wavelength 5-10 km), open, northwest-trending anticlines and synclines, which plunge gently towards their cores and basins, respectively.

3- A series of grabens and horsts controlled by several near-vertical normal faults with displacements of up to 1700 m (along the Redelinghuys Fault zone). The tilted strata that generally dip at up to 30 degrees should allow lateral groundwater movement, which would be confined by shaley aquicludes in the Graafwater and Cedarberg Formations.

4- East of the series of horst and grabens the TMG sequence thins out, dipping gently eastward under the Karoo sequence without major structural disturbance. A feature of interest however is a northwest-trending Karoo dolerite dyke at 32°02'53"S, 19°19'55"E. This intrudes about 1350 m of Table Mountain Group overlain by 300 m of Bokkeveld Group with no apparent vertical displacement. The dyke has probably compartmentised the Table Mountain Group aquifer and may have marginal fracture zones that would provide good features for water movement along side the structure and water barrier across it.

**Profile 2**

Profile 2 starts on the farm Uitvlug 135 (18° 32' 20"E, 32° 55' 00"S) which is situated west of Piketberg. It trends in a north- easterly direction, at 32°37'24"S, 19°03'16"E it diverts in a due easterly direction and passes south of Citrusdal. Extending over the mountains the profile crosses the Ceres- Karoo where it again diverts at the Soekor borehole KL 1/65 (32°37'00"S, 20°27'15"E)in a north easterly direction towards the Soekor borehole QU 1/65 (31°49'35"S, 21°26'20"E) on the farm Quagga◘s Fontein 357, situated on the 3120 Williston 1:250 000 sheet. The main stratigraphy intersected by the profile comprises the Malmesbury Group, Table Mountain Group, Bokkeveld Group, Witteberg Group and the Dwyka-, Ecca- and Beaufort Groups of the Karoo Supergroup. The TMG sequence along the profile comprises the following formations geochronologically: Piekenierskloof Formation (conglomerate), Graafwater Formation (shale), Peninsula Formation (sandstone), Cedarberg Formation (shale) which includes the Pakhuis Formation (conglomerate and sandstone) and the Nardouw Subgroup (arenite and sandstone).

The Table Mountain Group attains its larger thickness in the Clanwilliam with a maximum of 3500 m occurring in the Citrusdal syncline. There is a progressive northeasterly thinning of the TMG away from the zone of grabens and an overburden of Bokkeveld Group up to 1000 m thick.

***Five structural compartments can be defined along the profile from West to East:***

1- The outlier of the TMG sequence around Piketberg shows strata that have been tilted along faults. These faults are mainly normal faults and no information about their inclinations could be deduced from the maps along the profile. These are therefore inferred as vertical, creating grabens and horsts.

2- The second structural compartment corresponds to the syncline south west of Citrusdal. The exact shape of the structure at depth is unknown and was interpreted from surface structural readings.

3- On the large anticlinal structure further east, several faults displace the formations vertically producing horsts and grabens. The amount of displacement is unknown, but due to the relative known thicknesses of the formations the vertical section uncover the total thickness of the TMG in the profile.

4- Further to the east along the profile a reduction of the intensity of the structure is evident. Regular low amplitude folds and undisturbed horizontal layers are prominent where thick Bokkeveld and Witteberg Groups overlie the TMG.

5- The rest of the profile corresponds to thickening of the Karoo Supergroup. Formations of the TMG also starts to become thinner and pinch out with major folding of faulting being seen from surface analysis. Dolerite dykes and sills are prominent in the eastern part of the profile and could have deformed the formations.

**Profile 3**

Profile 3 runs north-south through the Cape Fold Belt syntaxis, starting at 34°50'00"S, 19°50'00"E until 32°37'00"S, 19°50'00"E' where it intersects Profile 2 on 3219DB Kapelsfontein. It spans the eastern part of the 3319 Worcester sheet from south to north as well as the lower eastern part of 3218 Clanwilliam. The stratigraphy consists of basement (Malmesbury Group and Cape Granite Suite), the Peninsula Formation (the Piekenierskloof and Graafwater Formations wedge out west of the profile), Cedarberg Formation (Pakhuis Formation included), Nardouw Subgroup, Bokkeveld Group, Witteberg Group and the Dwyka and Ecca Groups combined. A small area in the south is underlain by the Mesozoic Uitenhage Group.

Thickness control for the Table Mountain Group can only be verified at Bredasdorp, Riviersonderend and the Langeberg Mountains where it reaches 2700 m thick.

***Seven structural compartments can be defined along the profile from South to North:***

1- Tight folding and overturn folding seems to be concentrated in the southern zone near the coast. Thrust faulting is probably more frequent than shown on the profile, but this is due to poor outcrops in the profile areas. The east rim of this domain is downfaulted along a basement uplift along a fault next to Bredarsdorp.

2- The second zone corresponds to a gently folded flat syncline structure. Its southern limb is uplifted and tilted against a horst associated with a granite pluton and its northern limb is truncated by another uprise of the granitic basement (Riviersonderend fault). The Bokkeveld Group underlies most of the area, field control in these areas is poor due to a scarcity of outcrops.

3- The third zone corresponds to another flat syncline showing the same structural pattern: uplifted in the south and

truncated in the North at the contact with the Worcester fault. Synclines have a low plunge to the east (like zones 1 and 2), probably as a result of the proximity of the syntaxis. In the southern part of profile 4 the synclines plunge to the West giving rise to a north/south striking syncline between the two profiles. North/south crossfolding have also been recognised further to the east (Du Preez, 1944). The faults cutting through the synclinorium are mainly normal faults with relatively high angles, with displacement of the strata to the south.

4- It corresponds to a horst with a perched synclinal structure. The southern limb of the syncline is uplifted against a basement high. The northern limb is thrusted northward over another syncline.

5- Another syncline with a southern limb thrusted (high angle fault) over structural compartment 6 along the Kango fault. Between the Waboomsberg and Witberg Mountains, a zone with high fault intensity occurs. These faults are mainly inverted, down faulted to the north.

6- It forms a synclinorium that progressively gets buried under the thick sequence of the Bokkeveld and Witteberg Groups as well as Karoo Supergroup. On its southern boundary the syncline of zone 4 is thrusted over with a high angle along the Kango fault.

7- In this last zone the TMG forms a vast undulating basin under a thick sequence of Karoo sediments.

**Profile 4**

Profile 4 trends N-S along longitude 20° 42'00"E. It starts from the coast at 34°28'00"S until it intersects the latitude of borehole KL1 at 32°38'00"S, where it ends. It spans the western side of the 3420 Riversdale and 3320 Ladysmith sheets and part of the Sutherland sheet. The stratigraphy consists of basement (Malmesbury Group), the Peninsula Formation, the Cedarberg Formation, Nardouw Subgroup, Bokkeveld Group, Witteberg Group and the Karoo Supergroup.

Thickness control for the Table Mountain Group (up to 4500 m thick) can be verified at several places like Hamerkop, Langeberg, Warrmwaterberg and Anysberg. The depth of the top of the basement attains 8000 m below sea level.

***Six structural compartments can be defined along the profile from South to North:***

1- A very small tectonic block on the coast where the TMG sequence is down faulted to the south (probably similar to zone 2 of profile 3).

2- A vast flat synclinal structure, similar to zone 3 of profile 3, with an uplifted southern limb and a down faulted northern limb against the Worcester Fault. The syncline has a low plunge to the West.

3- A syncline sharply overturned against basement rise along the Worcester fault in the south and down-faulted in the North. This zone is the equivalent to zone 4 of profile 3.

4- A perched synclinal structure similar to zone 5 of profile 3. Its southern rim is limited by a series of normal faults with displacement to the south. Its northern rim corresponds to an anticline bringing the Peninsula Formation few hundred meters below the surface.

5- This zone is very wide and corresponds to a synclinorium made of large open synclines and anticlines. It can be divided into two structural domains: a southern domain where the TMG is outcropping and a northern domain where the TMG is plunging under the Karoo sediment. The limit with zone 6 corresponds to where the base of the TMG sequence and the base of the Karoo Basin reach the deepest point (8000 m).

6- A zone where the TMG sequence thins-out and remains undisturbed.

**Profile 5**

Profile 5 trends N-S along longitude 21°51'00"E. It extends from the coast at 34°22'15"S until it intersects borehole SA1 at 32°38'00"S. It runs parallel to the Prince Albert profile of Halbich (1983). It spans the eastern side of the 3420 Riversdale and 3320 Ladysmith sheets and part of the Sutherland sheet. The stratigraphy consists of basement (Malmesbury Group), the Peninsula Formation, the Cedarberg Formation, Nardouw Subgroup, Bokkeveld Group, Witteberg Group and the Karoo Supergroup. Three large Cretaceous grabens are filled with the Uitenhage Group. The Cenozoic Grahamstown Formation is also present on the profile.

Thickness control for the Table Mountain Group can be verified at several places, where the top and the bottom of both Peninsula Formation and Nardouw Subgroup outcrop: Groot Goliatsberg, Gamkasberg (about 3200 m thick)

***Six structural compartments can be defined along the profile from South to North:***

1 and 2- Two zones are combined in this coastal region underlain by the Uitenhage Group or by more recent deposits, where TMG outcrops are very small. It seems to correspond to a flat syncline with down-faulting on its northern boundary at the Worcester Fault. The structure is divided into two basins separated by a flower-like horst limited by north-verging thrusts in the North and south-verging thrusts in the South. These two basins could correspond to zone 1 and 2 of profiles 3 and 4.

3- A syncline with north verging overturned second order folds. The south  limb of the syncline is strongly overturned and thrusted in place, A major north verging thrust- fold divides the structure in two smaller basins. The syncline has a low plunge to the East. It corresponds to structural zone no 2 of Halbich (1983) where shortening has been calculated between 30% for the northern part and 76% for the southern thrusted part.
4- The Oudtshoorn Basin (filled with Cretaceous Uitenhage Group) corresponds to another syncline. It is separated from the syncline of zone 3 by an anticline. The northern side of the basin is limited by a series of antithetic faults also corresponding to the Kango fault. A maximum Cretaceous sediment thickness of 1900 m is suggested for the Oudtshoorn basin (Kleywegt, 1972).

5- It corresponds to a large synclinorium with north verging overturned second order folds and thrust-folds. The synclinorium can be divided in two parts: a southern part where the TMG is outcropping showing overturned and thrusted  structure (zone 4 of Hallbich at 33% shortening) and a northern part where the TMG  plunges under the Karoo basin and where it reaches its deepest (8000 m), corresponding  to zone 3 off Halbich (1983).

6- A zone where the TMG sequence thins-out and remain undisturbed.

**Profile 6**

Profile 6 runs north-south along the longitude 22°33'00"E, with the southern point at co-ordinates 33°57'00" and the northern end at 32°30'00" S. The area covered is the 1:250 000 map sheet of Oudtshoorn (3322), and part of 1:250 000 mapsheet of Beaufort West (3222). The stratigraphy intersected by the profile is made up of the Kango and Kaaimans Group rocks, forming the basement, the Cape Supergroup (Table Mountain Group, Bokkeveld Group and the Witterberg Group), the Dwyka, Ecca and Beaufort Group of the Karoo Supergroup.

At locations where the Table Mountain Group (TMG) is well exposed like the large anticlinorial mountain ranges of Outeniqua, Kammanassie and the Swartberg/ Meiringspoort, a maximum of 3200 m thickness could be measured.

***Four structural compartments can be defined along the profile from South to North:***

1- A large syncline with north verging inclined or overturned second order folds and local thrusts. This zone seems equivalent to zone 4 of profile 3, and zone 3 of profiles4 and 5.

2- This zone corresponds to an overturned syncline. The Kammanassie anticline marks the limit between zone 1 and 2 in the south, whereas in the north the sequence is downfaulted along the Kango fault with a displacement of about 4000 m. This zone is equivalent to zone 5 of profile 3, and zone 4 of profiles 4 and 5.

3- This zone correspond to a vast synclinorium, similar to zone 6 of profile 3, and zone 5 of profiles 4 and 5. It shows north verging overturned second order folds and thrust-folds. The synclinorium can be divided in two parts: a southern part where the TMG is outcropping and a northern part where the sinuosity is higher and where the TMG plunges under the Karoo basin and where it reaches its deepest (8000 m).

4- After the trough where the base of the TMG reaches its deepest, the sequence thins out and remains undisturbed.

**Profile 7**

Profile 7 trends north-northeast across the strike of the Table Mountain Group from 34º00'00"S, 023º37'21"E at Grootbank in the south, to 33º45'00"S, 023º50'40"E in the north where it reaches borehole SC3. It spans the eastern portion of the 1:250000 3322 Oudtshoorn sheet. The stratigraphy indicated on the profile consists of: Sardinia Bay, Peninsula and Cedarberg Formations, the Nardouw Subgroup of the Table Mountain Group and the overlying Ceres and Traka Subgroups of the Bokkeveld Group, all of the Cape Supergroup. Although in some parts the pre-Cape Gamtoos Group lies very close to the surface, none of this basement is exposed along the profile.

The thickness of the entire Table Mountain Group varies throughout the length of the profile from approximately 3500 m in the south to 4000 m towards the north in relation to the distance from the geosynclinal axis of the Cape Basin.

Thrust faulting with a northerly displacement occurs throughout the profile. Some of the thrusts in Profile 7 are inferred due to bed thickness and fold style constraints encountered during the drawing of the section.

***Five structural compartments can be defined along the profile from South to North:***

1- Two south verging overturned synclines. This is the only zone of the Cape Fold Belt where the folds are verging south, towards the sea.

2- A series of north verging overturned synclinoriums and anticlinoriums. The plunges of the fold axes are very variable. The TMG attains a high degree of shortening. The northern boundary of this domain corresponds to a basement rise and a normal fault (the Kango fault). The folding of the resistant Peninsula Formation has a pronounced effect on the topography of the region within the profile. All the prominent mountain ranges of the area are remnants of large anticlinorium within the TMG. The typical macro-folding occurs in wavelengths of some 5-12 km, with fold amplitudes in the region of 1-2 km. Secondary folding within these broad constraints commonly leads to spectacular tightly-folded and convoluted beds, down to the micro-level in places. This deformation typically occurs in the vicinity of the larger thrust faults, particularly in the compressed southern side.

3- A vast synclinorium where the shortening seems to be less. The tectonics is similar to the one of other zones north of the Kango fault for section 3, 4, 5 and 6. This zone is limited to the North by a normal fault.

4- From the profile, it is apparent that the deformation of the Cape Supergroup becomes somewhat less intense towards the very northern end.

5- After the last folds the sequence thins out and remains undisturbed.

**Profile 8**

Profile 8 consists of an 81.5 km section trending north-northeast across the strike of the Cape Fold Bet from (34º06'08"S, 024º19'17"E ) at Otterbaai in the south, to (33º25'00"S, 024º35'12"E) at Erekroonspoort in the north. It spans the eastern portion of the 1:250000 3324 Port Elizabeth sheet. The stratigraphy indicated on the profile consists of: Sardinia Bay, Peninsula and Cedarberg Formations, the Nardouw Subgroup of the Table Mountain Group and the overlying Ceres and Traka Subgroups of the Bokkeveld Group, all of the Cape Supergroup. Although in some parts the pre-Cape Gamtoos Group lies very close to the surface, none of this basement is exposed along the profile.

Thickness control for the Table Mountain Group can be verified at several places along the profile where outcrops and structural readings are numerous. The thickness of the entire Table Mountain Group varies throughout the length of the profile from approximately 3000 m in the south to 4500 m towards the north in relation to the distance from the geosynclinal axis of the Cape Basin.

***Two structural compartments can be defined along the profile from South to North:***

**1-** Typical north-vergent macro-folding occurs throughout the profile. Both the prominent mountain ranges of the area, the Baviaanskloof and Grootwinterhoek Mountains are situated within large anticlinorium.

Overfolding and secondary folding is evident, especially on the compressed hanging-walls situated to the south of the large thrust faults like the Kareedouw thrust near the Krom River (Booth and Shone, 2002). Wavelengths are generally 6-10 km long, with fold amplitudes in the region of 2 km. The general east-west trends of the fold axes evident on the western side of the profile, is common throughout the southern limb of the fold belt. On the eastern side of the profile however, the trend tend to rotate slightly southward. This, along with the low-angle eastward plunge of the fold axes may be associated with a later influence of the left-lateral Agulhas fracture. Thrust faulting, both bedding transgressive and bedding-parallel, occurs throughout the profile. Displacement along these faults is northwards. The large thrusts indicated in the profile have displacements between 2 and 4 km. In places, smaller bedding-parallel thrusts (not indicated) within individual units make them thicker than they originally were at the time of deposition. Many of the thrusts in profile 8 are inferred due to bed thickness and structural constraints encountered during the drawing of the section. The profile also transects three left-lateral strike slip faults trending northeast-southwest.

2- A vast anticlinorium similar to zone 3 of section 7.

## HYDRO-STRUCTURAL DOMAINS

Several hydro-structural compartments were drawn based on the analysis of the profiles. The result is shown on **Figure 4**. Each compartment that could be characterised by its own flow dynamics is bound by major discontinuities and defined by a specific tectonic style.

The major discontinuities are mainly normal faults developed by inversion of fault zones of the Cape Orogeny during the Mesozoic rifting and break-up of Gondwanaland (Viljoen, 1992).The tectonic style inside each compartment (overturned synclines, flat anticlinorium, monoclines, thrusted folds, etc...) was acquired during the Cape Fold Belt compressional orogeny.The prolongation of the structural domains off shore the Southern coast was taken from Bate and Malan (1992) and Fouché et al. (1992).

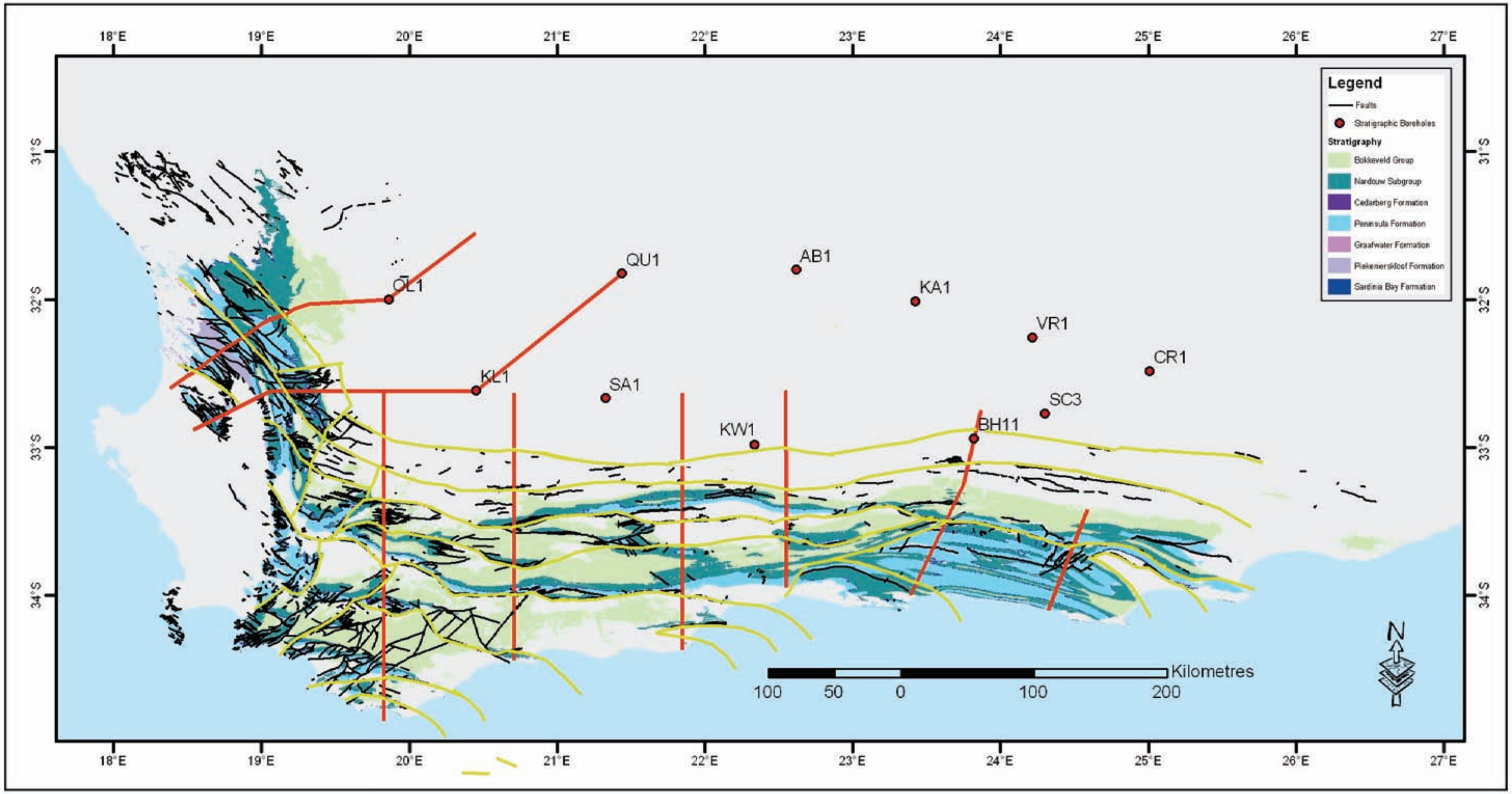


**Figure 4: Hydro-structural domains of the TMG aquifer.**

## REFERENCES


Bate, K.J and Malan, J.A., 1992. Tectonostratigraphic evolution of the Alggoa, Gamtoos and Pletmos Basins, offshore South africa. In: M.J. De Wit and I.G.D. Ransome eds, Inversion tectonics of the Cape Fold Belt, Karoo and Cretaceous Basins of Southern Africa. 61-76

Booth, P. W. K. and Shone, R. W., 2002. A Review of Thrust Faulting in the Eastern Cape Fold Belt, South Africa, and the Implications for Current Lithostratigraphic Interpretations of the Cape Supergroup. *Journal of African Earth Sciences*. **34**, 179-190.

Du Preez, J.W., 1944. Lithology, structure and mode of deposition of the Cretaceous deposits in the Oudtshoorn area: Annals, University of Stellenbosch, 22A, 209-237.

Fouché, K.J., Bate, K.J and Van der Merwe, R., 1992. Plate tectonic setting of the Mesozoic Basins, southern offshore, South Africa: A review. In: M.J. De Wit and I.G.D. Ransome eds, Inversion tectonics of the Cape Fold Belt, Karoo and Cretaceous Basins of Southern Africa. 33-48

Gresse, P.G. and Theron, J.N., 1992. The geology of the Worcester area: Explanation of Sheet 3319 Worcester (1:250 000), Geological Survey of South Africa, 79 pp.

Halbich, I.W., 1983. A tectogenesis of the Cape Fold Belt. Spec. Publ. geol. Soc. S. Afr., 12, 165-175.

Haughton, S.H., Blignaut, J.J.G., Rossouw, P.J., Spies, J.J. and Zagt, S., 1953. Results of an investigation into the possible presence of oil in Karroo rocks in parts of the Union of South Africa: Memoir, Geological Survey of South Africa, 45, 130 pp.

Hill, R.S.,1988. Quaternary faulting in the south-eastern Cape Province. South African Journal of Geology, v. 91, No. 3, p. 399-403.

Johnson, M.R., Theron, J.N. and Rust, I.C., 1999. Table Mountain Group: Catalogue of South African Lithostratigraphic Units, South African Committee for Stratigraphy, Council for Geoscience, 6, 43-45.

Kleywegt, R.J., 1972. Interpretation of a gravity profile across the Oudtshoorn Cretaceous basin. Ann Geol. Surv. (1971-1972). Dep of Mines, Rep. Of S. Afr., 125-128.

Rowsell, D.M. and De Swardt, A.M..J., 1976. Diagenesis in Cape and Karroo sediments, South Africa, and its bearing on their hydrocarbon potential. Transactions Geological Society of South Africa, 79, p. 81-145.

Rust, I.C., 1967. On the sedimentation of the Table Mountain Group in the Western Cape Province: D.Sc. thesis, Geology Department, University of Stellenbosch (unpublished), 110 pp.

Rust, I.C., 1973. The evolution of the Palaeozoic Cape basin, southern margin of Africa *in* The Ocean Basins and Margins, Volume 1. The South Atlantic (A.E.M. Nairn and F.G. Stehli, eds.): Plenum, New York, p. 247-276.

South African Committee for Stratigraphy (SACS), 1980. Stratigraphy of South Africa. Part 1: Lithostratigraphy of the Republic of South Africa, South West Africa/Namibia, and the Republics of Bophuthatswana, Transkei and Venda: Handbook Geological Survey of South Africa, 8, 690 pp.

Theron, J.N. and Loock, J.C., 1988. Devonian deltas of the Cape Supergroup, South Africa *in* Devonian of the World, Volume 1. Regional Synthesis (N.J. McMillan, A.F. Embry and D.J. Glass, eds.): Canadian Society of Petroleum Geologists, Memoir 14, p. 729-740.

Theron, J.N. and Johnson, M.R., 1991. Bokkeveld Group (including the Ceres, Bidouw and Traka Subgroups): Catalogue of South African Lithostratigraphic Units, South African Committee for Stratigraphy, Council for Geoscience, 3, 3-5.

Truswell, J. F., 1977. The Geological Evolution of South Africa. Purnell and Sons.

Viljoen, J.H.A. , 1992. The statigraphy of the Heidelberg/Riversdale Mesozoic Basin. In: M.J. De Wit and I.G.D. Ransome eds, Inversion tectonics of the Cape Fold Belt, Karoo and Cretaceous Basins of Southern Africa. 77-85.

Winter, H. de la R. and Venter, J.J., 1970. Lithostratigraphic correlation of recent deep boreholes in the Karroo-Cape sequence Africa *in* Proceedings and Papers, 2nd Gondwana Symposium (S.H. Haughton, ed.): CSIR, Pretoria, p. 395-408.

# Appendix B TABLE MOUNTAIN GROUP AQUIFER WELLFIELD DEVELOPMENT – AN OVERVIEW

PN ROSEWARNE

## INTRODUCTION

The main wellfields and wellfield areas developed in the Table Mountain Group Aquifer (TMGA) are shown on Figure 1 and details given in Table 1. The distinction is made between wellfields and wellfield areas because the former are distinct clusters of boreholes operated as a unit, eg Ceres Municipality, while the latter refers to areas of general borehole development, eg Hex River Valley. Exploitation of the TMGA is spread along most of its outcrop. The main gaps in development are in the northern and eastern extremities and in the mountainous inland area of the Eastern Cape.

Prior to the late 1980s, early 1990s, the main use of the TMGA was restricted to the general areas mentioned above, including the Hex, Ceres, Breede and Agter Witzenberg Valleys and small-scale municipal use by small towns along the coastal and inland outcrop areas of the TMGA.

## WELLFIELD DEVELOPMENT

In the Hex Valley, ~400 production boreholes pump ~20 million $m^3$/a of groundwater for use in irrigating of vines for export table grape production. Most of these boreholes tap the Bokkeveld Aquifer directly but indirectly obtain about 75% of their groundwater via leakage from the surrounding TMGA, mainly the Nardouw Subgroup. The same is true of the other valley areas mentioned above although the actual volumes of water pumped are less well documented. The Valley is in the syntaxis area of the Cape Fold Belt and joints and bedding plane openings appear to be the main conduits for groundwater flow and storage. Elipsoid drawdown zones have been noted around test boreholes, with the longer axis being developed parallel to the main fold direction, ie NE-SW. Water levels are monitored in about 20 boreholes by the Hex Valley Irrigation Board. There is a need to optimise the location and operation of production boreholes in the valley to minimise the risk of overabstraction in places and inflow of poor quality groundwater from the Bokkeveld rocks to the north-east of the valley. There is a surplus of groundwater in the south-western parts of the valley and scope for developing a more assured annual yield for the valley rather than increasing overall yield.

In the period 1987 to 1990 two projects came on stream where specific wellfields were developed. These were in the Klein Karoo area near Oudtshoorn and Calitzdorp, and at St Francis Bay.

The Klein Karoo Rural Water Supply Scheme (KKRWSS) was commissioned in 1987. The original design yield was 4,7 million $m^3$/a from two wellfield areas, an Eastern Wellfield near Dysselsdorp and a Western Wellfield near Calitzdorp. Monitoring has shown that the capacity of the scheme is closer to 1,3 million $m^3$/a. The earlier over-estimation was as a result of poor understanding of the conceptual flow model and incorrect analysis of test pumping data. The scheme has also been dogged by problems of iron bacteria formation in the boreholes developed in the Nardouw Subgroup, which has lead to clogging of screens and the need for continual rehabilitation of boreholes. The Calitzdorp Wellfield yield has declined to a trickle. The wellfields are used all year round and there is a detailed monitoring programme in place with telemetric monitoring of water levels and abstraction.

Two adjacent wellfields were developed at St Francis Bay in 1990, the Santa and Airfield Wellfields, to cater for increased development and water demand in the area. These boreholes were all drilled into the Nardouw Subgroup. A feature of the development of these wellfields is that the boreholes were sited “blind” through a ~40 m thick sand and calcrete cover but only one borehole out of 15 was unsuccessful. Wellfield management is of critical importance in coastal resort towns such as this as boreholes and aquifers are usually over-stressed during holiday periods when water use increases exponentially. The peak yield of the scheme is 60 l/s and the normal demand yield is 24 l/s. The wellfields are used all year round with particular stress being placed on the aquifer during the Christmas and Easter holiday periods.

At nearby Jeffreys Bay, seven production boreholes all yielding >5 l/s supply the town with domestic water supplies. These boreholes are developed in the Nardouw Subgroup.

Other municipal wellfield schemes to be developed in the 1990s include those at Ceres, Hermanus, Bredasdorp, Prince Albert, Kleinmond and Citrusdal. Some of these are described below.

At Ceres five production boreholes were developed in the Nardouw Subgroup along the western margin of the town. Yields are mostly moderate at 8 to 10 l/s. An interesting feature of this area is the higher yields obtained from production boreholes in the Bokkeveld Aquifer, where yields of 20 l/s are attained. The wellfield is mainly used as a summer bridging supply for when surface water supplies are short. There is scope for further development of the TMGA along the southern margins of the town.

A number of high yielding (>20 l/s) but unused boreholes were known in the Hermanus area prior to 1995. A production borehole was then developed on the approach to the town from the Onrus side in 1996 with an immediate yield of up to 40 l/s and sustainable yield of up to 20 l/s. This borehole penetrated through the Cedarberg Shale into the Peninsula Formation at a relatively shallow depth. Further deeper drilling was carried out in 2001-2002 in the same area and further strong boreholes established. The supply capacity of the wellfield is ~1,5 million $m^3$/a. A possible concern here is the boreholes being located on the coastal fringe, with main water strikes being located >100 m below sea level coupled with high pumping rates. Excessive pumping here would seem to carry a very real threat of seawater intrusion. A monitoring programme has been drawn-up in consultation with DWAF to track changes in water level and water quality. Once all aprties have agreed to the monitoring requirements and constraints abstraction will start.

Boreholes with very high ( one with >100 l/s) blow-out yields were developed at Boschkloof near Citrusdal in 1997/98. These are developed in the Peninsula Formation. However, critical evaluation of the test pumping data by several experienced hydrogeologists suggests that the long term sustainable yields are only of the order of 25 l/s and there is mutual interference between boreholes and influence on a nearby river. The boreholes have only been used intermittently by the municipality. A detailed review of the capacity of the wellfield was carried out in 2003 as part of a DANIDA funded project on trial implement DWAF's Intergrated Water Resources Management approach to catchment water use.

A more recent addition to the list of TMGA wellfields is a scheme in the Koo Valley, between Worcester and Montagu. This scheme was developed in response to a period of prolonged drought in the area and a subsequent shortage of irrigation water for the mainly peach and pear orchards. Twenty three exploration boreholes were subsequently drilled in 2002 and a sustainable yield of ~60 l/s estimated. These boreholes tap the Nardouw Subgroup. The scheme was commissioned in 2003 and a detailed monitoring programme is in place, including DIVER continuous EC and water level recorders installed by DWAF in three observation boreholes.. The scheme is currently running to expectations.

The biggest potential wellfield development in the TMGA is taking place in the mountains to the east of Cape Town. A number of target areas are being investigated and it is intended to develop a pilot wellfield to yield ~3,5 million $m^3$/a. This is to test borehole siting, drilling and construction methods and get an initial indication of environmental impacts of such a scheme. Yields of 100 l/s are proposed for successful production boreholes, which may be as deep as 1 000 m. The investigation is being carried out for the City of Cape Town to see if TMGA groundwater can provide a significant supply to help alleviate future shortages. A key aspect of this study is the potential ecological impact of large-scale groundwater use from high yielding boreholes/wellfields. It was originally proposed that only confined areas of the TMGA be exploited, ie where the Peninsula Formation is confined by the overlying Pakhuis and Cedarberg Formations. However, this has apparently proved to be more difficult than originally thought and may not be feasible. Groundwater resources are also being investigated in the so-called "Deep South" area of the Cape Peninsula to the west of Simonstown as part of a separate project.

## WELLFIELD RANKINGS

An attempt has been made to "rank" the main TMG Aquifer wellfields in Table 2. This is a subjective ranking done by the author based on personal involvement at some stage or other in most of these wellfields. Within this subjective ranking, four possible groups are distinguishable, below average (24, 25), average (26-28), above average (30) and exceptional (39).

### Below Average Ranking

These wellfields comprise those of the Klein Karoo, Jeffreys Bay, Ceres Municipality and Boschkloof.

- **Klein Karoo**

  This wellfield scores badly because of a combination of:

  - poor borehole design
  - fragmented and widely spaced wellfields
  - chronic Fe problems

It has underperformed from commissioning in 1993 but has one of the most comprehensive monitoring programmes in place, including telemetry and has had some of the most detailed research carried out in terms of geological mapping, resource evaluation and environmental impacts of pumping.

- **Jeffreys Bay**

  This wellfield scores badly on monitoring and aquifer parameters. DWAF possibly have further information that could increase the ranking on these aspects.

- **Ceres Municipality**

  Initial wellfield development took place along the western margin of the town in the mid1990s (and in the associated Bokkeveld Aquifers). Groundwater was required as a summer top-up when supplies from the existing Ceres Dam became inadequate and also during construction of the new Ceres Dam. However, despite further boreholes being sited along the southern margin of the town, these were not developed and groundwater use is sporadic and there is no monitoring programme.

- **Boschkloof**

  The Boschkloof boreholes were drilled amongst much fanfare in 1998, with blow-out yields of >100 ℓ/s apparently being obtained. However, subsequent evaluation of test pumping and monitoring data by a number of experts has shown that:

  - sustainable yields are ~25 ℓ/s per borehole
  - all boreholes show mutual interference when pumped and are sited far too closely together
  - pumping affects nearby surface water flow.

The wellfield is also ranked below average because it is rarely used, only when surface water supplies fail.

Average Ranking

These include three of the 'diffuse' wellfields, Hex, Ceres and Agter Witzenberg, plus St Francis Bay. In the case of the former wellfields, their rankings suffer because:

- Much of the actual abstraction is from the Bokkeveld Aquifer;
- There is no scientific input in terms of borehole siting, design and derivation of aquifer parameters;
- Monitoring is sporadic and data are not analysed by a qualified hydrogeologist.

Above Average Ranking

Two wellfields fall into this category, Koo Valley and Hermanus. These are relatively recently developed wellfields where all aspects have been supervised by suitably qualified hydrogeologists. In both cases there is a detailed monitoring programme in place and extensive aquifer testing and derivation of aquifer parameters has taken place. This is what distinguishes these two wellfields from the Average Ranked wellfields.

Exceptional Ranking

There is only one such wellfield and it is somewhat unfair to include it in the current rankings as it doesn't yet exist! This is the wellfield development proposed to augment water supply to the Greater Cape Town Area. This wellfield or more likely series of wellfields, gets full marks on all ranking aspects apart from quality because:

- There is sufficient budget available to ensure optimum design and derivation of aquifer parameters;
- Development is taking place in some of the prime areas regarding recharge and exploitation material;
- The project is being carried out by a multi-disciplinary team of experts;
- Environmental concerns will ensure that a detailed monitoring programme is implemented. Indeed, an initial three year pilot study will be carried out first to test wellfield development criteria;
- If the project lives up to hype, the wellfield(s) will comprise the highest yielding production boreholes (>100 ℓ/s) in the country.

However, the author doubts that such yields will be consistently sustainable in the long-term, particularly without causing unacceptable environmental impacts of some kind.

PN ROSEWARNE Pr Sci Nat
Principal Hydrogeologist
SRK Consulting

MAIN TMG AQUIFER WELLFIELDS : RANKING MATRIX

| Main Wellfield | Design | Recharge | Exploitation Potential | Current Potential | Volume abstracted | Quality | Monitoring Programme | Aquifer parameters | Total |
|---|---|---|---|---|---|---|---|---|---|
| Hex Valley | 3 | 5 | 5 | 4 | 4 | 3 | 2 | 2 | 28 |
| Agter Witzenberg | 3 | 5 | 5 | 4 | 4 | 3 | 2 | 2 | 28 |
| Ceres Valley | 3 | 5 | 5 | 4 | 4 | 3 | 1 | 1 | 26 |
| Klein Karoo | 2 | 2 | 3 | 4 | 3 | 1 | 5 | 4 | 24 |
| St Francis Bay | 4 | 4 | 4 | 4 | 3 | 3 | 3 | 3 | 28 |
| Jeffreys Bay | 4 | 4 | 4 | 4 | 3 | 4 | 1 | 1 | 25 |
| Ceres Municipality | 4 | 5 | 4 | 2 | 2 | 4 | 1 | 3 | 25 |
| Hermanus | 4 | 3 | 3 | (4) | (3) | 4 | (5) | 4 | (30) |
| Boschkloof | 3 | 3 | 3 | 2 | 2 | 4 | 3 | 5 | 25 |
| Koo Valley | 4 | 3 | 4 | 4 | 3 | 3 | 5 | 4 | 30 |
| Cape Town | (5) | (5) | (5) | (5) | (5) | (4) | (5) | (5) | (39) |

Rating of 1 = Poor; 5 = Good

**Notes:**

1. Ratings in brackets indicate that wellfield has yet to be commissioned (Hermanus) or developed (Cape Town).
2. Some wellfields are diffuse and spread extensively in an aquifer/catchment, e.g. Hex Valley or consist of a number of widely spaced wellfields, eg. Klein Karoo.
3. Most TMG wellfields have very low EC/TDS but are downgraded to at least a 4 on quality because of inherent problems of corrosiveness and dissolved Fe.
4. Klein Karoo wellfields are plagued by chronic Fe problems.
5. The Cape Town 'wellfield(s)' is rated highest because it is being developed in one of the best areas regarding structure and recharge and it has sufficient budget to ensure optimum borehole/wellfield design and monitoring. However, borehole yields of >100 ℓ/s have been projected by the consultants and such high expectations may not be met or have unacceptable environmental impacts.

# Appendix C Borehole core logging

| Well ID | UWC BH-1 | Well Log: Lithology and Construction | | | |
|---|---|---|---|---|---|
| | | Gevoden, Rawsonville | | | |
| Drilling method: | | Core drilling | Contract No. | | none |
| Coordinate | X | 19.24558333 | Scale | H | 7 |
| | Y | 33.71851666 | | V | 400 |
| Surface Elevation (m) | | 273.55 | Diameter (mm) | | 75 |
| Well depth (m) | | 270.55 | Commencing date | | 20051120 |
| Casing depth (m) | | 179 | Ending date | | 20061129 |

| Layer No. | Strata | Thick (m) | Elev. (m) | Depth (m) | Column map | Lithology | Remark |
|---|---|---|---|---|---|---|---|
| 1 | Q4 | 7.55 | 266 | 7.55 | 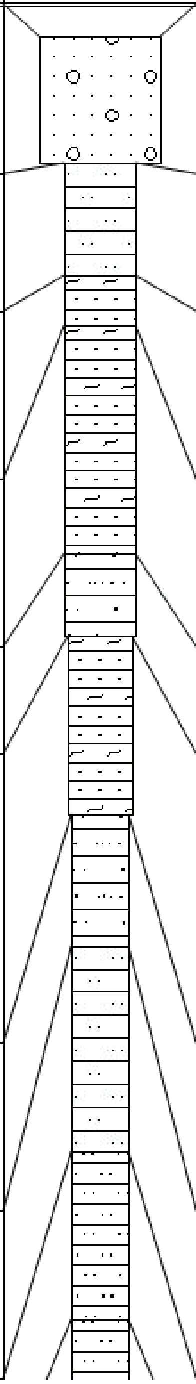 | Alluvial & pluvial deposits: Grit, gravel and boulder. | borhole inclination of 60°, dipping to the west. |
| 2 | Nardouw | 6.69 | 259.31 | 14.24 | | Brown, reddish, blueish and strongly weathered medium~coarse grained sandstones | |
| 3 | Nardouw | 2.94 | 256.37 | 17.18 | | Weathered brown~reddish sandstone with a clay band of 80mm in thickness | Packer tests from 16m to 120m with each interval of 6m |
| 4 | Nardouw | 13.54 | 242.83 | 30.72 | | Fault zone.highly fractured brown, blueish~reddish sandstones sandwiching shales of 50~80 mm in thickness. | |
| 5 | Nardouw | 4.88 | 237.95 | 35.6 | | Lightly fractured blueish~reddish litharenites and siltstones. | |
| 6 | Nardouw | 10.62 | 227.33 | 46.22 | | Dark grey~reddish, medium grained litharenites, lightly fractured, with shale bands of 50~100mm in thickness. | Borehole diverted at 41.82m, the followings are loggings with redrilled hole at the same position |
| 7 | Nardouw | 7.78 | 219.55 | 54 | | highly fractured brown~reddish medium~coarse grained sandstone with minor shales. | Wire drilling |
| 8 | Nardouw | 12.16 | 207.39 | 66.16 | | Lightly~moderately fractured grey blueish~grey reddish sandstones with extensive iron diffusion and veins in fractures. | |

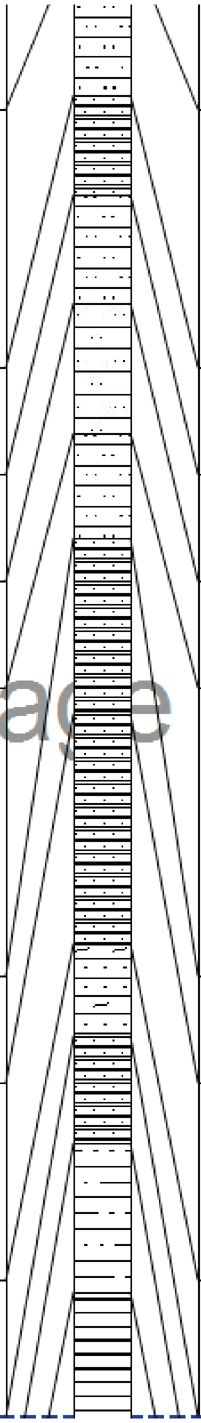

| | | | | | | |
|---|---|---|---|---|---|---|
| 9 | Nardouw | 10 | 197.39 | 76.16 | Grey~blueish medium grained quartz sandstone, lightly fractured. | |
| 10 | Nardouw | 9.01 | 188.38 | 85.17 | Grey~blueish thickbedded medium grained quartz sandstone and mica-feldspar sandstone, lightly fractured. | First conductive zone at 77.5~78.8m, artesian flow Q=0.083 l/s from a steep fracture. |
| 11 | Nardouw | 5.96 | 182.42 | 91.13 | Dark grey sandstones interbedding with silty shales. | |
| 12 | Nardouw | 6.44 | 175.98 | 97.57 | Grey ~ blueish thickbedded medium grained quartz sandtones. | |
| 13 | Nardouw | 7.68 | 168.3 | 105.25 | Highly fractured dark grey midbedded sandstone and siltstone. | |
| 14 | Nardouw | 6.27 | 162.03 | 111.52 | Grey - dark grey, thin to midbedded sandtones and siltstones, lightly-moderately fractured. | Second conductive zone at 106m, total artesian flow Q=0.15 l/s, from a subvertical fracture |
| 15 | Nardouw | 10.51 | 151.52 | 122.03 | Grey~dark grey, medium- to thickbedded litharenites with minor shaly siltstones. | |
| 16 | Nardouw | 13.62 | 137.9 | 135.65 | Lightly fractured grey~dark grey, medium- to thickbedded litharenite, quartz sandstone with minor shaly siltstone and silty shale. | |
| 17 | Cedarberg | 5.46 | 132.44 | 141.11 | Dark grey, thinbedded to medium-bedded sandstone and siltstone with minor silty shales. | |

| | | | | | | | |
|---|---|---|---|---|---|---|---|
| 18 | Cedarberg | 6.39 | 126.05 | 147.5 | 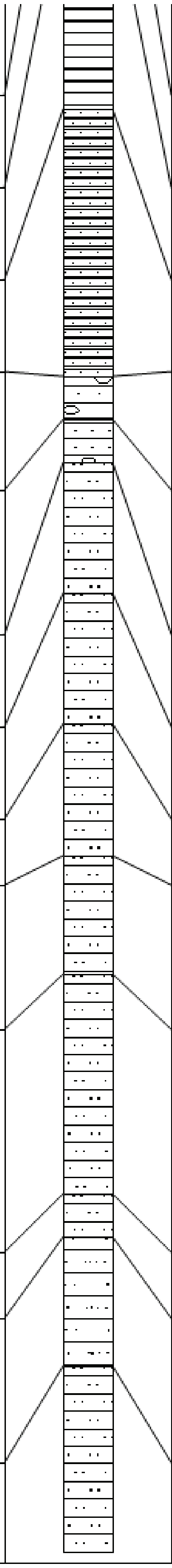 | Grey~dark grey, litharenite and siltstone with minor shales and silty shales. | |
| 19 | Cedarberg | 8.85 | 117.2 | 156.35 | | Dark grey~ grey interbedded shaly siltstone, siltstone and shales. | |
| 20 | Cedarberg | 14.74 | 102.46 | 171.09 | | Dark grey midbedded silty shales with minor sandwiched shaly siltstones | |
| 21 | Cedarberg | 18.44 | 84.02 | 189.53 | | Dark grey thinbedded silty shales sandwiched shaly siltstone and siltstone | |
| 22 | Peninsula | 3 | 81.02 | 192.53 | | Dark grey medium- to thickbedded coarse grained pebble-surported sandstone with minor siltstones. | |
| 23 | Peninsula | 3 | 78.02 | 195.53 | | Dark grey medium- to thickbedded quartz sandstone, with minor pebble-surported litharenites. | |
| 24 | Peninsula | 8.95 | 69.07 | 204.48 | | Highly fractured light grey thin- to mid-bedded quartz sandstone | |
| 25 | Peninsula | 9.01 | 60.06 | 213.49 | | Highly fractured grey fine-mid grained quartz sandstone | |
| 26 | Peninsula | 9.11 | 50.95 | 222.6 | | Grey mid-bedded fine-grained quartz sandstone | |
| 27 | Peninsula | 8.2 | 42.75 | 230.8 | | Grey thin- to mid-bedded fine-grained quartz sandstone with minor grey shale bands, a magnetite concretion at 228.5m. | |
| 28 | Peninsula | 15.1 | 27.65 | 245.9 | | Moderately fractured grey fine to medium grained quatz sandstone. | Third conductive zone at 245.5m total flow Q=0.25 l/s, from a steep fracture. |
| 29 | Peninsula | 2.95 | 24.7 | 248.85 | | Grey fine-grain quartz sandstone | |
| 30 | Peninsula | 8.9 | 15.8 | 257.75 | | Grey~ dark grey mid- to thick-bedded, mid- to coarse-grained quartz sandstone with minor litharenites | |
| 31 | Peninsula | 12.8 | 3 | 270.55 | | Grey thickbedded, mid- to coarse-grained quartz sandstone | |

| Well ID | UWC BH-2 | Well Log: Lithology and Construction | | | |
|---|---|---|---|---|---|
| | | Gevoden, Rawsonville | | | |
| Drilling method: | | Core drilling | Contract No. | none | |
| Coordinate | X | 19.24601667 | Scale | H | 7 |
| | Y | 33.71863333 | | V | 500 |
| Surface Elevation (m) | | 273.06 | Diameter (mm) | 75 | |
| Well depth (m) | | 201.06 | Commencing date | 20060305 | |
| Casing depth (m) | | 65 | Ending date | 20060915 | |

| Layer No. | Strata | Thick (m) | Elev. (m) | Depth (m) | Column map | Lithology | Remark |
|---|---|---|---|---|---|---|---|
| 1 | Q4 | 5.51 | 267.55 | 5.51 | 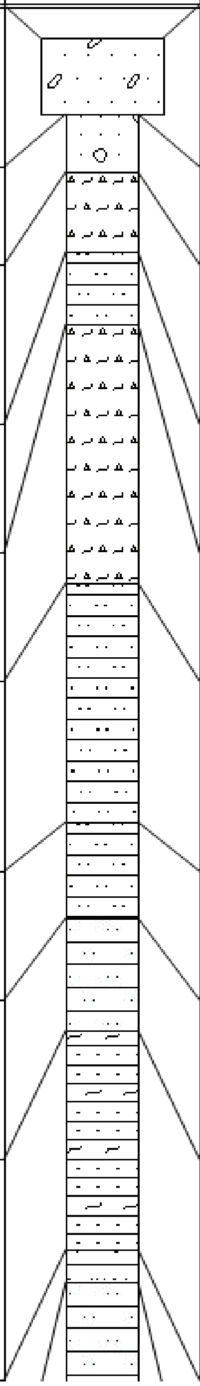 | Brown-reddish grit and gravel | Rest water level: 1.61m to surface |
| 2 | Q4 | 4.29 | 263.26 | 9.8 | | Brown-reddish grit, gravel, and boulder | |
| 3 | TMG | 5.81 | 257.45 | 15.61 | | Fault zone. Jointed mottled cataclastite with extensive iron diffusion in fractures, highly weathered. | |
| 4 | TMG | 5.34 | 252.11 | 20.95 | | Fault zone. Extensively weathered, jointed, greyish, reddish sandstones. | |
| 5 | TMG | 18.95 | 233.16 | 39.9 | | Fault zone. Weathered, iron cemented fault cataclasite with minor sandstones, | |
| 6 | TMG | 17.5 | 215.66 | 57.4 | | Fult zone. Brown-reddish, medium grained quartz sandstone, highly fractured, with iron and manganese diffusions in fractures | Packer tests from 3.8m to bottom with each interval of 6m |
| 7 | TMG | 7 | 208.66 | 64.4 | | Fault zone. Grey, blueish-grey qaurtz sandstones with minor cataclasite. | |
| 8 | Penisula | 8.2 | 200.46 | 72.6 | | Grey, Grey-brown medium grained quartz sandtone, iron diffusion along major fractures | |
| 9 | Penisula | 15.97 | 184.49 | 88.57 | | Grey- dark grey medium-coarse grained quartz sandtone with minor shale bands of 5~15cm in thickness.slight iron diffusion along fractures. | |

| | | | | | | | |
|---|---|---|---|---|---|---|---|
| 10 | Penisula | 2.38 | 182.11 | 90.95 | | Brown medium grained sandstone, extensively jointed with strong iron diffusion along fractures. | |
| 11 | Penisula | 29.05 | 153.06 | 120 | | Grey - dark grey, mudium- to thick-bedded, medium-coarse grained qaurtz sandtones and litharenites with slight iron and manganese diffusion along fractures. | |
| 12 | Penisula | 18.77 | 134.29 | 138.77 | | Greyish medium- to thick-bedded quartz sandtone with minor siltstone and shales. | |
| 13 | Penisula | 26.53 | 107.76 | 165.3 | | Dark grey, mediumbedded shaly siltstones and sandstones. | |
| 14 | Penisula | 9.79 | 97.97 | 175.09 | | Grey - dark grey, mudium- to thick-bedded, medium-coarse grained qaurtz sandtone with minor shaly siltstones. | |
| 15 | Penisula | 9.32 | 88.65 | 184.41 | | Dark grey, medium- to thick-bedded, coarse-grained sandstone and minor shaly siltstones. | |
| 16 | Penisula | 9.1 | 79.55 | 193.51 | | Dark grey shaly siltstones and sandstones | |
| 17 | Penisula | 4.55 | 75 | 198.06 | | Dark grey, medium- to thick-bedded, cross-bedding coarse-grained sandstones with minor shaly siltstones. | |
| 18 | Penisula | 3 | 72 | 201.06 | | Dark grey, thickbedded quartz sandstone. | |

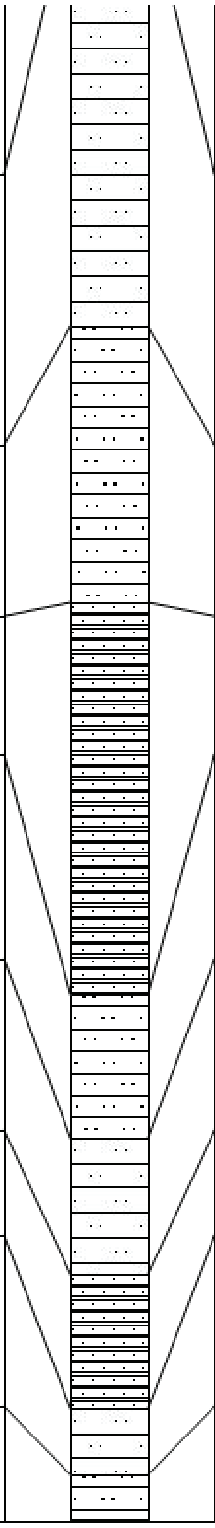

# Appendix D Fracture data from field measurements

| Dip Direction | Strike | Dip angle | Spacing (mm) | Aperture (mm) |
|---|---|---|---|---|
| 85 | 175 | 20 | 890 | |
| 90 | 180 | 18 | 900 | 0.11 |
| 110 | 20 | 16 | 760 | 0.15 |
| 115 | 25 | 17 | 630 | |
| 82 | 172 | 19 | 780 | |
| 96 | 6 | 21 | 920 | 0.26 |
| 95 | 5 | 25 | 1100 | |
| 92 | 2 | 17 | 860 | 0.22 |
| 80 | 170 | 22 | 790 | |
| 99 | 9 | 19 | 900 | |
| 112 | 22 | 20 | | 0.18 |
| 111 | 21 | 21 | 590 | 0.16 |
| 117 | 27 | 15 | 1000 | |
| 69 | 159 | 16 | | |
| 93 | 3 | 20 | 590 | |
| 110 | 20 | 18 | 866 | |
| 83 | 173 | 21 | 895 | |
| 88 | 178 | 22 | | |
| 75 | 165 | 19 | 946 | |
| 73 | 163 | 22 | 970 | |
| 84 | 174 | 17 | 855 | |
| 87 | 177 | 16 | 770 | 0.22 |
| 70 | 160 | 19 | | |
| 89 | 179 | 21 | 880 | |
| 91 | 1 | 21 | | |
| 98 | 8 | 16 | | 0.15 |
| 92 | 2 | 18 | | |
| 92 | 2 | 15 | | 0.2 |
| 92 | 2 | 21 | | 0.19 |
| 113 | 23 | 17 | | |
| 95 | 5 | 22 | | |
| 94 | 4 | 17 | | 0.22 |
| 90 | 180 | 18 | 860 | |
| 120 | 30 | 20 | | |
| 107 | 17 | 22 | | 0.18 |
| 125 | 35 | 17 | 750 | 0.2 |
| 88 | 178 | 21 | | |
| 117 | 27 | 21 | | 0.19 |
| 76 | 166 | 22 | | |
| 103 | 13 | 14 | 1002 | |
| 107 | 17 | 28 | | |
| 120 | 30 | 18 | | |
| 95 | 5 | 24 | 1005 | |
| 90 | 180 | 25 | | |
| 104 | 14 | 17 | | |
| 91 | 1 | 22 | | |
| 105 | 15 | 19 | | |
| 78 | 168 | 18 | 850 | |
| 86 | 176 | 17 | | |
| 77 | 167 | 23 | | |
| 92 | 2 | 20 | | |
| 96 | 6 | 20 | | |
| 96 | 6 | 23 | | |

| | | | | |
|---|---|---|---|---|
| 92 | 2 | 25 | | |
| 123 | 33 | 20 | | |
| 75 | 165 | 25 | | |
| 205 | 115 | 88 | 350 | |
| 210 | 120 | 89 | 500 | 0.3 |
| 220 | 130 | 85 | 550 | 0.26 |
| 216 | 126 | 82 | | 0.21 |
| 225 | 135 | 84 | 400 | |
| 223 | 133 | 78 | 650 | 0.17 |
| 200 | 110 | 45 | 350 | |
| 211 | 121 | 65 | 460 | 0.25 |
| 215 | 125 | 88 | 470 | |
| 212 | 122 | 72 | | 0.33 |
| 203 | 113 | 55 | 450 | |
| 217 | 127 | 77 | | 0.35 |
| 198 | 108 | 39 | 590 | |
| 214 | 124 | 65 | | 0.29 |
| 220 | 130 | 84 | 660 | |
| 205 | 115 | 51 | | 0.3 |
| 222 | 132 | 68 | 670 | |
| 214 | 124 | 66 | | |
| 221 | 131 | 87 | 450 | |
| 209 | 119 | 72 | 433 | |
| 227 | 137 | 71 | 500 | |
| 217 | 127 | 72 | | |
| 199 | 109 | 67 | 900 | |
| 230 | 140 | 61 | | |
| 208 | 118 | 70 | | |
| 218 | 128 | 62 | 460 | |
| 223 | 133 | 68 | | |
| 224 | 134 | 65 | 520 | |
| 199 | 109 | 88 | | |
| 215 | 125 | 79 | 490 | |
| 194 | 104 | 85 | | 0.29 |
| 213 | 123 | 73 | | |
| 217 | 127 | 84 | 530 | |
| 213 | 123 | 75 | | |
| 216 | 126 | 76 | | |
| 207 | 117 | 58 | | |
| 207 | 117 | 80 | | |
| 218 | 128 | 68 | 550 | |
| 207 | 117 | 79 | | 0.22 |
| 212 | 122 | 62 | | |
| 211 | 121 | 71 | | |
| 226 | 136 | 79 | | |
| 215 | 125 | 74 | | |
| 230 | 140 | 60 | | |
| 216 | 126 | 67 | | 0.26 |
| 221 | 131 | 69 | | |
| 220 | 130 | 71 | | |
| 203 | 113 | 49 | | |
| 219 | 129 | 86 | | 0.35 |
| 208 | 118 | 62 | | |
| 211 | 121 | 81 | | |
| 204 | 114 | 86 | | 0.27 |
| 216 | 126 | 70 | | |
| 192 | 102 | 65 | | |

| | | | | |
|---|---|---|---|---|
| 212 | 122 | 73 | 505 | |
| 225 | 135 | 59 | | |
| 218 | 128 | 70 | | |
| 200 | 110 | 73 | | |
| 207 | 117 | 52 | | 0.22 |
| 214 | 124 | 41 | | |
| 198 | 108 | 70 | 540 | |
| 208 | 118 | 71 | | 0.19 |
| 233 | 143 | 73 | | |
| 205 | 115 | 78 | | |
| 213 | 123 | 87 | | |
| 206 | 116 | 70 | | |
| 203 | 113 | 68 | | |
| 216 | 126 | 75 | | |
| 211 | 121 | 72 | | |
| 217 | 127 | 66 | | |
| 219 | 129 | 77 | | |
| 206 | 116 | 82 | 520 | |
| 211 | 121 | 67 | | |
| 207 | 117 | 74 | | |
| 210 | 120 | 84 | | |
| 227 | 137 | 76 | | |
| 208 | 118 | 67 | | |
| 197 | 107 | 73 | | |
| 222 | 132 | 50 | | |
| 212 | 122 | 89 | | |
| 222 | 132 | 75 | | |
| 140 | 50 | 88 | 250 | |
| 145 | 55 | 89 | 400 | 0.12 |
| 150 | 60 | 85 | | |
| 150 | 60 | 86 | 350 | |
| 155 | 65 | 87 | | |
| 135 | 45 | 78 | 600 | 0.01 |
| 130 | 40 | 79 | | |
| 161 | 71 | 81 | | |
| 135 | 45 | 83 | 300 | 0.02 |
| 150 | 60 | 76 | 330 | |
| 152 | 62 | 73 | 350 | |
| 159 | 69 | 73 | | 0.08 |
| 146 | 56 | 74 | | |
| 140 | 50 | 86 | | 0.1 |
| 138 | 48 | 70 | 330 | |
| 153 | 63 | 81 | | |
| 147 | 57 | 84 | | 0.01 |
| 147 | 57 | 83 | | 0.09 |
| 138 | 48 | 81 | 510 | 0.04 |
| 156 | 66 | 77 | | |
| 148 | 58 | 84 | 600 | 0.03 |
| 131 | 41 | 84 | | |
| 153 | 63 | 82 | 640 | 0.02 |
| 162 | 72 | 87 | | |
| 157 | 67 | 84 | 400 | |
| 164 | 74 | 83 | | |
| 158 | 68 | 87 | 470 | |
| 148 | 58 | 79 | | |
| 138 | 48 | 80 | 495 | |
| 144 | 54 | 89 | | |

| | | | | |
|---|---|---|---|---|
| 150 | 60 | 87 | 390 | |
| 132 | 42 | 80 | | |
| 138 | 48 | 73 | | |
| 139 | 49 | 87 | 330 | |
| 140 | 50 | 82 | | |
| 159 | 69 | 87 | | |
| 162 | 72 | 79 | | |
| 129 | 39 | 90 | 335 | |
| 152 | 62 | 76 | 390 | |
| 144 | 54 | 77 | | |
| 145 | 55 | 81 | 400 | |
| 153 | 63 | 89 | | |
| 144 | 54 | 87 | 410 | |
| 148 | 58 | 74 | | |
| 145 | 55 | 79 | | |
| 165 | 75 | 89 | 488 | |
| 146 | 56 | 89 | | |
| 148 | 58 | 80 | | |
| 138 | 48 | 80 | 520 | |
| 152 | 62 | 82 | | |
| 134 | 44 | 75 | | |
| 152 | 62 | 85 | | |
| 144 | 54 | 85 | | |
| 153 | 63 | 83 | | |
| 145 | 55 | 82 | | |
| 128 | 38 | 80 | | |
| 158 | 68 | 83 | | |
| 139 | 49 | 89 | | |
| 155 | 65 | 82 | | 0.09 |
| 141 | 51 | 83 | | |
| 141 | 51 | 85 | | |
| 145 | 55 | 79 | | 0.05 |
| 148 | 58 | 86 | | |
| 145 | 55 | 77 | | 0.03 |
| 157 | 67 | 83 | | |
| 141 | 51 | 90 | | |
| 133 | 43 | 81 | 500 | |
| 150 | 60 | 87 | | |
| 145 | 55 | 78 | | |
| 157 | 67 | 84 | | |
| 150 | 60 | 85 | | |
| 152 | 62 | 78 | 420 | |
| 161 | 71 | 81 | | |
| 142 | 52 | 82 | | |
| 147 | 57 | 80 | | |
| 139 | 49 | 80 | | 0.03 |
| 126 | 36 | 77 | | |
| 127 | 37 | 84 | | |
| 135 | 45 | 74 | | |
| 140 | 50 | 80 | | |
| 145 | 55 | 79 | | |
| 144 | 54 | 87 | | |
| 156 | 66 | 85 | | |
| 142 | 52 | 80 | | |
| 147 | 57 | 76 | | |
| 145 | 55 | 78 | | |
| 152 | 62 | 86 | | |

| | | | | |
|---|---|---|---|---|
| 141 | 51 | 70 | | |
| 142 | 52 | 78 | | |
| 127 | 37 | 79 | 440 | 0.01 |
| 153 | 63 | 89 | | |
| 140 | 50 | 81 | 400 | 0.08 |
| 123 | 33 | 84 | | |
| 133 | 43 | 90 | | |
| 148 | 58 | 78 | | |
| 147 | 57 | 86 | 470 | 0.06 |
| 141 | 51 | 86 | | |
| 146 | 56 | 88 | | |
| 143 | 53 | 80 | | |
| 139 | 49 | 89 | | |
| 148 | 58 | 72 | 355 | |
| 150 | 60 | 84 | | |
| 131 | 41 | 84 | | |
| 152 | 62 | 80 | | |
| 126 | 36 | 82 | | |
| 123 | 33 | 78 | 380 | |
| 148 | 58 | 88 | | |
| 150 | 60 | 82 | 400 | |
| 135 | 45 | 67 | | |
| 157 | 67 | 83 | | |
| 169 | 79 | 85 | | |
| 145 | 55 | 82 | | |
| 250 | 160 | 88 | | |
| 270 | 0 | 89 | | |
| 265 | 175 | 85 | 600 | |
| 260 | 170 | 83 | 650 | 0.15 |
| 289 | 19 | 84 | | 0.05 |
| 300 | 30 | 75 | 350 | |
| 275 | 5 | 76 | 450 | |
| 255 | 165 | 72 | | |
| 268 | 178 | 81 | 605 | |
| 290 | 20 | 83 | | |
| 295 | 25 | 85 | 510 | |
| 272 | 2 | 76 | | 0.11 |
| 255 | 165 | 80 | 400 | 0.15 |
| 263 | 173 | 81 | | 0.04 |
| 270 | 0 | 87 | | |
| 280 | 10 | 81 | | |
| 276 | 6 | 85 | | |
| 276 | 6 | 84 | | |
| 267 | 177 | 82 | | |
| 254 | 164 | 86 | 670 | |
| 255 | 165 | 80 | | |
| 268 | 178 | 74 | | |
| 278 | 8 | 85 | | |
| 271 | 1 | 76 | 650 | 0.05 |
| 249 | 159 | 82 | 460 | 0.17 |
| 297 | 27 | 83 | 500 | |
| 277 | 7 | 87 | | |
| 271 | 1 | 88 | | |
| 292 | 22 | 87 | | |
| 268 | 178 | 83 | 380 | 0.06 |
| 276 | 6 | 80 | 390 | |
| 282 | 12 | 87 | | |

| | | | | |
|---|---|---|---|---|
| 273 | 3 | 84 | | |
| 258 | 168 | 78 | 390 | 0.05 |
| 250 | 160 | 87 | 410 | |
| 296 | 26 | 88 | | |
| 280 | 10 | 86 | | |
| 288 | 18 | 70 | | |
| 286 | 16 | 81 | | |
| 264 | 174 | 87 | 620 | |
| 290 | 20 | 80 | 540 | |
| 274 | 4 | 83 | | |
| 259 | 169 | 78 | 600 | |
| 268 | 178 | 78 | | |
| 292 | 22 | 84 | 570 | |
| 292 | 22 | 83 | | |
| 255 | 165 | 89 | | |
| 281 | 11 | 79 | | |
| 294 | 24 | 78 | 585 | |
| 284 | 14 | 74 | 615 | |
| 265 | 175 | 83 | | |
| 289 | 19 | 84 | | |
| 276 | 6 | 84 | | |
| 260 | 170 | 75 | | |
| 252 | 162 | 79 | | |
| 248 | 158 | 71 | | |
| 242 | 152 | 86 | | |
| 265 | 175 | 81 | 670 | |
| 249 | 159 | 80 | 600 | |
| 265 | 175 | 77 | | |
| 289 | 19 | 76 | | |
| 243 | 153 | 78 | | |
| 277 | 7 | 79 | | |
| 235 | 145 | 75 | | |
| 305 | 35 | 76 | | |
| 272 | 2 | 89 | | |
| 317 | 47 | 74 | 390 | |
| 293 | 23 | 76 | 590 | |
| 282 | 12 | 76 | | |
| 267 | 177 | 81 | | |
| 270 | 180 | 74 | | |
| 294 | 24 | 85 | 540 | |
| 298 | 28 | 87 | 610 | |
| 268 | 178 | 74 | | |
| 283 | 13 | 90 | | |
| 292 | 22 | 86 | | |
| 286 | 16 | 77 | | |
| 251 | 161 | 74 | 500 | 0.15 |
| 271 | 1 | 80 | 600 | |
| 278 | 8 | 73 | | |
| 276 | 6 | 74 | | |
| 280 | 10 | 80 | | |
| 295 | 25 | 76 | 430 | |
| 306 | 36 | 85 | | |
| 266 | 176 | 72 | | |

# Appendix E Constant discharge pumping test BH-5

Site: Rawsonville, Borehole: BH5, Conductor: H.Jia &L. Lin , Dat: 23~24/may/06

Borehole depth:170_m; R.WL: 5.570 m; pump inlet depth:100 m; Pump type:Submersible

| T (min.) | WL (m) | Sw(m) | Q(*l/s.*) |
|---|---|---|---|
| **R.W.L.** | **5.570** | | |
| 0.5 | 7.120 | 1.550 | 1.30 |
| 1 | 8.400 | 2.830 | |
| 1.5 | 9.480 | 3.910 | |
| 2 | 10.450 | 4.880 | |
| 2.5 | 11.605 | 6.035 | |
| 3 | 12.700 | 7.130 | |
| 4 | 14.550 | 8.980 | |
| 5 | 15.270 | 9.700 | |
| 6 | 16.250 | 10.680 | |
| 7 | 17.290 | 11.720 | |
| 8 | 18.280 | 12.710 | |
| 9 | 19.280 | 13.710 | |
| 10 | 20.073 | 14.503 | |
| 11 | 20.740 | 15.170 | |
| 12 | 21.415 | 15.845 | |
| 15 | 23.062 | 17.492 | |
| 20 | 25.743 | 20.173 | |
| 25 | 26.620 | 21.050 | |
| 30 | 27.673 | 22.103 | |
| 35 | 28.515 | 22.945 | |
| 40 | 29.173 | 23.603 | |
| 45 | 29.696 | 24.126 | |
| 50 | 30.160 | 24.590 | |
| 55 | 30.490 | 24.920 | |
| 60 | 30.840 | 25.270 | |
| 70 | 31.210 | 25.640 | 1.30 |
| 80 | 31.682 | 26.112 | |
| 90 | 32.042 | 26.472 | |
| 100 | 32.280 | 26.710 | |
| 110 | 32.535 | 26.965 | |
| 120 | 32.745 | 27.175 | |
| 140 | 33.145 | 27.575 | |
| 160 | 33.443 | 27.873 | |
| 180 | 33.692 | 28.122 | |
| 210 | 34.054 | 28.484 | |
| 240 | 34.366 | 28.796 | |
| 270 | 34.555 | 28.985 | |
| 300 | 34.775 | 29.205 | |
| 330 | 34.890 | 29.320 | 1.30 |
| 360 | 35.000 | 29.430 | |
| 420 | 35.210 | 29.640 | |
| 480 | 35.364 | 29.794 | |
| 540 | 35.490 | 29.920 | |
| 600 | 35.685 | 30.115 | |
| 660 | 35.900 | 30.330 | |
| 720 | 36.060 | 30.490 | |
| 780 | 36.165 | 30.595 | |
| 840 | 36.297 | 30.727 | |
| 900 | 36.390 | 30.820 | |

| | | |
|---|---|---|
| 1000 | 36.435 | 30.865 |
| 1100 | 36.600 | 31.030 |
| 1200 | 36.662 | 31.092 |
| 1320 | 36.725 | 31.155 |
| 1440 | 36.790 | 31.220 |

# Appendix F Constant discharge pumping test BH-3

Site: Rawsonville, Borehole: BH3, Conductor: L. Lin & B. Mfanby Dat: 28~30/Nov/06

Borehole depth:200 m, R.WL: 3.28 m, pump inlet depth:47 m, Pump type:Submersible

| **T (min.)** | **WL (m)** | **$s_w$(m)** | **Q(l/s.)** |
|---|---|---|---|
| **R.W.L.** | **3.280** | | |
| 0 | 3.28 | -0.720 | 1.80 |
| 1 | 4 | 0.000 | |
| 2 | 4.34 | 0.340 | |
| 3 | 4.59 | 0.590 | |
| 4 | 4.77 | 0.770 | |
| 5 | 4.91 | 0.910 | |
| 6 | 5.09 | 1.090 | |
| 7 | 5.16 | 1.160 | |
| 8 | 5.31 | 1.310 | |
| 9 | 5.33 | 1.330 | |
| 10 | 5.42 | 1.420 | |
| 11 | 5.5 | 1.500 | |
| 12 | 5.53 | 1.530 | |
| 13 | 5.68 | 1.680 | |
| 14 | 5.74 | 1.740 | |
| 15 | 5.78 | 1.780 | |
| 16 | 5.78 | 1.780 | |
| 17 | 5.85 | 1.850 | |
| 18 | 5.87 | 1.870 | |
| 19 | 5.94 | 1.940 | |
| 20 | 6.01 | 2.010 | |
| 25 | 6.17 | 2.170 | |
| 30 | 6.3 | 2.300 | |
| 35 | 6.44 | 2.440 | |
| 40 | 6.59 | 2.590 | |
| 45 | 6.67 | 2.670 | |
| 50 | 6.77 | 2.770 | |
| 55 | 6.81 | 2.810 | |
| 60 | 6.96 | 2.960 | 1.80 |
| 70 | 7 | 3.000 | |
| 75 | 7.12 | 3.120 | |
| 80 | 7.2 | 3.200 | |
| 90 | 7.39 | 3.390 | |
| 95 | 7.38 | 3.380 | |
| 100 | 7.39 | 3.390 | |
| 110 | 7.5 | 3.500 | |
| 120 | 7.54 | 3.540 | |
| 130 | 7.63 | 3.630 | |
| 140 | 7.71 | 3.710 | |
| 150 | 7.8 | 3.800 | |
| 160 | 7.85 | 3.850 | |
| 170 | 7.86 | 3.860 | |
| 180 | 8.01 | 4.010 | |
| 200 | 8.05 | 4.050 | |
| 220 | 8.05 | 4.050 | |
| 240 | 8.19 | 4.190 | |
| 270 | 8.3 | 4.300 | |
| 300 | 8.33 | 4.330 | |
| 330 | 8.43 | 4.430 | |
| 360 | 8.51 | 4.510 | |

| | | | |
|---|---|---|---|
| 400 | 8.6 | 4.600 | |
| 420 | 8.58 | 4.580 | |
| 480 | 8.74 | 4.740 | |
| 540 | 8.86 | 4.860 | 1.80 |
| 600 | 8.89 | 4.890 | |
| 660 | 9.03 | 5.030 | |
| 720 | 9.1 | 5.100 | |
| 780 | 9.14 | 5.140 | |
| 900 | 9.28 | 5.280 | |
| 1036 | 9.3 | 5.300 | |
| 1100 | 9.28 | 5.280 | |
| 1200 | 9.3 | 5.300 | |
| 1300 | 9.42 | 5.420 | |
| 1400 | 9.45 | 5.450 | |
| 1440 | 9.49 | 5.490 | |
| 1500 | 9.5 | 5.500 | 1.80 |
| 1564 | 9.54 | 5.540 | |

## Appendix G Mean annual surplus (MAS) from soil water balance calculation for quaternary catchments of the TMG outcrop areas

| Quaternary Catchment | Outcrop Area ($Km^2$) | Quaternary MAP (mm) | Outcrop_MAS (mm) | Surplus Rate (%) | Surplus Volume ($Mm^3$) |
|---|---|---|---|---|---|
| E10A | 133.06 | 898.59 | 108.38 | 12.06% | 14.42 |
| E10B | 166.61 | 736.31 | 145.85 | 19.81% | 24.30 |
| E10C | 191.81 | 586.91 | 80.56 | 13.73% | 15.45 |
| E10D | 234.62 | 518.44 | 62.76 | 12.11% | 14.72 |
| E10E | 362.40 | 419.03 | 55.52 | 13.25% | 20.12 |
| E10F | 385.82 | 406.98 | 54.42 | 13.37% | 21.00 |
| E10G | 508.42 | 407.45 | 57.02 | 13.99% | 28.99 |
| E10H | 162.16 | 494.87 | 69.14 | 13.97% | 11.21 |
| E10J | 468.44 | 343.98 | 101.17 | 29.41% | 47.39 |
| E10K | 191.83 | 283.59 | 46.59 | 16.43% | 8.94 |
| E21A | 15.59 | 620.03 | 170.11 | 27.44% | 2.65 |
| E21D | 105.02 | 626.57 | 134.22 | 21.42% | 14.10 |
| E21E | 73.44 | 360.34 | 118.33 | 32.84% | 8.69 |
| E21F | 50.17 | 288.89 | 132.00 | 45.69% | 6.62 |
| E21G | 111.81 | 475.12 | 112.69 | 23.72% | 12.60 |
| E21H | 404.25 | 428.52 | 102.67 | 23.96% | 41.51 |
| E21J | 233.06 | 337.97 | 119.13 | 35.25% | 27.77 |
| E21K | 265.36 | 351.89 | 104.82 | 29.79% | 27.81 |
| E22C | 1.01 | 323.92 | 169.73 | 52.40% | 0.17 |
| E24A | 236.86 | 392.57 | 113.76 | 28.98% | 26.94 |
| E24B | 3.41 | 272.43 | 142.30 | 52.23% | 0.48 |
| E24J | 357.20 | 235.18 | 113.18 | 48.12% | 40.43 |
| E24K | 340.51 | 237.68 | 77.48 | 32.60% | 26.38 |
| E24L | 459.04 | 310.58 | 106.30 | 34.23% | 48.79 |
| E24M | 503.53 | 264.99 | 106.64 | 40.24% | 53.70 |
| E32E | 233.79 | 192.60 | 68.18 | 35.40% | 15.94 |
| E33A | 0.03 | 135.94 | 0.00 | 0.00% | 0.00 |
| E33B | 6.45 | 113.90 | 0.00 | 0.00% | 0.00 |
| E33C | 17.29 | 139.70 | 63.78 | 45.65% | 1.10 |
| E33F | 156.03 | 212.30 | 94.53 | 44.53% | 14.75 |
| E33G | 228.83 | 186.01 | 24.80 | 13.33% | 5.67 |
| E33H | 197.08 | 133.77 | 0.00 | 0.00% | 0.00 |
| E40C | 199.53 | 285.29 | 91.80 | 32.18% | 18.32 |
| E40D | 494.43 | 284.26 | 104.54 | 36.78% | 51.69 |
| F60E | 20.42 | 115.63 | 0.00 | 0.00% | 0.00 |
| G10A | 129.61 | 1580.24 | 292.59 | 18.52% | 37.92 |
| G10B | 119.39 | 1245.12 | 251.32 | 20.18% | 30.00 |
| G10C | 41.45 | 1009.21 | 440.16 | 43.61% | 18.25 |
| G10D | 9.11 | 625.39 | 392.87 | 62.82% | 3.58 |
| G10E | 100.03 | 639.95 | 180.24 | 28.16% | 18.03 |
| G10F | 19.66 | 514.65 | 239.74 | 46.58% | 4.71 |

| Quaternary Catchment | Outcrop Area ($Km^2$) | Quaternary MAP (mm) | Outcrop_MAS (mm) | Surplus Rate (%) | Surplus Volume ($Mm^3$) |
|---|---|---|---|---|---|
| G10G | 184.26 | 912.31 | 61.30 | 6.72% | 11.29 |
| G10H | 28.60 | 411.34 | 170.56 | 41.46% | 4.88 |
| G10J | 39.31 | 446.98 | 361.91 | 80.97% | 14.23 |
| G10K | 271.50 | 381.85 | 151.23 | 39.60% | 41.06 |
| G10M | 5.67 | 300.29 | 149.99 | 49.95% | 0.85 |
| G22A | 236.68 | 683.68 | 320.05 | 46.81% | 75.75 |
| G22B | 82.70 | 922.56 | 224.01 | 24.28% | 18.53 |
| G22C | 9.90 | 605.43 | 349.61 | 57.75% | 3.46 |
| G22D | 29.12 | 737.93 | 384.52 | 52.11% | 11.20 |
| G22F | 36.84 | 1464.50 | 362.61 | 24.76% | 13.36 |
| G22H | 4.51 | 669.23 | 588.94 | 88.00% | 2.65 |
| G22J | 14.72 | 1002.14 | 741.78 | 74.02% | 10.92 |
| G22K | 5.43 | 769.08 | 318.09 | 41.36% | 1.73 |
| G30A | 331.33 | 259.70 | 86.40 | 33.27% | 28.63 |
| G30B | 51.34 | 393.60 | 146.37 | 37.19% | 7.51 |
| G30C | 327.93 | 409.52 | 112.01 | 27.35% | 36.73 |
| G30D | 241.74 | 384.31 | 141.05 | 36.70% | 34.10 |
| G30E | 331.32 | 248.55 | 65.20 | 26.23% | 21.60 |
| G30F | 762.76 | 285.23 | 78.29 | 27.45% | 59.72 |
| G30G | 603.79 | 252.96 | 71.94 | 28.44% | 43.44 |
| G30H | 1068.31 | 213.96 | 29.73 | 13.90% | 31.76 |
| G40A | 67.95 | 1120.50 | 203.64 | 18.17% | 13.84 |
| G40B | 121.60 | 936.61 | 239.31 | 25.55% | 29.10 |
| G40C | 142.60 | 1367.07 | 284.69 | 20.82% | 40.60 |
| G40D | 327.00 | 983.80 | 231.50 | 23.53% | 75.70 |
| G40E | 151.02 | 721.78 | 323.77 | 44.86% | 48.89 |
| G40F | 28.14 | 515.27 | 285.87 | 55.48% | 8.04 |
| G40G | 142.28 | 723.85 | 255.58 | 35.31% | 36.36 |
| G40H | 90.55 | 697.83 | 217.80 | 31.21% | 19.72 |
| G40J | 115.38 | 613.42 | 234.53 | 38.23% | 27.06 |
| G40K | 33.47 | 495.81 | 220.21 | 44.41% | 7.37 |
| G40L | 202.28 | 569.04 | 210.25 | 36.95% | 42.53 |
| G40M | 322.68 | 573.53 | 175.82 | 30.66% | 56.73 |
| G50A | 218.89 | 545.04 | 160.41 | 29.43% | 35.11 |
| G50B | 203.99 | 531.07 | 176.91 | 33.31% | 36.09 |
| G50C | 113.06 | 488.76 | 143.31 | 29.32% | 16.20 |
| G50D | 108.21 | 431.43 | 176.48 | 40.91% | 19.10 |
| G50E | 61.19 | 448.41 | 120.41 | 26.85% | 7.37 |
| G50F | 62.02 | 453.14 | 152.02 | 33.55% | 9.43 |
| G50H | 7.69 | 370.52 | 106.55 | 28.76% | 0.82 |
| G50K | 63.84 | 440.63 | 0.00 | 0.00% | 0.00 |
| H10A | 5.58 | 512.39 | 35.38 | 6.91% | 0.20 |
| H10B | 112.73 | 707.75 | 154.71 | 21.86% | 17.44 |
| H10C | 173.46 | 673.63 | 26.47 | 3.93% | 4.59 |

| Quaternary Catchment | Outcrop Area ($Km^2$) | Quaternary MAP (mm) | Outcrop_MAS (mm) | Surplus Rate (%) | Surplus Volume ($Mm^3$) |
|---|---|---|---|---|---|
| H10D | 96.78 | 1018.86 | 12.36 | 1.21% | 1.20 |
| H10E | 81.61 | 1403.76 | 462.32 | 32.93% | 37.73 |
| H10F | 125.48 | 783.69 | 170.07 | 21.70% | 21.34 |
| H10G | 136.91 | 787.83 | 225.94 | 28.68% | 30.93 |
| H10H | 79.63 | 885.81 | 26.09 | 2.95% | 2.08 |
| H10J | 175.77 | 1594.86 | 488.48 | 30.63% | 85.86 |
| H10K | 188.81 | 1224.84 | 586.83 | 47.91% | 110.80 |
| H10L | 28.00 | 476.16 | 171.40 | 36.00% | 4.80 |
| H20A | 24.20 | 357.14 | 105.37 | 29.50% | 2.55 |
| H20B | 78.17 | 590.35 | 170.45 | 28.87% | 13.32 |
| H20C | 58.87 | 642.96 | 67.20 | 10.45% | 3.96 |
| H20D | 100.43 | 695.97 | 9.45 | 1.36% | 0.95 |
| H20E | 94.49 | 906.39 | 280.47 | 30.94% | 26.50 |
| H20F | 91.81 | 796.88 | 184.63 | 23.17% | 16.95 |
| H20G | 55.86 | 680.13 | 142.40 | 20.94% | 7.96 |
| H30A | 66.52 | 442.57 | 157.15 | 35.51% | 10.45 |
| H30B | 70.59 | 374.37 | 66.46 | 17.75% | 4.69 |
| H30C | 188.28 | 479.55 | 62.60 | 13.05% | 11.79 |
| H30D | 52.13 | 385.11 | 77.91 | 20.23% | 4.06 |
| H30E | 20.37 | 440.89 | 61.57 | 13.97% | 1.25 |
| H40A | 87.92 | 426.20 | 87.65 | 20.57% | 7.71 |
| H40B | 141.05 | 577.49 | 91.38 | 15.82% | 12.89 |
| H40C | 37.38 | 374.92 | 82.70 | 22.06% | 3.09 |
| H40D | 83.20 | 556.67 | 341.84 | 61.41% | 28.44 |
| H40E | 110.40 | 539.13 | 393.97 | 73.08% | 43.49 |
| H40F | 3.09 | 292.83 | 216.27 | 73.85% | 0.67 |
| H40G | 102.30 | 416.95 | 239.14 | 57.35% | 24.46 |
| H40H | 29.47 | 460.80 | 155.39 | 33.72% | 4.58 |
| H40J | 38.85 | 416.95 | 106.42 | 25.52% | 4.13 |
| H40K | 185.45 | 405.74 | 157.82 | 38.90% | 29.27 |
| H40L | 9.46 | 381.32 | 114.67 | 30.07% | 1.09 |
| H50A | 55.94 | 335.28 | 197.06 | 58.77% | 11.02 |
| H50B | 30.07 | 389.23 | 4.79 | 1.23% | 0.14 |
| H60A | 59.31 | 1894.50 | 527.01 | 27.82% | 31.26 |
| H60B | 145.60 | 1126.69 | 335.95 | 29.82% | 48.91 |
| H60C | 131.57 | 891.00 | 458.09 | 51.41% | 60.27 |
| H60D | 104.33 | 651.84 | 222.85 | 34.19% | 23.25 |
| H60E | 71.25 | 639.74 | 275.76 | 43.11% | 19.65 |
| H60F | 81.03 | 581.64 | 210.79 | 36.24% | 17.08 |
| H60H | 60.66 | 464.01 | 143.14 | 30.85% | 8.68 |
| H60J | 102.08 | 457.44 | 182.95 | 39.99% | 18.68 |
| H60K | 55.38 | 371.23 | 84.39 | 22.73% | 4.67 |
| H60L | 19.97 | 360.76 | 86.17 | 23.89% | 1.72 |
| H70A | 8.08 | 414.40 | 135.96 | 32.81% | 1.10 |

| Quaternary Catchment | Outcrop Area ($Km^2$) | Quaternary MAP (mm) | Outcrop_MAS (mm) | Surplus Rate (%) | Surplus Volume ($Mm^3$) |
|---|---|---|---|---|---|
| H70B | 35.30 | 694.37 | 161.53 | 23.26% | 5.70 |
| H70C | 66.67 | 372.52 | 147.46 | 39.58% | 9.83 |
| H70D | 99.29 | 634.75 | 87.73 | 13.82% | 8.71 |
| H70E | 76.94 | 741.05 | 179.08 | 24.17% | 13.78 |
| H70F | 6.54 | 573.22 | 231.64 | 40.41% | 1.52 |
| H70H | 38.89 | 395.42 | 81.63 | 20.65% | 3.18 |
| H70K | 38.52 | 458.42 | 42.31 | 9.23% | 1.63 |
| H80A | 148.92 | 596.95 | 18.73 | 3.14% | 2.79 |
| H80B | 78.37 | 791.68 | 206.14 | 26.04% | 16.15 |
| H80C | 27.26 | 479.37 | 33.24 | 6.93% | 0.91 |
| H90A | 125.09 | 644.68 | 61.66 | 9.56% | 7.71 |
| H90B | 116.68 | 663.76 | 77.20 | 11.63% | 9.01 |
| H90C | 18.37 | 466.68 | 95.06 | 20.37% | 1.75 |
| J11H | 132.19 | 239.58 | 40.53 | 16.92% | 5.36 |
| J11J | 151.34 | 303.70 | 12.35 | 4.07% | 1.87 |
| J11K | 47.46 | 220.61 | 16.01 | 7.26% | 0.76 |
| J12A | 94.21 | 436.97 | 142.88 | 32.70% | 13.46 |
| J12B | 36.59 | 268.18 | 64.85 | 24.18% | 2.37 |
| J12D | 35.60 | 289.31 | 117.98 | 40.78% | 4.20 |
| J12F | 121.42 | 245.27 | 44.23 | 18.03% | 5.37 |
| J12G | 72.30 | 276.66 | 62.47 | 22.58% | 4.52 |
| J12H | 196.14 | 259.53 | 24.24 | 9.34% | 4.75 |
| J12J | 75.52 | 250.03 | 34.97 | 13.99% | 2.64 |
| J12K | 44.20 | 192.47 | 51.95 | 26.99% | 2.30 |
| J12L | 110.59 | 314.06 | 131.89 | 42.00% | 14.59 |
| J12M | 100.70 | 289.94 | 93.53 | 32.26% | 9.42 |
| J13A | 96.29 | 295.24 | 29.37 | 9.95% | 2.83 |
| J13B | 96.71 | 305.67 | 58.92 | 19.27% | 5.70 |
| J13C | 78.97 | 350.51 | 82.73 | 23.60% | 6.53 |
| J23E | 77.77 | 328.97 | 86.16 | 26.19% | 6.70 |
| J23F | 66.10 | 194.23 | 70.65 | 36.38% | 4.67 |
| J23H | 59.58 | 199.38 | 52.54 | 26.35% | 3.13 |
| J23J | 128.66 | 307.70 | 49.03 | 15.93% | 6.31 |
| J24F | 21.44 | 221.70 | 28.05 | 12.65% | 0.60 |
| J25A | 266.73 | 288.59 | 50.04 | 17.34% | 13.35 |
| J25B | 265.59 | 325.57 | 27.22 | 8.36% | 7.23 |
| J25C | 159.62 | 288.13 | 16.11 | 5.59% | 2.57 |
| J25D | 53.85 | 365.23 | 82.67 | 22.63% | 4.45 |
| J25E | 159.51 | 244.46 | 51.82 | 21.20% | 8.27 |
| J31A | 311.14 | 441.05 | 50.93 | 11.55% | 15.85 |
| J31B | 112.65 | 359.19 | 83.65 | 23.29% | 9.42 |
| J31C | 103.30 | 369.20 | 20.35 | 5.51% | 2.10 |
| J31D | 31.07 | 299.98 | 18.06 | 6.02% | 0.56 |
| J32E | 63.80 | 234.34 | 26.24 | 11.20% | 1.67 |

| Quaternary Catchment | Outcrop Area ($Km^2$) | Quaternary MAP (mm) | Outcrop_MAS (mm) | Surplus Rate (%) | Surplus Volume ($Mm^3$) |
|---|---|---|---|---|---|
| J33A | 173.77 | 392.53 | 78.51 | 20.00% | 13.64 |
| J33B | 220.15 | 436.91 | 134.69 | 30.83% | 29.65 |
| J33C | 98.83 | 292.90 | 56.44 | 19.27% | 5.58 |
| J33D | 93.30 | 378.95 | 74.35 | 19.62% | 6.94 |
| J33E | 115.94 | 445.73 | 81.81 | 18.35% | 9.49 |
| J33F | 47.69 | 343.28 | 73.17 | 21.32% | 3.49 |
| J34A | 220.05 | 476.51 | 97.36 | 20.43% | 21.43 |
| J34B | 211.37 | 569.32 | 162.25 | 28.50% | 34.30 |
| J34C | 243.29 | 673.55 | 252.89 | 37.55% | 61.53 |
| J34D | 179.09 | 470.83 | 128.69 | 27.33% | 23.05 |
| J34E | 120.72 | 426.68 | 138.52 | 32.47% | 16.72 |
| J34F | 85.65 | 415.04 | 176.01 | 42.41% | 15.07 |
| J35A | 96.55 | 418.28 | 102.62 | 24.53% | 9.91 |
| J35B | 237.24 | 410.49 | 194.11 | 47.29% | 46.05 |
| J35C | 181.80 | 373.04 | 101.97 | 27.34% | 18.54 |
| J35D | 46.64 | 406.50 | 66.74 | 16.42% | 3.11 |
| J35E | 29.52 | 269.88 | 53.89 | 19.97% | 1.59 |
| J35F | 146.41 | 341.33 | 71.56 | 20.96% | 10.48 |
| J40A | 237.58 | 417.88 | 74.72 | 17.88% | 17.75 |
| J40B | 212.11 | 431.15 | 65.18 | 15.12% | 13.82 |
| J40C | 211.16 | 521.32 | 81.53 | 15.64% | 17.22 |
| J40D | 14.28 | 445.61 | 116.99 | 26.25% | 1.67 |
| K10C | 115.86 | 492.70 | 66.23 | 13.44% | 7.67 |
| K10D | 2.88 | 454.11 | 79.53 | 17.51% | 0.23 |
| K10E | 88.58 | 679.30 | 86.44 | 12.72% | 7.66 |
| K10F | 1.34 | 502.44 | 17.89 | 3.56% | 0.02 |
| K20A | 62.73 | 721.97 | 83.17 | 11.52% | 5.22 |
| K30A | 53.21 | 752.85 | 153.29 | 20.36% | 8.16 |
| K30B | 39.84 | 787.16 | 93.40 | 11.86% | 3.72 |
| K30C | 77.51 | 805.11 | 116.81 | 14.51% | 9.05 |
| K30D | 87.23 | 724.31 | 97.40 | 13.45% | 8.50 |
| K40A | 79.08 | 705.57 | 92.24 | 13.07% | 7.29 |
| K40B | 70.91 | 845.63 | 117.90 | 13.94% | 8.36 |
| K40C | 51.90 | 930.39 | 120.57 | 12.96% | 6.26 |
| K40D | 16.64 | 756.73 | 85.93 | 11.36% | 1.43 |
| K40E | 220.03 | 864.32 | 108.31 | 12.53% | 23.83 |
| K50A | 235.46 | 849.64 | 115.42 | 13.58% | 27.18 |
| K50B | 202.86 | 881.94 | 93.02 | 10.55% | 18.87 |
| K60A | 161.46 | 663.86 | 156.90 | 23.63% | 25.33 |
| K60B | 143.20 | 753.60 | 118.07 | 15.67% | 16.91 |
| K60C | 160.85 | 744.43 | 110.30 | 14.82% | 17.74 |
| K60D | 292.62 | 814.63 | 136.55 | 16.76% | 39.96 |
| K60E | 98.53 | 774.54 | 72.57 | 9.37% | 7.15 |
| K60F | 188.96 | 806.46 | 82.29 | 10.20% | 15.55 |

| Quaternary Catchment | Outcrop Area (Km$^2$) | Quaternary MAP (mm) | Outcrop_MAS (mm) | Surplus Rate (%) | Surplus Volume (Mm$^3$) |
|---|---|---|---|---|---|
| K60G | 125.18 | 860.00 | 87.11 | 10.13% | 10.90 |
| K70A | 170.41 | 920.11 | 75.30 | 8.18% | 12.83 |
| K70B | 106.50 | 997.24 | 77.12 | 7.73% | 8.21 |
| K80A | 146.00 | 1029.50 | 82.14 | 7.98% | 11.99 |
| K80B | 208.44 | 1031.08 | 99.49 | 9.65% | 20.74 |
| K80C | 189.01 | 1016.84 | 105.71 | 10.40% | 19.98 |
| K80D | 173.20 | 936.19 | 135.82 | 14.51% | 23.52 |
| K80E | 245.38 | 894.73 | 202.54 | 22.64% | 49.70 |
| K80F | 157.73 | 545.68 | 131.92 | 24.18% | 20.81 |
| K90A | 213.81 | 716.15 | 168.52 | 23.53% | 36.03 |
| K90B | 145.81 | 774.13 | 283.65 | 36.64% | 41.36 |
| K90C | 255.45 | 596.31 | 128.44 | 21.54% | 32.81 |
| K90D | 116.30 | 692.62 | 162.05 | 23.40% | 18.85 |
| K90E | 54.77 | 676.22 | 148.76 | 22.00% | 8.15 |
| K90F | 125.70 | 698.55 | 160.51 | 22.98% | 20.18 |
| K90G | 152.97 | 653.85 | 124.04 | 18.97% | 18.97 |
| L30A | 0.16 | 283.94 | 1.12 | 0.40% | 0.00 |
| L50A | 41.29 | 294.71 | 43.51 | 14.76% | 1.80 |
| L70A | 49.92 | 248.48 | 45.63 | 18.36% | 2.28 |
| L70B | 0.05 | 236.33 | 14.02 | 5.93% | 0.00 |
| L70C | 89.70 | 224.18 | 46.08 | 20.55% | 4.13 |
| L70D | 33.37 | 252.52 | 37.08 | 14.69% | 1.24 |
| L70F | 111.86 | 315.95 | 21.75 | 6.88% | 2.43 |
| L70G | 445.24 | 503.87 | 57.50 | 11.41% | 25.60 |
| L81A | 331.78 | 526.84 | 92.40 | 17.54% | 30.66 |
| L81B | 261.41 | 427.84 | 58.51 | 13.67% | 15.29 |
| L81C | 332.49 | 436.73 | 59.30 | 13.58% | 19.72 |
| L81D | 308.12 | 393.02 | 61.58 | 15.67% | 18.97 |
| L82A | 269.28 | 595.06 | 86.87 | 14.60% | 23.39 |
| L82B | 404.92 | 677.73 | 151.77 | 22.39% | 61.45 |
| L82C | 362.33 | 685.75 | 162.50 | 23.70% | 58.88 |
| L82D | 591.39 | 577.91 | 101.01 | 17.48% | 59.74 |
| L82E | 365.49 | 584.48 | 150.37 | 25.73% | 54.96 |
| L82F | 168.84 | 511.83 | 112.02 | 21.89% | 18.91 |
| L82G | 265.75 | 472.12 | 64.35 | 13.63% | 17.10 |
| L82H | 230.32 | 450.54 | 63.64 | 14.12% | 14.66 |
| L82J | 161.73 | 491.00 | 68.06 | 13.86% | 11.01 |
| L90A | 260.91 | 541.59 | 66.84 | 12.34% | 17.44 |
| L90B | 83.89 | 596.68 | 108.19 | 18.13% | 9.08 |
| L90C | 60.83 | 607.44 | 152.74 | 25.14% | 9.29 |
| M10A | 258.50 | 533.15 | 30.27 | 5.68% | 7.83 |
| M10B | 249.62 | 557.46 | 68.40 | 12.27% | 17.07 |
| M10C | 216.09 | 564.56 | 59.88 | 10.61% | 12.94 |
| M10D | 62.61 | 470.64 | 39.62 | 8.42% | 2.48 |

| Quaternary Catchment | Outcrop Area ($Km^2$) | Quaternary MAP (mm) | Outcrop_MAS (mm) | Surplus Rate (%) | Surplus Volume ($Mm^3$) |
|---|---|---|---|---|---|
| M20A | 302.59 | 659.51 | 66.90 | 10.14% | 20.24 |
| M20B | 124.83 | 724.94 | 126.78 | 17.49% | 15.83 |
| M30A | 65.94 | 451.23 | 12.93 | 2.87% | 0.85 |
| N40B | 130.69 | 318.50 | 0.00 | 0.00% | 0.00 |
| N40E | 40.72 | 363.65 | 4.44 | 1.22% | 0.00 |

**Note:**

Outcrop Area: The TMG outcrop area in the quaternary catchment;

Quaternary MAP: MAP (Mean Annual Precipitation) of the quaternary catchment;

Outcrop_MAS: MAS (Mean Annual soil water Surplus) on the TMG outcrop of the quaternary catchment;

Surplus Rate: The ratio of MAS to MAP;

Surplus Volume: The mean annual volume of soil water surplus.

## **Appendix H** Baseflow separation results for quaternary catchments of the TMG outcrop areas

| Quaternary | MAR4Q | MAP4Q | Area4Q | Outcrop Area | Area_Ratio | MAB4Q | MAB_OC | MAB | MAB/MAR | MAB/MAP |
|---|---|---|---|---|---|---|---|---|---|---|
| Catchment | ($10^6$ $m^3$) | (mm) | ($Km^2$) | ($Km^2$) | (%) | ($10^6$ $m^3$) | ($10^6$ $m^3$) | (mm) | (%) | (%) |
| E10A | 61.27 | 898.59 | 133.71 | 133.06 | 99.51% | 12.04 | 11.98 | 90.02 | 19.65% | 10.02% |
| E10B | 69.78 | 736.31 | 201.94 | 166.61 | 82.51% | 13.61 | 11.23 | 67.4 | 19.50% | 9.15% |
| E10C | 49.93 | 586.91 | 192.46 | 191.81 | 99.66% | 9.51 | 9.47 | 49.39 | 19.05% | 8.42% |
| E10D | 48.98 | 518.44 | 234.9 | 234.62 | 99.88% | 9.27 | 9.26 | 39.48 | 18.93% | 7.62% |
| E10E | 52.38 | 419.03 | 365.78 | 362.4 | 99.08% | 9.83 | 9.74 | 26.87 | 18.77% | 6.41% |
| E10F | 52.58 | 406.98 | 385.82 | 385.82 | 100.00% | 9.84 | 9.84 | 25.51 | 18.71% | 6.27% |
| E10G | 69.13 | 407.45 | 508.42 | 508.42 | 100.00% | 12.92 | 12.92 | 25.42 | 18.69% | 6.24% |
| E10H | 33.53 | 494.87 | 162.16 | 162.16 | 100.00% | 6.53 | 6.53 | 40.29 | 19.48% | 8.14% |
| E10J | 30.02 | 343.98 | 468.44 | 468.44 | 100.00% | 6.21 | 6.21 | 13.26 | 20.69% | 3.85% |
| E10K | 4.71 | 283.59 | 235.42 | 191.83 | 81.48% | 0.45 | 0.37 | 1.92 | 9.55% | 0.68% |
| E21A | 34.9 | 620.03 | 189.92 | 15.59 | 8.21% | 7.38 | 0.61 | 38.84 | 21.15% | 6.26% |
| E21D | 45.37 | 626.57 | 241.82 | 105.02 | 43.43% | 9.57 | 4.16 | 39.58 | 21.09% | 6.32% |
| E21E | 19.59 | 360.34 | 292.74 | 73.44 | 25.09% | 4.13 | 1.04 | 14.11 | 21.08% | 3.92% |
| E21F | 16.47 | 288.89 | 378.44 | 50.17 | 13.25% | 3.46 | 0.46 | 9.15 | 21.01% | 3.17% |
| E21G | 30.6 | 475.12 | 266.02 | 111.81 | 42.03% | 6.52 | 2.74 | 24.52 | 21.31% | 5.16% |
| E21H | 38.13 | 428.52 | 404.25 | 404.25 | 100.00% | 8.09 | 8.09 | 20.02 | 21.22% | 4.67% |
| E21J | 18.78 | 337.97 | 316.59 | 233.06 | 73.62% | 3.96 | 2.91 | 12.5 | 21.09% | 3.70% |
| E21K | 21.53 | 351.89 | 330.24 | 265.35 | 80.35% | 4.64 | 3.73 | 14.05 | 21.55% | 3.99% |
| E22C | 13.36 | 323.92 | 489.29 | 1.01 | 0.21% | 1.47 | 0 | 3 | 11.00% | 0.93% |
| E24A | 17.27 | 392.57 | 254.64 | 236.86 | 93.02% | 2.04 | 1.9 | 8 | 11.81% | 2.04% |
| E24B | 10.29 | 272.43 | 467.54 | 3.41 | 0.73% | 1.16 | 0.01 | 2.49 | 11.27% | 0.91% |
| E24J | 20.48 | 235.18 | 1077.61 | 357.2 | 33.14% | 2.28 | 0.76 | 2.11 | 11.13% | 0.90% |
| E24K | 10.17 | 237.68 | 651.88 | 340.51 | 52.23% | 1.16 | 0.61 | 1.78 | 11.41% | 0.75% |
| E24L | 23.21 | 310.58 | 515.82 | 459.04 | 88.99% | 4.76 | 4.24 | 9.23 | 20.51% | 2.97% |
| E24M | 9.78 | 264.99 | 528.67 | 503.53 | 95.24% | 1.05 | 1 | 1.99 | 10.74% | 0.75% |
| E32E | 2.6 | 192.6 | 1001.12 | 233.79 | 23.35% | 0.28 | 0.07 | 0.28 | 10.77% | 0.15% |
| E33A | 0.95 | 135.94 | 1355.16 | 0.03 | 0.00% | 0.1 | 0 | 0.07 | 10.53% | 0.05% |
| E33B | 0.28 | 113.9 | 702.12 | 6.45 | 0.92% | 0.03 | 0 | 0.04 | 10.71% | 0.04% |
| E33C | 0.98 | 139.7 | 980.35 | 17.29 | 1.77% | 0.1 | 0 | 0.11 | 10.20% | 0.08% |
| E33F | 3.33 | 212.3 | 724.88 | 156.03 | 21.53% | 0.36 | 0.08 | 0.49 | 10.81% | 0.23% |
| E33G | 2.5 | 186.01 | 894.74 | 228.83 | 25.58% | 0.28 | 0.07 | 0.31 | 11.20% | 0.17% |
| E33H | 0.57 | 133.77 | 719.04 | 197.08 | 27.41% | 0.06 | 0.02 | 0.09 | 10.53% | 0.07% |
| E40C | 6.78 | 285.29 | 529.98 | 199.53 | 37.65% | 0.79 | 0.3 | 1.49 | 11.65% | 0.52% |
| E40D | 7.02 | 284.26 | 543.98 | 494.43 | 90.89% | 0.81 | 0.73 | 1.48 | 11.54% | 0.52% |
| F60E | 0.32 | 115.63 | 794.19 | 20.44 | 2.57% | 0.03 | 0 | 0.03 | 9.38% | 0.03% |
| G10A | 174.27 | 1580.24 | 171.78 | 129.61 | 75.45% | 42.45 | 32.03 | 247.13 | 24.36% | 15.64% |
| G10B | 91.48 | 1245.12 | 125.97 | 119.39 | 94.78% | 21.79 | 20.65 | 172.94 | 23.82% | 13.89% |

| Quaternary | MAR4Q | MAP4Q | Area4Q | Outcrop Area | Area_Ratio | MAB4Q | MAB_OC | MAB | MAB/MAR | MAB/MAP |
|---|---|---|---|---|---|---|---|---|---|---|
| Catchment | ($10^6$ $m^3$) | (mm) | ($Km^2$) | ($Km^2$) | (%) | ($10^6$ $m^3$) | ($10^6$ $m^3$) | (mm) | (%) | (%) |
| G10C | 146.84 | 1009.21 | 328.09 | 41.45 | 12.63% | 9.51 | 1.2 | 28.97 | 6.48% | 2.87% |
| G10D | 115.51 | 625.39 | 687.61 | 9.11 | 1.33% | 24.8 | 0.33 | 36.06 | 21.47% | 5.77% |
| G10E | 68.34 | 639.95 | 394.07 | 100.03 | 25.39% | 14.57 | 3.7 | 36.96 | 21.32% | 5.78% |
| G10F | 60.84 | 514.65 | 539.39 | 19.66 | 3.65% | 12.95 | 0.47 | 24.01 | 21.29% | 4.67% |
| G10G | 124.02 | 912.31 | 185.57 | 184.26 | 99.29% | 25.04 | 24.87 | 134.95 | 20.19% | 14.79% |
| G10H | 21.18 | 411.34 | 674.62 | 28.6 | 4.24% | 4.44 | 0.19 | 6.58 | 20.96% | 1.60% |
| G10J | 34.87 | 446.98 | 867.68 | 39.31 | 4.53% | 7.18 | 0.33 | 8.28 | 20.59% | 1.85% |
| G10K | 25.16 | 381.85 | 1176.42 | 271.5 | 23.08% | 3.14 | 0.72 | 2.67 | 12.48% | 0.70% |
| G10M | 17.44 | 300.29 | 2006.58 | 5.67 | 0.28% | 2.11 | 0.01 | 1.05 | 12.10% | 0.35% |
| G22A | 31.61 | 683.68 | 238.14 | 236.69 | 99.39% | 6.17 | 6.14 | 25.93 | 19.52% | 3.79% |
| G22B | 32.42 | 922.56 | 109.47 | 82.71 | 75.56% | 5.83 | 4.41 | 53.29 | 17.98% | 5.78% |
| G22C | 23.31 | 605.43 | 254.36 | 9.9 | 3.89% | 4.77 | 0.19 | 18.76 | 20.46% | 3.10% |
| G22D | 40.69 | 737.93 | 246.14 | 29.12 | 11.83% | 7.75 | 0.92 | 31.5 | 19.05% | 4.27% |
| G22F | 57.03 | 1464.5 | 65.69 | 36.84 | 56.07% | 14.92 | 8.37 | 227.1 | 26.16% | 15.51% |
| G22H | 25.14 | 669.23 | 227.35 | 4.51 | 1.98% | 5.18 | 0.1 | 22.77 | 20.60% | 3.40% |
| G22J | 58.89 | 1002.14 | 128.21 | 14.72 | 11.48% | 14.94 | 1.72 | 116.55 | 25.37% | 11.63% |
| G22K | 23.95 | 769.08 | 79.83 | 5.43 | 6.81% | 6.04 | 0.41 | 75.66 | 25.22% | 9.84% |
| G30A | 4.8 | 259.7 | 761.81 | 331.33 | 43.49% | 0.52 | 0.23 | 0.68 | 10.83% | 0.26% |
| G30B | 18.9 | 393.6 | 658.54 | 51.34 | 7.80% | 4.03 | 0.31 | 6.11 | 21.32% | 1.55% |
| G30C | 11.31 | 409.52 | 351.3 | 327.93 | 93.35% | 2.39 | 2.23 | 6.81 | 21.13% | 1.66% |
| G30D | 11.92 | 384.31 | 534.67 | 241.74 | 45.22% | 1.42 | 0.64 | 2.65 | 11.91% | 0.69% |
| G30E | 1.9 | 248.55 | 352.19 | 331.32 | 94.07% | 0.2 | 0.19 | 0.57 | 10.53% | 0.23% |
| G30F | 6.79 | 285.23 | 780.29 | 762.76 | 97.76% | 0.76 | 0.74 | 0.97 | 11.19% | 0.34% |
| G30G | 3.49 | 252.96 | 647.52 | 603.79 | 93.25% | 0.19 | 0.17 | 0.29 | 5.44% | 0.11% |
| G30H | 3.34 | 213.96 | 1077.93 | 1068.31 | 99.11% | 0.35 | 0.35 | 0.32 | 10.48% | 0.15% |
| G40A | 38.44 | 1120.5 | 71.53 | 67.95 | 95.00% | 10.2 | 9.69 | 142.59 | 26.53% | 12.73% |
| G40B | 49.37 | 936.61 | 122.44 | 121.61 | 99.32% | 12.87 | 12.78 | 105.1 | 26.07% | 11.22% |
| G40C | 105.29 | 1367.07 | 144.58 | 142.6 | 98.63% | 27.99 | 27.6 | 193.57 | 26.58% | 14.16% |
| G40D | 142.48 | 983.8 | 327.18 | 327 | 99.94% | 37.21 | 37.19 | 113.74 | 26.12% | 11.56% |
| G40E | 37.45 | 721.78 | 277.55 | 151.02 | 54.41% | 6.94 | 3.77 | 24.99 | 18.53% | 3.46% |
| G40F | 21.71 | 515.27 | 422.36 | 28.14 | 6.66% | 4.53 | 0.3 | 10.72 | 20.87% | 2.08% |
| G40G | 29.96 | 723.85 | 220.45 | 142.28 | 64.54% | 5.53 | 3.57 | 25.09 | 18.46% | 3.47% |
| G40H | 11.7 | 697.83 | 95.93 | 90.55 | 94.39% | 2.19 | 2.07 | 22.8 | 18.72% | 3.27% |
| G40J | 14.56 | 613.42 | 168.46 | 115.38 | 68.50% | 2.9 | 1.98 | 17.2 | 19.92% | 2.80% |
| G40K | 19.31 | 495.81 | 428.98 | 33.47 | 7.80% | 4.06 | 0.32 | 9.46 | 21.03% | 1.91% |
| G40L | 21.49 | 569.04 | 384.99 | 202.28 | 52.54% | 4.51 | 2.37 | 11.71 | 20.99% | 2.06% |
| G40M | 22.6 | 573.53 | 392.91 | 322.68 | 82.12% | 4.72 | 3.87 | 12 | 20.88% | 2.09% |
| G50B | 15.3 | 531.07 | 339.12 | 203.99 | 60.15% | 3.24 | 1.95 | 9.55 | 21.18% | 1.80% |
| G50C | 14.71 | 488.76 | 421.17 | 113.06 | 26.85% | 3.17 | 0.85 | 7.51 | 21.55% | 1.54% |
| G50D | 15.51 | 431.43 | 572.09 | 108.21 | 18.92% | 3.28 | 0.62 | 5.74 | 21.15% | 1.33% |

| Quaternary | MAR4Q | MAP4Q | Area4Q | Outcrop Area | Area_Ratio | MAB4Q | MAB_OC | MAB | MAB/MAR | MAB/MAP |
|---|---|---|---|---|---|---|---|---|---|---|
| Catchment | ($10^6$ $m^3$) | (mm) | ($Km^2$) | ($Km^2$) | (%) | ($10^6$ $m^3$) | ($10^6$ $m^3$) | (mm) | (%) | (%) |
| G50E | 9.52 | 448.41 | 313.05 | 61.19 | 19.55% | 2.01 | 0.39 | 6.41 | 21.11% | 1.43% |
| G50F | 7.9 | 453.14 | 290.22 | 62.02 | 21.37% | 1.74 | 0.37 | 5.99 | 22.03% | 1.32% |
| G50H | 15.3 | 370.52 | 889.07 | 7.69 | 0.86% | 3.3 | 0.03 | 3.71 | 21.57% | 1.00% |
| G50K | 4.2 | 440.63 | 162.66 | 63.84 | 39.25% | 0.94 | 0.37 | 5.8 | 22.38% | 1.32% |
| H10A | 39.23 | 512.39 | 233.6 | 5.58 | 2.39% | 7.87 | 0.19 | 33.69 | 20.06% | 6.58% |
| H10B | 46.74 | 707.75 | 162.42 | 112.73 | 69.41% | 9.48 | 6.58 | 58.39 | 20.28% | 8.25% |
| H10C | 69.1 | 673.63 | 259.55 | 173.46 | 66.83% | 14.03 | 9.38 | 54.07 | 20.30% | 8.03% |
| H10D | 50.38 | 1018.86 | 96.94 | 96.78 | 99.83% | 10.43 | 10.41 | 107.56 | 20.70% | 10.56% |
| H10E | 90.2 | 1403.76 | 84.81 | 81.61 | 96.23% | 21.23 | 20.43 | 250.35 | 23.54% | 17.83% |
| H10F | 86.56 | 783.69 | 247.85 | 125.48 | 50.62% | 17.79 | 9.01 | 71.78 | 20.55% | 9.16% |
| H10G | 95.54 | 787.83 | 270.39 | 136.91 | 50.63% | 19.64 | 9.94 | 72.63 | 20.56% | 9.22% |
| H10H | 79.21 | 885.81 | 187.44 | 79.63 | 42.48% | 16.31 | 6.93 | 87.03 | 20.59% | 9.82% |
| H10J | 183.62 | 1594.86 | 213.76 | 175.77 | 82.23% | 43.71 | 35.94 | 204.46 | 23.80% | 12.82% |
| H10K | 110.94 | 1224.84 | 193.52 | 188.81 | 97.57% | 26.81 | 26.16 | 138.55 | 24.17% | 11.31% |
| H10L | 8.99 | 476.16 | 95.77 | 28 | 29.24% | 1.24 | 0.36 | 12.91 | 13.79% | 2.71% |
| H20A | 4.72 | 357.14 | 140.4 | 24.2 | 17.24% | 0.54 | 0.09 | 3.84 | 11.44% | 1.08% |
| H20B | 4.12 | 590.35 | 124.34 | 78.17 | 62.87% | 0.81 | 0.51 | 6.55 | 19.66% | 1.11% |
| H20C | 3.58 | 642.96 | 80.54 | 58.87 | 73.09% | 0.68 | 0.5 | 8.41 | 18.99% | 1.31% |
| H20D | 27.91 | 695.97 | 100.64 | 100.43 | 99.79% | 6 | 5.98 | 59.58 | 21.50% | 8.56% |
| H20E | 40.29 | 906.39 | 95.17 | 94.49 | 99.28% | 8.69 | 8.62 | 91.26 | 21.57% | 10.07% |
| H20F | 11.26 | 796.88 | 116.53 | 91.81 | 78.79% | 1.91 | 1.5 | 16.38 | 16.96% | 2.06% |
| H20G | 4.71 | 680.13 | 85.05 | 55.86 | 65.68% | 0.87 | 0.57 | 10.22 | 18.47% | 1.50% |
| H30A | 16.32 | 442.57 | 284.03 | 66.52 | 23.42% | 2.04 | 0.48 | 7.16 | 12.50% | 1.62% |
| H30B | 10.99 | 374.37 | 314.79 | 70.59 | 22.42% | 1.24 | 0.28 | 3.94 | 11.28% | 1.05% |
| H30C | 23.32 | 479.55 | 326.94 | 188.28 | 57.59% | 3 | 1.73 | 9.18 | 12.86% | 1.91% |
| H30D | 4.8 | 385.11 | 127.03 | 52.13 | 41.04% | 0.55 | 0.23 | 4.34 | 11.46% | 1.13% |
| H30E | 8.89 | 440.89 | 153.66 | 20.37 | 13.25% | 1.29 | 0.17 | 8.4 | 14.51% | 1.91% |
| H40A | 6.51 | 426.2 | 184.3 | 87.92 | 47.70% | 0.77 | 0.37 | 4.16 | 11.83% | 0.98% |
| H40B | 3.7 | 577.49 | 240.42 | 141.05 | 58.66% | 1.05 | 0.62 | 4.37 | 28.38% | 0.76% |
| H40C | 14.19 | 374.92 | 271.69 | 37.38 | 13.76% | 1.8 | 0.25 | 6.63 | 12.68% | 1.77% |
| H40D | 24.77 | 556.67 | 181.7 | 83.2 | 45.79% | 3.55 | 1.63 | 19.54 | 14.33% | 3.51% |
| H40E | 36.05 | 539.13 | 285.35 | 110.4 | 38.69% | 5.1 | 1.97 | 17.88 | 14.15% | 3.32% |
| H40F | 9.11 | 292.83 | 339.79 | 3.09 | 0.91% | 1.08 | 0.01 | 3.17 | 11.86% | 1.08% |
| H40G | 17.38 | 416.95 | 263.26 | 102.3 | 38.86% | 2.58 | 1 | 9.8 | 14.84% | 2.35% |
| H40H | 18.19 | 460.8 | 207.81 | 29.47 | 14.18% | 2.46 | 0.35 | 11.84 | 13.52% | 2.57% |
| H40J | 10.59 | 416.95 | 203.47 | 38.85 | 19.09% | 1.51 | 0.29 | 7.45 | 14.26% | 1.79% |
| H40K | 12.47 | 405.74 | 270.42 | 185.45 | 68.58% | 1.76 | 1.21 | 6.51 | 14.11% | 1.60% |
| H40L | 6.1 | 381.32 | 158.83 | 9.46 | 5.96% | 0.84 | 0.05 | 5.31 | 13.77% | 1.39% |
| H50A | 6.88 | 335.28 | 264.35 | 55.94 | 21.16% | 0.93 | 0.2 | 3.5 | 13.52% | 1.04% |
| H50B | 16.66 | 389.23 | 430.3 | 30.08 | 6.99% | 2.27 | 0.16 | 5.26 | 13.63% | 1.35% |

| Quaternary | MAR4Q | MAP4Q | Area4Q | Outcrop Area | Area_Ratio | MAB4Q | MAB_OC | MAB | MAB/MAR | MAB/MAP |
|---|---|---|---|---|---|---|---|---|---|---|
| Catchment | ($10^6$ $m^3$) | (mm) | ($Km^2$) | ($Km^2$) | (%) | ($10^6$ $m^3$) | ($10^6$ $m^3$) | (mm) | (%) | (%) |
| H60A | 87.67 | 1894.5 | 72.64 | 59.31 | 81.64% | 19.91 | 16.26 | 274.1 | 22.71% | 14.47% |
| H60B | 118.4 | 1126.69 | 209.99 | 145.6 | 69.34% | 26.39 | 18.3 | 125.69 | 22.29% | 11.16% |
| H60C | 83.76 | 891 | 216.86 | 131.57 | 60.67% | 18.61 | 11.29 | 85.84 | 22.22% | 9.63% |
| H60D | 41.67 | 651.84 | 226.78 | 104.33 | 46.01% | 8.69 | 4 | 38.33 | 20.85% | 5.88% |
| H60E | 29.68 | 639.74 | 170.42 | 71.25 | 41.81% | 6.07 | 2.54 | 35.59 | 20.45% | 5.56% |
| H60F | 23.29 | 581.64 | 164.87 | 81.03 | 49.15% | 4.74 | 2.33 | 28.75 | 20.35% | 4.94% |
| H60H | 19.71 | 464.01 | 252.86 | 60.66 | 23.99% | 4.19 | 1.01 | 16.57 | 21.26% | 3.57% |
| H60J | 22.01 | 457.44 | 292.97 | 102.08 | 34.84% | 4.69 | 1.63 | 16 | 21.31% | 3.50% |
| H60K | 11.62 | 371.23 | 262.04 | 55.38 | 21.13% | 2.34 | 0.49 | 8.91 | 20.14% | 2.40% |
| H60L | 9.51 | 360.76 | 230.13 | 19.97 | 8.68% | 1.91 | 0.17 | 8.31 | 20.08% | 2.30% |
| H70A | 13.18 | 414.4 | 223.62 | 8.08 | 3.62% | 2.64 | 0.1 | 11.82 | 20.03% | 2.85% |
| H70B | 41.23 | 694.37 | 152.98 | 35.31 | 23.08% | 13.51 | 3.12 | 88.32 | 32.77% | 12.72% |
| H70C | 14.03 | 372.52 | 287.18 | 66.67 | 23.21% | 1.44 | 0.33 | 5 | 10.26% | 1.34% |
| H70D | 39.1 | 634.75 | 170.29 | 99.29 | 58.30% | 12.72 | 7.42 | 74.68 | 32.53% | 11.77% |
| H70E | 47.55 | 741.05 | 156.72 | 76.94 | 49.09% | 15.72 | 7.72 | 100.28 | 33.06% | 13.53% |
| H70F | 22.88 | 573.22 | 120.76 | 6.54 | 5.41% | 7.42 | 0.4 | 61.43 | 32.43% | 10.72% |
| H70H | 7.4 | 395.42 | 399.76 | 38.89 | 9.73% | 1.69 | 0.16 | 4.23 | 22.84% | 1.07% |
| H70K | 6.01 | 458.42 | 207.11 | 38.52 | 18.60% | 1.34 | 0.25 | 6.49 | 22.30% | 1.42% |
| H80A | 31.11 | 596.95 | 148.92 | 148.92 | 100.00% | 9.75 | 9.75 | 65.47 | 31.34% | 10.97% |
| H80B | 42.48 | 791.68 | 122.87 | 78.37 | 63.79% | 13.66 | 8.72 | 111.22 | 32.16% | 14.05% |
| H80C | 8.2 | 479.37 | 284.61 | 27.26 | 9.58% | 2.07 | 0.2 | 7.27 | 25.24% | 1.52% |
| H90A | 41.32 | 644.68 | 178.95 | 125.09 | 69.90% | 13.3 | 9.3 | 74.32 | 32.19% | 11.53% |
| H90B | 28.74 | 663.76 | 118.09 | 116.68 | 98.81% | 9.26 | 9.15 | 78.38 | 32.22% | 11.81% |
| H90C | 5.59 | 466.68 | 217.41 | 18.37 | 8.45% | 1.42 | 0.12 | 6.51 | 25.40% | 1.39% |
| J11H | 2.41 | 239.58 | 650.9 | 132.19 | 20.31% | 0.3 | 0.06 | 0.46 | 12.45% | 0.19% |
| J11J | 3.78 | 303.7 | 449.48 | 151.34 | 33.67% | 0.46 | 0.15 | 1.02 | 12.17% | 0.34% |
| J11K | 1.6 | 220.61 | 515.49 | 47.46 | 9.20% | 0.18 | 0.02 | 0.36 | 11.25% | 0.16% |
| J12A | 6.8 | 436.97 | 180.75 | 94.21 | 52.12% | 0.85 | 0.44 | 4.7 | 12.50% | 1.08% |
| J12B | 2.41 | 268.18 | 250.85 | 36.59 | 14.58% | 0.26 | 0.04 | 1.03 | 10.79% | 0.38% |
| J12D | 9.64 | 289.31 | 830.34 | 35.6 | 4.29% | 1.09 | 0.05 | 1.31 | 11.31% | 0.45% |
| J12F | 4.47 | 245.27 | 709.39 | 121.42 | 17.12% | 0.47 | 0.08 | 0.67 | 10.51% | 0.27% |
| J12G | 4.49 | 276.66 | 760.29 | 72.3 | 9.51% | 0.57 | 0.05 | 0.74 | 12.69% | 0.27% |
| J12H | 4.29 | 259.53 | 548.95 | 196.14 | 35.73% | 0.45 | 0.16 | 0.83 | 10.49% | 0.32% |
| J12J | 2.91 | 250.03 | 548.51 | 75.52 | 13.77% | 0.31 | 0.04 | 0.57 | 10.65% | 0.23% |
| J12K | 1.6 | 192.47 | 516.22 | 44.2 | 8.56% | 0.16 | 0.01 | 0.31 | 10.00% | 0.16% |
| J12L | 7.12 | 314.06 | 757.02 | 110.59 | 14.61% | 0.86 | 0.13 | 1.14 | 12.08% | 0.36% |
| J12M | 3.48 | 289.94 | 482.63 | 100.7 | 20.87% | 0.42 | 0.09 | 0.88 | 12.07% | 0.30% |
| J13A | 3.88 | 295.24 | 517.59 | 96.29 | 18.60% | 0.49 | 0.09 | 0.94 | 12.63% | 0.32% |
| J13B | 3.42 | 305.67 | 401.51 | 96.71 | 24.08% | 0.42 | 0.1 | 1.06 | 12.28% | 0.35% |
| J13C | 5.7 | 350.51 | 434.76 | 78.96 | 18.17% | 0.71 | 0.13 | 1.63 | 12.46% | 0.47% |

| Quaternary | MAR4Q | MAP4Q | Area4Q | Outcrop Area | Area_Ratio | MAB4Q | MAB_OC | MAB | MAB/MAR | MAB/MAP |
|---|---|---|---|---|---|---|---|---|---|---|
| Catchment | ($10^6$ $m^3$) | (mm) | ($Km^2$) | ($Km^2$) | (%) | ($10^6$ $m^3$) | ($10^6$ $m^3$) | (mm) | (%) | (%) |
| J23E | 7.41 | 328.97 | 224.99 | 77.77 | 34.56% | 1.3 | 0.45 | 5.77 | 17.54% | 1.75% |
| J23F | 4.39 | 194.23 | 477.3 | 66.1 | 13.85% | 0.5 | 0.07 | 1.05 | 11.39% | 0.54% |
| J23H | 2.59 | 199.38 | 264.01 | 59.58 | 22.57% | 0.3 | 0.07 | 1.12 | 11.58% | 0.56% |
| J23J | 6.58 | 307.7 | 228.48 | 128.66 | 56.31% | 1.19 | 0.67 | 5.2 | 18.09% | 1.69% |
| J24F | 0.79 | 221.7 | 282.15 | 21.44 | 7.60% | 0.09 | 0.01 | 0.34 | 11.39% | 0.15% |
| J25A | 8.7 | 288.59 | 353.4 | 266.73 | 75.48% | 1.59 | 1.2 | 4.5 | 18.28% | 1.56% |
| J25B | 13.61 | 325.57 | 396.56 | 265.59 | 66.98% | 2.5 | 1.68 | 6.31 | 18.37% | 1.94% |
| J25C | 1.1 | 288.13 | 180.43 | 159.62 | 88.47% | 0.14 | 0.12 | 0.76 | 12.73% | 0.26% |
| J25D | 9.61 | 365.23 | 210.24 | 53.85 | 25.61% | 1.76 | 0.45 | 8.38 | 18.31% | 2.29% |
| J25E | 1 | 244.46 | 286.34 | 159.51 | 55.71% | 0.13 | 0.07 | 0.44 | 13.00% | 0.18% |
| J31A | 9.61 | 441.05 | 447.04 | 311.14 | 69.60% | 2.2 | 1.53 | 4.93 | 22.89% | 1.12% |
| J31B | 2.31 | 359.19 | 200.56 | 112.65 | 56.17% | 0.57 | 0.32 | 2.83 | 24.68% | 0.79% |
| J31C | 2 | 369.2 | 167.97 | 103.3 | 61.50% | 0.47 | 0.29 | 2.81 | 23.50% | 0.76% |
| J31D | 2 | 299.98 | 303.65 | 31.07 | 10.24% | 0.51 | 0.05 | 1.67 | 25.50% | 0.56% |
| J32E | 5.15 | 234.34 | 971.15 | 63.8 | 6.57% | 0.5 | 0.03 | 0.51 | 9.71% | 0.22% |
| J33A | 5.12 | 392.53 | 449.46 | 173.77 | 38.66% | 1.22 | 0.47 | 2.71 | 23.83% | 0.69% |
| J33B | 9.22 | 436.91 | 590.72 | 220.15 | 37.27% | 2.14 | 0.8 | 3.63 | 23.21% | 0.83% |
| J33C | 2.61 | 292.9 | 427.93 | 98.83 | 23.10% | 0.29 | 0.07 | 0.68 | 11.11% | 0.23% |
| J33D | 12.4 | 378.95 | 258.86 | 93.3 | 36.04% | 2.24 | 0.81 | 8.66 | 18.06% | 2.29% |
| J33E | 24.59 | 445.73 | 328.67 | 115.94 | 35.27% | 4.75 | 1.68 | 14.45 | 19.32% | 3.24% |
| J33F | 11.7 | 343.28 | 365.62 | 47.69 | 13.05% | 2.54 | 0.33 | 6.94 | 21.71% | 2.02% |
| J34A | 5.6 | 476.51 | 252.19 | 220.05 | 87.25% | 1.27 | 1.1 | 5.02 | 22.68% | 1.05% |
| J34B | 12.88 | 569.32 | 341.55 | 211.37 | 61.89% | 2.72 | 1.68 | 7.95 | 21.12% | 1.40% |
| J34C | 21.3 | 673.55 | 318.9 | 243.29 | 76.29% | 4.21 | 3.21 | 13.2 | 19.77% | 1.96% |
| J34D | 7.72 | 470.83 | 354.2 | 179.09 | 50.57% | 1.82 | 0.92 | 5.13 | 23.58% | 1.09% |
| J34E | 4.31 | 426.68 | 257.98 | 120.72 | 46.79% | 1.07 | 0.5 | 4.16 | 24.83% | 0.97% |
| J34F | 4.71 | 415.04 | 319.96 | 85.65 | 26.77% | 1.15 | 0.31 | 3.61 | 24.42% | 0.87% |
| J35A | 22.66 | 418.28 | 427.35 | 96.55 | 22.59% | 4.72 | 1.07 | 11.05 | 20.83% | 2.64% |
| J35B | 9.38 | 410.49 | 651.13 | 237.24 | 36.44% | 2.34 | 0.85 | 3.59 | 24.95% | 0.87% |
| J35C | 2.81 | 373.04 | 264.48 | 181.8 | 68.74% | 0.74 | 0.51 | 2.78 | 26.33% | 0.75% |
| J35D | 25.31 | 406.5 | 506.95 | 46.64 | 9.20% | 5.31 | 0.49 | 10.48 | 20.98% | 2.58% |
| J35E | 4.31 | 269.88 | 215.16 | 29.52 | 13.72% | 0.87 | 0.12 | 4.06 | 20.19% | 1.50% |
| J35F | 18.31 | 341.33 | 500.04 | 146.41 | 29.28% | 3.63 | 1.06 | 7.27 | 19.83% | 2.13% |
| J40A | 31.89 | 417.88 | 453.31 | 237.58 | 52.41% | 6.17 | 3.23 | 13.6 | 19.35% | 3.25% |
| J40B | 17.2 | 431.15 | 221.84 | 212.11 | 95.61% | 3.47 | 3.32 | 15.65 | 20.17% | 3.63% |
| J40C | 39.14 | 521.32 | 435.99 | 211.16 | 48.43% | 8.77 | 4.25 | 20.12 | 22.41% | 3.86% |
| J40D | 25.48 | 445.61 | 654.5 | 14.28 | 2.18% | 5.55 | 0.12 | 8.47 | 21.78% | 1.90% |
| K10C | 11.2 | 492.7 | 158.94 | 115.86 | 72.90% | 2.66 | 1.94 | 16.71 | 23.75% | 3.39% |
| K10D | 5.71 | 454.11 | 163.88 | 2.88 | 1.76% | 1.34 | 0.02 | 8.16 | 23.47% | 1.80% |
| K10E | 31.39 | 679.3 | 132.5 | 88.59 | 66.86% | 9.49 | 6.34 | 71.6 | 30.23% | 10.54% |

| Quaternary | MAR4Q | MAP4Q | Area4Q | Outcrop Area | Area_Ratio | MAB4Q | MAB_OC | MAB | MAB/MAR | MAB/MAP |
|---|---|---|---|---|---|---|---|---|---|---|
| Catchment | ($10^6$ m$^3$) | (mm) | (Km$^2$) | (Km$^2$) | (%) | ($10^6$ m$^3$) | ($10^6$ m$^3$) | (mm) | (%) | (%) |
| K10F | 4.89 | 502.44 | 105.73 | 1.34 | 1.27% | 1.12 | 0.01 | 10.59 | 22.90% | 2.11% |
| K20A | 40.32 | 721.97 | 168.4 | 62.73 | 37.25% | 14.11 | 5.26 | 83.81 | 35.00% | 11.61% |
| K30A | 52.52 | 752.85 | 195.94 | 53.21 | 27.16% | 18.51 | 5.03 | 94.47 | 35.24% | 12.55% |
| K30B | 41.59 | 787.16 | 138.59 | 39.84 | 28.75% | 14.77 | 4.25 | 106.58 | 35.51% | 13.54% |
| K30C | 54.03 | 805.11 | 190.06 | 77.51 | 40.78% | 18.99 | 7.74 | 99.91 | 35.15% | 12.41% |
| K30D | 37.87 | 724.31 | 177.82 | 87.23 | 49.05% | 13.18 | 6.46 | 74.1 | 34.80% | 10.23% |
| K40A | 18.7 | 705.57 | 87.47 | 79.08 | 90.41% | 7.19 | 6.5 | 82.16 | 38.45% | 11.64% |
| K40B | 26.7 | 845.63 | 111.56 | 70.91 | 63.56% | 10.15 | 6.45 | 91 | 38.01% | 10.76% |
| K40C | 33.77 | 930.39 | 99.6 | 51.9 | 52.11% | 13.23 | 6.89 | 132.79 | 39.18% | 14.27% |
| K40D | 32.95 | 756.73 | 129.82 | 16.64 | 12.81% | 12.81 | 1.64 | 98.69 | 38.88% | 13.04% |
| K40E | 53.12 | 864.32 | 267.61 | 220.03 | 82.22% | 17 | 13.98 | 63.52 | 32.00% | 7.35% |
| K50A | 53.89 | 849.64 | 235.46 | 235.46 | 100.00% | 19.9 | 19.9 | 84.5 | 36.93% | 9.95% |
| K50B | 48.47 | 881.94 | 202.91 | 202.86 | 99.98% | 17.89 | 17.88 | 88.15 | 36.91% | 10.00% |
| K60A | 13.93 | 663.86 | 161.46 | 161.46 | 100.00% | 4.56 | 4.56 | 28.27 | 32.74% | 4.26% |
| K60B | 17.42 | 753.6 | 143.2 | 143.2 | 100.00% | 7.16 | 7.16 | 49.97 | 41.10% | 6.63% |
| K60C | 20.07 | 744.43 | 160.85 | 160.85 | 100.00% | 8.57 | 8.57 | 53.25 | 42.70% | 7.15% |
| K60D | 44.57 | 814.63 | 292.62 | 292.62 | 100.00% | 18.73 | 18.73 | 63.99 | 42.02% | 7.86% |
| K60E | 10.12 | 774.54 | 100.2 | 98.53 | 98.33% | 4.54 | 4.47 | 45.34 | 44.86% | 5.85% |
| K60F | 23.6 | 806.46 | 242.13 | 188.96 | 78.04% | 10.46 | 8.16 | 43.19 | 44.32% | 5.36% |
| K60G | 19.06 | 860 | 166.64 | 125.19 | 75.12% | 8.43 | 6.33 | 50.57 | 44.23% | 5.88% |
| K70A | 25.86 | 920.11 | 170.42 | 170.41 | 99.99% | 10.43 | 10.43 | 61.18 | 40.33% | 6.65% |
| K70B | 40.56 | 997.24 | 106.5 | 106.5 | 100.00% | 14.55 | 14.55 | 136.6 | 35.87% | 13.70% |
| K80A | 70.04 | 1029.5 | 146 | 146 | 100.00% | 26.78 | 26.78 | 183.42 | 38.24% | 17.82% |
| K80B | 94.71 | 1031.08 | 208.44 | 208.44 | 100.00% | 35.5 | 35.5 | 170.31 | 37.48% | 16.52% |
| K80C | 79.11 | 1016.84 | 189.01 | 189.01 | 100.00% | 29.13 | 29.13 | 154.12 | 36.82% | 15.16% |
| K80D | 65.95 | 936.19 | 173.21 | 173.2 | 100.00% | 23.76 | 23.76 | 137.2 | 36.03% | 14.66% |
| K80E | 54.17 | 894.73 | 266.25 | 245.38 | 92.16% | 14.47 | 13.33 | 54.33 | 26.71% | 6.07% |
| K80F | 33.97 | 545.68 | 221.32 | 157.73 | 71.27% | 9.3 | 6.63 | 42 | 27.38% | 7.70% |
| K90A | 30.34 | 716.15 | 213.81 | 213.81 | 100.00% | 7.55 | 7.55 | 35.29 | 24.88% | 4.93% |
| K90B | 25.54 | 774.13 | 149.84 | 145.81 | 97.31% | 6.39 | 6.22 | 42.63 | 25.02% | 5.51% |
| K90C | 13.59 | 596.31 | 267.46 | 255.45 | 95.51% | 3.97 | 3.79 | 14.84 | 29.21% | 2.49% |
| K90D | 17.11 | 692.62 | 215.66 | 116.3 | 53.93% | 4.83 | 2.61 | 22.41 | 28.23% | 3.24% |
| K90E | 12.03 | 676.22 | 176.77 | 54.77 | 30.98% | 3.54 | 1.1 | 20.03 | 29.43% | 2.96% |
| K90F | 18.82 | 698.55 | 250.86 | 125.7 | 50.11% | 5.46 | 2.74 | 21.76 | 29.01% | 3.12% |
| K90G | 17.13 | 653.85 | 287.16 | 152.97 | 53.27% | 5.01 | 2.67 | 17.44 | 29.25% | 2.67% |
| L30A | 2.99 | 283.94 | 360.95 | 0.16 | 0.04% | 0.31 | 0 | 0.85 | 10.37% | 0.30% |
| L50A | 4.38 | 294.71 | 466.79 | 41.29 | 8.85% | 0.45 | 0.04 | 0.97 | 10.27% | 0.33% |
| L70A | 3.08 | 248.48 | 582.22 | 49.92 | 8.57% | 0.31 | 0.03 | 0.53 | 10.06% | 0.21% |
| L70B | 1.32 | 236.33 | 441.24 | 0.05 | 0.01% | 0.13 | 0 | 0.3 | 9.85% | 0.13% |
| L70C | 2.65 | 224.18 | 662.89 | 89.7 | 13.53% | 0.27 | 0.04 | 0.41 | 10.19% | 0.18% |

| Quaternary | MAR4Q | MAP4Q | Area4Q | Outcrop Area | Area_Ratio | MAB4Q | MAB_OC | MAB | MAB/MAR | MAB/MAP |
|---|---|---|---|---|---|---|---|---|---|---|
| Catchment | ($10^6$ m$^3$) | (mm) | (Km$^2$) | (Km$^2$) | (%) | ($10^6$ m$^3$) | ($10^6$ m$^3$) | (mm) | (%) | (%) |
| L70D | 2.68 | 252.52 | 536.8 | 33.37 | 6.21% | 0.28 | 0.02 | 0.53 | 10.45% | 0.21% |
| L70F | 3.31 | 315.95 | 307.07 | 111.86 | 36.43% | 0.35 | 0.13 | 1.14 | 10.57% | 0.36% |
| L70G | 14.51 | 503.87 | 470.68 | 445.24 | 94.59% | 4.17 | 3.95 | 8.86 | 28.74% | 1.76% |
| L81A | 17.7 | 526.84 | 332.39 | 331.78 | 99.82% | 3.7 | 3.69 | 11.12 | 20.90% | 2.11% |
| L81B | 8.41 | 427.84 | 261.41 | 261.41 | 100.00% | 1.84 | 1.84 | 7.04 | 21.88% | 1.65% |
| L81C | 11.39 | 436.73 | 332.49 | 332.49 | 100.00% | 2.54 | 2.54 | 7.64 | 22.30% | 1.75% |
| L81D | 8.18 | 393.02 | 308.12 | 308.12 | 100.00% | 1.89 | 1.89 | 6.13 | 23.11% | 1.56% |
| L82A | 15.02 | 595.06 | 269.28 | 269.28 | 100.00% | 3.67 | 3.67 | 13.62 | 24.43% | 2.29% |
| L82B | 31.49 | 677.73 | 404.92 | 404.92 | 100.00% | 7.45 | 7.45 | 18.4 | 23.66% | 2.71% |
| L82C | 28.6 | 685.75 | 362.33 | 362.33 | 100.00% | 6.89 | 6.89 | 19.03 | 24.09% | 2.78% |
| L82D | 31.31 | 577.91 | 591.39 | 591.39 | 100.00% | 8.11 | 8.11 | 13.72 | 25.90% | 2.37% |
| L82E | 18.51 | 584.48 | 365.49 | 365.49 | 100.00% | 4.83 | 4.83 | 13.22 | 26.09% | 2.26% |
| L82F | 5.68 | 511.83 | 168.84 | 168.84 | 100.00% | 1.63 | 1.63 | 9.64 | 28.70% | 1.88% |
| L82G | 7.11 | 472.12 | 265.75 | 265.75 | 100.00% | 2.08 | 2.08 | 7.83 | 29.25% | 1.66% |
| L82H | 5.29 | 450.54 | 230.32 | 230.32 | 100.00% | 1.52 | 1.52 | 6.61 | 28.73% | 1.47% |
| L82J | 5 | 491 | 164.28 | 161.73 | 98.45% | 1.45 | 1.42 | 8.8 | 29.00% | 1.79% |
| L90A | 19.91 | 541.59 | 517 | 260.92 | 50.46% | 5.76 | 2.91 | 11.14 | 28.93% | 2.06% |
| L90B | 37.68 | 596.68 | 366.69 | 83.89 | 22.88% | 7.85 | 1.8 | 21.42 | 20.83% | 3.59% |
| L90C | 34.28 | 607.44 | 319.73 | 60.83 | 19.03% | 7.19 | 1.37 | 22.49 | 20.97% | 3.70% |
| M10A | 15.97 | 533.15 | 265.09 | 258.5 | 97.52% | 2.66 | 2.6 | 10.04 | 16.66% | 1.88% |
| M10B | 26.48 | 557.46 | 393.96 | 249.62 | 63.37% | 4.4 | 2.79 | 11.17 | 16.62% | 2.00% |
| M10C | 30.57 | 564.56 | 431.31 | 216.09 | 50.09% | 5.11 | 2.56 | 11.84 | 16.72% | 2.10% |
| M10D | 5.61 | 470.64 | 307.55 | 62.61 | 20.36% | 0.49 | 0.1 | 1.59 | 8.73% | 0.34% |
| M20A | 20.31 | 659.51 | 362.72 | 302.79 | 83.48% | 2.1 | 1.75 | 5.78 | 10.34% | 0.88% |
| M20B | 41.39 | 724.94 | 308.39 | 124.83 | 40.48% | 7.36 | 2.98 | 23.88 | 17.78% | 3.29% |
| M30A | 5.05 | 451.23 | 258.71 | 65.94 | 25.49% | 0.47 | 0.12 | 1.81 | 9.31% | 0.40% |
| N40B | 8.23 | 318.5 | 1213.03 | 130.68 | 10.77% | 0.66 | 0.07 | 0.55 | 8.02% | 0.17% |
| N40E | 3.98 | 363.65 | 511.82 | 40.72 | 7.96% | 0.34 | 0.03 | 0.67 | 8.54% | 0.18% |

**Note:**

MAR4Q: MAR (Mean Annual Riverflow) of the quaternary catchment;

MAP4Q: MAP(Mean Annual Precipitation) of the quaternary catchment;

Area4Q: Area of the quaternary catchment;

Outcrop Area: The TMG outcrop area in the quaternary catchment;

Area_Ratio: The percentage of TMG outcrop area in the quaternary catchment;

MAB4Q: MAB (Mean Annual Baseflow) of the quaternary catchment;

MAB_OC: The MAB that can be attributed to TMG outcrop areas.

MAB (mm): The MAB in the unit of mm of the quaternary catchment;

MAB/MAR: The ratio of MAB to MAR, presented in percentage.

MAB/MAP: The ratio of MAB to MAP, presented in Percentage.